Finite element modelling of steel-concrete composite structures

By

Jawed Qureshi

Submitted in accordance with the requirements for the degree of
Doctor of Philosophy

The University of Leeds
School of Civil Engineering

November, 2010

Acknowledgements

I would like to express my sincere gratitude to my supervisors Prof. Dennis Lam and Dr. Jianqiao Ye for their help, support, encouragement and positive feedback in every step of this PhD research.

I wish to thank Mehran University of Engineering and Technology, Jamshoro, Sindh, Pakistan for sponsoring my PhD study and The Metal Cladding and Roofing Manufacturers Association (MCRMA) for their financial assistance of this research project.

The school of Civil Engineering, University of Leeds is particularly acknowledged for providing experimental and computing facilities, and a conducive environment to conduct this research study. The author would also like to acknowledge the skilled assistance provided by the technical staff in the School of Civil Engineering at University of Leeds.

Finally, I am greatly indebted to my parents who have always supported and prayed for my success in every walk of life. It would not have been possible for me to complete my study without support, love and patience of my wife and son.

Abstract

The main objective of this research is to contribute to the knowledge and understanding of the behaviour of the headed stud shear connector in composite beams with trapezoidal profiled metal decking laid perpendicular to the axis of the beam through experimental and numerical studies. Push tests are used to study the behaviour of composite beams. A three-dimensional finite element model of the push test is developed using the general purpose finite element program ABAQUS and the push test is analysed using different concrete material models, and analysis procedures. The Concrete Damaged Plasticity model with dynamic explicit analysis procedure is found to have matched with experimental results very well in terms of the shear connector resistance, load-slip behaviour and failure mechanisms. The post-failure behaviour of the push test, which has not been modelled in the past, is accurately predicted in this study with the help of this modelling technique.

The experimental investigation is conducted with a single-sided horizontal push test arrangement to study the influence of various parameters such as normal load, number of shear studs, reinforcement bar at the bottom trough, number of layers of mesh, position of mesh, position of normal load and various push test arrangements. To assess the accuracy and reliability of the developed finite element model, it is validated against push test experiments conducted in this study and variety of push tests carried out by other authors with different steel decks and shear stud dimensions, positions of the shear stud within a rib and push test arrangements. The results obtained from the finite element analysis showed excellent agreement with the experimental studies.

The validated finite element model is used in a parametric study to investigate the effect of shear stud position, thickness of the profiled sheeting, shear connector spacing and staggering of shear studs on the performance of the shear stud. The results of the parametric study are evaluated and findings are used to propose the design equations for shear connector resistance taking into account the position of the shear stud and thickness of the profiled sheeting. The coefficient of correlation between experimental and predicted results is nearly equal to one, which indicates that the predicted results are accurate, and the proposed equations are suitable for future predictions.

Contents

Figures

Tables

Chapter 1
Introduction

Chapter 1
Introduction

1.1. Introduction

Steel-concrete composite structures are a common and economical form of construction used in a wide variety of structural types. Composite construction consisting of steel and concrete has been used since the early 1920s. It gained widespread use in bridges in the 1950s and in buildings in the 1960s. Traditionally, steel beams have been used with solid concrete slabs to form composite beams. Today, steel-concrete composite beams using profiled sheeting are becoming increasingly popular in modern construction industry on account of being lightweight, strong, building services friendly and economical in terms of saving in labour cost and construction time. The steel deck acts as a permanent formwork during concrete casting and as a tensile reinforcement after concrete has hardened. The geometry of the profiled sheeting results in reduced self weight of the composite system and thus, leads to reduced foundation loads.

Structural action of composite floor system involves three distinct aspects namely construction phase, composite slab action and composite beam action. In construction phase, the profiled sheeting is subjected to the wet concrete loading, any other load from workman, storage and tools. As no composite action develops between the steel deck and the concrete slab during this phase, the steel deck should, at least, be able to carry the weight of the wet concrete. In other words, the steel deck acts as a permanent formwork during construction phase.

During composite slab action, the profiled sheeting acts compositely with the hardened concrete and thus, forms a composite slab which should be able to support imposed live loading. The composite slab action provides spanning capability for the slab in one direction only. In this phase, the steel deck not only acts as permanent formwork but also as a tensile reinforcement. In order to achieve the required composite action between the profiled sheeting and the concrete slab, the shear forces have to be transferred between them, which is ensured by pressing a pattern of embossments or indentations on the steel deck surface. Besides transfer of these horizontal shear forces, the imposed bending action can create vertical separation between the steel deck and

concrete slab, which can be resisted by the shape of the profile. Both dovetailed or re-entrant and trapezoidal or open rib profiles can be used as steel decks; however, latter is more common. The extent of the shear bond characteristics of a deck profile depends on many factors such as the height, shape, orientation and frequency of embossments, the geometry and flexibility of the profiled sheeting.

The composite beam action ensures composite action between the steel beam and slab which altogether gives a two-way spanning capability for the composite floor slab. In steel-concrete composite beams, the slab could be either solid concrete slab, hollow core slab or composite slab with profiled sheeting. As shown in Figure 1.1, the most common form of achieving composite action between the steel beam and profiled sheeting slab is through mechanical action of shear connectors. The main function of shear connectors is to resist shear forces at the steel-concrete interface, and to prevent vertical separation between the slab and steel beam. The headed shear stud, being equally efficient in resisting shear forces in all directions due to its circular shape, is the most commonly used shear connector.

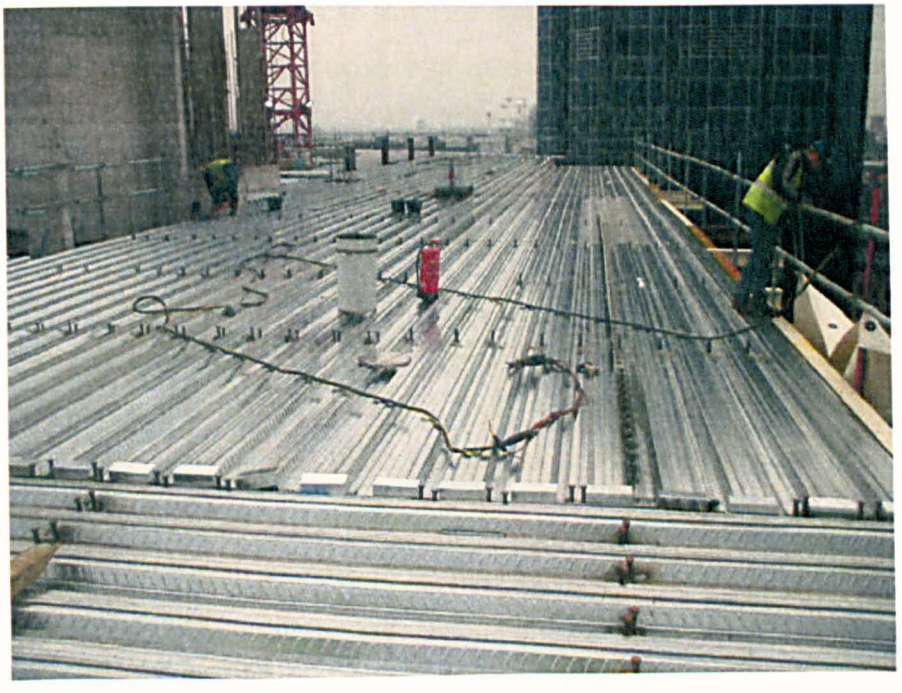

Figure 1.1 Composite beam with profiled sheeting during construction

Predominantly, the performance of the shear connector in composite beams with profiled steel sheeting has been based on empirical studies. Both large scale beam and

small scale push tests can be used to determine the shear connector resistance and load-slip behaviour of the shear stud. However, in practice, push tests are well-established as a cost-effective alternative to more expensive and time consuming full-scale composite beam tests. Research conducted by Johnson and Yuan (1998) on push tests with profiled sheeting slab suggests that the shear connector resistance from composite beam tests has given inconsistent results, and therefore the design equations are mainly based on push tests. For this reason, push tests are often used to evaluate wide variety of parameters and beam tests are only used to verify the results of methods developed from push tests.

Conventional push test arrangement consisting of a short steel beam connected to two small concrete slabs by means of shear connectors, with the exception of slight variations in its geometry, has hardly changed ever since its inception in the 1930s. Both concrete slabs remain bedded on the floor and a uniform vertical compressive load is applied to the upper end of the steel beam. The shear connector resistance is assumed to be the failure load divided by the number of studs. The slip is measured between the steel beam and concrete slab at various locations and the average slip is plotted against load per stud. The standard push test arrangement in Eurocode 4 was originally devised to study the behaviour headed shear studs in solid slabs. No provisions are given in Eurocode 4 about the changes that need to be made in the standard push test arrangment if profiled sheeting slab is used instead of solid concrete slab.

Majority of push tests conducted using the standard push test arrangement has resulted in a slip at the steel-concrete interface in a push test that is well below the slip observed in beam tests. It is generally believed that the reason of poor performance of the shear stud in a push test is due to the absence of a curvature and normal load which exist in the real beam from the imposed floor loading. A few attempts have been made by Easterling et al. (1993) and Bradford et al. (2006) to devise the standard push test arrangement through use of normal load on the top surface of the slab in addition to the horizontal shear load. The research conducted by Ernst et el. (2009) made use of the waveform reinforcement and stud performance enhancing devices to address the problem of low ductility of the shear stud in composite beams with profiled sheeting. Although the slip at the steel-concrete interface attained in these studies met the Eurocode 4 requirement of 6 mm slip for ductile shear connector failure, the push test specimens were heavily reinforced in most of the cases. Therefore, there is a need to

develop a standard push test arrangement for composite beams with profiled sheeting that can ensure ductile shear connector failure.

Finite element models, if validated properly against experimental results, can be used as an efficient tool to study the behaviour of shear connectors in composite beams with profiled sheeting in conjunction with experimental investigations. However, on account of complex interactions among concrete slab, profiled sheeting, wire mesh, shear stud and steel beam; there has been limited success in effectively modelling the behaviour of headed shear studs in composite beams with profiled sheeting. All numerical studies conducted so far are based on the assumption that the concrete slab and profiled sheeting nodes remain connected throughout the analysis, which means that the effect of separation of concrete slab from profiled sheeting is neglected. This is contrary to the push test experiment, where the steel deck is usually delaminated from the concrete slab after failure.

The post-failure behaviour of a push test with steel deck has not been modelled in the past, which is very important in determining the accurate load and slip at failure, and identifying the actual failure mechanisms in a push test. Previous research on finite element modelling of the shear connector behaviour is mainly focussed on a single stud per rib with primary variables as concrete strength, size of the shear stud and the deck rib width. A finite element model that can represent the true behaviour of the push test with profiled sheeting in terms of post-failure softening behaviour, failure mechanisms and accurate slip at failure needs to be developed, which will be very useful in getting greater insight into the behaviour of headed shear studs in composite beams

The appearance of small central stiffening rib at the bottom of the trough in modern profiled sheeting has resulted in shear studs being placed in the off-centre position either on the favourable or unfavourable side of the rib. A favourable location is where the zone of concrete under compression in front of the stud in its load bearing direction is larger than the compressive zone behind the stud. On the other hand, an unfavourable location is where the zone of concrete in compression in front of the stud in its loaded direction is very small compared with the zone behind it. In a beam, the stud placed on side of the central stiffener away form the mid span is in the favourable location, while the stud placed closest to the location of maximum moment for a simply supported

beam is in the unfavourable position. Favourable and unfavourable shear stud locations are also termed as strong and weak stud positions respectively in America. The shear stud is considered to be strong in the favourable position and weak in the unfavourable position.

It is recommended by majority of the researchers and design codes that the studs should be placed in the favourable position. However, it is not practically possible to ensure the favourable position of studs all the time. The review of the literature also indicates that limited research exists for the influence of shear stud spacing, layout and position, and profiled sheeting thickness on the strength and ductility of the shear connector in composite beams with profiled metal decking. Therefore, in order to bridge the gaps in knowledge and understating of the behaviour of the headed shear stud in composite beams, an investigation must be carried out by way of experimental and numerical studies.

1.2. Objectives of the research

The main objective of this research is to develop a three-dimensional finite element model to study the behaviour of the headed shear stud in a composite beam with trapezoidal profiled sheeting by utilizing the best available material models and analysis procedures in ABAQUS. The specific combination of the material model and the analysis procedure that gives results which are comparable with the experimental results in terms of shear connector resistance, load-slip behaviour and failure modes will be considered to be representative of the true behaviour of the shear stud in a push test and will be used for further validation against experimental push tests conducted in this study and previous experimental studies. The validated finite element model will be used to carry out an extensive parametric study.

The experimental study employing a single-sided horizontal push test arrangement will also be conducted to verify the developed finite element model and to investigate the influence of various parameters such as normal load, number of shear studs, reinforcement bar at the bottom trough, number of layers of mesh, position of mesh, position of normal load and various push test arrangements on the strength and ductility of the headed shear stud in composite beams with profiled sheeting.

A parametric study to investigate the effect of shear connector spacing, layout and position, and profiled sheeting thickness on the strength, ductility and failure mechanisms of the headed shear connector in a push test will be carried out. The size of the shear stud, concrete slab and wire mesh fabric, and geometry of the steel deck will be kept constant throughout the parametric study. Design equations for the shear connector resistance, based on the position of shear stud within a sheeting pan and profiled sheeting thickness, will also be proposed, and will be verified against experimental studies and separate set of numerical studies, where experimental data is not available.

1.3. Scope of the thesis

The scope of this research is limited to the behaviour of headed shear studs in composite beams with profiled sheeting slab in secondary beam applications.

The review of previous research related to composite beams with profiled sheeting is presented in Chapter 2. The literature review is focussed on experimental and numerical studies of push test with profiled sheeting along with some discussion of standard push test arrangement and design equations to calculate the shear connector resistance.

The results of the experimental investigation of push tests are reported in Chapter 3. It also presents the push test set up, instrumentation, loading procedure, material tests, failure patterns and summary of push test results.

Chapter 4 presents the discussion of the push test results. The effect of various parameters on the behaviour of the shear stud, and comparison of shear connector resistances obtained from push tests and different strength prediction methods are also presented in this chapter.

Preliminary development of the finite element model of the push test with profiled sheeting is covered in Chapter 5. The main purpose is to highlight different concrete material models and analysis procedures available in the general purpose finite element program ABAQUS; and to facilitate selection of an appropriate modelling technique that represents the true behaviour of the headed shear connector.

After selection of a suitable modelling approach in Chapter 5, the developed finite element model is extensively validated in Chapter 6 against the experimental push test results conducted in this study and experimental studies conducted by other authors in terms of the strength, ductility and failure modes of the headed shear stud.

A parametric study using validated finite element model is presented in Chapter 7. The main parameters are the effect of shear connector spacing, layout and position, and profiled sheeting thickness on the strength and ductility of the shear connector.

Finally, Chapter 8 presents conclusions drawn from numerical and experimental work, and recommendations for future work.

Chapter 2
Literature Review

Chapter 2
Literature Review

2.1. Introduction

This chapter deals with details of the shear connection in composite beams with profiled sheeting and review of previous research related to experimental and numerical studies of composite beams with profiled sheeting. The main purpose is to identify gaps in the knowledge and understanding of the shear connector behaviour in steel-concrete composite beams with profiled sheeting and bridge those gaps in subsequent chapters.

2.2. Shear connection in composite beam

Composite beams using a composite slab with profiled metal decking are a common and economical form of construction these days. This type of construction is lightweight, strong, building services friendly and economical in terms of savings in labour cost and construction time. The efficiency of a steel-concrete composite beam lies in ensuring composite action between the steel beam and composite slab. Headed shear studs are commonly used to achieve composite action in a steel- concrete composite beam. Their main function is to resist longitudinal shear forces across steel-concrete interface, and to prevent vertical separation of the concrete slab from the steel beam. The strength of the shear connection in a steel-concrete composite beam depends on two important factors, namely shear strength of the shear stud and the resistance of concrete or composite slab against longitudinal cracking.

2.2.1. Shear connectors

Although shear connectors are available in a variety of shapes and sizes such as, bar and channel connectors, the headed shear stud remains the most commonly used shear connector on account of relative ease with which it can be installed, and it offers little obstruction to the reinforcement in the concrete slab. Additionally, it is believed that the headed shear stud, being circular in shape, is equally efficient in resisting shear forces in all directions, and the head of the shear stud prevents the concrete slab from lifting away from the steel beam. According to Eurocode 4, the ultimate tensile strength of the stud should be at least 450 N/mm^2 and minimum elongation should be 15%. Further, it is mentioned in this code that the stud should be welded and the minimum head diameter

should be 1.5d and head depth should be 0.4d, where d is the shank diameter of the stud. The diameter of the stud varies from 13 to 25 mm and the height of the stud ranges from 65 mm to 150 mm. The headed shear stud is shown in Figure 2.1.

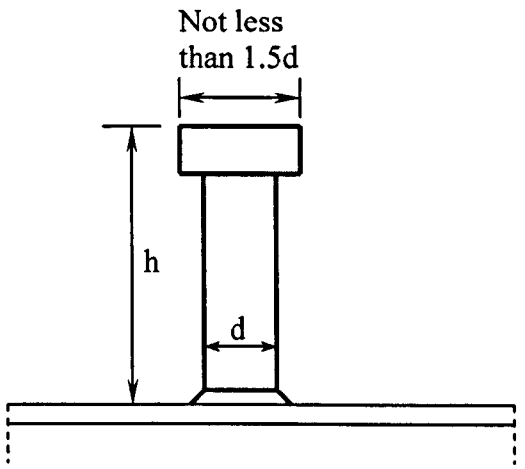

Figure 2.1 Headed stud shear connector

In steel-concrete composite beams, the slab that rests on the steel beam can be either solid reinforced concrete slab, pre-cast hollow core slab or composite slab with profiled sheeting. The way, the shear stud is welded to the beam, can be different for all of these slabs. For example, in case of solid slab and pre-cast hollow core slab shear studs are welded directly to the beam. On the other hand, for composite slab, the stud is welded through the steel deck to the beam, and thereby, it ensures the composite action among steel beam, metal deck and concrete slab.

2.2.2. Push test

The behaviour of the shear stud depends upon its strength, and slip at the steel-concrete interface. The load-slip curve is plotted to assess the performance of the shear connector. Mostly, the performance of shear connector in composite beams with profiled steel sheeting has been based on empirical studies. Both large scale beam and small scale push tests can be used to study the behaviour of the headed shear stud, but push tests are more commonly used to determine the performance of the shear stud.

The conventional vertical push test arrangement has hardly changed ever since it was introduced in 1930s. This push test consists of two slabs connected to the steel beam with the help of shear studs and with vertical load applied to the top of the beam. The shear connector strength is the maximum load applied to the push test divided by total

number of studs. The existing standard push test arrangement has previously been reviewed by Lam (2007). The standard push test arrangement in Eurocode 4 was originally intended to study the behaviour of headed shear studs in solid slabs. It is important to note that no provision is given in this code for any changes that need to be made in the standard push test arrangement, when the steel deck is present. The standard push test arrangement as per Eurocode 4 is shown in Figure 2.2.

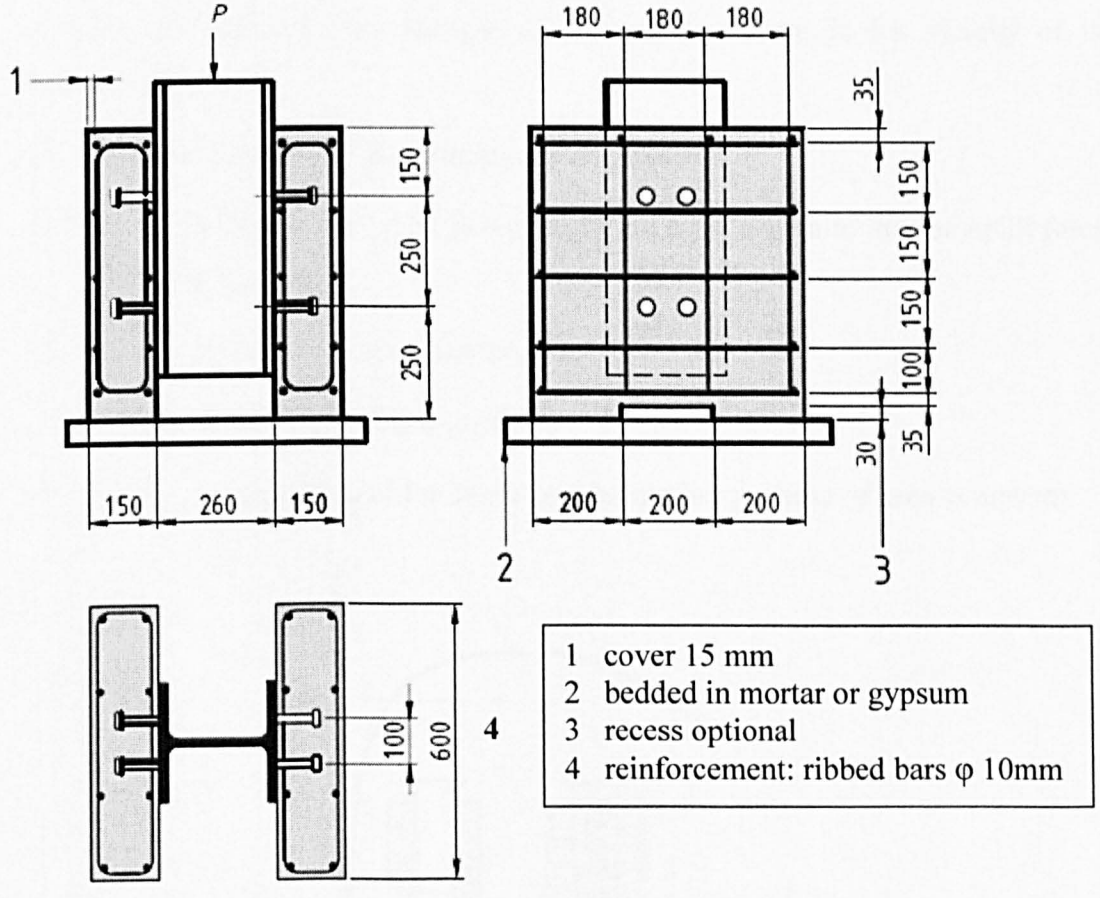

Figure 2.2 Standard push out test specimen according to Eurocode 4

According to Eurocode 4, if three nominally identical push tests are carried out, and the individual test result does not deviate more than 10% of the mean value, the characteristic resistance of the shear connector P_{RK} is equal to 0.9 times the minimum failure load per stud. The ductility of the shear connector is determined from its slip capacity δ_u. The slip capacity is defined as a value of slip at which the characteristic shear resistance of the stud P_{RK} intersects the falling branch of the load-slip curve as shown in Figure 2.3. The characteristic slip capacity δ_{uk} is taken as a minimum value of

the slip capacity δ_u with 10% reduction or it can also be determined from the statistical analysis of push test results. The load-slip behaviour of shear connectors, obtained from push tests using solid slab, is influenced by many factors as mentioned by Johnson (2004)

1. number of connectors in the test specimen,
2. mean longitudinal stress in the concrete slab surrounding the connectors,
3. size, arrangement, and strength of slab reinforcement in the vicinity of the connectors,
4. thickness of concrete surrounding the connectors,
5. freedom of the base of each slab to move laterally, and so to impose uplift forces on the connectors,
6. bond at the steel-concrete interface,
7. strength of the concrete slab, and
8. degree of compaction of the concrete surrounding the base of each connector

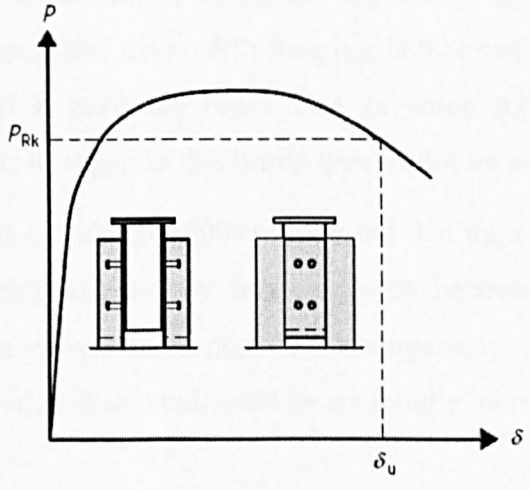

Figure 2.3 Determination of slip capacity δ_u according to Eurocode 4

The current standard push test arrangement in Eurocode 4 is not suitable for use in composite slab with profiled steel sheeting based on following reasons:

1. The size of the push test arrangement and the position of the shear stud in a sheeting pan are dictated by the geometry of the steel deck. For example, the

Eurocode 4 specifies the longitudinal spacing between studs as 250 mm, which is difficult to be maintained for different deck geometries.

2. In the absence of a standard push test arrangement, when the profiled sheeting is used, it is not clear that how many number of connected profiled sheeting ribs per push test slab should be used.

3. No guidance is given in Eurocode 4 about the changes that need to be made in the standard push test arrangement when the steel decking is present.

4. In conventional vertical push test set up, two profiled sheeting slabs are prone to asymmetrical transfer of load from steel beam, especially in the inelastic load range.

5. The limited width of the slab could cause rib shear failure. This type of failure is reported by Patrick (2000) and it takes place both in push tests and in beam tests with profiled sheeting transverse to the beam. It occurs when a crack forms at the top corner of the steel deck rib and extends horizontally to the other top corner of the trough, while locally passing over the head of the stud. This is a brittle failure and can significantly reduce the strength and ductility of the shear connector. It is considered as a potential mode of failure especially in composite edge beams employing deep trapezoidal decks. Rib shearing failure can be avoided if wider test specimens are used in push and beam tests, or some authors have used special reinforcing elements to suppress this brittle type of failure mode.

6. Work by Hicks and Couchman (2004) suggested that the shear connector capacity could be significantly affected by friction forces between the test slab and the reaction floors in a conventional push test arrangement. Consequently, the shear resistance of the headed shear stud could be artificially increased.

2.3. Shear connector strength prediction equations

This section presents a review of different strength prediction equations for both composite beams with solid slabs and composite beams with profiled sheeting slabs. The equations employed by different design codes are also explained. Separate design equations are given for composite beam with profiled sheeting laid transverse and parallel to the axis of the steel beam.

2.3.1. Shear connector embedded in solid concrete slab

One of the earliest empirical equations for predicting the shear strength of stud connectors in a solid concrete slab was presented by Ollgaard et al (1971). The results of 48 push-out tests showed that the strength of the shear connector was mainly affected by the compressive strength and modulus of elasticity of concrete. For design purposes, the authors proposed the following equation to estimate the ultimate strength of shear studs Q_u embedded in both normal and lightweight concrete slabs.

$$Q_u = 0.5 A_s \sqrt{f_c' E_c} \tag{2.1}$$

where

A_s = nominal area of the stud shear connector

f_c' = concrete compressive strength (cylindrical)

E_c = modulus of elasticity of concrete

The Equation (2.1) was adopted in CP 117. However, in BS 5950-3.1 1990, the characteristic resistance Q_k of headed shear connectors is given in Table 5 of the code corresponding to some selected values of the size of the shear connector and compressive strength of concrete. According to BS EN 1994-1-1:2004 Eurocode 4 clause 6.6.3.1, the design shear resistance P_{Rd} should be determined from the smaller of the following two equations:

$$P_{Rd} = \frac{0.8 f_u \pi \frac{d^2}{4}}{\gamma_V} \tag{2.2}$$

Or

$$P_{Rd} = \frac{0.29 \alpha d^2 \sqrt{f_{ck} E_{cm}}}{\gamma_V} \tag{2.3}$$

whichever is smaller with:

$$\alpha = 0.2\left(\frac{h_{sc}}{d} + 1\right) \quad \text{for} \quad 3 \le \frac{h_{sc}}{d} \le 4$$

$$\alpha = 1 \quad \text{for} \quad \frac{h_{sc}}{d} > 4$$

γ_V = is the partial safety factor taken as 1.25 for the ultimate condition

d = is the diameter of the shank of the stud, 16 mm $\leq d \leq$ 25 mm

f_u = is the specified ultimate tensile strength of the material of the stud but not greater than 500 N/mm^2

f_{ck} = is characteristic cylinder compressive strength of the concrete at the age considered, of density not less than 1750 kg/m^3

h_{sc} = is the overall nominal height of the stud

2.3.2. Shear connector embedded in composite slab

It has long been known that the presence of trapezoidal profiled metal decking not only weakens the shear connector, but also reduces the slip capacity of the headed shear stud (Wright et al (1987), Lloyd and Wright (1990), Easterling et al (1993) and Patrick (2000)). To take into account the weakening effect of the profiled sheeting, the most popular approach has been to apply a reduction factor to the shear connector resistance of push tests with solid slabs. Early equations for the shear connector strength were primarily for composite beams with solid slabs and were based on the results from push tests. The equation for strength of the shear connector embedded in the profiled sheeting slab, which is based on the application of empirical reduction factor to the solid slab shear connector strength (P_{Rd}), is given in Equation (2.4).

$$P_r = k P_{Rd} \tag{2.4}$$

where 'k' is the empirical reduction factor which depends upon direction of the sheeting

Perhaps, the shear capacity of composite beams with profiled sheeting was first determined by Fisher (1970). The equation is based on results of composite beams with formed metal deck and is given by

$$Q_{rib} = 0.36\frac{w}{h}Q_{sol} \tag{2.5}$$

where 'Q_{rib}' is ultimate shear connector strength in composite slab, 'w' is average rib width, 'h' is rib height and 'Q_{sol}' is ultimate shear connector strength in solid slab.

As a matter of fact, the Equation (2.5) had inherent limitation that it did not include the height of the shear stud and number of shear connectors in a rib as variables. These concerns were first addressed by Grant et al (1977) and these two factors were included by the authors. Therefore, a modified empirical reduction factor, which had to be multiplied by the shear connector resistance of the solid slab in order to get the strength of the shear stud in a beam with a composite slab, was proposed by Grant et al (1977) as given in (2.6).

$$k_r = \frac{0.85}{\sqrt{N}}\left(\frac{H-h}{h}\right)\left(\frac{w}{h}\right) \leq 1 \qquad (2.6)$$

where *'N'* is number of studs in a rib and *'H'* is height of stud shear connector.

This empirical relation became very popular and gained widespread acceptance across the world. It has been adopted by various design codes such as American, British and European codes with a slight variation. However, the recent American Code AISC (2005) uses a unified equation for the shear connector resistance of composite beams with both solid and composite slabs. The main problem is that the reduction factor and solid slab shear connector resistance are both empirically based relations and using one empirical relation on the basis of the other makes this approach quite questionable. In spite of this, the use of this reduction factor has remained a preferred approach in the design codes.

2.3.3. Shear connector resistance with ribs parallel to supporting beams

The profiled sheeting can be placed on supporting beams in two ways, it may be continuous across the beam, thus providing lateral support to the concrete around studs, and it may be discontinuous having a breadth of b_o that is generally more than breadth of ordinary trough of the profiled sheeting. When the profiled sheeting is discontinuous, studs are enclosed in a region of concrete that has the shape of a haunch as shown in Figure 2.4.

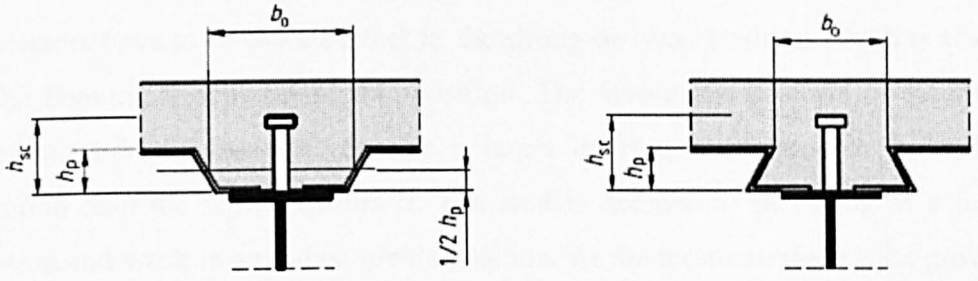

Figure 2.4 Beam with profiled steel sheeting parallel to the beam

As per Eurocode 4, the design resistance of the shear connector placed in a composite slab with profiled sheeting parallel to the axis of the beam is equal to the resistance of the solid slab multiplied by a reduction factor k_l expressed by the following equation:

$$k_l = 0.6\frac{b_o}{h_p}\left(\frac{h_{sc}}{h_p} - 1\right) \leq 1.0 \qquad (2.7)$$

where

h_p is the overall depth of sheeting excluding embossments

h_{sc} is the overall height of the stud, but not greater than $h_p + 75$ mm

2.3.4. Shear connector resistance with ribs transverse to supporting beams

According to Eurocode 4, the design shear connector resistance of a composite beam with profiled sheeting slab is equal to the shear connector resistance of a composite beam with solid slab in Equations (2.2) and (2.3) (f_u should not be greater than 450 N/mm^2) multiplied by the reduction factor k_t which is given by the following equation:

$$k_t = \frac{0.7}{\sqrt{n_r}}\frac{b_o}{h_p}\left(\frac{h_{sc}}{h_p} - 1\right) \leq 1.0 \qquad (2.8)$$

where

n_r = is the number of stud connectors in one rib at a beam intersection, not to exceed 2 in computations.

The widespread use of modern trapezoidal profiled sheeting with a central stiffening rib at the bottom of the trough has led to studs being placed off centre. As a result, shear connectors have to be placed either in the strong or weak position which is also termed as the favourable or unfavourable position. The favourable position of the stud is the location where the zone of concrete is larger in front of the stud in its load bearing direction than the region behind it. The stud is deemed to be strong in a favourable position and weak in an unfavourable position. At the moment, there is no provision for the position of the stud in Eurocode 4. However, the American code AISC (2005) takes into account the position of the shear connector by introducing position effect factor, which is 0.75 for favourable positioned studs and 0.6 for unfavourable positioned studs, in its shear connector resistance prediction equation (2.9). The explanation regarding different variables in this equation is given in section 4.4.3 of Chapter 4.

$$Q_n = 0.5 A_{sc} \sqrt{f_c' E_c} \leq R_g R_p A_{sc} F_u \qquad (2.9)$$

2.4. Previous studies on behaviour of shear stud in composite slab

A comprehensive experimental study was conducted in 1977 to investigate the behaviour of shear studs in composite beams with formed metal deck by Grant et al (1977). The behaviour of 19 mm diameter or smaller studs was evaluated. The authors performed 17 composite beam tests, and used the results of 58 tests from other researchers. They used wide slabs with widths equal to 16 times the slab thickness. The main parameters were the weight and strength of concrete, diameter and height of stud shear connectors, type of slab reinforcement, and type of loading.

The authors made a modification to the equation proposed by Fisher (1970) and thus, included the height of the stud shear connector. Therefore, the strength of the shear stud in ribs of composite beams with formed steel deck can be expressed by Equation (2.10). The authors concluded that the flexural strength of a composite beam with formed steel deck can be estimated more accurately if the slab force is assumed to act at the mid-depth of the solid portion of the slab above the ribs rather than at the centroid of the concrete stress block.

$$Q_{rib} = \frac{0.85}{\sqrt{N}}\left(\frac{H-h}{h}\right)\left(\frac{w}{h}\right)Q_{sol} \leq Q_{sol} \quad (2.10)$$

where, Q_{rib} = strength of a stud in formed steel deck, N = number of studs in a rib, H = height of stud shear connector, h = height of rib, w = average rib width and Q_{sol} = strength of the stud shear connector in a solid slab

$$Q_{sol} = 0.5A_s\sqrt{f_c' E_c} \quad (2.11)$$

where, A_s = Area of studs, f_c' = concrete compressive strength, E_c = modulus of elasticity of concrete

In 1984, Hawkins and Mitchell (1984) conducted 10 solid slab push-out tests under reversed cyclic loading and compared the results with 13 composite slab push-out specimens tested monotonically to study the behaviour of shear connectors. Mostly, the profiled steel sheeting was placed perpendicular to the axis of the beam except one case in which it ran parallel to the steel beam. The diameter of the stud was 19 mm, profiled sheeting depths ranged from 38 and 76 mm and profiled sheeting widths were 38 to 127 mm. The effect of type of loading, presence of ribbed metal deck, geometry of metal deck, and orientation of metal deck were studied.

Four different failure modes were observed by Hawkins and Mitchell (1984) including stud shearing, concrete pull-out, rib shearing and rib punching. The studs that failed in stud shearing showed ductile behaviour. The shear connector strength in the push test subjected to reversed cyclic loads was 17% lower than the monotonically tested push test. Staggering of the studs or using large stud spacings increased the shear connector strength. In concrete pull-out failure, studs may also fail due to a tensile force in the stud caused by large deformations and this failure was very brittle, can cause a large decrease in strength and ductility of the stud compared to stud shearing failure. The shear connector strength in push tests with concrete pull-out failure, based on pyramidal cone-shaped failure surface in concrete, can be calculated from Equation (2.12). The authors proposed equations for calculating area of concrete pull-out failure surface (A_c) for single and double studs per rib.

$$V_c = 5.4\sqrt{f_c'}A_c \qquad (2.12)$$

where

V_c = shear strength due to concrete pull-out (psi)

f_c' = concrete compressive strength (psi)

A_c = area of concrete pull-out failure surface (in^2)

In 1987, Wright et al (1987) conducted performance testing to study the composite beam and composite slab action. The authors conducted forty push-out tests to calculate stud strengths for various grades of concrete. It was concluded that the presence of the profile sheeting and position of the stud within the trough weakens the stud. Stud strengths obtained from push-out tests were used to determine the strength and stiffness of composite beams by a design method recommended by CONSTRADO. Eight full scale beam tests were carried out in order to assess the suitability of this method for composite beams with profiled sheeting. The results showed that the design method generally underestimated the ultimate strength of the composite beam. It was also noted that use of light weight concrete has little effect on short term strength and stiffness of the composite beam. The authors noted that the stiffness calculated by the design method was reasonably close to the test results. It was concluded that the results obtained from the design method were generally conservative.

The behaviour of the composite interior beam (perpendicular metal deck), spandrel beam (perpendicular metal deck) and girder (parallel metal deck) was studied by Robinson (1988). The author performed 49 push tests with 51 mm and 76 mm deep metal deck, and two beam tests with 76 mm deep metal deck. Both the interior and exterior beam-type push test specimens failed by "cracking through the solid part of the concrete slab at the root of the concrete rib on both sides of the rib." The slip and shear connector resistance for pair of studs per rib were approximately 1.3 times more than that for single stud per rib.

The girder type push test specimen failed by shearing off of one or both shear connectors. Ultimate shear strengths obtained from push tests were used to calculate ultimate flexural moment capacities of two composite beams; and the ratio of the calculated ultimate flexural moment to the measured ultimate flexural moment was 0.999. It was concluded that shear strength obtained from push tests, having the same shear connector and profile sheeting as that of composite beams, can be reliably used in the design of composite beams and girders.

The empirical equations for shear connector resistance were proposed by Jayas and Hosain (1988) based on 18 full-size push-out tests and 4 pull-out tests. Five of the push-out specimens had solid concrete slabs, five had composite slabs with ribbed metal deck parallel to the steel beam, and remaining eight had the metal deck perpendicular to the steel beam. The main parameters were longitudinal spacing of the headed studs and rib geometry of metal decks. Two types of deck heights namely 38 mm and 76 mm were used with corresponding headed stud size of 16 × 76 mm and 19 × 125 mm respectively. The concrete slab thickness was chosen in such a way so as to provide a clear cover of 25 mm to the stud head.

Several failure modes were observed in push-out tests such as shearing off of studs, crushing of concrete near the stud, longitudinal shearing of the concrete slab, stud pull-out together with a concrete wedge, and rib shear failure. The first three failure modes occurred only in solid slabs and specimens having metal deck parallel to the beam. For these specimens, when the stud spacing was more than six times the diameter, shearing off of studs was the principal mode of failure. However, in case of closely spaced studs, spacing equal to six diameters, concrete related failures were dominant. In case of closely spaced studs, the stud strength reduced by 7% for solid slabs, and 14% for parallel ribbed slabs. It was recommended that concrete failures for studs spaced less than six diameters should be checked in the design.

The stud pull-out failure was the predominant failure mode in case of specimens with a perpendicular metal deck. This resulted in as much as 40% and 50% reduction in the stud strength for wide (where the rib width-to-rib height ratio, W_r/h_r, is greater than four) and narrow rib profiles respectively as compared to the similar specimen with

solid slab. It was further observed that the stud spacing did not have much influence on the stud strength for tests with perpendicular metal decks. The authors concluded that North American codes overestimated the stud strength for the deck placed perpendicular to the steel beam. Similarly, the equation proposed by Hawkins and Mitchell (1984) underestimated the stud strength for 38 mm high metal deck and overestimated the stud strength when 76 mm high metal deck was used.

The authors proposed two separate empirical equations (2.13) and (2.14), based on the linear regression analysis, for 38 and 76 mm decks heights.

For a 76 mm deck

$$V_c = 0.35\lambda\sqrt{f'_c}A_c \leq Q_u \qquad (2.13)$$

For a 38 mm deck

$$V_c = 0.61\lambda\sqrt{f'_c}A_c \leq Q_u \qquad (2.14)$$

where

V_c = shear strength due to concrete pull-out failure (N)

f'_c = concrete compressive strength (MPa)

A_c = concrete pull-out failure surface area (Hawkins and Mitchell 1984) (mm^2)

λ = factor dependent upon type of concrete

= 1.0 for normal density concrete

= 0.85 for semi-low density concrete

= 0.75 for structural low density concrete

Q_u = ultimate shear stud strength from Ollgaard et al (1971) (N)

These empirical equations were verified with the help of four full scale composite beam and two full size push-off tests in a separate study by Jayas and Hosain (1989). The beams were designed with partial shear connection, and deck geometry and longitudinal stud spacing were the principal parameters. The concrete pull-out was the predominant mode of failure. Only, one of the beam and push-off specimens failed by a combination of concrete pull-out and stud shearing failure. It was concluded that the shear capacity of the stud is dependent on the deck geometry and stud layout rather than on the

longitudinal stud spacing. The flexural capacity, calculated indirectly using equation proposed by Jayas and Hosain (1988) for 76 mm deck, was in close agreement with those observed in full scale beam specimens.

The effect of slab dimensions, and position and amount of reinforcement, and application of transverse load to the slab were studied by Lloyd and Wright (1990) with the help of 42 push-out tests on headed shear studs welded through-deck. The stud size used was 19 × 100 mm and the slab was 115 mm thick with normal weight concrete. The slab width varied from 450 mm to 1350 mm.

Major failure modes observed were wedged shear-cone failure; stud shear and rib shear failure. Predominantly, the wedge-shaped failure cones formed around the studs instead of pyramidal-shaped cones as suggested by Hawkins and Mitchell (1984). It was concluded that the capacity of the shear stud welded through-deck depends upon the geometry of the sheeting and stud height. The authors developed expression for the shear connector resistance, based on the concrete surface area of wedge-shaped cone for cone failures. This expression is given by

$$Q_K = 0.92\left(A_C\sqrt{f_{cu}}\right)^{0.349} \tag{2.15}$$

where

f_{cu} = concrete strength

A_c = surface area of concrete failure cone

For design purpose, the above equation was simplified as

$$Q_K = \left(A_C\sqrt{f_{cu}}\right)^{0.34} \tag{2.16}$$

Different equations were proposed for the surface area of concrete considering wedge-shaped cone failure and rib shear failure with single and double shear stud per rib. The authors proposed an expression to predict a minimum specimen width before the rib shear failure occurs. The standard size of the push-out test was also proposed. It was suggested that at least three full pitches of the sheeting profile should be used and a width 200 mm wider than the limiting rib-shear width should be used. It was concluded that the capacity of the shear connector with profiled sheeting was considerably lower

than that of the solid slab. Variations in size and position of reinforcement, and increasing the width of the specimen appeared to have no significant effect on the shear connector resistance.

In 1990, Mottram and Johnson (1990) conducted 35 push-out tests on studs welded through profiled sheeting with ribs laid transverse to the steel beam. Three types of steel decks with normal and light weight concrete were used. The influence of short-fired pins, which were used to fix profiled sheeting, was studied in three tests. Studs had a diameter of 19 mm, and the nominal length after welding was either 95 mm or 120 mm.

The push test results showed that the failure occurred in concrete ribs instead of shear studs, particularly when two studs per rib were used. The stud strength was approximately proportional to $f_{cu}^{0.27}$, where f_{cu} is the cube strength of concrete. The resistance per stud for two studs per rib was less than that for one stud per rib. The strength per stud for two studs placed diagonally was slightly less than for an unfavourable stud. On the other hand, the maximum slip was greatly reduced in diagonally placed studs. Two studs in line were stronger than two diagonally placed, even though the diagonal studs were farther apart. Tests showed that studs placed in the unfavourable side can be 35% weaker than the favourable side studs. However, this weakening effect was less prominent in unfavourable studs placed in shallower slab.

The authors compared the reduction factors for rib geometry due to Grant et al (1977) and the following equation which was later modified and published by Lawson (1992).

$$SRF = \frac{0.75r}{\sqrt{N_R}}\left(\frac{H_s}{H_s + h_R}\right) \leq 1.0 \qquad (2.17)$$

where

r = factor to account for position of stud in rib

for central or favourable position studs ($e > b_o/2$):

r is the lesser of b_0/h_a and 2.0

for studs placed in unfavourable position ($e > b_o/2$):

r is the least of b_0/h_a , $(e/h_a) + 1$ and 2.0

N_R = number of studs per rib

H_s = height of stud

h_R = depth of steel deck

b_o = average width of rib

e = distance from centre of stud to mid-height of deck web on loaded side

The authors concluded that the equation proposed by Lawson (1992) was more consistent with test results than the equation due to Grant et al (1977). In contrast to the equation proposed by Grant et al (1977), Equation (2.17) accounts for the position of studs within a rib which can be central, favourable or unfavourable position. It was also found that a decrease in the transverse spacing of studs from 76 mm to 50 mm resulted in a 6% reduction in the strength. One stud per trough had a higher slip capacity than two studs per rib. This loss of slip capacity can be overcome by either increasing longitudinal shear resistance or slab thickness when designing the slabs.

In the same year, Wright and Francis (1990) performed four full-scale composite beams tests with composite slabs, having shear studs welded through profiled sheeting, along with three push-out tests. The number of studs used was varied, while the deck type and stud size remained constant. Both the beams and push-off tests failed due to concrete shear failure cones around studs. It was observed by the authors that "the beams were approximately 20% stiffer when tested in a web-cleated condition than when tested with roller supports." Further, the dynamic behaviour did not seem to be affected by the connection level.

A few attempts have been made to devise a standard push test arrangement for headed shear studs in profiled steel sheeting. The push test arrangement proposed by Easterling et al. (1993) consisted of a vertical push test arrangement with three profiled sheeting ribs. The steel beam was split into two to form structural tee so that same concrete could be poured in both test slabs. In addition to the shear load, a normal load equal to 10 percent of the expected shear load was applied to the face of the slab. The focus of this research was to study the effect of strong versus weak positioned studs on the shear connector resistance. The studs in the weak position failed by rib punching, and their strength depended more on the strength of the steel deck rather than the concrete compressive strength.

The authors found that the AISC equations for stud strength were unconservative for push-out tests with one stud per rib. The push-off tests showed that strong position studs had strengths approximately 70% of predicted strengths using AISC specifications, while weak position studs had strengths only 60% of the predicted strength. This discrepancy in results might be due to the fact that the AISC equations were primarily developed from push tests using pairs of studs. The authors suggested that for single stud per rib, the stud reduction factor should not exceed 0.75. The authors suggested that studs be placed in a strong position, if possible.

Design equations based on theoretical models were developed for seven failure modes observed in push tests with profiled sheeting by Johnson and Yuan (1998). The authors used results of 269 push tests from previous research and performed 34 push tests to study existing design rules for the strength of the shear connector in composite beams with profiled sheeting. They observed that the existing rules for the strength of the shear stud were of limited scope and low accuracy, particularly for studs placed off-centre in a rib. It was found that the data was most scarce for the influence of position of stud, thickness of profiled sheeting, lightweight aggregate, profiled ribs having average width less than twice the rib depth and parallel sheeting. The authors identified seven failure modes including shank shearing, rib punching, rib punching with shank shearing, rib punching with concrete pull-out and concrete pull-out for push tests with transverse sheeting; and splitting of concrete and concrete pull-out for push tests with parallel sheeting. Although the equations proposed by Johnson and Yuan (1998) are based on the actual failure mechanism that happens in the push test and good understanding of the shear connector behaviour, the method is tedious and difficult to use in practice, because the failure mode has to be identified first before using any equation.

A novel reinforcing component to prevent rib shearing failure in composite edge beams with transverse sheeting was first developed by Patrick (2000). Rib shearing failure has been found to be a potential mode of longitudinal shear failure in composite edge beams. The conventional way of controlling longitudinal splitting is to use transverse horizontal reinforcement. However, previous research by Grant et al (1977) showed that this type of reinforcement could not prevent the rib shear failure.

Initially, push-out tests were performed using both re-entrant and trapezoidal profiled sheeting. Once the rib-shearing failure mode was identified in push tests, short and long span beam tests were performed to see whether or not the same failure occurred in full scale beam tests. Both push tests with re-entrant and trapezoidal profile failed in a very brittle manner with a slip less than 1 mm. In the short beam, rib shearing failure occurred accompanied by severe delamination of the slab. It was evident that U-bars successfully controlled the longitudinal splitting but failed to prevent the rib shearing failure. Long beams failed in a similar manner as that of short beams.

Preliminary testing using trial reinforcing components was conducted which led to final reinforcing component consisting of "a waveform piece of welded-wire fabric made from cold reduced, ribbed wire with a nominal diameter of 6 mm and nominal yield stress of 500 MPa." Push-out tests were conducted on both re-entrant and trapezoidal profile with reinforcing component included. The rib shearing failure did not occur and sufficient improvement in the ductility was achieved. Short and long beam tests were also conducted using the reinforcing component and they showed satisfactory results.

It was concluded by Patrick (2000) that the reinforcing component resulted in a stronger and more ductile shear connection between the steel beam and composite slab. It was urged that this type of component was especially required for edge beams incorporating profiled sheeting having either re-entrant or trapezoidal profile. Also, it can be advantageously used in regions of negative moment and regions over large steel web penetrations. It was also found that the reinforcing component could contain other failure modes as well, such as punch through or Type 2 longitudinal shear failure.

The validity of provisions of both British and European codes for the design shear connector strength of beams with profiled sheeting were discussed by Johnson (2005) in the wake of recent developments in modern profiled sheeting. The author argued that generally codes of practice, and especially BS 5950-3.1 and EN 1994-1-1, do not take sufficient account of the new developments such as presence of small upstanding ribs above the main top surface of the sheeting profile, sheetings with high yield strengths like 550 N/mm^2 as against code limit of 350 N/mm^2 and sheetings with a central rib at the bottom of trough.

The author suggests that in design, 'overall depth' should always include any small upstanding rib at the top of the sheeting. Further, the use of unfavourable studs should be avoided wherever possible. Pair of studs in unfavourable position should never be used, because they can result in brittle failure. If two studs are needed, then they should be placed in opposite sides of the trough. As the sheeting with a central stiffening rib in the trough can reduce ductility, and should be avoided wherever possible. The reinforcement above the sheeting should always be provided and its height above the stud should always conform to 30 mm rule of EN 1994-1-1 which states that the surface of shear stud should always extend not less than 30 mm above the bottom reinforcement. This practice would increase the height of stud and thus thickness of concrete slab.

At supports of composite slabs, the minimum area of reinforcement should be increased from that in British code to that in EN 1994-1-1 according to Johnson (2005). This is particularly useful in case of propped construction. The author terms the EN 1994-1-1 provision for maximum spacing of bottom bars above stud connectors too liberal i.e. it allows upto 350 mm or 2h (where h is the overall depth of slab) whichever is the lesser. Even the BS 5950 rule of 200 mm spacing should ideally be reduced to 150 mm. As an alternate, the Australian practice of using 'wave-form' reinforcement into troughs can be used which not only improves the shear capacity but slip capacity of shear studs too.

In an attempt to address the issue of brittleness and premature failure in push tests with deep trapezoidal slab, Bradford et al. (2006) proposed a new horizontal push test arrangement. The size of the specimen was 1400 mm long and 1200 mm wide, which facilitated larger number of studs, and thus improved the statistical evaluation of the results. A maximum normal load of 10 percent of the horizontal force was applied to the specimen, besides shear load. This test arrangement significantly improved the slip capacity of the shear stud and allowed better extrapolation of push test results for use in full-scale composite beams. However, the push test specimen presented in this paper seemed quite heavily reinforced, which might be the reason for improvement in the slip capacity.

Another attempt to propose a new push test arrangement for composite beams with transverse sheeting was made by Hicks (2007) with the help of two full-scale beam tests

and six companion push tests. The author proposed a standard push test arrangement for composite slabs having three studded ribs while keeping the first and last rib unstudded. Different stud layouts were considered in beam tests such as a single stud, pair of studs, and studs placed in the favourable, unfavourable and central positions. Tests with a single stud per rib exhibited higher shear connector resistance than push tests with double studs per rib. The highest ductility was achieved in case of push tests with favourable studs. It was observed that less slip was needed for the stud in the unfavourable position to reach peak resistance as compared with the favourable and centrally welded studs. The results showed that there was no similarity between beam and push tests in terms of load-slip behaviour with slip in push tests being much lower than the beam tests. The author argued that the reason of a poor performance of push-off tests was the absence of a curvature and normal force, which existed in the real composite beam from the floor loading.

The characteristic resistance of centrally welded studs, obtained experimentally from beam tests, showed close agreement with the characteristic resistance predicted from BS 5950-3.1 using depth of sheeting which excluded the top upstanding rib. Thus, the current practice of using depth of sheeting without upstanding top rib (net depth) in BS 5950-3.1 should be maintained. For a single stud per rib placed either in the favourable or unfavourable position, the predicted resistance given by BS 5950-3.1 is conservative as compared to that obtained from beam tests. For all cases, the prediction for the characteristic resistance from the Eurocode 4 seemed to be overly conservative for push tests with a single stud per rib. The author believes that the requirement of Eurocode 4 that the studs should be placed alternatively in two sides of the trough, where studs cannot be placed in central position, appears to be appropriate. The resistance and ductility obtained from beam tests were higher than push tests by 46% and 269% respectively. On the contrary, in case of pair of studs the shear connector resistance was almost same for both beam and push tests.

It was observed that "the resistance of the pairs of studs from the beam test is lower than expected." According to authors, the main reason for their poor performance was relatively high longitudinal spacing. The author thought that the reduction factor given in BS 5950-3.1 was too high. Further, "the current code assumption that the resistance of pairs of studs is proportional to $1/\sqrt{n_r}$ (where n_r is the number of studs per rib), does

not appear to be appropriate." Following modified reduction factor formula was suggested as an interim measure.

$$k = 0.37\left(\frac{b_o}{h_p}\right)\left\{\left(\frac{h_{sc}}{h_p}\right)-1\right\} \quad \text{but } k \le 0.75 \text{ for } n_r = 2 \qquad (2.18)$$

where

b_o = breadth of the concrete rib

h_p = depth of the profiled steel sheet excluding top upstanding rib (provided that the stud projects at least 35 mm above the shoulder of the deck)

h_{sc} = height of the stud

The waveform reinforcement elements and spiral stud performance-enhancing devices surrounding the studs were used by Ernst et al (2009) to improve the strength and ductility of the shear connector in composite beams with profiled sheeting in secondary beam applications. Based on results of 65 push tests, the authors proposed a new design method which distinguished between various failure modes and specified suitable reinforcing measures to ensure ductile shear connector behaviour. The application of these extra reinforcing devices inhibited concrete related failures, improved the strength and ductility of the shear connector which satisfied the minimum ductility requirement of Eurocode 4. The use of proposed reinforcing devices in Australian type metal decking resulted in the shear connector behaviour similar to that of the solid slab in case of push tests with a single stud per rib. The shear connector resistance obtained from the method proposed by the authors matched well with the experimental results as compared to the prediction of Eurocode 4.

The results from full-scale beams tests and companion push tests using composite slabs were compared by Ernst et al (2010). Two composite beams representing internal secondary beam and secondary edge beam applications were tested along with 4 companion push test detailed similar to the beams tests. One half of the beam was conventionally reinforced as per Eurocode 4 provisions, and the other half included waveform reinforcing elements and spiral stud performance-enhancing devices. It was found that the shear connector resistance and failure modes of beam tests compared

very well with the companion push test. Therefore, the authors concluded that the small scale push test can be used to predict the shear connector behaviour in a full-scale beam.

It was concluded by Ernst et al (2010) that the concrete related premature failures that were typically experienced in push tests could also occur in full-scale composite beams. The stud pull-out failure was observed in conventionally reinforced internal secondary beams and rib shearing failure occurred in edge beams; these failure modes were very brittle. On the contrary, the special reinforcing components overcame brittle effects observed in conventionally reinforced beams and resulted in a ductile load-slip behaviour. The combined use of waveform reinforcing elements and spiral stud performance-enhancing devices resulted in 25% increase in the shear connector resistance.

The effect of mesh position, transverse spacing of shear connectors, number of shear connectors per rib and the slab depth on the shear connector resistance in composite beams with profiled sheeting was studied by Smith and Couchman (2010). This was probably the first experimental investigation in which the effect of transverse spacing of shear studs was studied. However, the transverse spacing was restricted to the limits which could be implemented practically. The authors concluded that within the tested limits of transverse spacings of 75 to 140 mm, there was very little effect of the transverse spacing on the performance of the shear stud. In addition, including a third shear connector in a rib gave no benefit over using pairs of shear connectors. An improvement of 30% in the shear connector resistance was witnessed by locating the wire mesh fabric directly on top of the trapezoidal steel deck. The results also indicted that the shear connector resistance increased with an increase in the slab depth, but it was unclear if it was due to an experimental error or a genuine effect of the composite construction.

2.5. Previous studies on numerical modelling of push test

The accurate numerical modelling of composite beams with profiled sheeting involves complex contact interactions among various components of the composite beam and definition of nonlinear material models consisting of the material damage. On account of complex nature of a composite beam or a push test, there has been limited success in

the realistic numerical modelling, which could compare well with the experimental results in terms of the load-slip behaviour and failure patterns.

Perhaps, the first attempt to numerically model push test with profiled sheeting was made by Kim et al (2001). The authors used 13 × 65 mm studs welded through the unembossed profiled sheeting. Mainly, three types of failure modes were observed namely the concrete pull-out, stud shearing and local concrete crushing around the foot of the stud. Push tests were analysed using linear and nonlinear two-dimensional finite element models, and a linear three-dimensional model using the program LUSAS. In case of two-dimensional anaylsis, the steel beam, concrete slab and shear stud were modelled using plane stress elements, while bar elements were used to model the profiled sheeting. The headed shear stud, which was originally circular in cross section, was assumed to be of a rectangular cross section. As yielding can possibly occur before the stud fails, half stiffness was assigned to the bottom elements of the stud to take into account this effect.

It was observed by Kim et al (2001) that the nonlinear two-dimensional analysis resulted in a linear load-slip curve, contrary to the expected nonlinear curve, despite using nonlinear material properties. In addition to this, headed shear studs did not yield in spite of using nonlinear materials. Based on the wedged cone failure, a new expression for the effective slab width in the two-dimensional analysis was proposed. For three-dimensional analysis, the steel beam and profiled sheeting were modelled using shell elements and the stud using beam elements. The concrete was represented by volume elements. The results showed that the linear three-dimensional analysis gave better results when compared with push test experiments. However, the nonlinear three-dimensional analysis would give better results as compared to the linear. It was also found that the shear connector resistance is highly influenced by the loading and boundary conditions at the base of the concrete slab.

A three-dimensional finite element model for composite beams with profiled sheeting was developed by Ellobody and Young (2006) using the finite element program ABAQUS. The authors modelled push test specimens conducted by Kim et al (2001) and Lloyd and Wright (1990) using three-dimensional eight node and six node solid

elements. The steep slope trapezoidal profiled sheeting was modelled using an equivalent rectangular shape, while the mild slope sheeting was modelled as the actual trapezoidal shape. The circular reinforcement was modelled as rectangular. In this study, nodes of the concrete slab remained connected to the profiled sheeting during the analysis, which meant that the effect of vertical separation of the concrete slab from the sheeting was neglected. This assumption seems too simplistic and highly questionable as vertical separation does occur at the steel-concrete interface in reality.

A parametric study, consisting of 44 push test specimens, was conducted to investigate the effect of profiled sheeting geometries, diameter and height of the headed stud, and strength of concrete on the capacity and behaviour of the shear connector; and the results were compared with design codes. It was found that the American and British codes overestimated the capacity of the shear connector; while design strengths calculated using the European Code were generally conservative.

The behaviour of the shear connector under elevated temperature using a three-dimensional nonlinear finite element model was studied by Mirza and Uy (2009). The shear connector was embedded in both solid slab, and composite slab with profiled sheeting. The results of push tests under fire were compared with selected push tests under ambient temperatures. The results of the numerical analysis were compared with selected experimental results. Push tests with a solid slab failed by stud shearing and tests with composite slab failed by concrete cracking.

It was concluded that push tests with profiled sheeting slab and solid slab can withstand 60% and 40% of their ultimate load at elevated temperature compared to ambient temperature respectively. The authors also found that solid slab can resist fire for 30 minutes before failure occurs and profiled sheeting slab can withstand fire for more than 180 minutes because the steel deck acts as protective layer for the composite slab during fire. Although good results have been achieved in this paper, the failure modes show that the steel deck and concrete slab were assumed to be tied during the entire analysis, and load-slip behaviour did not exhibit any softening response. However, in push test experiments the profiled sheeting separates from the concrete slab at failure and the

softening response of load-slip curve is generally observed; it seems that both of these features are ignored in the modelling carried out by Mirza and Uy (2009).

The effect of combined actions of the shear and axial tensile loading was studied by Mirza and Uy (2010) with the help of a three-dimensional finite element model for both solid and profiled sheeting slabs. After validation of the numerical model against experimental studies, the model was used to carry out a parametric study having different loading conditions including shear and axial loading, shear stud sizes and concrete strengths. It was found that application of the axial tensile load greatly reduced the shear connector resistance. The authors proposed caged reinforcement instead of confined reinforcement to overcome this reduction in the strength. For a solid slab, the results showed that a thicker concrete slab led to higher shear connector strength. However, the axial tensile strength was reduced when a thick concrete slab was used, mainly because the thicker concrete slab caused more tensile cracking. On the other hand, in case of the profiled sheeting slab, the thicker slab led to a higher shear and axial tensile resistance of the shear stud.

The results of the parametric study conducted by Mirza and Uy (2010) showed that the shear connector resistance was significantly influenced by loading conditions, reinforcement layout schemes, thickness of slabs, shear stud size and concrete strength. The authors also presented interaction diagram for combined axial tension and shear loading in case of both solid and profiled sheeting slabs. Despite application of the axial tensile loading, the failure modes in numerical model developed by Mirza and Uy (2010) did not show any separation between the steel deck and concrete slab, which suggested that the steel deck and concrete slab were assumed to be tied. Moreover, the load-slip behaviour of the finite element model did not show any softening, which makes it difficult to determine the accurate slip capacity of the shear connector.

2.6. Summary and Conclusions

A comprehensive review of experimental and numerical studies with steel-concrete composite beams using trapezoidal profiled metal decking is carried out. The equations predicting the shear connector resistance from different design codes and equations developed by various authors are also presented. The main parameters of various

experimental and numerical studies related to composite beams with profiled sheeting slab are tabulated in Table 2.1.

Table 2.1 Summary of main parameters studied in previous studies

Author	**Type of study**	**Main parameters**
Grant et al (1977)	Experimental	Yield strength of steel beams, geometry of metal deck, weight and strength of concrete, diameter and height of stud shear connectors
Hawkins and Mitchell (1984)	Experimental	Type of loading, presence of ribbed metal deck, geometry and orientation of metal deck
Wright et al (1987)	Experimental	Strength and weight of concrete, orientation of steel deck, presence of profiled sheeting, position of shear stud
Robinson (1988)	Experimental	Number of shear studs, Interior and Exterior beam-type push tests
Jayas and Hosain (1988)	Experimental	Longitudinal stud spacing, rib geometry of metal decks
Jayas and Hosain (1989)	Experimental	Longitudinal stud spacing, rib geometry of metal decks
Lloyd and Wright (1990)	Experimental	Slab width, slab height, amount and position of reinforcement
Mottram and Johnson (1990)	Experimental	Layout and position of shear stud, number of shear studs, weight and strength of concrete, influence of short-fired pins
Wright and Francis (1990)	Experimental	Number of studs, comparison between roller supports and web-cleated connections of beam
Easterling et al. (1993)	Experimental	Position of shear stud, effect of normal load on the surface of concrete slab
Johnson and Yuan (1998)	Experimental	Orientation of steel deck, position and layout of shear studs, weight and strength of concrete
Patrick (2000)	Experimental	Effect of waveform reinforcement on composite edge beams
Kim et al (2001)	Experimental/ Numerical	Width of concrete slab, inclusion of profiled sheeting, loading and support conditions
Bradford et al. (2006)	Experimental	Effect of normal load on the surface of concrete slab
Ellobody and Young (2006)	Numerical	Geometry of steel deck, size of headed shear stud, strength of concrete

Table 2.1 Summary of main parameters studied in previous studies

Author	**Type of study**	**Main parameters**
Hicks (2007)	Experimental	Position of shear stud, comparison of beam and push test results
Ernst et al (2009)	Experimental	Effect of waveform reinforcement elements and spiral stud performance-enhancing devices
Mirza and Uy (2009)	Numerical	Comparison of push tests with solid and profiled sheeting slabs under different fire conditions
Ernst et al (2010)	Experimental	Comparison of beam and push test results using waveform reinforcement elements and spiral stud performance-enhancing devices
Smith and Couchman (2010)	Experimental	Mesh position, transverse spacing of shear connectors, number of shear connectors, slab depth
Mirza and Uy (2010)	Numerical	Effect of combined actions of shear and axial tensile loading, concrete strength, size of shear stud

The review of previous research studies suggested that there are some gaps in the knowledge and understanding of composite beams with profiled sheeting laid perpendicular to the longitudinal axis of the steel beam. The following conclusions can be drawn based on the review of previous studies:

1. The main focus of previous studies has remained on the effect of concrete strength, size of shear stud, and depth and width of the profiled sheeting on the behaviour of the shear stud.

2. To the best of author's knowledge, no study has been conducted so far related to the effect of profiled sheeting thickness on the strength and ductility of the shear stud. Additionally, the effect of transverse spacing of shear studs on the performance of shear stud has hardly been studied previously

3. There is a limited experimental research on the position and layout of the shear stud within a rib, and no numerical study is found in the literature related to these parameters.

4. There are only few papers on the finite element modelling of composite beams with profiled sheeting and that too present a simplistic way of modelling these beams. Predominantly, numerical studies of composite beams with profiled sheeting are based on the assumption that the steel deck and the concrete slab are tied together, which means no separation of the steel deck from the concrete slab occurs. In addition, the post-failure softening response of the load-slip curve of the push test with profiled sheeting has never modelled in the past, and therefore, the maximum failure load has been determined by looking at stress contours of the concrete slab and shear stud to see if they have reached their maximum stress levels. Further, the accurate slip at failure has never been determined using numerical modelling. The assumption in previous studies that the profiled sheeting does not delaminate from the concrete slab, and the load-slip curve does not extend beyond the maximum failure load level seems contrary to the push test experiment, where the steel deck separates from the concrete slab, and the load-slip curve is taken past the maximum load level.

5. The finite element modelling approach adopted in the past by many researchers can only predict concrete related failure of the push test with shear studs placed in only favourable or central locations. A favourable location of the shear stud is explained in subsequent chapters. However, in reality the push test with profiled sheeting slab can fail by stud shearing, rib punching and rib shear as well depending upon the concrete strength, sheeting thickness and location of the shear stud in a deck rib.

6. Most previous studies have used static implicit finite element procedures to model a push test, which is the reason that there has been limited success in effectively modelling a push test. Usually, the finite element analysis using static implicit procedures experiences convergence difficulties when a problem involves material damage and a lot of surfaces coming into contact simultaneously.

In order to address some of these gaps in knowledge and understanding of the behaviour of composite beams with profiled sheeting identified in preceding paragraphs, experimental and numerical investigations will be carried in subsequent chapters.

Chapter 3
Experimental investigation of push test

Chapter 3
Experimental investigation of push test

3.1. Introduction

Push tests were conducted to study the behaviour of headed shear connectors with profiled sheeting spanning perpendicular to the beam. A single-sided horizontal push test arrangement was used for the testing. The experimental investigation was divided into two series with 24 push tests in total to study the behaviour of composite beams with profiled sheeting. The first series consisted of application of only horizontal shear load to push test specimens; while in the second series a normal load equal to 10% of the horizontal shear laod was also applied to the top surface of the concrete slab, in addition to the horizontal load, to replicate the load on the slab that would exist in a real beam. The steel beam in real life supports longer spans of composite slabs than the push tests tested in this study. The justification for applying a normal load equal to 10% of the horizontal load is that it is equivalent to the self weight of the composite slab in a real life situation. The main parameters investigated in the experimental investigation were the effect of mesh position, number of mesh layers, number of shear connectors, inclusion of reinforcement bar at the bottom of the trough, the concrete strength and the push test arrangement. This chapter includes the push test arrangement, instrumentation, material testing, and results and summary of the push tests.

3.2. Test set up

Push tests were conducted under a single-sided horizontal push test arrangement. The horizontal push test has previously been used by Bradford et al. (2006) and Ernst et al. (2009) for composite beams with transverse profiled sheeting, and by Lam (2007) for composite beams with hollowcore slabs. In this study, the test specimen consisted of a concrete slab cast on a profiled sheeting connected to the steel beam with the help of through-welded stud shear connectors. A 1500 mm square concrete slab having a depth of 140 mm was used. Lengthening the test slab allowed more number of shear studs to be used, which ensured greater distribution of shear forces across the specimen, and thus resembled more closely the full-scale beam behaviour. The steel section 254 × 254 × 73 UC or HE206B, 3500 mm long was used as a steel beam.

The experimental investigation includes push tests with both single and double shear studs per rib. The general arrangement of push tests for double and single studs is shown in Figure 3.1 and Figure 3.2 respectively. The profiled steel sheeting had a depth (h_p) of 60 mm, average width (b_o) of 150 mm and sheeting thickness (t) of 0.9 mm. The profiled sheeting was laid transverse to the axis of the steel beam. The geometry and dimensions of the profiled metal decking consisting of a Multideck 60-V2 profile are shown in Figure 3.3. Headed shear studs 19 mm × 100 mm long were welded through the profiled sheeting to the steel beam. Because of the central stiffening rib in the profiled sheeting trough, the shear studs had to be welded off-centre either in the favourable or unfavourable location. A favourable or strong position, within a sheeting pan, is where the zone of the concrete under compression in front of the stud in the direction of the applied shear loading is greater than the compressive zone behind the shear stud. Thus, all shear studs were placed in the favourable position of each trough.

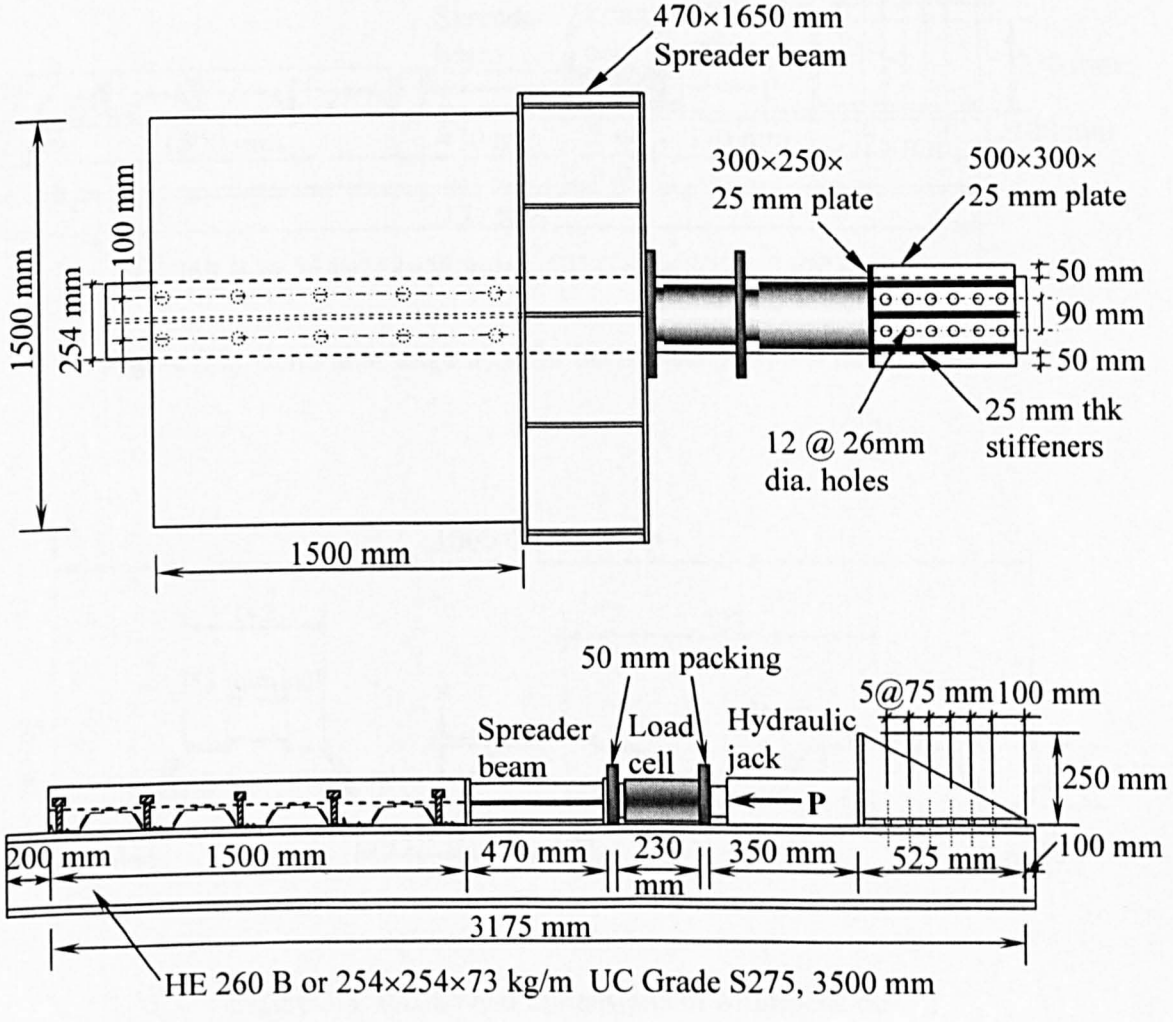

Figure 3.1 General arrangement for horizontal push test using double studs

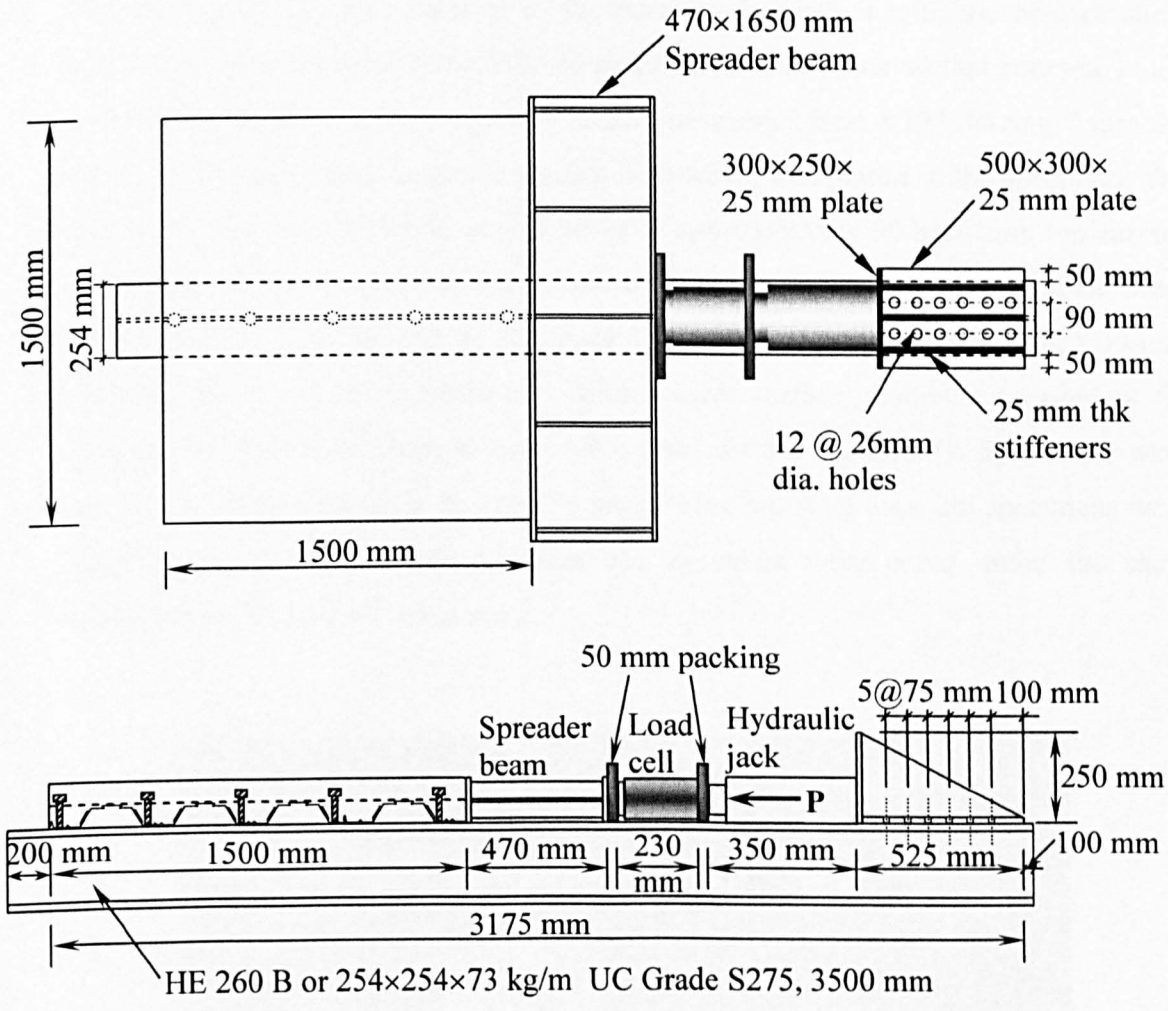

Figure 3.2 General arrangement for horizontal push test using single stud

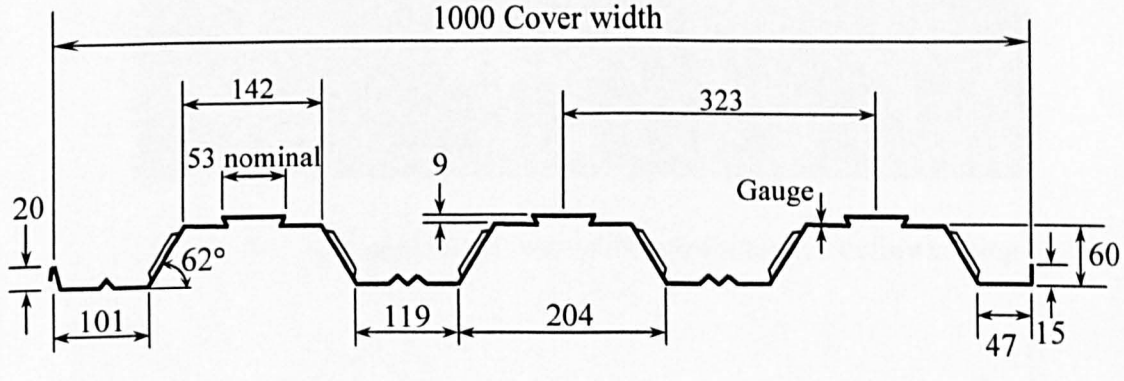

Figure 3.3 Profile and dimensions of Multideck 60-V2

After the steel deck was attached to the beam underneath it with the help of shear connectors, the edge trims were fixed to outer sides of the deck so that concrete could be poured in it. The standard square welded wire mesh fabric A193, having 7 mm dia bars with 200 mm centre to centre spacing both ways, was placed in the specimen. The arrangement of the wire mesh, with a cover of approximately 30 mm from top surface of the slab, placed in a push test specimen is shown in Figure 3.4. All specimens were cast horizontally as suggested by Eurocode 4. Concrete was compacted using a 30 mm vibrating poker and then, finished to form a level surface. Cubes and cylinders for compressive and tensile strength tests were also cast simultaneously. Specimens were cured by a wet hessian cloth. In order to prevent the moisture loss, test specimens were covered by polythene sheeting. Cubes and cylinders were cured under the same conditions as the push test specimens.

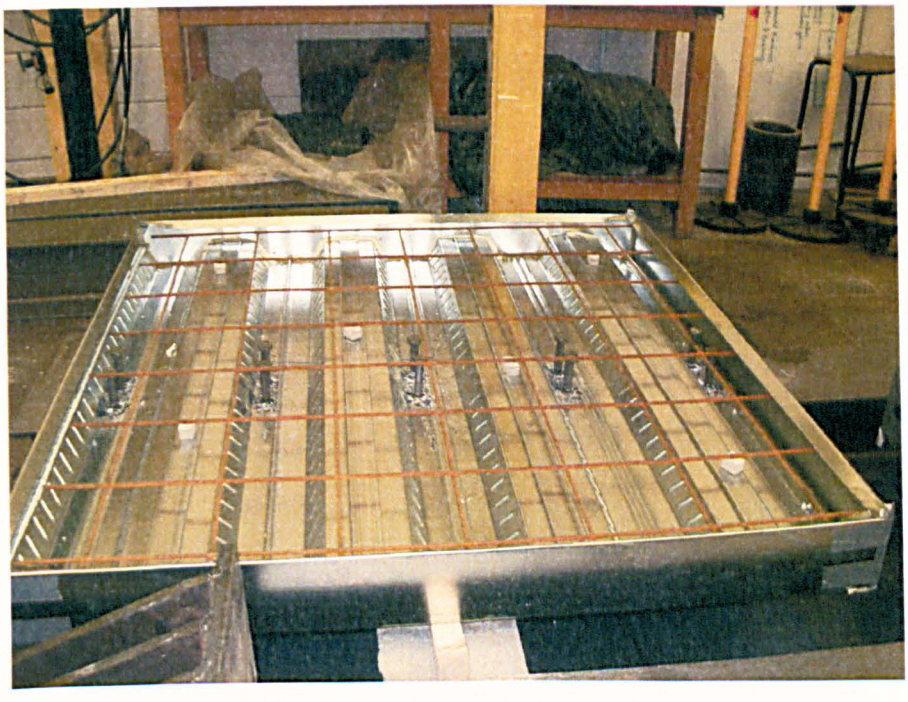

Figure 3.4 Arrangement of wire mesh reinforcement before casting

3.3. Loading frame

The test rig consisted of one 100 tonne hydraulic jack, with a stroke of 250 mm, placed at the centre of the specimen. The horizontal load was applied at the centre of the spreader beam with the help of a hydraulic jack and measured through a load cell. The complete test set up for the horizontal push test including the position of displacement

transducers, the hydraulic jack and load cell is shown in Figure 3.5. The edge trims were removed before load application, and a layer of plaster was applied on the side of the slab to stick it to the spreader beam, which ensured equal distribution of the load. A spreader plate was placed between the hydraulic jack and load cell to improve the distribution of the load. The pressure was supplied to the hydraulic jack with the help of Enerpec hydraulic pump as shown in Figure 3.6 .

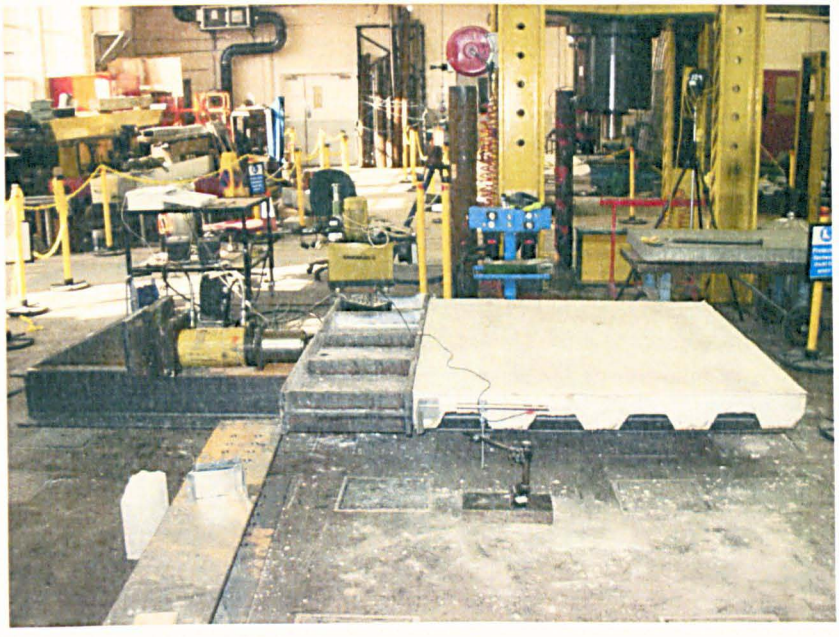

Figure 3.5 Complete test set up for horizontal push test

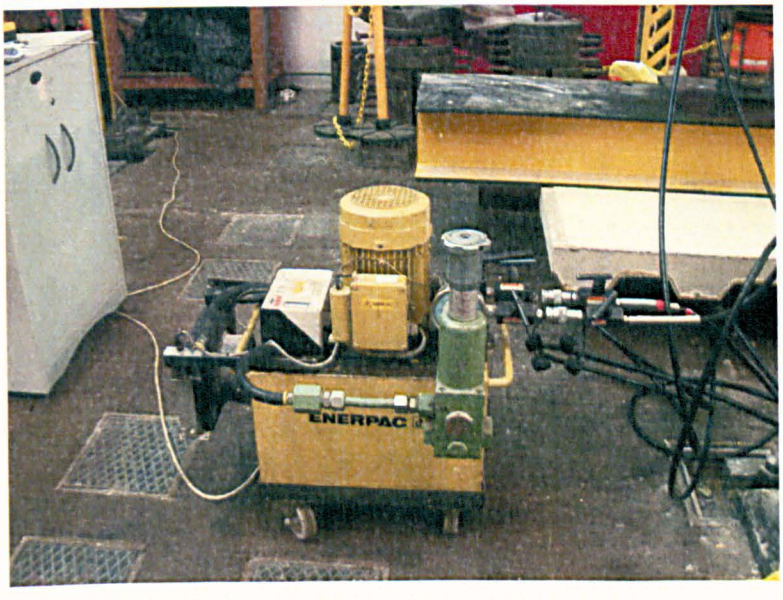

Figure 3.6 Hydraulic pump used in the push test

3.4. Instrumentation

The test specimen consists of two linear voltage displacement transducers (LVDTs) placed at two sides of the concrete slab near the spreader beam as shown in Figure 3.7. Two thin steel brackets were glued to the sides of the concrete slab to position the LVDTs. These LVDTs recorded relative slip between the steel beam and concrete slab at each load increment. All readings from LVDTs and load cell were collected in a data logger and stored in a computer simultaneously as shown in Figure 3.8. The data was transformed into the spreadsheet format so that it could be analyzed.

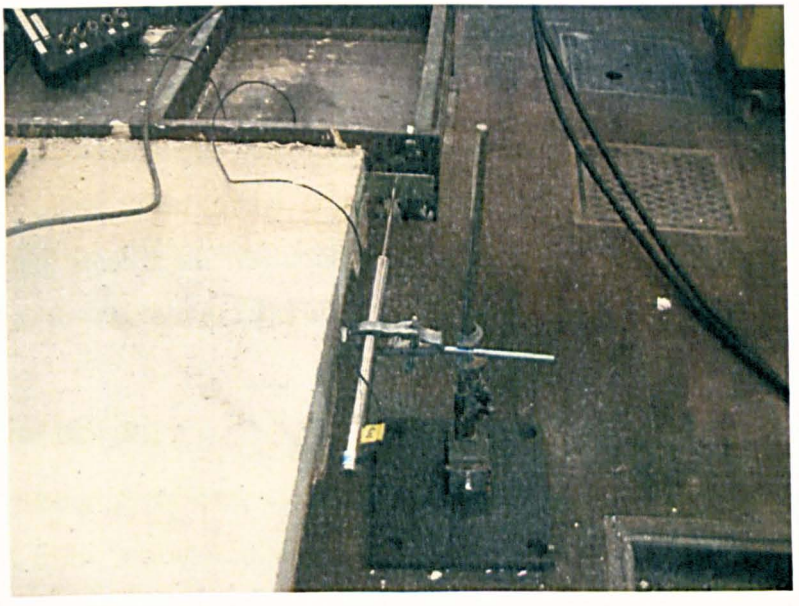

Figure 3.7 Positioning of LVDT using brackets and magnetic clamps

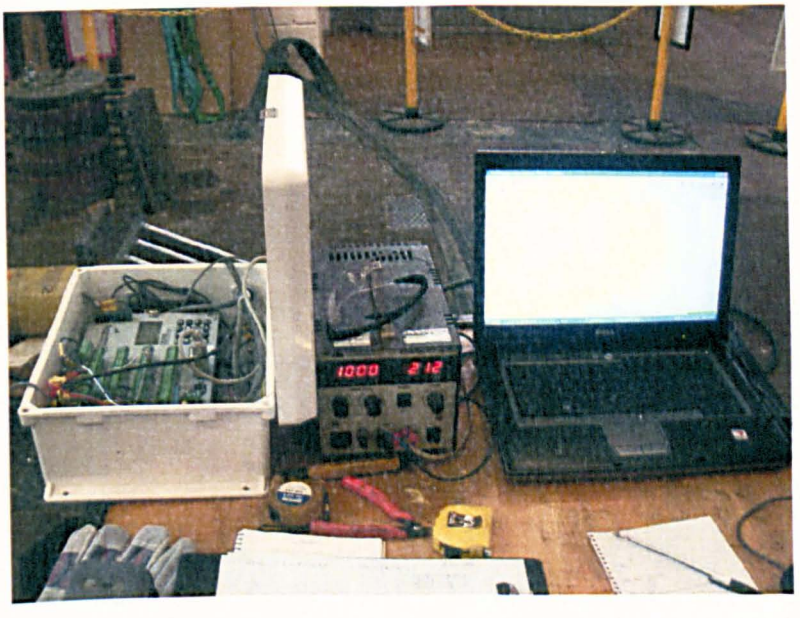

Figure 3.8 Data logger used in the push tests

3.5. Loading procedure

Each test contained a minimum of two specimens. Initially, for the first specimen, the load was applied in 40 kN increments until 60% of the expected failure load was reached and after that, load increments were decreased to 10 kN increments. The expected failure load was established from Eurocode 4 provisions. Once the failure load was obtained from the experimental push test of the first specimen, it was used as a reference failure load for the second specimen. The load was applied to the second specimen in increments up to 40% of the failure load and cycled 25 times between 5% and 40% of the failure load, obtained from the first specimen. Thereafter, load increments were reduced in such a way, so that failure did not occur in less than 15 minutes. The purpose of cyclic loading was to break any chemical bond between the profiled sheeting and concrete slab. Chemical bond is formed as a result of chemical adherence of cement paste to the steel sheeting. The longitudinal slip between the concrete slab and steel beam was continuously measured until the load dropped to at least 20% below the maximum failure load.

3.6. Material testing

The material properties of concrete, reinforcing bars, shear connector and steel deck were obtained from various material tests. The measured material properties will be used in the three-dimensional finite element model to predict the true behaviour of the headed shear connector in a push test with profiled sheeting.

3.6.1. Concrete

The compressive strength of concrete was determined by the cylinder (150×300 mm) and cube (100×100×100 mm) compression tests. The compressive strength of concrete used in specimens was determined from a minimum of three cubes and cylinders on the day of testing; the strength results were valid for each group of specimens tested within 48 hours. Additionally, the growth of concrete strength was monitored by testing two cubes at each 7 and 14 and 28 days. The results of concrete compressive strength tests are presented in Table 3.1.

Table 3.1 Results of concrete compressive strength tests

Specimen	7 day	Test day		28 day	
	Cube Strength (N/mm^2)	Cube Strength (N/mm^2)	Cylindrical Strength (N/mm^2)	Cube Strength (N/mm^2)	Cylindrical Strength (N/mm^2)
PTS 1	32.7	34.0	21.7	38.2	28.1
PTS 2	21.4	27.5	20.8	37.5	27.9
PTD 1	21.4	27.9	20.9	37.5	27.9
PTD 2	21.4	28.0	21.1	37.5	27.9
PTSN 1	17.7	25.4	20.3	31.0	23.1
PTSN 2-1	13.2	21.2	17.3	23.2	17.6
PTSN 2-2	13.2	23.2	17.6	23.2	17.6
PTDN 1-1	22.0	28.2	22.5	41.6	33.2
PTDN 1-2	22.0	37.0	28.1	41.6	33.2
PTDN 2-1	34.0	58.8	40.1	63.6	40.8
PTDN 2-2	34.0	63.2	40.0	63.6	40.8
PSNM 1-1	26.3	32.8	26.3	40.4	28.9
PSNM 1-2	26.3	36.1	29.8	40.4	28.9
PSNM 2-1	25.6	32.3	24.2	38.8	28.1
PSNM 2-2	25.6	32.7	24.5	38.8	28.1
PDNM 1-1	42.1	46.0	35.7	57.3	41.6
PDNM 1-2	42.1	48.8	35.8	57.3	41.6
PDNM 2-1	24.7	30.7	23.6	38.2	27.6
PDNM 2-2	24.7	31.6	24.4	38.2	27.6

3.6.2. Steel reinforcement bar

The tensile tests on high yield reinforcing bars were conducted using the Instron universal testing machine according to BS EN 10002-1. The yield and ultimate strength were obtained from the tensile test. Typical stress-strain curve of the reinforcing bar

T16 is shown in Figure 3.9. The mechanical properties of the reinforcing bar T16 are presented in Table 3.2.

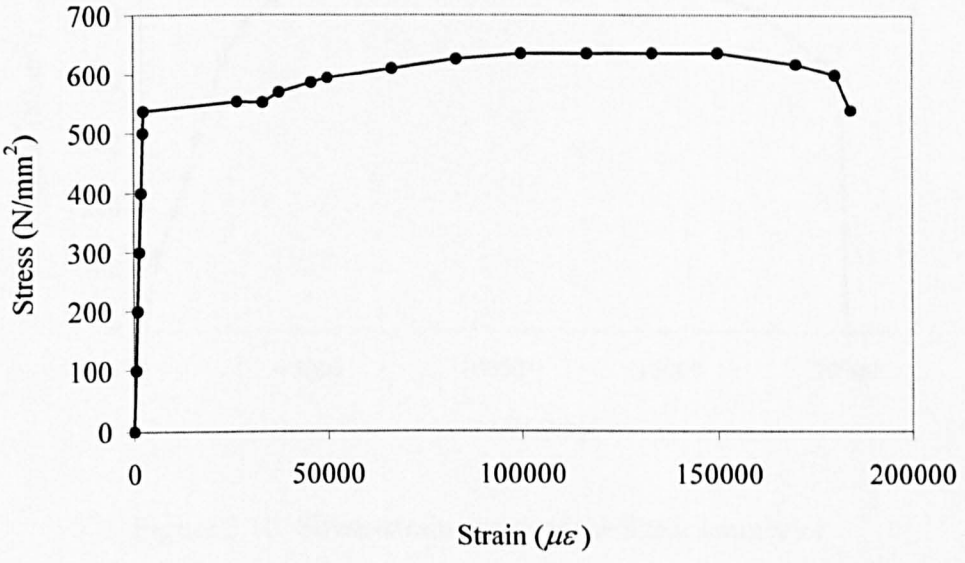

Figure 3.9 Typical stress-strain curve of the T16 reinforcing bar

Table 3.2 Tensile test results for reinforcing bars

Test Ref.	Yield Strength (N/mm^2)	Ultimate Strength (N/mm^2)	Cross-Sectional Area (mm^2)
T16-1	561.0	631.5	195.5
T16-2	499.0	645.2	195.4
T16-3	541.0	631.3	195.5

3.6.3. Shear stud

In all push tests, Nelson headed shear studs having dimensions 19 × 100 mm were welded through the sheeting to the steel beam. Tensile coupon specimens were machined form the shank of the shear connector and were used to conduct tensile tests using the Instron testing machine. The modulus of elasticity and yield stress of the shear stud material were found to be 193 GPa and 563 MPa respectively. The ultimate strength of the shear stud was found to be 610.5 N/mm^2. The stress-strain curve of the shear stud obtained from the tensile testing is shown in Figure 3.10.

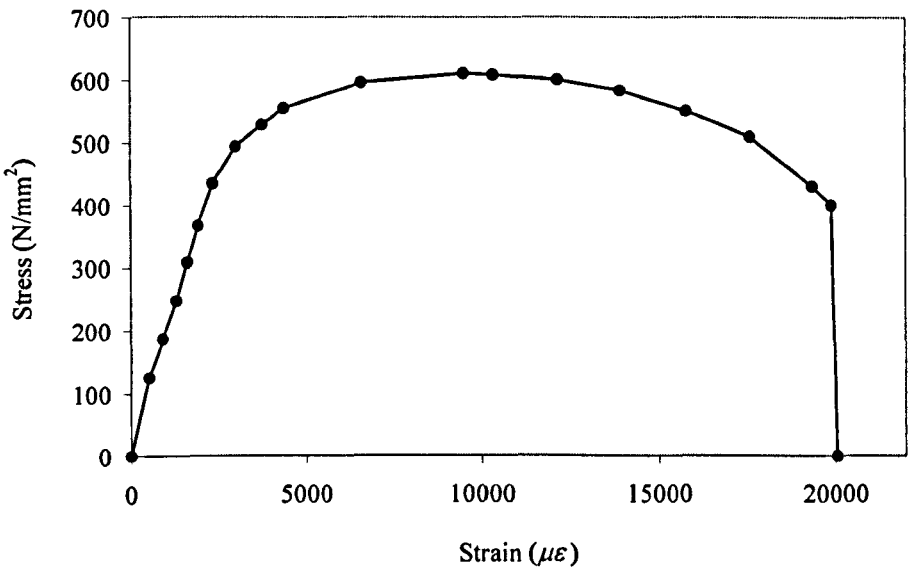

Figure 3.10 Stress-strain curve of the shear connector

3.6.4. Profiled sheeting

The material properties of the steel deck were determined from tensile coupon tests. The specimen for the coupon test was cut from the flat portion of the profiled sheeting. As much as 3 coupon tests were performed. The mean value of the test results was taken as the representative yield strength and modulus of elasticity of the steel deck profile. The mean values of the modulus of elasticity and the yield stress were 210 GPa and 418 MPa respectively. The average ultimate tensile strength of the profiled sheeting was found to be 437.4 MPa. The stress-strain curve obtained from the tensile testing of steel deck coupons using Instron Testing machine is shown in Figure 3.11.

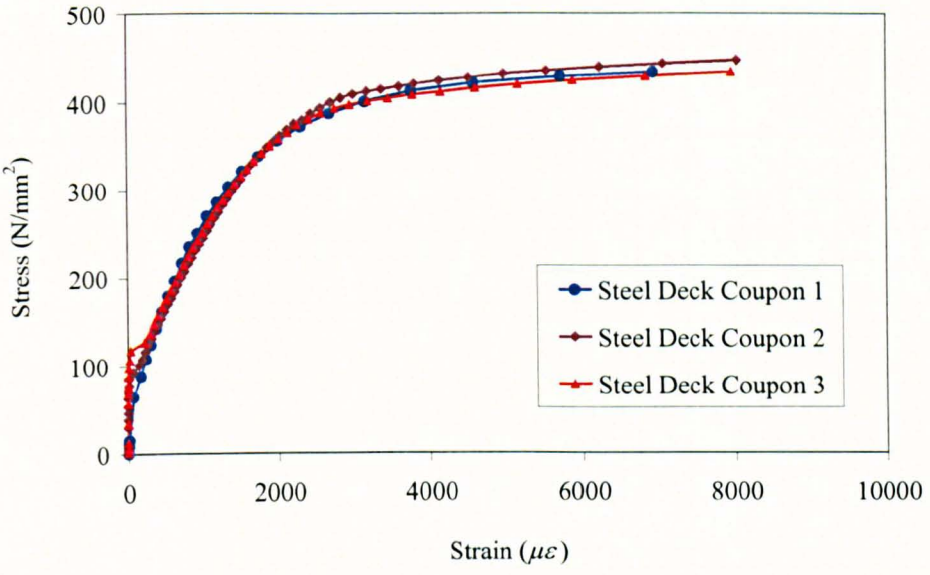

Figure 3.11 Stress-strain curve of the profiled sheeting

3.7. Test parameters to be investigated

The experimental investigation consisted of different test parameters of push tests including the effect of mesh position and number of layers of wire mesh, normal load, number of studs, high yield bar at bottom of the trough and push test arrangement. Test parameters, which will be investigated in this study, are presented in Table 3.3.

Table 3.3 Test parameters of push tests

Series	S. No.	Test Ref.	Concrete cube strength (MPa)	No. of Studs per rib, n_r	Total No. of studs per specimen	Studs in first rib	Studs in last rib	Mesh position	No. of mesh layers	Extra reinforce-ment	Normal load
First	1	PTS 1-1	34.0	1	5	Yes	Yes	Low	Single	---	---
	2	PTS 1-2	34.0	1	5	Yes	Yes	Low	Single	---	---
	3	PTS 2-1	27.5	1	5	Yes	Yes	High	Single	---	---
	4	PTS 2-2	27.5	1	5	Yes	Yes	High	Single	---	---
	5	PTD 1-1	27.9	2	10	Yes	Yes	High	Single	---	---
	6	PTD 1-2	27.9	2	10	Yes	Yes	High	Single	---	---
	7	PTD 2-1	28.0	2	10	Yes	Yes	High	Single	T16	---
	8	PTD 2-2	28.0	2	10	Yes	Yes	High	Single	T16	---
Second	9	PTSN 1-1	25.4	1	5	Yes	Yes	Low	Single	---	10%
	10	PTSN 1-2	25.4	1	5	Yes	Yes	Low	Single	---	10%
	11	PTSN 2-1	21.2	1	5	Yes	Yes	High	Single	---	10%
	12	PTSN 2-2	23.2	1	5	Yes	Yes	High	Single	---	10%
	13	PTDN 1-1	28.2	2	10	Yes	Yes	High	Single	---	10%
	14	PTDN 1-2	37.0	2	10	Yes	Yes	High	Single	---	10%
	15	PTDN 2-1	58.8	2	8	Yes	No	High	Single	---	10%
	16	PTDN 2-2	63.2	2	8	Yes	No	High	Single	---	10%

Note: Mesh located at low position is resting on top of the steel deck and high location is 30 mm below the top surface of the concrete slab. T16 bar is placed at the centre of the bottom flange of the sheeting. Normal load is applied as 10% of the horizontal shear load.

Table 3.3 Test parameters of push tests (continued)

Series	S. No.	Test Ref.	Concrete cube strength (MPa)	No. of Studs per rib, n_r	Total No. of studs per specimen	Studs in first rib	Studs in last rib	Mesh position	No. of mesh layers	Extra reinforce-ment	Normal load
Second	17	PSNM 1-1	32.8	1	4	Yes	No	Low & High	Double	---	10%
	18	PSNM 1-2	36.1	1	4	Yes	No	Low & High	Double	---	10%
	19	PSNM 2-1	32.3	1	4	Yes	No	Low & High	Double	---	10%
	20	PSNM 2-2	32.7	1	4	Yes	No	Low & High	Double	---	10%
	21	PDNM 1-1	46.0	2	8	Yes	No	Low & High	Double	---	10%
	22	PDNM 1-2	48.8	2	8	Yes	No	Low & High	Double	---	10%
	23	PDNM 2-1	30.7	2	6	No	No	Low & High	Double	---	10%
	24	PDNM 2-2	31.6	2	6	No	No	Low & High	Double	---	10%

Note: Mesh located at low position is resting on top of the steel deck and high location is 30 mm below the top surface of the concrete slab. T16 bar is placed at the centre of the bottom flange of the sheeting. Normal load is applied as 10% of the horizontal shear load.

3.8. First series of push tests with horizontal load only

The behaviour of the headed shear stud with trapezoidal metal deck is evaluated from a single-sided horizontal push test arrangement. The shear capacity, load-slip behaviour and failure patterns are investigated. The main parameters are the effect of mesh position and inclusion of reinforcement bar at the bottom trough. The push test PTS 1 had the mesh placed directly on top of the steel deck and all other push tests in this series had mesh 30 mm below the top surface of the concrete slab. All parameters in push tests PTD 1 and PTD 2 were the same except a reinforcement bar was placed at each bottom flange of the sheeting in case of push test PTD 2. The tests included both single and pair of shear studs per rib. Each test was repeated twice to ensure its statistical acceptance.

3.8.1. Test PTS 1

This test used a single stud shear connector per rib positioned on the favourable side of the sheeting pan, with a total of five shear studs per test specimen. The standard wire mesh reinforcement was placed directly on top of the profiled sheeting. The position of LVDTs in this test was somewhat different from all other push tests. Three LVDTs were located at the end of the test slab, opposite to the loading side as shown in Figure 3.12 . The specimen was loaded slowly in increments and the slip at the steel-concrete interface was measured. There were no obvious signs of cracking in the concrete slab until failure occurred.

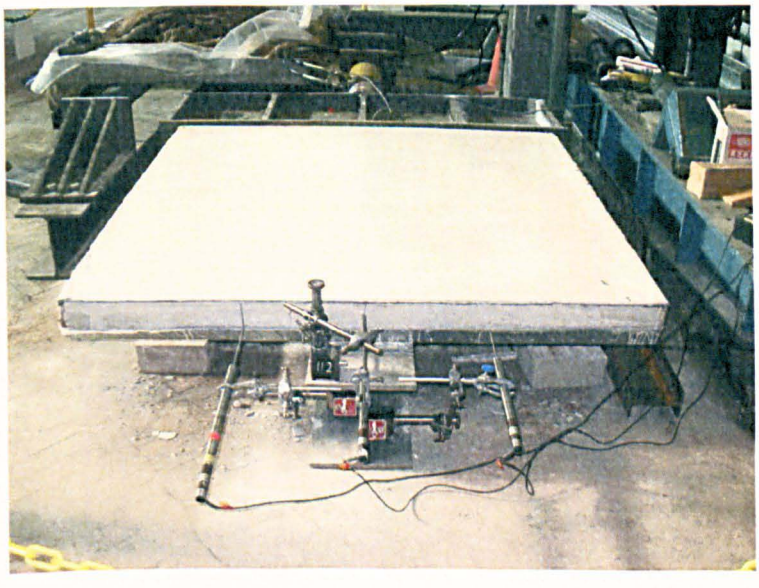

Figure 3.12 Position of LVDTs for push test PTS 1

The load application was continued until the concrete slab completely detached from the profiled metal decking and shear studs. At failure, a crack appeared in the last studded rib of the specimen near the top flange of the steel deck. It continued to widen resulting in rotation of the last rib. Both specimens failed by a combination of concrete conical failure and rotation of the last studded rib, typically known as 'back-breaking' as shown in Figure 3.13. In case of concrete cone failure, the tensile force acting on the stud forces the concrete slab to move up and over the metal decking, and consequently leaving behind a wedge shaped cone of concrete around the shear stud. The concrete slab was removed from the push test specimen to investigate the failure mechanism of shear studs. The view of concrete cone failure showing concrete cones attached to each shear stud in the profiled sheeting is shown in Figure 3.14 and Figure 3.15.

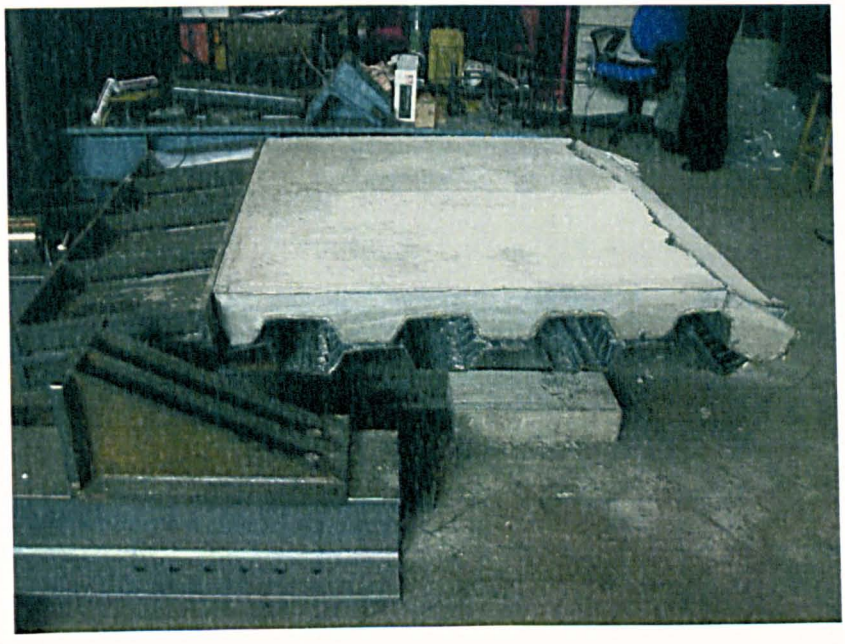

Figure 3.13 Push test specimen PTS 1-1 after failure

Figure 3.14 View of concrete cones attached to studs for test PTS 1-1

Figure 3.15 View of concrete cones attached to studs for test PTS 1-2

In case of test PTS 1-1, the first shear stud at the loading side completely bent to a horizontal position and the last shear stud also showed some bending in the direction of the applied load. Other three studs remained connected to the steel deck and exhibited less bending as compared to the first stud. The size of failure cones in the middle three ribs was larger than the size of cones in the first and last rib. The first stud in the push

test PTS 1-2 sheared off, and the last stud completely detached from the steel deck and remained embedded inside the concrete rib. The underside of the concrete slab of the push test PTS 1-2 showing pull-out failure surfaces of concrete is shown in Figure 3.16.

Figure 3.16 Underside of the slab of test PTS 1-2 showing pull-out failure surfaces

The load-slip curves for push test specimens PTS 1-1 and PTS 1-2 are shown in Figure 3.17. Both tests failed in a highly brittle manner, which meant that the load dropped very quickly as soon as the maximum load was reached. The specimen PTS 1-1 failed at a maximum load per stud of 75.7 kN with a slip of 0.60 mm. While, the maximum load per stud observed in PTS 1-2 was 78.8 kN at a slip of 0.70mm.

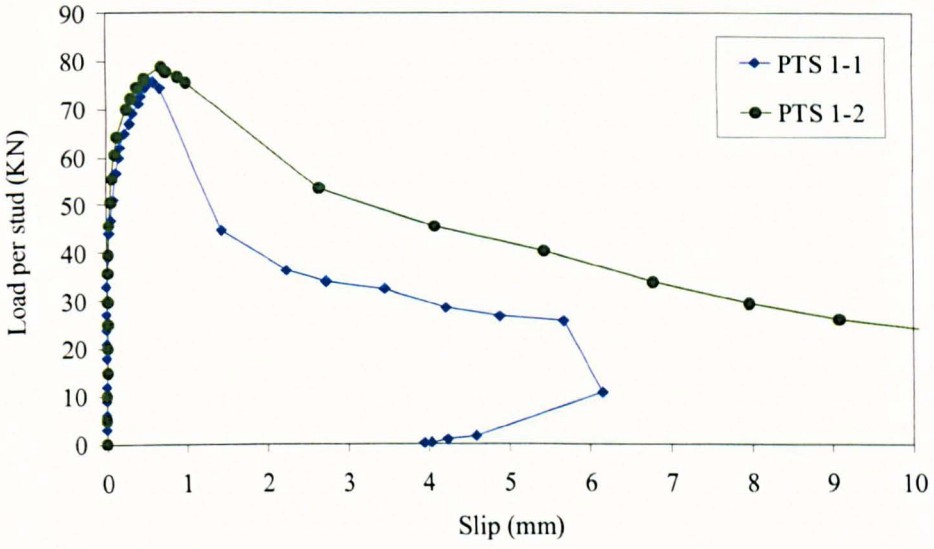

Figure 3.17 Load-slip curve for push test PTS 1

3.8.2. Test PTS 2

This test consisted of a single stud placed on the favourable side of the trough with wire mesh raised above the steel deck having a cover of 30 mm from top of the slab. The specimen was loaded slowly and no concrete cracking was observed before failure. At failure, a nearly horizontal crack formed near the top flange of the last studded rib normal to the direction of the loading. The load application was continued until the crack widened and the last rib rotated. The failure occurred on account of both concrete cracking around the stud and rotation of the last studded rib as shown in Figure 3.18.

The concrete slab was dismantled to inspect its condition. Similar to the push test PTS 1, the failure mode in this test was due to formation of concrete cones around the shear stud. The first shear connector nearly flattened in the direction of the loading, while the last stud was partially bent, and middle three studs were slightly bent. The underside of the concrete slab of the push test PTS 2-1 showing concrete pull-out surfaces, when it is detached from the steel deck and shear studs is shown in Figure 3.19. The formation of concrete cones around shear studs with concrete slab removed is shown in Figure 3.20. It can be observed that the size of concrete shear failure cones in this test essentially remained the same as that of the previous push test PTS 1.

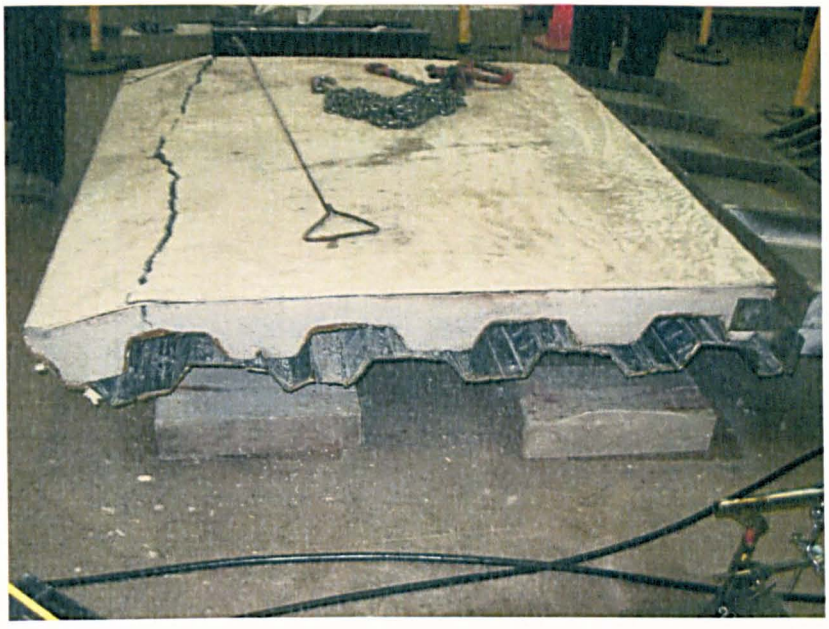

Figure 3.18 Push test specimen PTS 2-1 after failure

Figure 3.19 Underside of the slab of test PTS 2-1 showing pull-out failure surfaces

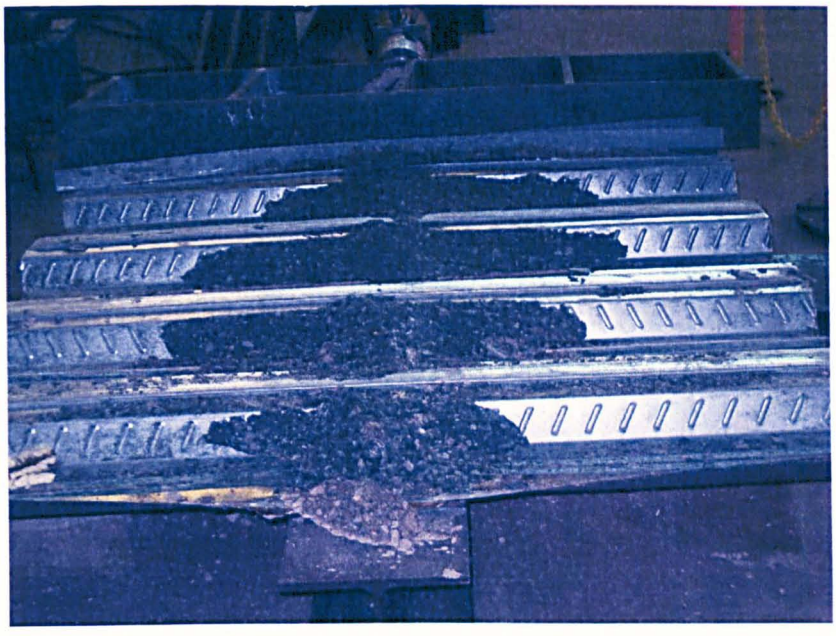

Figure 3.20 Formation of concrete cones for push test PTS 2-2

The load-slip curves for push test specimens PTS 2-1 and PTS 2-2 are shown in Figure 3.21. The maximum failure load per stud in case of PTS 2-1 was 69.0 kN with a slip of 1.67 mm. While, the specimen PTS 2-2 failed at a load per stud of 73.8 kN with a slip of 1.41 mm.

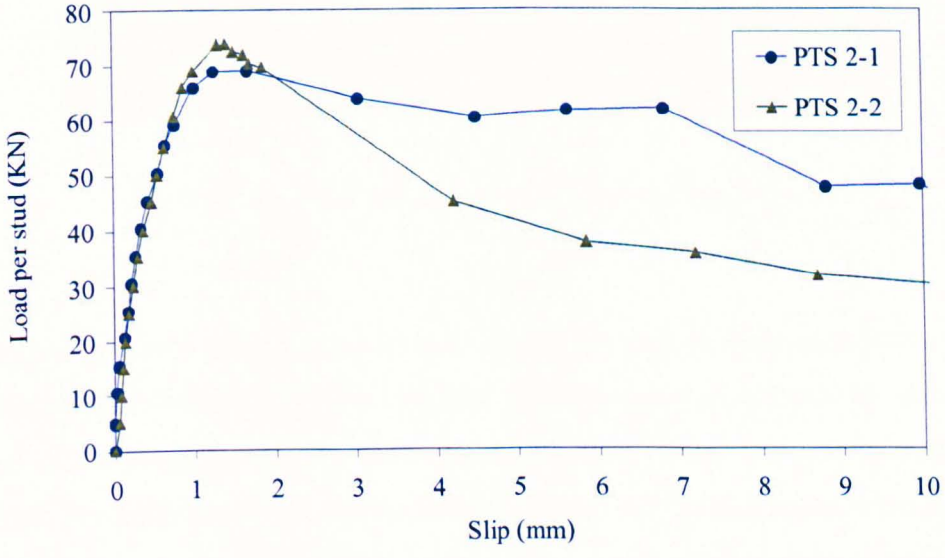

Figure 3.21 Load-slip curve for push test PTS 2

3.8.3. Test PTD 1

This test used double shear studs per rib placed on the favourable side of the rib. The wire mesh was positioned with a cover of 30 mm from top of the slab. The pairs of studs had a centre to centre transverse spacing of 100 mm. The load was applied to the specimen and no cracking was observed until failure occurred. The load was continued until the concrete slab completely lost interaction with studs and steel deck. Likewise single shear stud push tests, the failure in this test occurred due to cracking of concrete around shear studs and rotation of the last studded rib. The push test specimen PTD 1-1 after failure is shown in Figure 3.22.

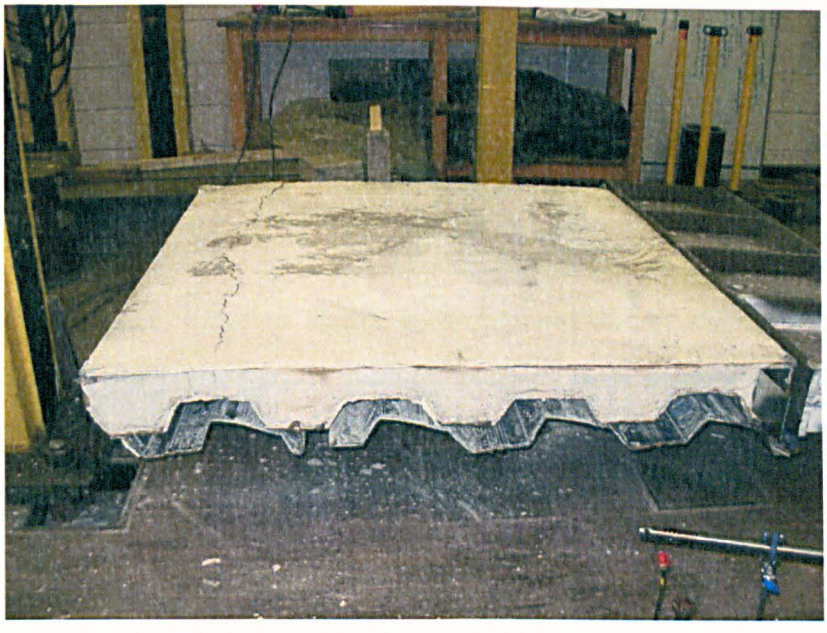

Figure 3.22 Push test specimen PTD 1-1 after failure

After failure, concrete wedges were formed around the pair of shear connectors. In push tests with a single shear stud per rib, concrete failure cones started from the underside of the head of the shear connector, while increasing in diameter along the length of the shear stud. For push tests with double shear studs per rib, failure cones were similar to the single shear stud per rib, but the cones around the shear stud were connected with each other. The concrete failure wedges for the push test PTD 1-2, which had double shear connecters per rib, are shown in Figure 3.23. All shear studs remained attached to the steel beam after failure. The first and last two studs bent in the direction of the loading, while studs in the middle three troughs remained more or less unchanged.

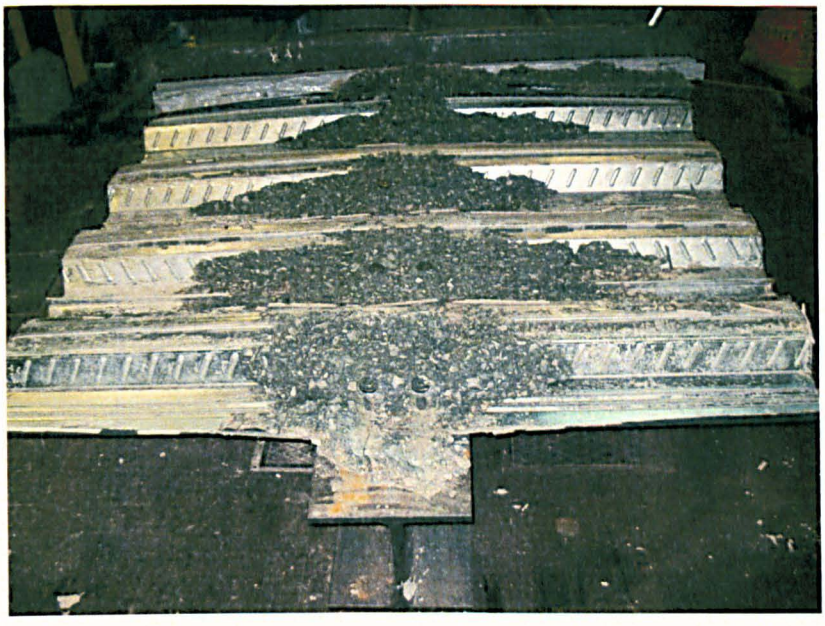

Figure 3.23 Concrete failures wedges for push test PTD 1-2

The load-slip behaviour for the push test PTD 1 is presented in Figure 3.24. As soon as the failure load reached, the load started to drop rapidly indicating a brittle concrete failure. The specimen PTD 1-1 failed at a load per stud of 52.1 kN with an average slip of 1.02 mm. While, the maximum load per stud observed in the push test specimen PTD 1-2 was 45.4 kN at an average slip of 0.94 mm.

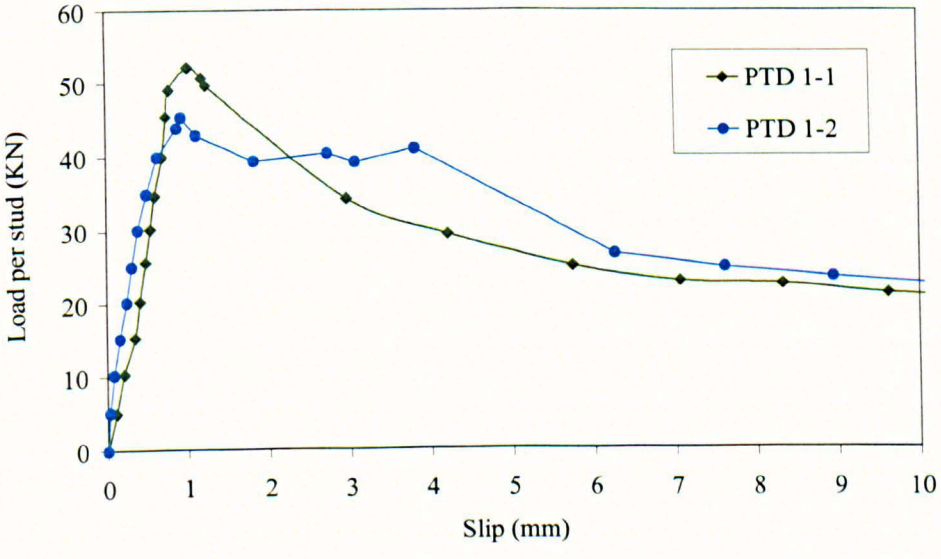

Figure 3.24 Load-slip curve for push test PTD 1

3.8.4. Test PTD 2

The push test PTD 2 had exactly same configuration as the push test PTD 1 except that it had a high yield bar T16 at each bottom trough of the profiled sheeting near a central stiffening rib. The main purpose of using this bar was to investigate its effect on the strength and ductility of the shear connector. The position of T16 bar within the profiled sheeting, before concrete is cast, is shown in Figure 3.25.

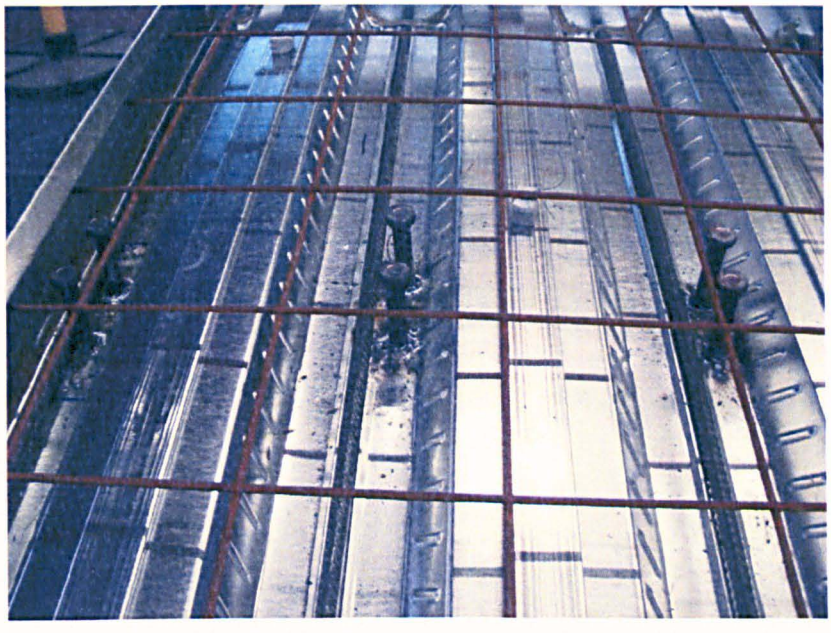

Figure 3.25 Position of T16 high yield bar within the sheeting trough

Both specimens failed due to concrete failure around shear studs and rotation of the last rib, similar to the push test without a bar at the bottom trough. The specimen PTD 2-1 after failure is shown in Figure 3.26. The concrete cones started to form underneath the head of shear connectors, spreading towards the end of the bottom flange of the profiled sheeting. The development of concrete failure surfaces around double shear connectors is shown in Figure 3.27. The first two studs nearly bent to the horizontal position and last two studs showed some bending as well in the direction of loading. However, shear studs in the middle three troughs remained nearly unbent.

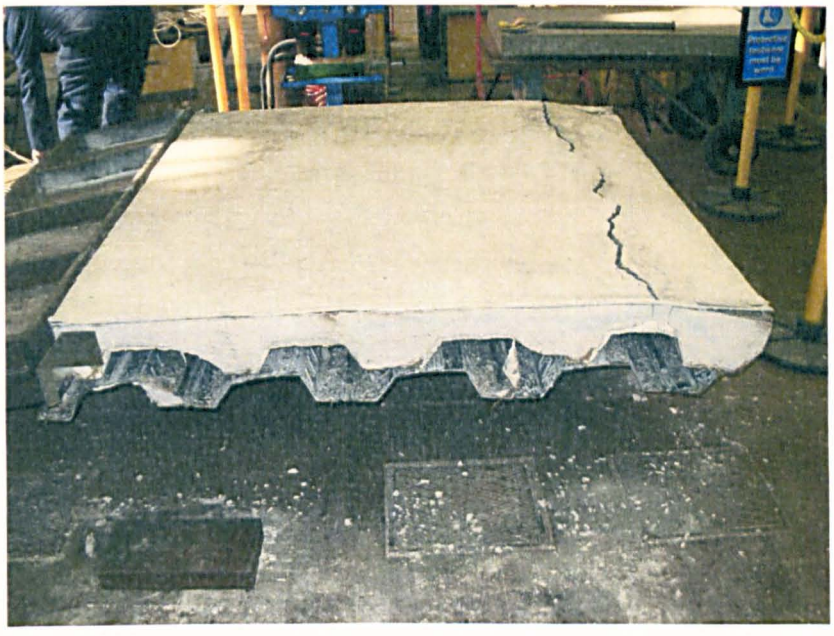

Figure 3.26 The specimen PTD 2-1 after failure

Figure 3.27 The concrete failure surfaces around shear studs for specimen PTD 2-1

The load-slip curve for the push test PTD 2 is plotted in Figure 3.28. The results obtained from this test are not much different from the push test having double studs per rib without reinforcement bar in the bottom trough. The load continued to drop rapidly as soon as concrete around the shear stud failed. For the push test specimen PTD 2-1, the maximum load per stud was 52.2 kN at an average slip of 1.23 mm. Similarly, the maximum failure load per stud in PTD 2-2 was 47.3 kN with a slip of 0.95 mm.

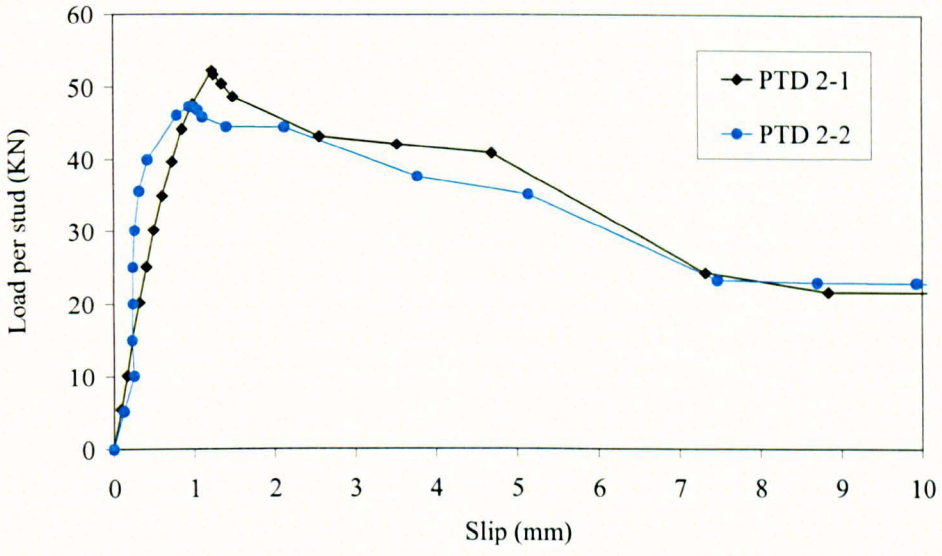

Figure 3.28 Load-slip curve for push test PTD 2

3.8.5. Summary of push test results from first series

Push tests have been conducted under a single-sided horizontal push test arrangement. The main parameters were position of the welded wire mesh fabric, number of shear connectors and effect of additional high yield reinforcement at the bottom flange of profiled sheeting. The square wire mesh fabric was located either at low or high position. The mesh located at the low position was resting directly on top flanges of the steel deck, while high positioned mesh was 30 mm below the top surface of the concrete slab. A single stud and double shear connectors per rib were used in the favourable location of the trough. Also, a T16 high yield reinforcement bar, located at the bottom flange of the sheeting pan near the central stiffeners, was tried in some of the tests to investigate any potential benefit for the strength and ductility of the shear connector. The strength of the shear connector, load-slip behaviour and failure mechanisms has been investigated. The purpose of the single sided horizontal push test arrangement was to achieve some improvement in the ductility of the headed shear connector as compared to the vertical push test set up and meet the Eurocode 4 requirement of 6 mm slip at steel-concrete interface for ductile shear connector. However, the horizontal push test set up did not result in any improvement over conventional vertical push test arrangement in terms of ductility of shear studs. The load-slip behaviour of the headed shear stud obtained from the horizontal push test arrangement was almost similar to the

one observed in the vertical push test set up. The results obtained from the first series of push tests are summarized in Table 3.4.

Table 3.4 Summary of push test results from first series

S. No.	Test Ref.	Concrete cube strength (MPa)	No. of studs per rib, n_r	Total No. of studs per specimen	Mesh position	Extra Reinforcement	Shear capacity per stud (kN)
1	PTS 1-1	34.0	1	5	Low	---	75.7
2	PTS 1-2	34.0	1	5	Low	---	78.8
3	PTS 2-1	27.5	1	5	High	---	69.0
4	PTS 2-2	27.5	1	5	High	---	73.8
5	PTD 1-1	27.9	2	10	High	---	52.1
6	PTD 1-2	27.9	2	10	High	---	45.4
7	PTD 2-1	28.0	2	10	High	T16	52.2
8	PTD 2-2	28.0	2	10	High	T16	47.3

Note: Mesh located at low position is resting on top of the steel deck. Mesh at high location is 30 mm below the top surface of the concrete slab. T16 bar is placed at the centre of the bottom flange of the sheeting.

3.9. Second series of push tests with horizontal and normal load

Push tests in second series include the normal load in addition to the horizontal shear load to replicate the real beam situation, where the normal load exists from superimposed composite slab loads. The main parameters in this series are the effect of normal load, mesh position, number of mesh layers, number of shear connectors, concrete strength and push test arrangement. The push test PTSN 1 had the mesh directly placed on top of the steel deck; while in case of push tests PTSN 2, PTDN 1 and PTDN 2 the mesh was positioned in such a way so that it had a 30 mm cover from top surface of the concrete slab. The test PTDN 2 had higher strength concrete than the other tests. Apart from push tests PTSN 1, PTSN 2 and PTDN 1, the last rib was kept unstudded in all other tests to prevent unwanted back-breaking failure. Additionally, the first rib in the push test PDNM 2 was kept unstudded. Push tests PSNM 1, PSNM 2, PDNM1 and PDNM 2 used double layers of wire mesh inside the concrete slab. The position of the normal load was directly on top of the first rib perpendicular to the axis of the beam in case of the push test PSNM 2 as against other push tests, where normal load was applied to all ribs along the axis of the beam. Similar to the first series, all push tests were repeated twice to ensure their statistical acceptance.

3.9.1 Test set up for second series

The push test set up for second series remained essentially the same as that of the first series apart from application of normal on top surface of the concrete slab. The normal load was applied with the help of two spreader beams placed on top surface of the concrete slab. A steel plate was placed on the spreader beams to distribute the load equally. The hydraulic jack and load cell were positioned at the centre of this steel plate. To allow horizontal movement of the push test specimen, a roller skate was located beneath the load cell. Apart from one LVDT placed on top of the concrete slab to measure its uplift, all other instrumentation remained the same as that of push tests in the first series. The general arrangement of the push test specimen adopted for the second series is shown in Figure 3.29.

Figure 3.29 General arrangement of push tests in second series

3.9.2 Test PTSN 1

This push test used a single stud in every sheeting pan with wire mesh placed directly on top of the steel deck. A normal load of 10% of the maximum horizontal shear load was applied to the specimen, before applying the horizontal shear load. The maximum horizontal shear load used for calculation of 10% normal load, was established from the companion push tests conducted earlier without normal load. The normal load remained constant during the entire test. The horizontal shear load was applied, while keeping the normal load constant, until the concrete slab completely separated from the steel deck.

The specimen did not develop any cracks on concrete surface until it failed. At failure, cracks formed in the concrete slab near the top flange of the steel deck in the first and last rib. Although, the normal load reduced uplift of the concrete slab, it could not completely prevent the premature failure caused by rotation of the last studded rib. The push test specimen PTSN 1-1 after failure is shown in Figure 3.30. The concrete slab rode over the profiled sheeting as the horizontal shear load was increased; and the portion of the concrete slab near the last stud spalled as shown in Figure 3.31.

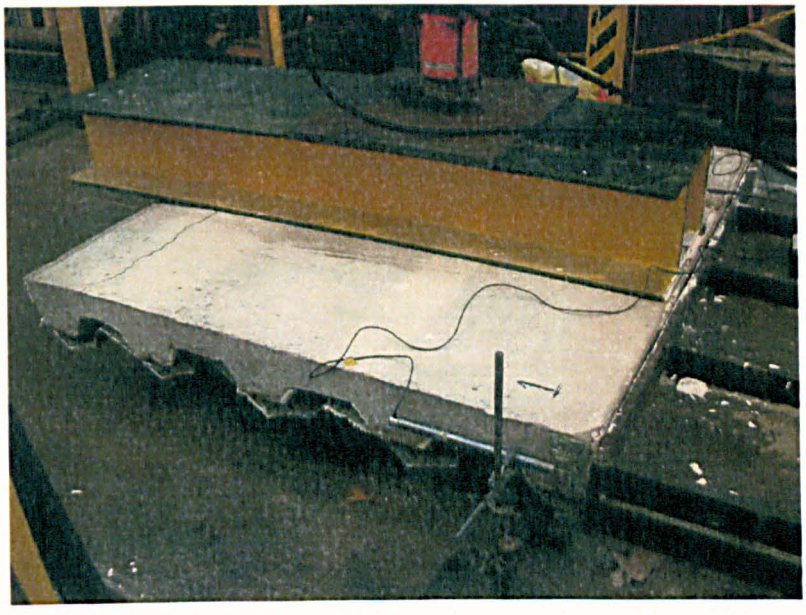

Figure 3.30 The specimen PTSN 1-1 after failure

Figure 3.31 Concrete spalling at free end of specimen PTSN 1-1

The load versus slip curve for the push test PTSN 1 is shown in Figure 3.32. Both of the specimens showed consistent load-slip behaviour. At a load level of 97.8 kN per stud with an average slip of 2.52 mm, the specimen PTSN 1-1 started to fail and the load dropped quickly thereafter. Similarly, the maximum load observed in the specimen PTSN 1-2 was 98.9 kN per stud with an average slip of 2.45 mm.

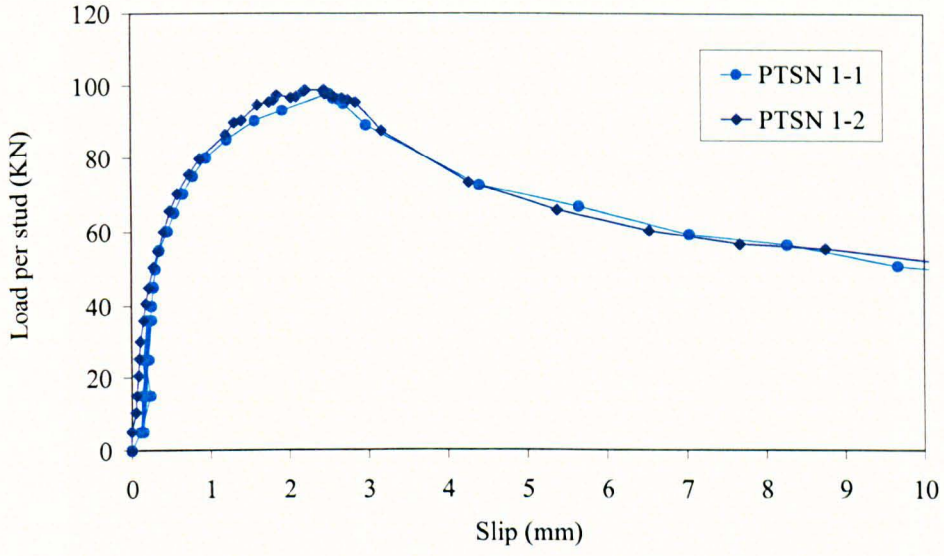

Figure 3.32 Load-slip curve for push test PTSN 1

3.9.3 Test PTSN 2

This test used a single shear stud per rib with the wire mesh located at a distance of 30 mm from top of the concrete slab. The loading procedure and instrumentation was same as that of the push test PTSN 1. The specimen failed by cracking in the concrete around the shear stud. Due to application of normal load in addition to shear load, the concrete near the last stud broke into fragments. After failure, the concrete slab was detached from the profiled sheeting and shear studs as shown in Figure 3.33. When the horizontal shear load was increased, while keeping normal load constant, the profiled sheeting showed increased buckling as the concrete slab tended to slide over it. The buckling of the steel deck, after concrete slab completely separated from it, is shown in Figure 3.34.

When the test terminated, the first shear stud almost bent to the horizontal position in the direction of loading. Remaining four shear studs also bent in a single curvature shape in the direction of loading. The concrete slab and profiled sheeting were detached

from the steel beam to inspect shear studs. The condition of shear studs with steel deck and concrete slab removed is shown in Figure 3.35. The load-slip curve for the test PTSN 2 is shown in Figure 3.36. The specimen PTSN 2-1 failed at a maximum load of 90.0 kN per stud with a slip of 1.40 mm. The failure in the specimen PTSN 2-2 occurred at a load level of 81.7 kN with a slip of 1.60 mm at the steel-concrete interface.

Figure 3.33 Underside of the concrete slab and failure cones in push test PTSN 2-1

Figure 3.34 Buckling of steel deck and concrete failure cones in push test PTSN 2-1

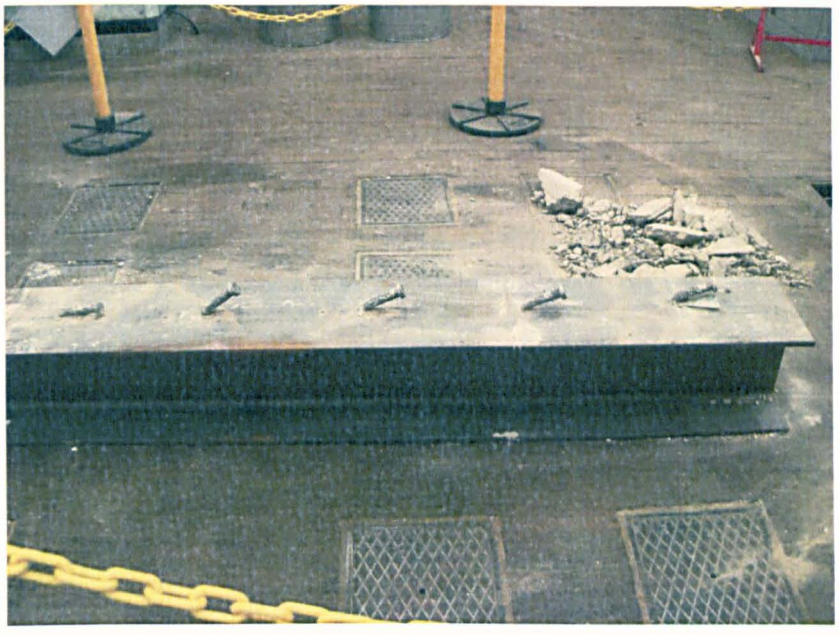

Figure 3.35 Shear studs for specimen PTSN 2-1 after failure

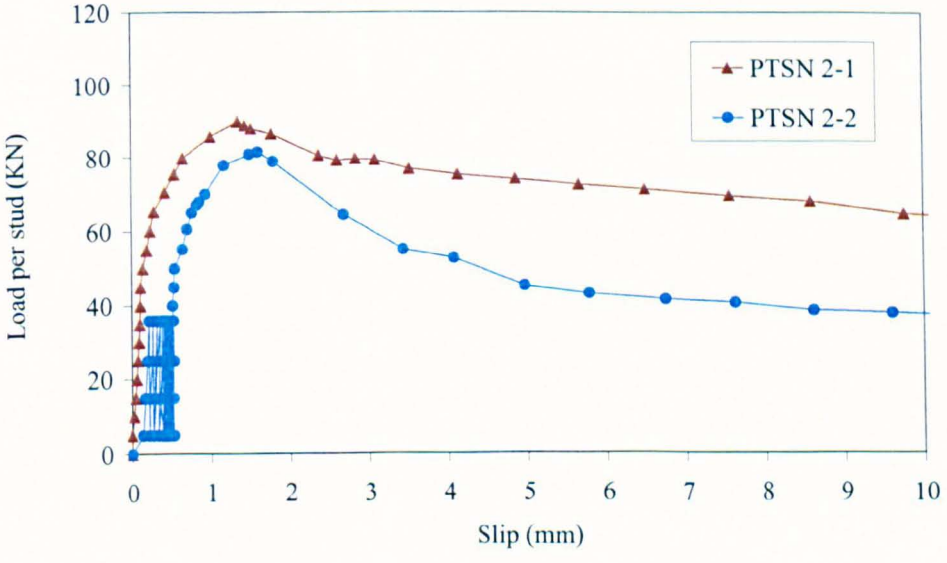

Figure 3.36 Load-slip curve for push test PTSN 2

3.9.4 Test PTDN 1

This test employed double shear studs per rib with wire mesh raised above the steel deck having a concrete cover of 30 mm from top surface of the slab. The test set up and load application procedure remained the same as that of push tests PTSN 1 and PTSN 2. The push test failed by formation of concrete failure cones and rotation of the last studded rib. Concrete around all shear studs cracked and failure cones formed as shown

in Figure 3.37. However, none of shear studs sheared off. In the specimen PTDN 1-1, first two shear studs almost flattened in the direction of loading, while other studs bent only marginally.

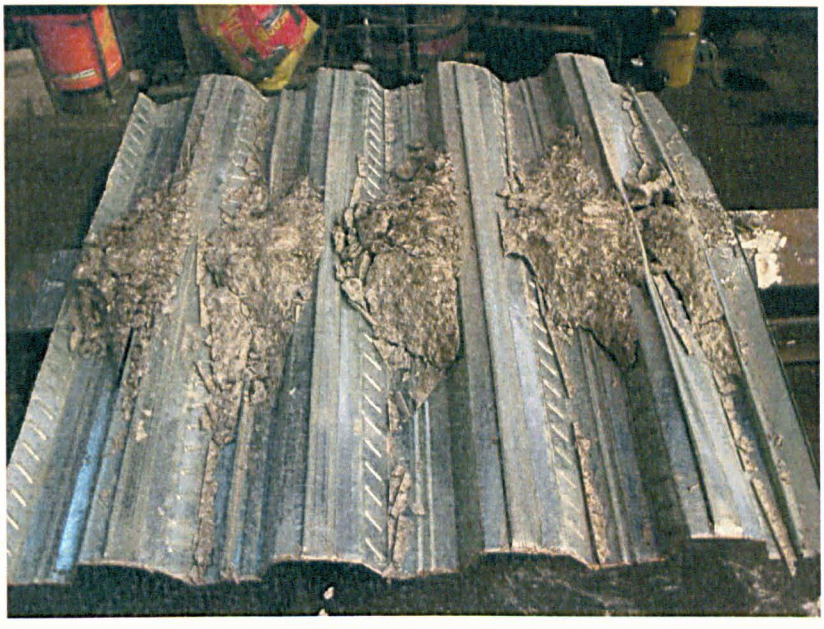

Figure 3.37 Formation of concrete cones in push test PTDN 1-1

In the specimen PTDN 1-2, all shear studs slightly bent in the direction of loading except first two studs, which sheared off due to proximity to the loading side. The specimen PTDN 1-2, after removal of the concrete slab, is shown in Figure 3.38. The load versus slip curve for the push test PTDN 1 is plotted in Figure 3.39. The maximum load at failure observed in the specimen PTDN 1-1 was 61.3 kN per stud with a corresponding slip of 1.40 mm. Similarly, the specimen PTDN 1-2 failed at a maximum load of 67.3 kN per stud with a slip of 1.22 mm.

Figure 3.38 Shear studs for specimen PTDN 1-1 after failure

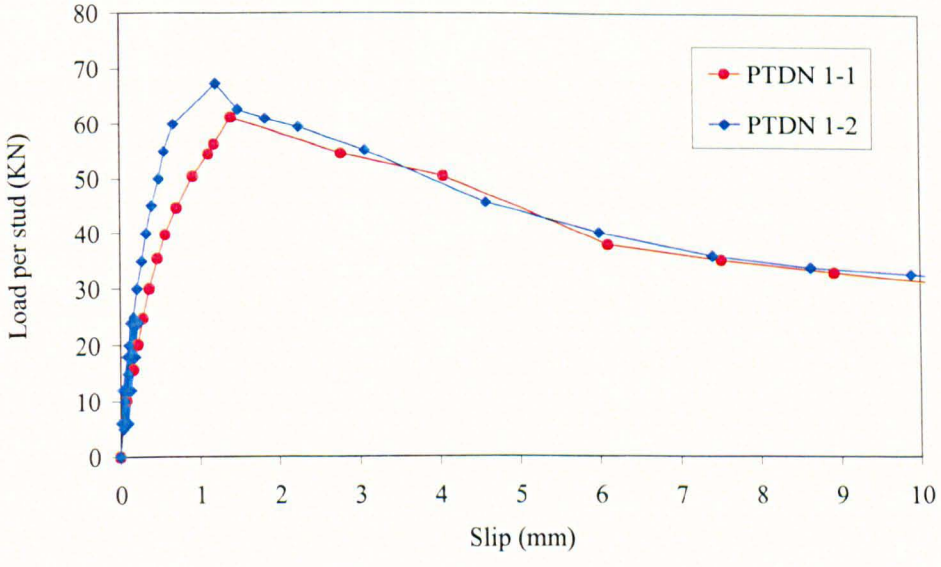

Figure 3.39 Load-slip curve for push test PTDN 1

3.9.5 Test PTDN 2

This test used double studs per rib with concrete grade of C40/50 and mesh fabric having a cover of 30 mm from top surface of the concrete slab. To prevent rotation of the last studded rib, as observed in previous tests, two shear studs in the last rib were chopped off. As a result, eight, instead of ten, shear connectors were used in the specimen as shown in Figure 3.40.

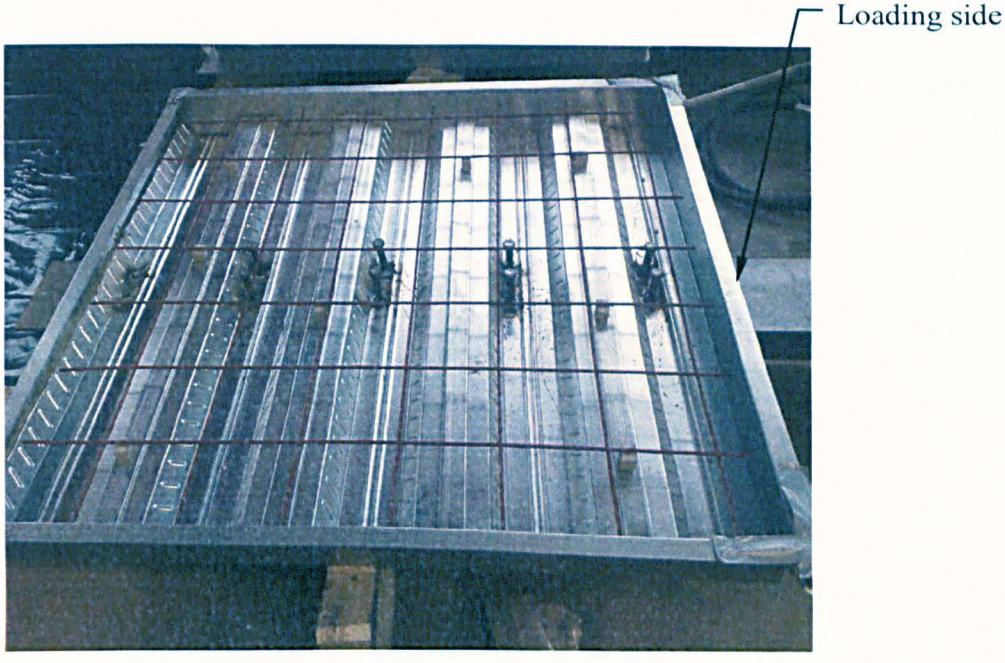

Figure 3.40 Arrangement of shear connectors in push test PTDN 2

The first push test specimen PTDN 2-1 was tested under load control, while the load in the second specimen PTDN 2-2 was applied in small increments under displacement control. A normal load of 70 kN was applied to both specimens, which was 10% of the expected horizontal failure load. The cracks in concrete slab, near top flange of the first sheeting trough, started to form when 80% of the failure load was reached. The rotation of the last rib was prevented by keeping it unstudded. The specimen PTDN 2-1 failed by formation of concrete shear failure wedges around the shear connectors. The size of failure wedges in the middle studded ribs was larger than the first and last studded rib. The last sheeting pan remained attached with the concrete slab, when the specimen was dismantled to inspect the failure patterns. The push test specimen PTDN 2-1 after failure is shown in Figure 3.41.

In the specimen PTDN 2-1, one of shear studs in the second last rib sheared off and other stud bent in the direction of horizontal loading. One of the pair of shear connectors in the first sheeting pan bent more than the other stud in single curvature in the direction of applied loading. The shear connectors in third sheeting pan showed slight bending and shear studs in second rib remained almost unchanged. The condition of shear studs and profile sheeting for PTDN 2-1, after concrete slab removal, is shown in Figure 3.42.

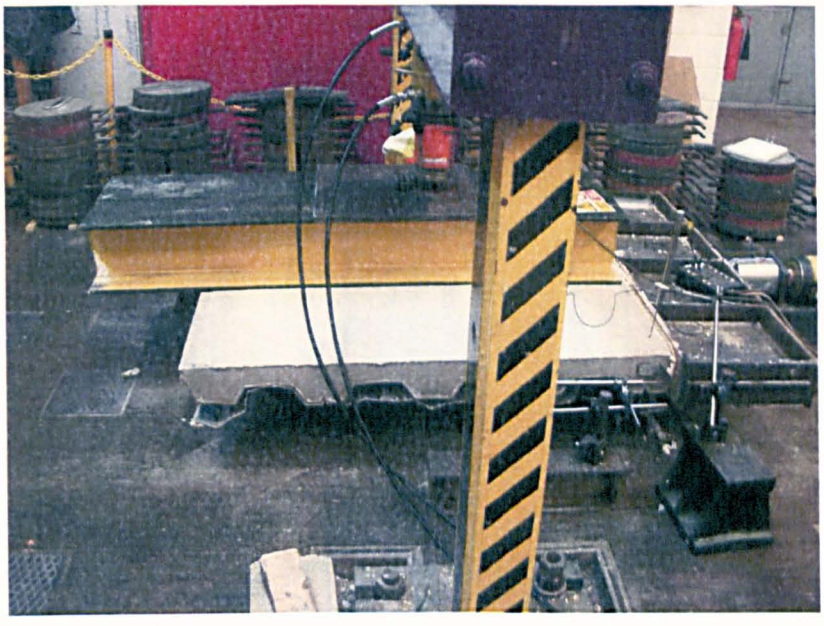

Figure 3.41 The specimen PTDN 2-1 after failure

Figure 3.42 The condition of shear studs and steel deck for PTDN 2-1 after concrete slab removal

The specimen PTDN 2-2 was subjected to the horizontal load under displacement control with the help of servo controlled hydraulic system. The displacement control was also tried in the previous test PTDN 2-1, but the insufficient pressure in the servo controlled system caused the test to be stopped at a total load of 400 kN and could not be continued until failure. Then, the specimen PTDN 2-1 was tested under load control.

In the specimen PTDN 2-2, the test set up was slightly modified. Two parallel hydraulic jacks were used, which were supplied with equal pressure from the servo controlled hydraulic system. Thus, two hydraulic jacks applied a load of 800 kN in total, which was enough to test the specimen until the expected total failure load of 700 kN.

The LVDT was mounted on one of the hydraulic jack to measure the applied displacement as shown in Figure 3.43. The specimen PTDN 2-2 was slowly displaced at a rate of 0.2 mm/min and the resulting load was measured with the help of the load cell. The position of LVDTs on this specimen was similar to the ones tested earlier. The load was cycled 25 times between 5% (35 kN) and 40% (280 kN) of the failure load determined from the previous test PTDN 2-1. After 25 cycles, the load was continued to be applied, under displacement control, until failure.

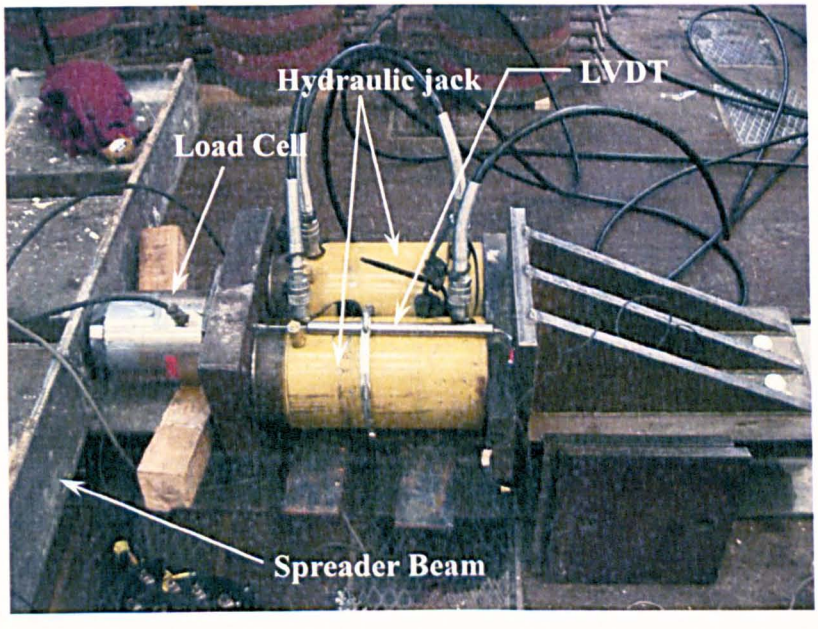

Figure 3.43 Arrangement of hydraulic jacks for specimen PTDN 2-2

The failure mode of the specimen PTDN 2-2 was essentially similar to the previous specimen PTDN 2-1. No back-breaking or rotation of the last rib occurred, primarily due to removal of shear connectors from the last rib. The portion of the concrete slab, above the top flange of the steel deck near the first and last rib, started to crack when almost 80% of the expected failure load was reached. The specimen PTDN 2-2 after failure is shown in Figure 3.44. Mainly, the specimen PTDN 2-2 failed on account of formation of concrete shear failure cones around the shear stud as shown in Figure 3.45.

Both shear studs in the first rib and one of the shear studs in the third rib completely sheared off. Remaining shear connectors bent in the direction of loading.

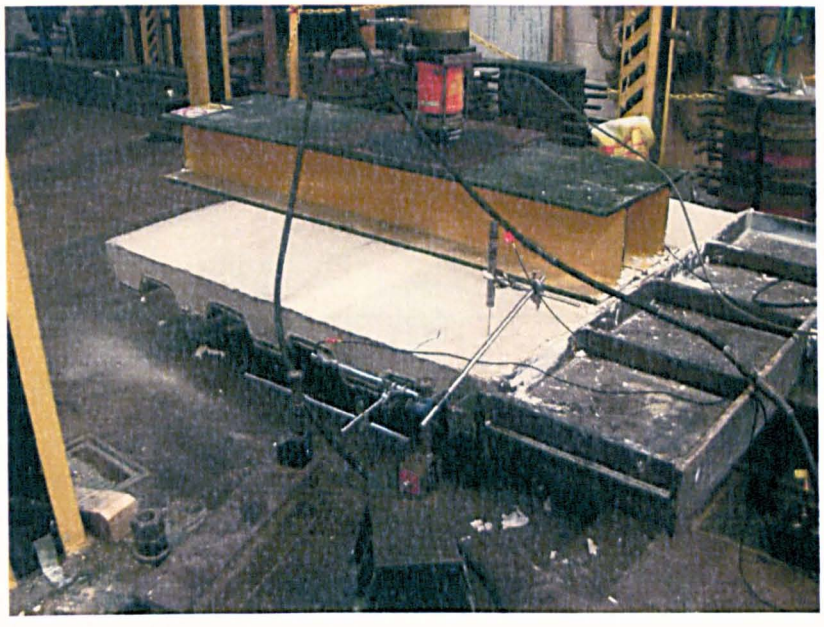

Figure 3.44 The specimen PTDN 2-2 after failure

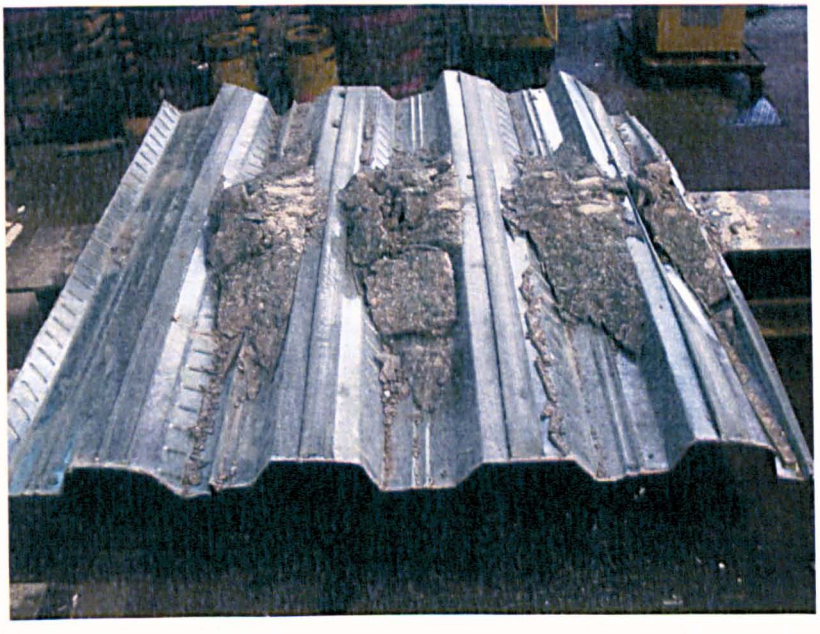

Figure 3.45 Formation of concrete failure cones in push test PTDN 2-2

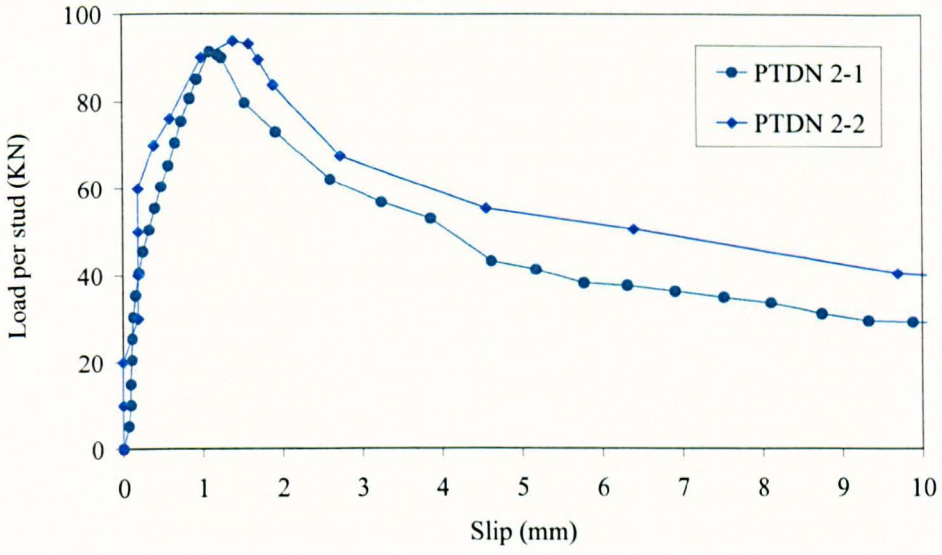

Figure 3.46 Load-slip curve for push test PTDN 2

The load-slip curve for the push test PTDN 2 is plotted in Figure 3.46. The maximum load per stud in case of the specimen PTDN 2-1, with load application under load control, was 91.3 kN with a slip of 1.11 mm at the steel-concrete interface. Similarly, the specimen PTDN 2-2, with displacement controlled loading procedure, failed at a load level of 93.7 kN per stud at a slip of 1.40 mm. The change of loading procedure from load to displacement control, apparently, did not have significant influence on the strength and ductility of the shear connector in the push test.

3.9.6 Test PSNM 1

This push test had a single shear stud per trough and in total 4 shear studs were used with last sheeting pan without any stud to prevent the back-breaking failure. A normal load of 40 kN, which was 10% of the expected horizontal shear load, was applied to the top surface of the slab parallel to the axis of the beam. The horizontal shear load was applied to the specimen under displacement control. The specimen failed by formation of failure cones around the shaft of the shear stud as shown in Figure 3.47. At failure, a crack in the concrete slab near top flanges of the first rib developed, and it grew wider as the load dropped beyond the maximum load. As no shear stud was used in the last rib, and two profiled sheetings were joined near the last rib, therefore, the last sheeting rib remained attached with the concrete slab when failure occurred.

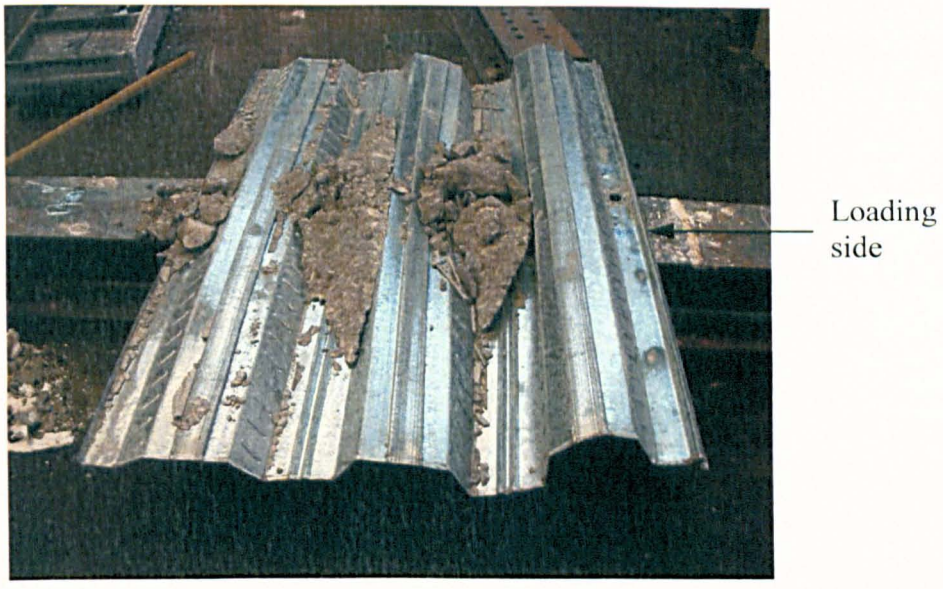

Figure 3.47 Formation of concrete cones in push test PSNM 1-1

The last shear stud near the free end, bent in the direction of the applied shear loading. The first shear stud remained embedded inside the concrete slab and detached from the beam and sheeting, leaving behind a hole in the steel deck as shown in Figure 3.47 and Figure 3.48. The underside of the concrete slab showing concrete pull-out failure surfaces is shown in Figure 3.48. The second stud also ripped off the beam without bending, and the condition of the studs indicated that they were detached due to welding failure rather than stud shearing failure. The first trough buckled and rose above the steel beam. When the studs pull out of the beam and sheeting without enough bending in the direction of the applied shear load, it is a sign of failure in welding around the shear stud. The failure cones developed around shear studs in the second and third sheeting rib, however, the failure cone around the shear connector in the third rib was larger than the failure cones in other ribs.

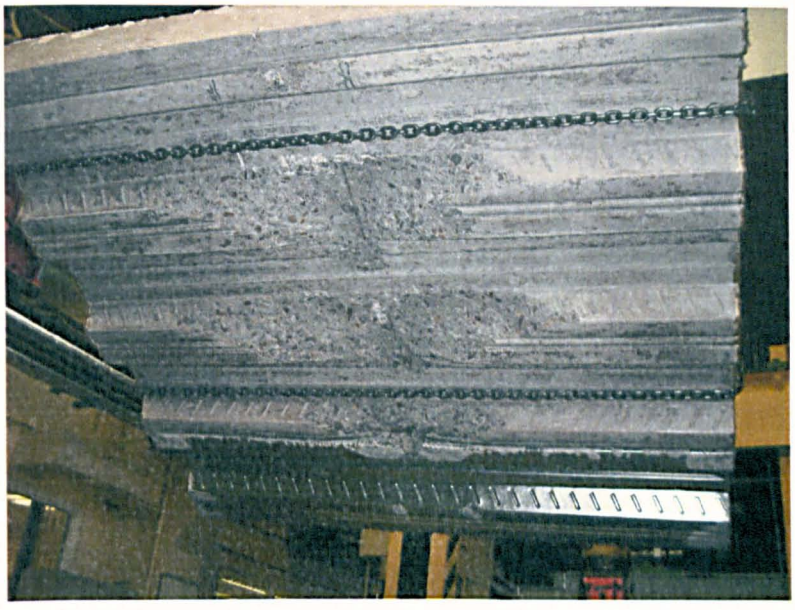

Figure 3.48 Underside of the slab of test PSNM 1-1 showing pull-out failure surfaces

The load-slip curve for push test PSNM 1 is plotted in Figure 3.49. The maximum load per stud in case of the push test specimen PSNM 1-1 was 113.0 kN with a corresponding slip of 2.71 mm. In the same way, the maximum load per stud observed in the specimen PSNM 1-2 was 138.4 kN with an average slip of 2.40 mm. Shear connector resistances of push test specimens PSNM 1-1 and PSNM 1-2 are normalized to a common concrete cube strength of 30 N/mm^2 using Equation 4.1 to make better comparison of shear connector capacites. Shear connector resistances of push test specimens PSNM 1-1 and PSNM 1-2 are calculated as 108.0 kN and 126.0 kN corresponding to a concrete cube strength of 30 N/mm^2, which indicates that the shear connector resistance of the specimen PSNM 1-2 is about 16% higher than the shear connector resistance of the push test specimen PSNM 1-1.

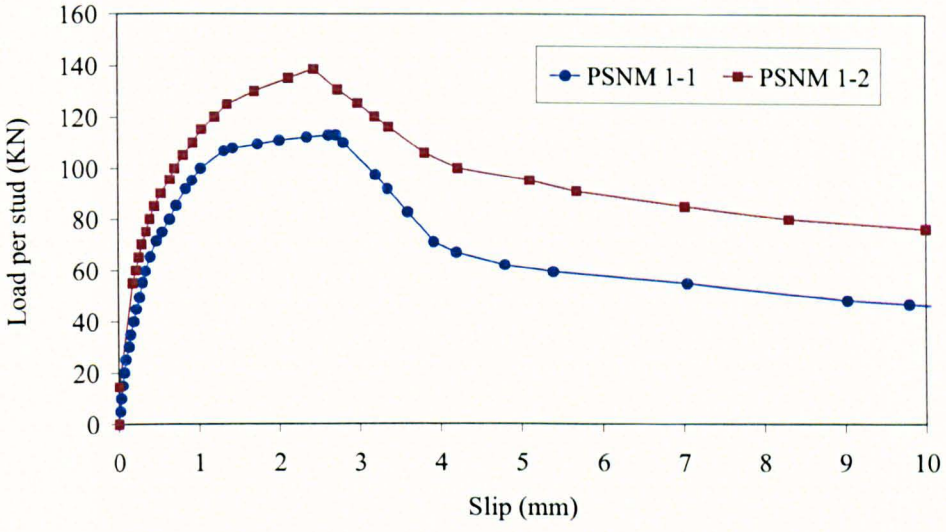

Figure 3.49 Load-slip curve for push test PSNM 1

3.9.7 Test PSNM 2

This push test used a single stud per rib with total of four shear studs in the specimen, and it had no shear connector in the last rib. The push test arrangement was modified slightly with normal load applied directly on top of the first rib perpendicular to the axis of the beam as shown in Figure 3.50. This set up prevented the unwanted uplift or rotation of the first rib. The horizontal shear load was applied to the specimen under displacement control, with initial loading rate of 0.5 mm/min. The loading rate was slowed down to 0.25 mm/min when 60% of the horizontal load was reached. It was further reduced to 0.1 mm/min when specimen started to crack. The surface of the concrete slab above the top flange of the steel deck near the last studded rib formed a crack when the specimen started to fail, which continued through the entire width of the slab as shown in Figure 3.51.

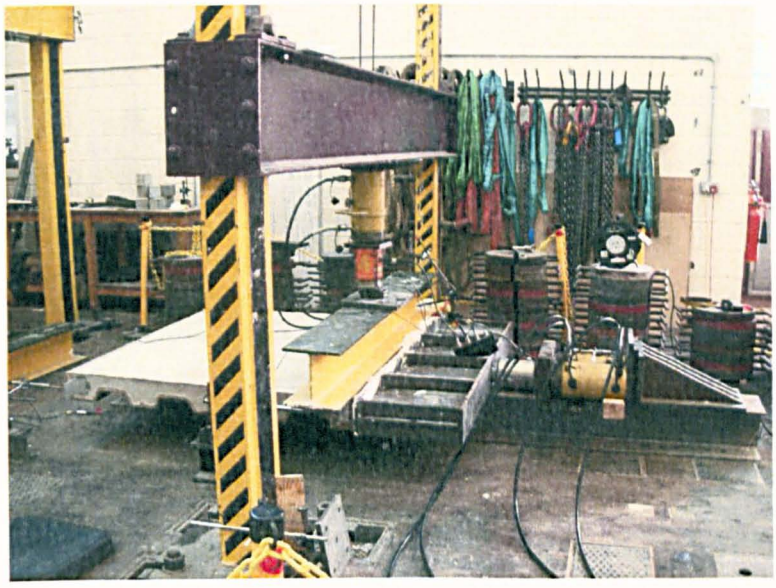

Figure 3.50 General arrangement of the push test PSNM 2

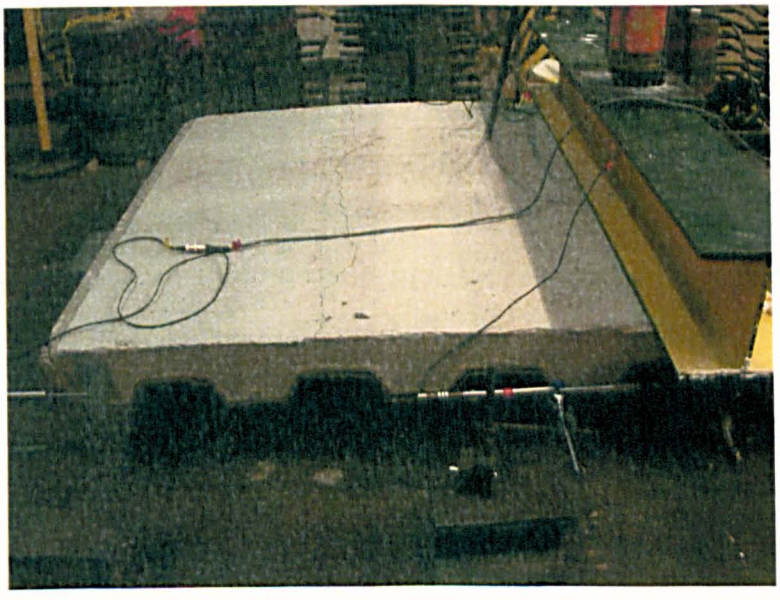

Figure 3.51 Formation of a crack across the width of push test PSNM 2-2

The load-slip behaviour of the push test PSNM 2 is presented in Figure 3.52. At the time of the testing, both specimens had almost similar concrete compressive strength. The push test specimen PSNM 2-1 failed at a load per stud of 127.2 kN with a slip of 2.30 mm at the steel-concrete interface. Similarly, the maximum shear connector resistance observed in the push test specimen PSNM 2-2, expressed as a load per stud, was 134.6 kN with a corresponding slip of 1.40 mm.

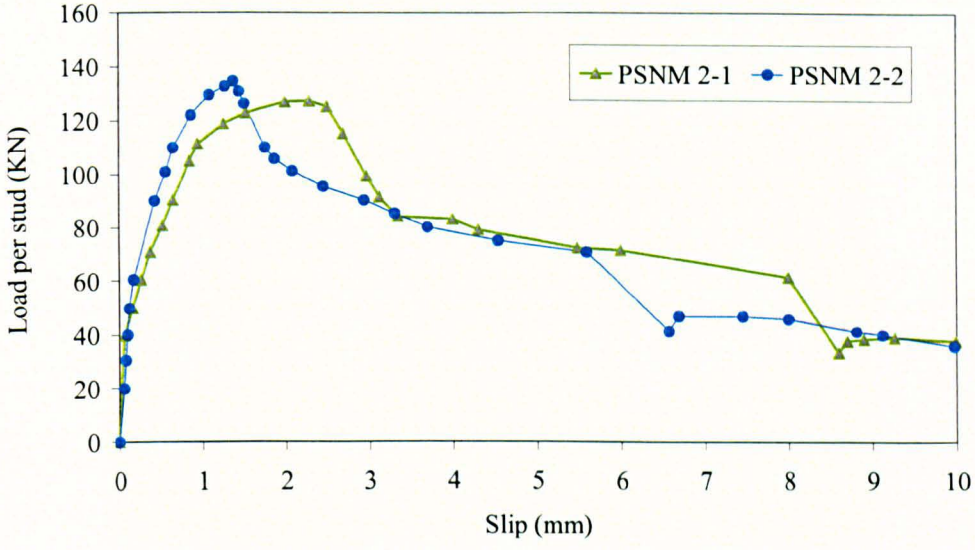

Figure 3.52 Load-slip curve for push test PSNM 2

3.9.8 Test PDNM 1

The push test PDNM 1 had double studs per trough with no studs in the last rib. The procedure for normal and shear loading remained the same as that of PSNM 1. The main failure mode was concrete cone failure. The concrete failure cones formed around the shear stud shaft in all studded ribs apart from the first rib where studs detached from the sheeting and beam as shown in Figure 3.53. The small fragments of concrete were left behind the first rib when the specimen was dismantled. In the specimen PDNM 1-1, one of the shear studs in the first rib completely detached from the sheeting due to applied shear load; and in the specimen PDNM 1-2 both of the shear studs in the first rib separated from the steel deck and beam. All shear studs bent in the direction of applied shear loading.

Figure 3.53 Formation of concrete cones in push test PDNM 1-2

The load-slip curves for the push test PDNM 1 are plotted in Figure 3.54. The maximum load per stud in the specimen PDNM 1-1 was 72.7 kN with a corresponding slip of 3.20 mm. While, the push test specimen PDNM 1-2 failed at a load of 81.8 kN with a slip of 1.40 mm. Although the compressive strength of both specimens was almost the same, the load in the specimen PDNM 1-2 was higher than the specimen PDNM 1-1.

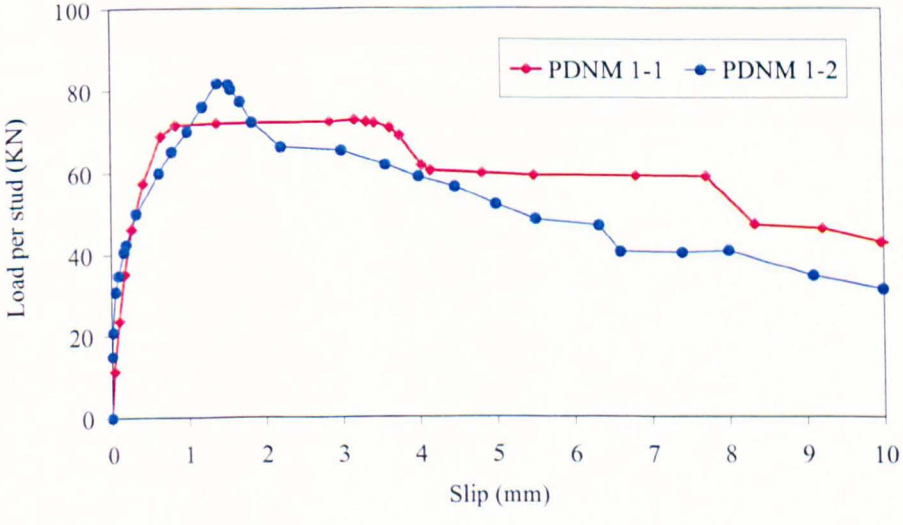

Figure 3.54 Load-slip curve for push test PDNM 1

3.9.9 Test PDNM 2

The push test arrangement for this test was modified with no shear studs in the first and last rib. This push test used double shear studs per rib. As there were no shear connectors in the first and last rib, the concrete failure cones formed in the middle three studded ribs as shown in Figure 3.55. The formation of concrete failure cones resembled with other push tests conducted in this study. When the push test failed, a crack in the concrete slab above the top flange of the steel deck in the first rib appeared as shown in Figure 3.56, which grew wider as the specimen was pushed until complete loss of the shear connection among slab, sheeting and shear studs occurred.

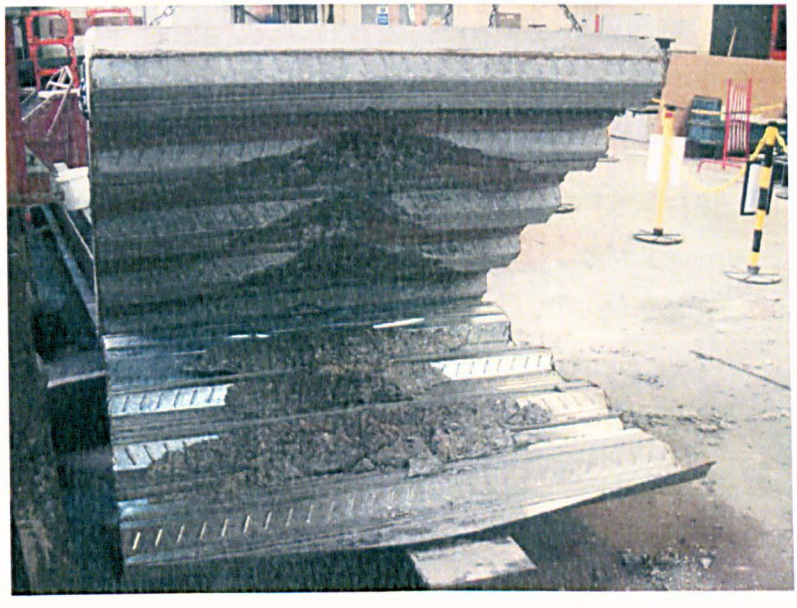

Figure 3.55 Formation of concrete failure cones and underside of slab in push test PDNM 2-1

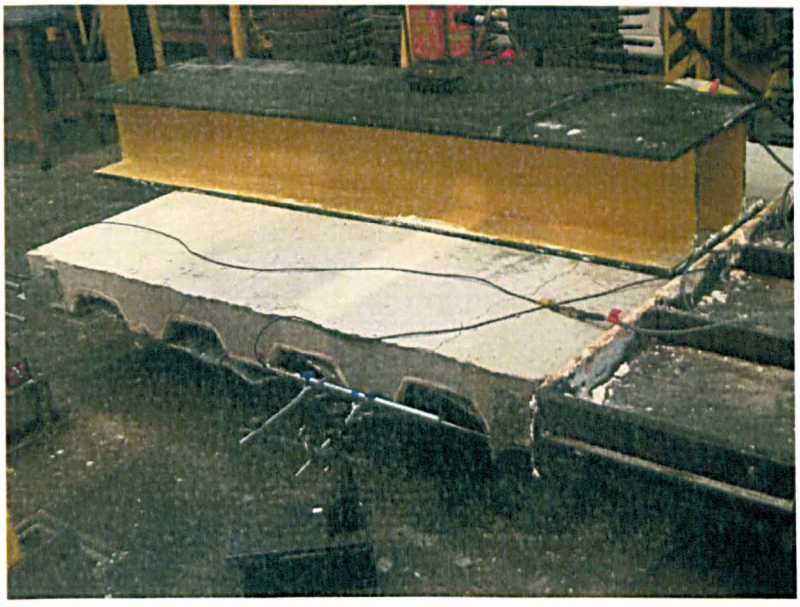

Figure 3.56 The push test specimen PDNM 2-2 after failure

The load-slip behaviour of the push test PDNM 2 is presented in Figure 3.57. The maximum shear connector resistance in the specimen PDNM 2-1 was 77.3 kN and the slip at failure was 0.84 mm. Similarly, the specimen PDNM 2-2 failed at a maximum load per stud of 76.8 kN with a corresponding slip of 1.30 mm.

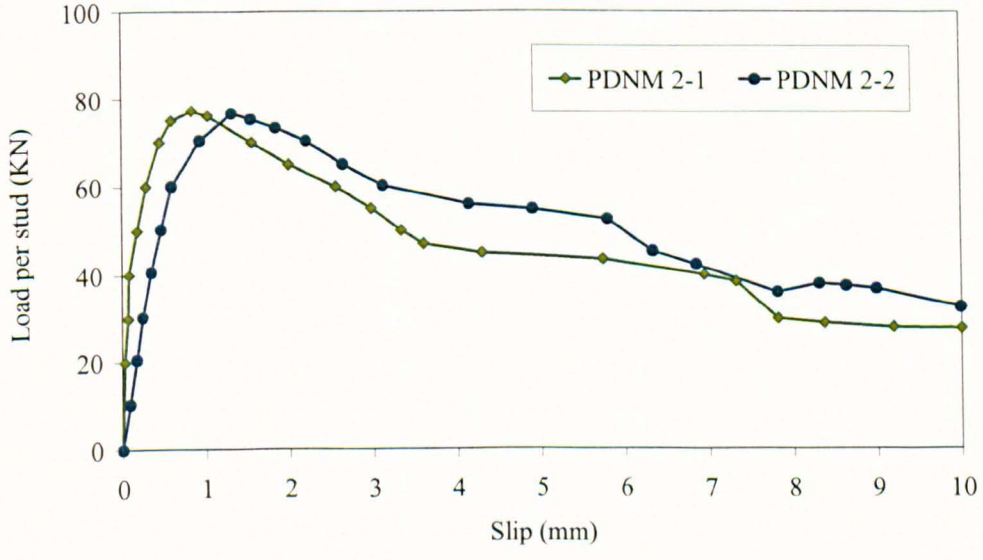

Figure 3.57 Load-slip curve for push test PDNM 2

3.9.10 Summary of push test results from second series

The second series of push tests consists of tests with horizontal as well as normal load equivalent to 10 % of the applied horizontal shear load. The key variables include the effect of mesh position, number of mesh layers, number of shear connectors, concrete strength, loading procedure and push test arrangement with normal load. Both single and double shear studs per rib were tried. The push test arrangement with last rib as unstudded and with no studs in the first and last rib were also tried to get rid of back-breaking failure. The horizontal shear load was applied under either load or deflection control to see its influence on the performance of the shear connector. The concrete strength was also varied in some specimens to study its impact on the strength and ductility of the shear connector. The push test results along with details of mesh location, concrete strength and number of studs are presented in Table 3.5.

Table 3.5 Summary of push test results from second series

S. No.	Test Ref.	Concrete cube strength (MPa)	No. of studs per rib, n_r	Total No. of studs per specimen	Mesh position	Shear capacity per stud (kN)
1	PTSN 1-1	25.4	1	5	Low	97.8
2	PTSN 1-2	25.4	1	5	Low	98.9
3	PTSN 2-1	21.2	1	5	High	90.0
4	PTSN 2-2	23.2	1	5	High	81.7
5	PTDN 1-1	28.2	2	10	High	61.3
6	PTDN 1-2	37.0	2	10	High	67.3
7	PTDN 2-1	58.8	2	8	High	91.3
8	PTDN 2-2	63.2	2	8	High	93.7
9	PSNM 1-1	32.8	1	4	Low & High	113.0
10	PSNM 1-2	36.1	1	4	Low & High	138.4
11	PSNM 2-1	32.3	1	4	Low & High	127.2
12	PSNM 2-2	32.7	1	4	Low & High	134.6
13	PDNM 1-1	46.0	2	8	Low & High	72.7
14	PDNM 1-2	48.8	2	8	Low & High	81.8
15	PDNM 2-1	30.7	2	6	Low & High	77.3
16	PDNM 2-2	31.6	2	6	Low & High	76.8

Note: Mesh located at low position is resting on top of the steel deck and high location is 30 mm below the top surface of the concrete slab.

3.10. Conclusions

In this chapter push test set up, instrumentation, loading procedure, material testing and push test results are explained in detail. The load-slip curves for each push test are plotted and failure patterns of each push test are presented. The push test results will be discussed in next chapter, and the results will also be compared with available design code provisions in the same chapter.

Chapter 4

Discussion of push test results

Chapter 4
Discussion of push test results

4.1. Introduction

This chapter deals with discussion of push tests conducted in previous chapter and comparison of push test results with various shear stud strength prediction methods. The influence of various parameters such as normal load, number of shear studs, reinforcement bar at the bottom trough, double layers of mesh, position of mesh, position of normal load and various push test arrangements have been discussed. The results of push tests are compared with the strength predicted from Eurocode 4 equations, Johnson and Yuan (1998) method and AISC (2005) specification.

4.2. Normalised shear connector resistance

The behaviour of the push test with profiled sheeting is significantly affected by concrete compressive strength. To study the effect of various parameters and make appropriate comparisons, ideally, the concrete compressive strength should be same for all test specimens. However, it is not practically possible to test all specimens on the same day, and thus, have the same concrete compressive strength. Therefore, in order to make good comparison between different push tests, the experimental shear connector resistances, P_e have been normalised to a common concrete strength of 30 N/mm^2 in proportion to the square root of the cube strength, $f_{cm,cube}$ of a particular push test using Equation (4.1). This equation has previously been used by Lloyd and Wright (1990) to compute the normalised shear connector resistance where concrete strength of otherwise identical specimens was different. The normalised strengths, $P_{e,norm}$ are presented in Table 4.1

$$P_{e,norm} = \frac{P_e}{\sqrt{\frac{f_{cm,cube}}{30}}} \qquad (4.1)$$

4.3. Effect of different parameters

The influence of different parameters on the performance of the headed shear stud embedded in the composite slab is discussed in this section. The main variables discussed include the effect of number of mesh layers and mesh position, normal load,

T16 bar at the bottom trough, number of shear connectors, different positions of normal load and different push test arrangements. The results are normalised to a common compressive strength, where necessary, to make appropriate comparisons.

Table 4.1 Determination of normalised shear connector resistance

S No.	Test Ref.	No. of Studs n_r	$f_{cm,cube}$ (MPa)	P_e (kN)	$P_{e,norm}$ (kN)	Mean ($P_{e,norm}$)	SD ($P_{e,norm}$)	COV ($P_{e,norm}$)
1	PTS 1-1	1	34.0	75.7	71.1	73.6	2.6	3.6%
2	PTS 1-2	1	34.0	78.8	74.0			
3	PTS 2-1	1	27.5	69.0	72.1			
4	PTS 2-2	1	27.5	73.8	77.1			
5	PTD 1-1	2	27.9	52.1	54.1	51.0	3.6	7.0%
6	PTD 1-2	2	27.9	45.4	47.1			
7	PTD 2-1	2	28.0	52.2	54.0			
8	PTD 2-2	2	28.0	47.3	48.9			
9	PTSN 1-1	1	25.4	97.8	106.4	103.5	7.1	6.9%
10	PTSN 1-2	1	25.4	98.9	107.6			
11	PTSN 2-1	1	21.2	90	107.1			
12	PTSN 2-2	1	23.2	81.7	92.8			
13	PTDN 1-1	2	28.2	61.3	63.2	63.4	2.0	3.2%
14	PTDN 1-2	2	37.0	67.3	60.6			
15	PTDN 2-1	2	58.8	91.3	65.2			
16	PTDN 2-2	2	63.2	93.7	64.6			
17	PSNM 1-1	1	32.8	113.0	108.1	121.4	9.28	7.64%
18	PSNM 1-2	1	36.1	138.4	126.2			
19	PSNM 2-1	1	32.3	127.2	122.6			
20	PSNM 2-2	1	32.7	134.6	128.9			
21	PDNM 1-1	2	46.0	72.7	58.7	68.5	8.52	12.43%
22	PDNM 1-2	2	48.8	81.8	64.1			
23	PDNM 2-1	2	30.7	77.3	76.4			
24	PDNM 2-2	2	31.6	76.8	74.8			

4.3.1. Effect of mesh position

The first variable tested was the location of welded wire mesh. The push test PTS 1 had the mesh placed directly on top of the steel deck, and in push test PTS 2 the mesh was placed at a distance of 30 mm from top surface of the slab. The normalised load versus slip curves for these single stud push tests are plotted in Figure 4.1. The mean strength of all four single stud push test specimens is 73.6 kN, the standard deviation is 2.6 and coefficient of variation is 3.6% as mentioned in Table 4.1, which suggests that there is little difference between the normalised shear connector resistances obtained from push tests PTS 1 and PTS 2. The discrepancy in the initial stiffness of the load-slip behaviour between PTS 1 and PTS 2 is due to the position of displacement transducers, which were placed at the back of the slab in case of PTS 1 and at the sides of the slab near the loaded end for PTS 2. Both push tests PTS 1 and PTS 2 failed in a similar manner by formation of concrete failure cones around the shear stud shaft with approximately identical shape and size of the failure cones.

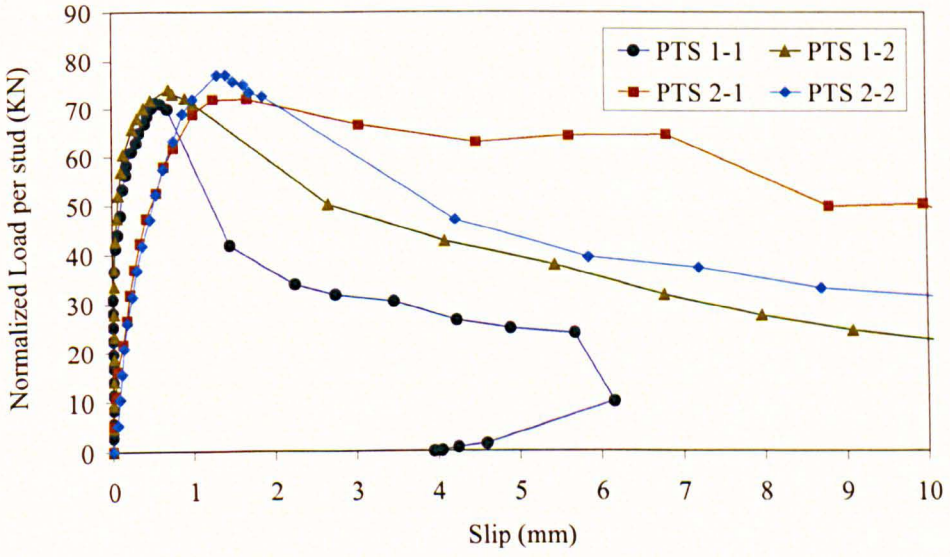

Figure 4.1 Normalised load versus slip curves for single stud push tests with horizontal shear loading only

The push tests PTSN 1 and PTSN 2 used a single stud per rib with 10% normal load in addition to the horizontal shear load with the mesh on the deck and raised mesh respectively. The average normalised strength achieved in all four push test specimens is 103.5 kN, the standard deviation is 7.1 and coefficient of variation is 6.9% as shown in Table 4.1. The normalised load versus slip curves for single stud push tests with

normal load are plotted in Figure 4.2. Again, the results indicate that the mesh location appears to have no influence on the shear connector resistance and the slip at the steel-concrete interface.

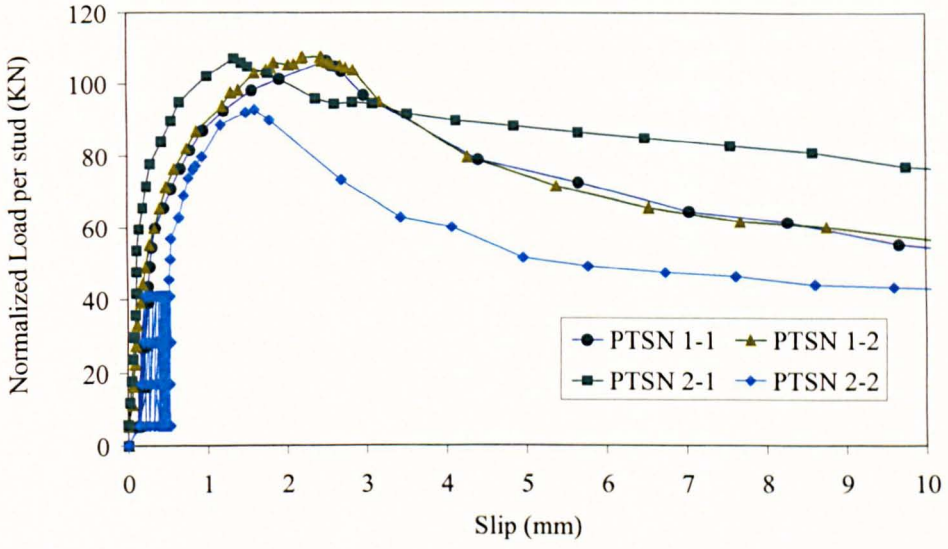

Figure 4.2 Normalised load versus slip curves for single stud push tests with normal and horizontal shear load

Thus, within the limits tested in this research, it is concluded that locating the mesh either directly on top of the profiled sheeting or at a distance of 30 mm from top surface of the slab does not have any influence on the strength and ductility of the headed shear stud. The concrete failure cones start from the underside of the head of the shear stud and progress towards the top corner of the profiled sheeting, where top flange and the web of the steel deck meet. Strength enhancement could have been achieved if the mesh would have been placed normal to the failure plane. However, in real situation, it is difficult to position the mesh in such a way, so that it can cross the failure surface.

4.3.2. Effect of extra T16 bar at the bottom of the rib

The effect of an extra T16 reinforcement bar placed at the bottom of the trough is investigated in push tests PTD 1 and PTD 2 with double studs per rib. The mean normalised shear connector resistance of all four push test specimens is 51.0 kN, the standard deviation is 3.6 and the coefficient of variation is 7% as shown in Table 4.1. The normalised load per stud versus slip curves are plotted for push tests with double studs per rib in Figure 4.3. The push test PTD 2 had an extra T16 high yield

reinforcement bar at the bottom of the sheeting pan and PTD 1 was without it. It appears from Figure 4.3 and Table 4.1 that the average shear connector resistance obtained from the push test with reinforcement bar is not much different from the one without it.

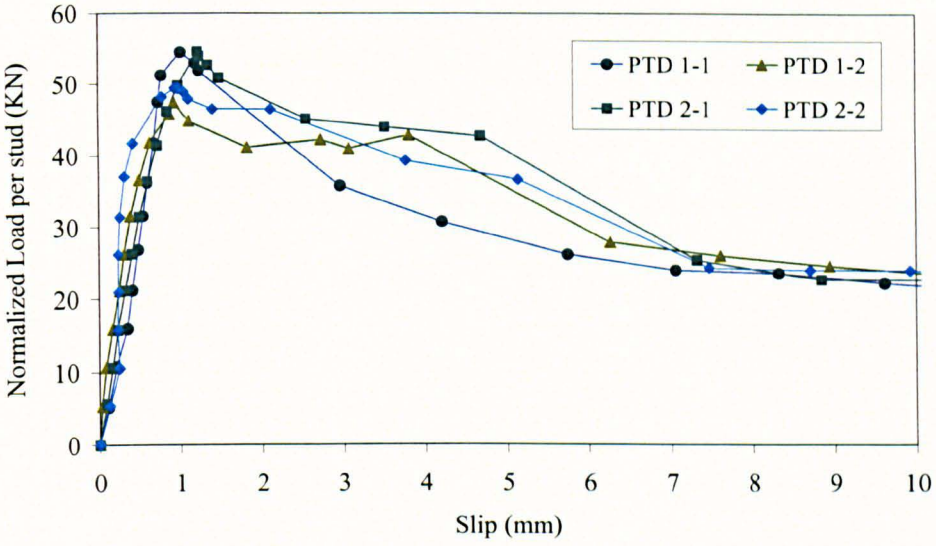

Figure 4.3 Normalised load versus slip curves for double studs push tests with horizontal shear loading only

The development of concrete failure wedges was also approximately same in all double studs push tests except in the push test PTD2, where some concrete fragments remained attached to the reinforcement bar. However, the concrete broken bits near the reinforcement bar at the bottom trough did not contribute towards either strength or ductility improvement. It is believed that the additional bar could have increased the shear connector strength, and possibly the ductility, if it was placed at a location closer to concrete failure surfaces. It is found that placing an additional high yield reinforcement bar at the bottom of the sheeting trough gives no extra benefit in terms of the strength and ductility of the shear connector as compared to the one without it.

4.3.3. Effect of normal load

The normalised load per stud versus slip curves for single stud push tests with and without 10% normal load are plotted in Figure 4.4, where PTS and PTSN indicate single stud push tests with and without normal load respectively. The results show that approximately 40% strength enhancement has been achieved on average, when a normal load of 10% of the horizontal shear load was applied to the push test with a single stud

per rib. Despite significant improvement in the shear connector resistance, the ductility of the shear connector could not be improved to attain the Eurocode 4 required slip capacity of 6 mm for ductile shear connector behaviour.

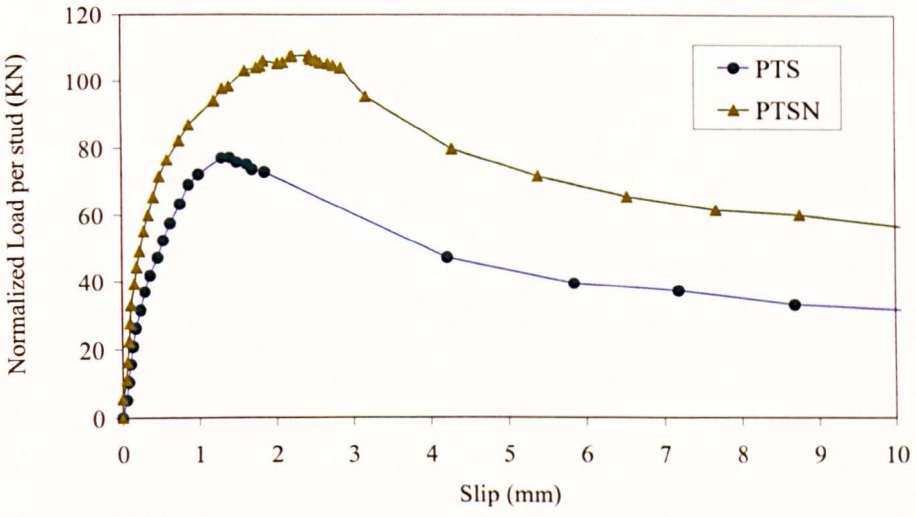

Figure 4.4 Comparison of push tests having single stud per rib with and without normal load

The comparison of push tests having double stud per rib with and without normal load is shown in Figure 4.5, where PTD represents a push test with double studs per rib and PTDN corresponds to a push test having double studs per trough with normal load. The results indicate that the shear connector resistance increases by about 23%, when 10% normal load is applied to the push test having pairs of shear connectors per rib. However, the ductility of the headed shear connector remained unaffected with application of the normal load. It was found that the normal load increased the shear connector resistance in general, in case of push tests with single and double studs per rib, but it did not have any influence on the slip at the steel-concrete interface.

The reason for 40% and 23% increase in the shear connector resistance of push tests with single and double shear studs per rib respectively is that the application of normal load on top surface of the composite slab increases confinement of concrete around shear connectors, and as a result, the push test with normal load takes more load than the one without it. It can also be noted that this increase in the shear connector resistance in case of double shear studs per rib is nearly half of the increase in strength using a single stud per rib. This is due to the fact the some area of concrete failure cones

between two shear connectors is duplicated in case of push tests with double studs per rib and it leads to relatively lesser increase in the shear connector resistance of push tests with double studs per rib as compared to push tests with a single stud per trough.

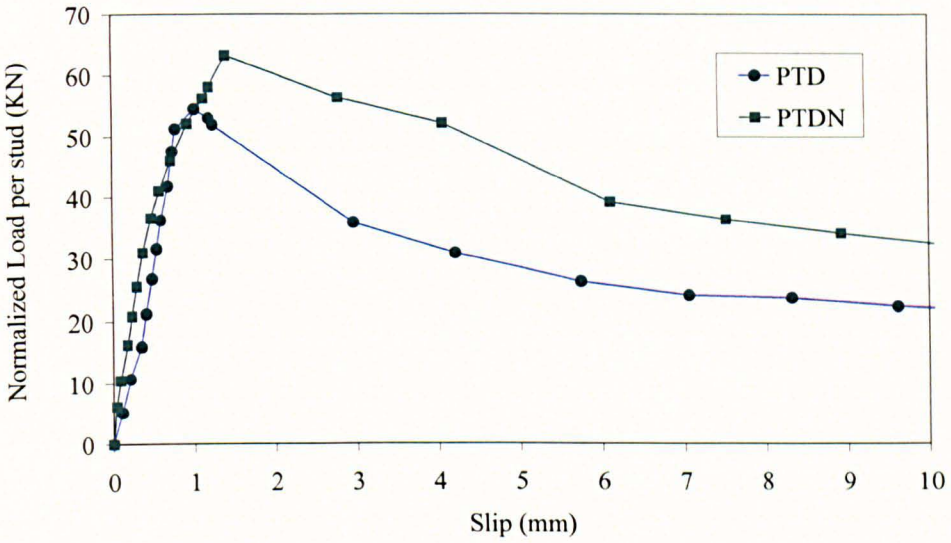

Figure 4.5 Comparison of push tests having double studs per rib with and without normal load

4.3.4. Effect of push test arrangement

Initially, the push test arrangement having shear studs in all sheeting pans was used. Later, it was modified with no studs in the last rib, and then, with no studs in the first and the last rib. The effect of removing shear studs from last rib in order to avoid back-breaking failure is investigated in push tests PTDN 1 and PTDN 2. Both push tests used double studs per rib with 10% normal load. In the push test PTDN 2, two shear studs were removed from the last rib to prevent it from rotating, and thus, avoiding the premature failure of the push test. The average normalised shear connector resistance is 63.4 kN for both push tests with standard deviation of 2.0 and coefficient of variation of 3.2% as shown in Table 4.1.

The normalised load per stud versus slip curves for push tests PTDN 1 and PTDN 2 are plotted in Figure 4.6. Although, keeping the last rib as unstudded prevents it from rotating, it did not have any effect on the strength and ductility of the shear connector as is evident form Figure 4.6. Furthermore, push tests PTDN 1 and PTDN 2 were tested

under load and displacement control respectively; and apparently, the results obtained from both tests are not hugely different. This suggests that the loading procedure and removal of studs from the last rib do not affect the behaviour of the shear stud in general.

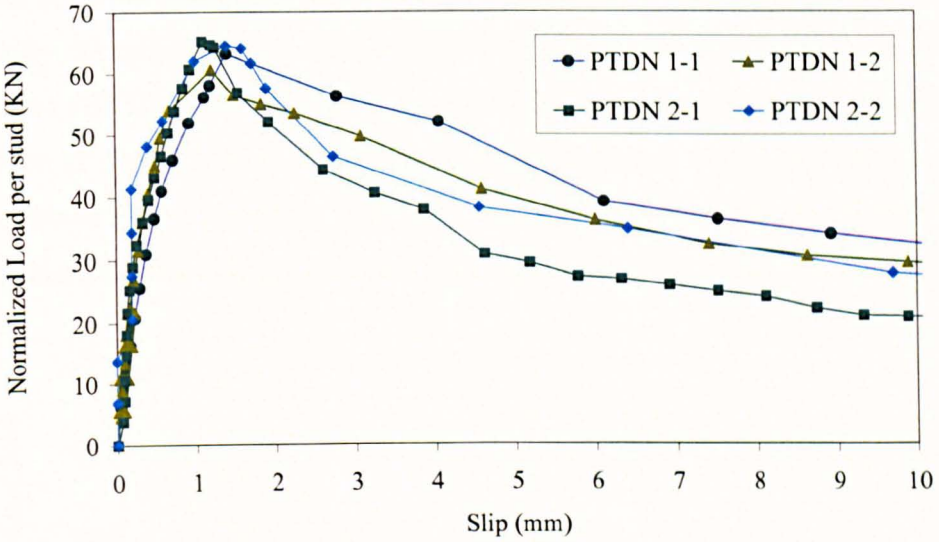

Figure 4.6 Normalised load versus slip curves for push tests having double studs per rib with normal and horizontal shear load

The comparison of push tests with no stud in the last rib, and no stud in the first and last rib is presented in Figure 4.7. The push test PDNM 1 had no stud in the last sheeting pan, while the push test PDNM 2 did not have any stud in the first and last rib. Both push tests had double layers of wire mesh, and the normal load was also applied to these tests besides conventional shear loading. The shear connector resistances presented in Figure 4.7 are normalised to a common concrete strength of 30 N/mm^2 in proportion to the square root of the concrete cube strength of the individual push test. The push test results suggest that the average shear connector resistance of the push test with no shear studs in the first and last rib was 23% higher than the average strength of headed shear stud in a push test with no stud in the last rib. However, the ductility of the shear stud still remained independent of the push testing arrangement.

The influence of the position of normal load on the performance of headed shear stud is studied in push tests PSNM 1 and PSNM 2. The push test PSNM 1 had normal load

applied to the centre of the concrete slab parallel to the longitudinal axis of the beam. On the other hand, in case of the push test PSNM 2, the normal load was applied on the surface of the concrete slab just above the first rib of the profiled sheeting perpendicular to the axis of the beam. The normalised load per stud versus slip curves for both push tests PSNM 1 and PSNM 2 are presented in Figure 4.8. The average shear connector resistance obtained from push tests PSNM 1 and PSNM 2 was 117.2 kN and 125.7 kN respectively. Although, the load per stud in case of the push test PSNM 2 is bit higher than the test PSNM 1, it is difficult to suggest if that is a genuine effect of the change in the position of normal load or it is due to experimental error. Based on these test results, it is interpreted that the position of normal load does not have significant influence on the performance of the headed shear stud in a push test with profiled sheeting.

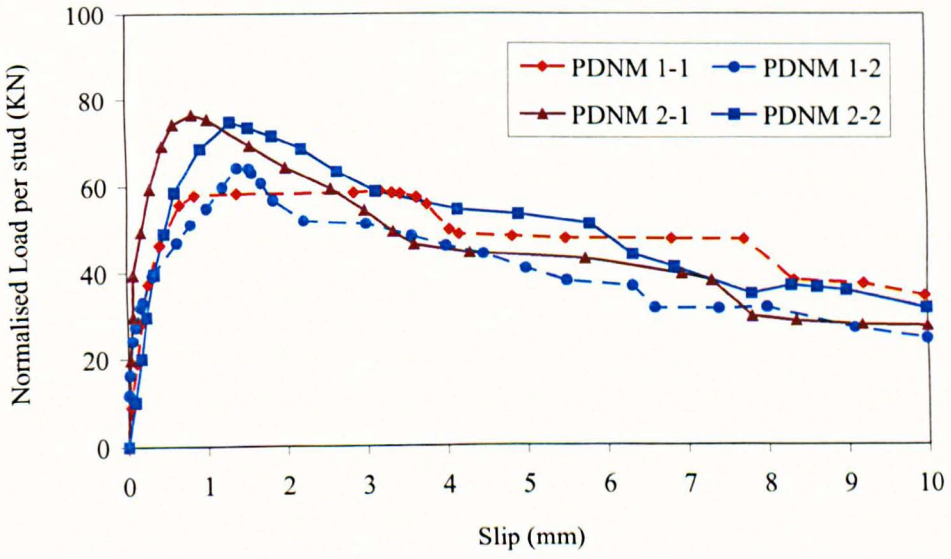

Figure 4.7 Comparison of push test arrangement with no stud in last rib, and no stud in first and last rib

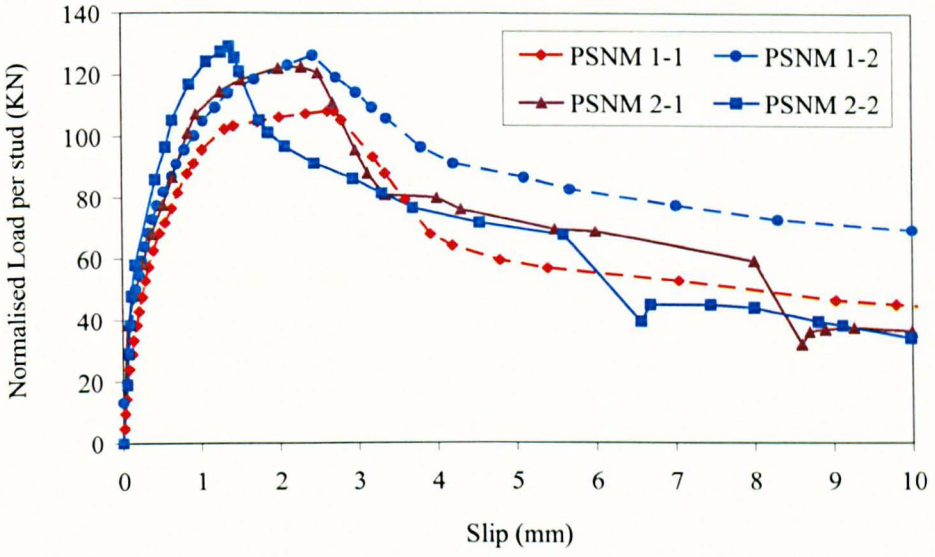

Figure 4.8 Effect of position of normal load on behaviour of push test

4.3.5. Effect of single and double layers of wire mesh

The first series of push tests included only single layer of wire mesh placed either on top of the steel deck or in a raised position with a concrete cover of 30 mm from top of the slab. However, the second series of push tests contained some push tests with double layers of mesh embedded inside the concrete slab. Double layers of wire mesh consisted of one layer placed directly on top of the steel deck and the other at a distance of 30 mm from the top surface of the concrete slab. The comparison of single and double layers of wire mesh in a push test with a single stud per rib and having normal load is presented in Figure 4.9. It can be observed that the shear connector resistance in case of the push test with double layers of mesh is 17% higher than the push test with a single layer of mesh, when a single stud per rib is used. However, the use of double layers of mesh did not result in any improvement in the slip capacity of the shear connector.

The comparison of single and double layers of wire mesh in a push test with double studs per rib is shown in Figure 4.10. It is evident that the normalised load per stud in case of the push test with double layers of mesh is about 18% higher than the normalised load per stud obtained from the push test with a single layer of mesh using double studs per rib. The push test PDNM 2 is used in this comparison, which used no studs in the first and last rib, rather than PDNM 1, which had no shear stud in the last rib only. In the push test PDNM 1, shear studs in the first rib detached from the sheeting

and beam due to welding failure, and this was the reason that the strength enhancement due to use of double layers of wire mesh could not be achieved.

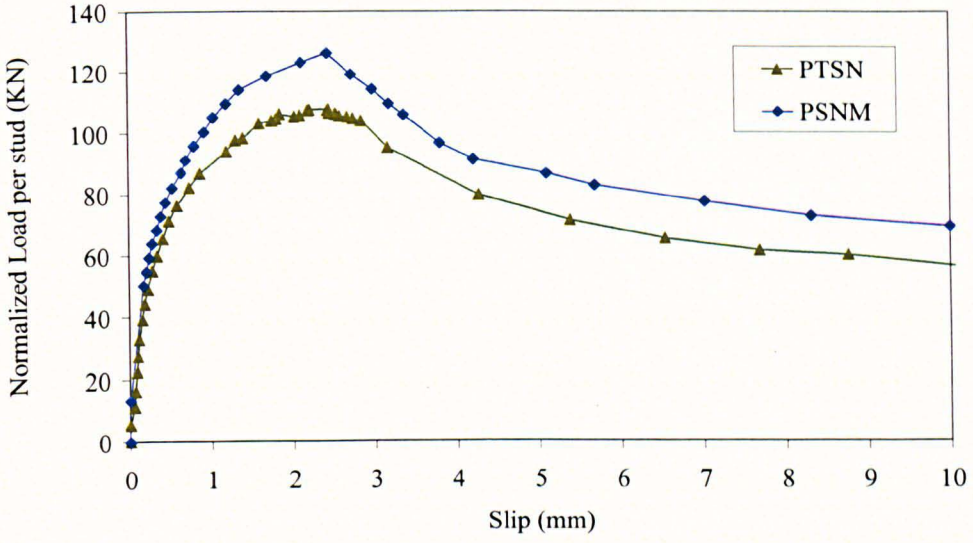

Figure 4.9 Comparison of single and double layers of wire mesh in a push test with single stud per rib

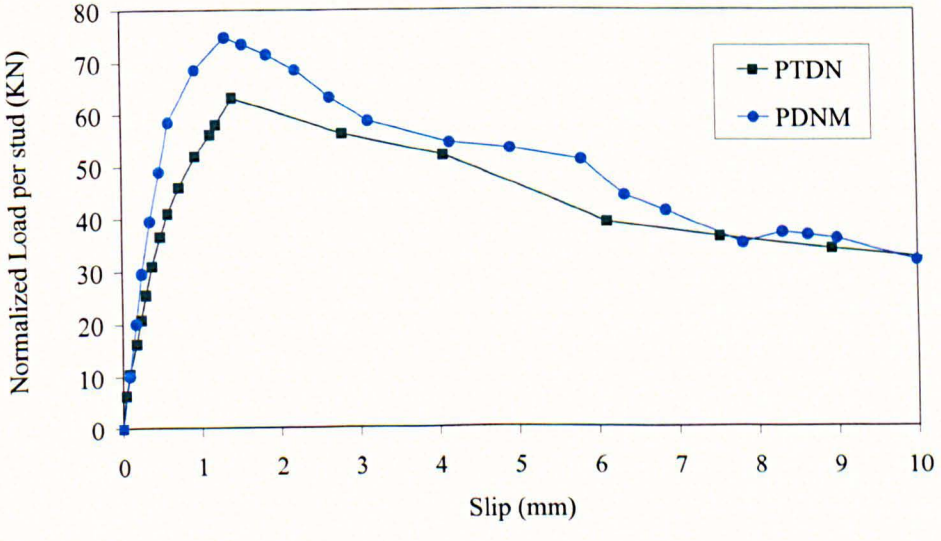

Figure 4.10 Comparison of single and double layers of wire mesh in a push test with double studs per rib

4.4. Comparison of push test results with strength prediction methods

The results obtained from push tests conducted in this study are compared to the predicted strengths from Eurocode 4 equations, Johnson and Yuan (1998) method and AISC (2005) provisions. The experimental shear connector strengths are plotted against predicted strengths to see how well the existing strength prediction methods estimate the shear connector resistance

4.4.1. Eurocode 4 Provisions

The results obtained from horizontal push tests are compared with the current design standard Eurocode 4 in order to investigate if this type of push test arrangement can be used to determine the shear connector resistance and slip capacity of the headed shear stud in composite beams with profiled metal decking. The experimental and theoretical shear connector resistances as well as slip capacity are presented in Table 4.2. The characteristic resistance and slip capacity for headed shear connectors were calculated using Eurocode 4 provisions.

Table 4.2 Measured and characteristic resistances for push test as per Eurocode 4

Test Ref.	$f_{cm,cube}$ (MPa)	f_{cm} (MPa)	E_{cm} [1] (GPa)	P_e (kN)	δ (mm)	$P_{Rk,e}$ [2] (kN)	$P_{Rk,t}$ [3] (kN)	δ_u (mm)	δ_{uk} [2] (mm)	$P_{Rk,e}/P_{Rk,t}$
PTS 1-1	34.0	25.5	29.1	75.7	0.60	68.1	63.5	0.82	0.74	1.07
PTS 1-2	34.0	25.5	29.1	78.8	0.70	70.9	63.5	1.38	1.24	1.12
PTS 2-1	27.5	20.6	27.3	69	1.67	62.1	52.3	3.80	3.42	1.19
PTS 2-2	27.5	20.6	27.3	73.8	1.41	66.4	52.3	2.18	1.96	1.27
PTD 1-1	27.9	20.9	27.3	52.1	1.02	46.9	43.6	1.50	1.35	1.08
PTD 1-2	27.9	20.9	27.3	45.4	0.94	40.9	43.6	1.60	1.44	0.94
PTD 2-1	28.0	21.1	27.3	52.2	1.23	47.0	43.9	1.80	1.62	1.07
PTD 2-2	28.0	21.1	27.3	47.3	0.95	42.6	43.9	2.60	2.34	0.97
PTSN 1-1	25.4	19.0	26.7	97.8	2.52	88.0	48.2	3.10	2.79	1.82
PTSN 1-2	25.4	19.0	26.7	98.9	2.45	89.0	48.2	3.10	2.79	1.85
PTSN 2-1	21.2	15.9	25.3	90	1.40	81.0	39.7	2.35	2.12	2.04
PTSN 2-2	23.2	17.4	26.0	81.7	1.60	73.5	44.1	2.15	1.94	1.67
PTDN 1-1	28.2	21.1	27.5	61.3	1.40	55.2	44.1	2.60	2.34	1.25
PTDN 1-2	37.0	27.7	29.9	67.3	1.22	60.6	56.3	2.00	1.8	1.08
PTDN 2-1	58.8	44.1	34.3	91.3	2.21	82.2	71.4	1.45	1.3	1.15
PTDN 2-2	63.2	47.4	35.1	93.7	1.40	84.3	71.4	1.90	1.71	1.18
PSNM 1-1	32.8	24.60	28.8	113.0	2.7	101.7	61.6	3.1	2.8	1.65
PSNM 1-2	36.1	27.08	29.7	138.4	2.4	124.6	66.9	3.0	3.7	1.86
PSNM 2-1	32.3	24.23	28.7	127.2	2.3	114.5	60.7	2.7	2.4	1.89
PSNM 2-2	32.7	24.53	28.8	134.6	1.4	121.1	61.4	1.6	1.4	1.97
PDNM 1-1	46.0	34.50	31.9	72.7	3.2	65.4	67.4	3.9	3.5	0.97
PDNM 1-2	48.8	36.60	32.5	81.8	1.4	73.6	70.6	1.8	1.6	1.04
PDNM 2-1	30.7	23.03	28.3	77.3	0.84	69.6	47.7	1.6	1.4	1.46
PDNM 2-2	31.6	23.70	28.5	76.8	1.3	69.1	49.0	2.0	1.8	1.41
									Mean	**1.38**
									Standard Deviation (SD)	**0.37**
									Coefficient of Variation (COV)	**26.7%**

computed [1] using Eurocode 2, [2] using Eurocode 4 Annex B, [3] using Eurocode 4, clause 6.6.3.1.

where:

$f_{cm,cube}$ = Mean value of concrete cube compressive strength (N/mm^2)

f_{cm} = Mean value of concrete cylinder compressive strength (N/mm^2)

E_{cm} = Secant modulus of elasticity of concrete (kN/mm^2)

P_e = Experimental maximum load per stud (kN)

$P_{Rk,e}$ = Experimental Characteristic Resistance (kN)

$P_{Rk,t}$ = Theoretical Characteristic Resistance (kN)

δ = Maximum slip at failure (mm)

δ_u = Slip Capacity (mm)

δ_{uk} = Characteristic slip capacity (mm)

The experimental characteristic shear connector resistance, $P_{Rk,e}$ is taken as the failure load per stud in a push test, reduced by 10%. However, this can only be used for tests for which the deviation of any individual test result from the mean test result is less than 10%. In this study, individual test results are within 10% of the mean results of two identical specimens. The slip capacity, δ_u is taken as the slip at a point where the horizontal line drawn at the characteristic load level touches the falling branch of the load-slip curve as shown in Figure 4.11. The characteristic slip capacity, δ_{uk} is taken as the minimum value of the slip capacity, δ_u reduced by 10%.

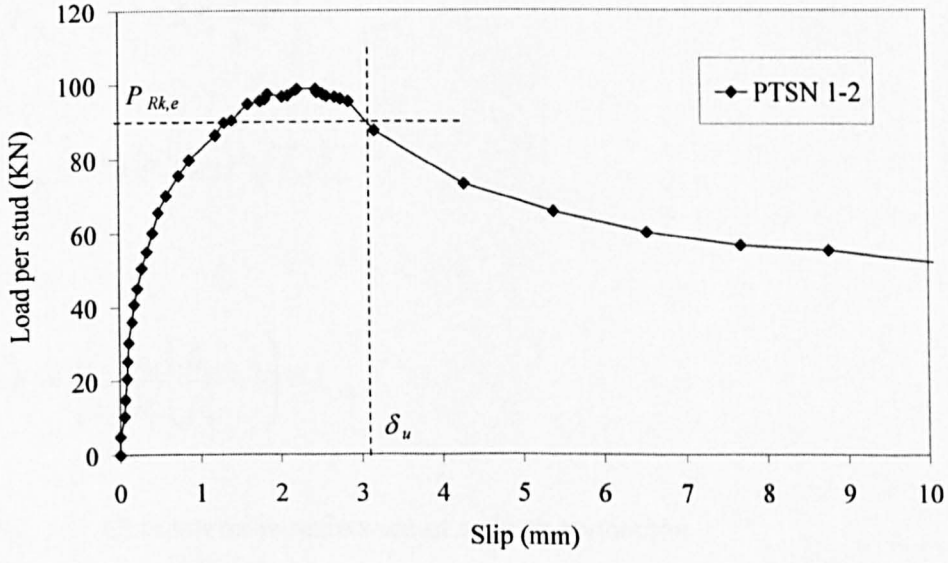

Figure 4.11 Determination of slip capacity

The compressive cube strength of concrete was converted to compressive cylinder strength using f_{cm} = 0.75 $f_{cm,cube}$ for 100-mm cubes as suggested by Stark and Hove (1991). The reason for using the calculated compressive cylinder strength with the help of Stark and Hove (1991) relation rather than the actual measured compressive cylinder strength is that the measured concrete cylinder strength gave inconsistent results in some cases on account of probably improper capping of the loading surface of the concrete cylinder. The modulus of elasticity of concrete, E_{cm}, for push test specimen was calculated using BS EN 1992-1-1 provisions as given in Equation (4.2)

$$E_{cm} = 22\left[\frac{f_{cm}}{10}\right]^{0.3} \qquad (f_{cm} \text{ in MPa}) \tag{4.2}$$

The theoretical characteristic resistance, $P_{Rk,t}$ in Table 4.2, was calculated using Eurocode 4 formula for the characteristic resistance of headed studs in composite slab with profiled steel sheeting laid transverse to the beam. The Eurocode 4 employs two equations for determination of the shear connector resistance based on the concrete related failure or the stud shearing failure as the controlling failure mode. The smaller of the following two equations should be used for calculating the shear connector resistance as per Eurocode 4.

$$P_{Rk} = k_t \times \left[0.8 f_u \frac{\pi}{4} d^2\right] \tag{4.3}$$

$$P_{Rk} = k_t \times \left(0.29 \alpha d^2 \sqrt{f_{ck} E_{cm}}\right) \tag{4.4}$$

where:

$$k_t = \frac{0.7}{\sqrt{n_r}} \frac{b_0}{h_p}\left(\frac{h_{sc}}{h_p} - 1\right) < k_{t,\max} \tag{4.5}$$

where:

P_{Rk} = Characteristic resistance of a shear connector

f_u = Specified ultimate strength of the stud material but not greater than 450 N/mm^2 for composite slab with profiled sheeting.

d = Diameter of the shank of the stud, 16 mm $\leq d \geq$ 25 mm

$$\alpha = 0.2\left(\frac{h_{sc}}{d}+1\right) \quad \text{for } 3 \le \frac{h_{sc}}{d} \le 4$$

$$\alpha = 1 \quad \text{for } \frac{h_{sc}}{d} > 4$$

k_t = Reduction factor based on the dimensions of the steel deck and the number of shear connectors per trough when the profiled sheeting is transverse to the beam, only applicable when h_p is not greater than 85 mm and a width b_0 not less than h_p.

$k_{t,max}$ = Maximum value of reduction factor, for single shear stud per trough: k_t = 0.85 for sheeting thickness $t \le 1$ mm and k_t = 1 for $t > 1$ mm, for double shear studs per trough: k_t = 0.7 for $t \le 1$ mm and k_t = 0.8 for $t > 1$ mm. These values are valid for through welded shear stud not exceeding 20 mm in diameter.

f_{ck} = characteristic cylinder strength of concrete

n_r = Number of shear connectors in one rib, not exceeding 2.

b_0 = Mean width of a concrete rib (minimum width for re-entrant sheeting profiles)

h_{sc} = Overall nominal height of a stud connector

h_p = Overall depth of the profiled steel sheeting excluding embossments

For the push test PTS 1 having a single shear stud per rib with the mesh on top flange of the steel deck, the average ratio of $P_{Rk,e}$ / $P_{Rk,t}$ is 1.1, which suggests that the results predicted by Eurocode 4 are conservative; and the average characteristic slip capacity is 0.99 mm. While, in case of the push test PTS 2 having a single stud per trough with raised mesh, the average ratio of $P_{Rk,e}$ / $P_{Rk,t}$ is 1.23, and the average characteristic slip capacity is 2.69 mm. It means that the results obtained from Eurocode 4 for the push test PTS 2 are more conservative than that for the test PTS 1. The reason for low slip capacity in case of PTS 1 is that in this test LVDTs were placed at the back of the concrete slab near the free end, while LVDTs in PTS 2 were positioned on the sides of the concrete slab near the loading end. The strength predictions using Eurocode 4 are close to the experimental results for push tests with double studs, PTD 1 and PTD 2. The average ratio of $P_{Rk,e}$ / $P_{Rk,t}$ is 1.01 and 1.02, the average characteristic slip capacity is 1.40 mm and 1.98 mm for push tests PTD 1 and PTD 2 respectively.

The average ratio of $P_{Rk,e}$ / $P_{Rk,t}$ is 1.85 for single stud push tests with normal load PTSN 1 and PTSN 2 with corresponding average characteristic slip capacity of 2.8 mm and 2.03 mm respectively. It appears that the strength of the shear connector predicted using Eurocode 4 is highly conservative for the push test with a single stud per rib with normal load. For push tests PTDN 1 and PTDN 2 having double studs per trough with normal load, the average ratio of $P_{Rk,e}$ / $P_{Rk,t}$ is 1.17 with the average characteristic slip capacity of 2.07 mm and 1.5 mm respectively. It is clear that in case of push tests with normal load, the shear connector strength predicted using Eurocode 4 equation is less conservative for push tests with double studs per rib than for push tests having a single stud per trough.

For push tests with a single stud per rib having double layers of wire mesh, PSNM 1 and PSNM 2, the average ratio of $P_{Rk,e}$ / $P_{Rk,t}$ is 1.76 and 1.93 respectively. The average slip capacity for push tests PSNM 1 and PSNM 2 was computed as 3.25 mm and 1.9 mm respectively. In case of push tests PDNM 1 and PDNM 2 having pairs of shear connectors per rib with double layers of wire mesh and normal load, the average ratio of experimental over theoretical shear connector resistance $P_{Rk,e}$ / $P_{Rk,t}$ is 1.0 and 1.4 with corresponding slips of 2.6 mm and 1.4 mm respectively. Due to immediate pull-out of shear studs from the first rib in the push test PDNM 1, the strength enhancement on account of double layers of wire mesh could not be achieved and this was the reason that the shear connector resistance obtained from it matched well with the Eurocode 4 predictions. However, the shear connector resistance predictions obtained from Eurocode 4 for the push test PDNM 2, which had no studs in the first and last rib, were conservative with estimated load per stud being almost 70% of the actual shear connector resistance observed in the experiment. Generally, the Eurocode 4 predictions for push tests having a single stud per rib, double layers of wire mesh and normal load were highly conservative with estimated values nearly equivalent to half of the experimental results.

The predicted characteristic shear connector strengths using Eurocode 4 equations are compared with experimental characteristic resistances in Figure 4.12 and Table 4.2. It can be seen that Eurocode 4 estimations are generally conservative for all push tests, except double stud tests without normal load for which the results nearly match the experimental strengths. The average ratio of $P_{Rk,e}$ / $P_{Rk,t}$ is 1.38 with the minimum value

of 0.94 and the maximum value of 2.04, and the standard deviation is 0.37 with corresponding coefficient of variation as 26.7%.

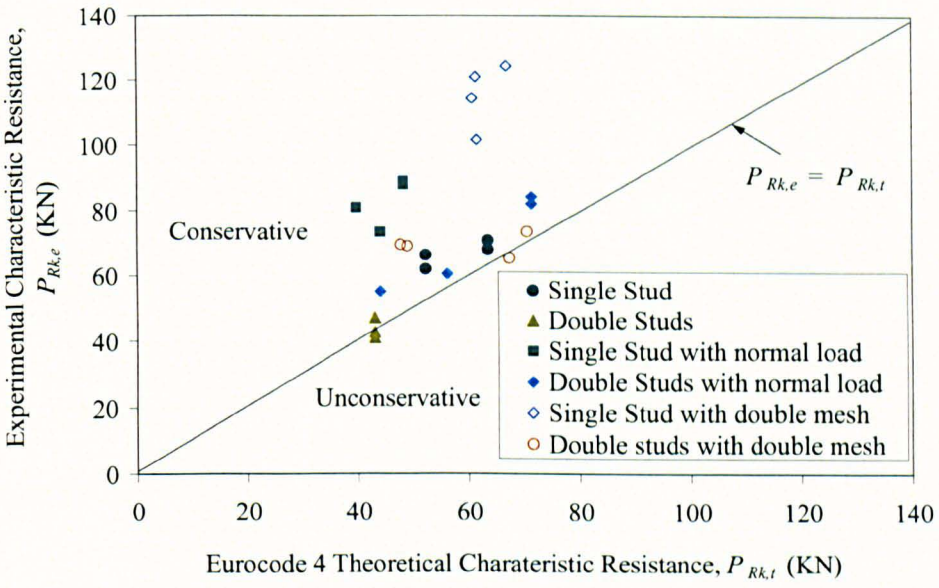

Figure 4.12 Experimental versus Eurocode 4 predicted characteristic resistance

4.4.2. Johnson and Yuan (1998) method

The results obtained from push tests are compared with the shear connector resistance obtained from Johnson and Yuan (1998), who developed theoretical models for predicting the shear connector resistance depending on the failure modes usually observed in the push test with transverse sheeting. The authors presented theoretical models for five failure modes namely shank shearing (SS), rib punching (RP), rib punching with shank shearing (RPSS), rib punching with concrete pull-out (RPCP), and concrete pull-out (CPT). However, due to concrete cone failure being the predominant failure mode in this study, only theoretical model for concrete pull-out failure (CPT) is described here. The strength of the shear stud according to this method is determined from the following equation:

$$P_r = k_{cp} P_{rs} \tag{4.6}$$

$$P_{rs} = \min \begin{pmatrix} 0.29 d^2 \sqrt{f_{ck} E_{cm}} \\ 0.8 \frac{\pi}{4} d^2 f_u \end{pmatrix} \tag{4.7}$$

$$k_{cp} = \frac{\eta_{cp} + \lambda_{cp}\left(1 - \eta_{cp}^{\ 2} + \lambda_{cp}^{\ 2}\right)^{0.5}}{1 + \lambda_{cp}^{\ 2}} \leq 1.0 \tag{4.8}$$

$$\eta_{cp} = \frac{0.56 v_{tu} h^2 \left(b_o - \frac{h}{4}\right)}{h_p N_r P_{rs}} \leq 1.0 \tag{4.9}$$

$$\lambda_{cp} = \frac{e_r T_y}{h_p P_{rs}} \tag{4.10}$$

$$T_y \cong 0.8 A_s f_u \tag{4.11}$$

$$v_{tu} = 0.8 f_{cu}^{\ 0.5} \leq 5 \tag{4.12}$$

where

P_{rs} = shank shearing resistance of the stud in a solid concrete slab

k_{cp} = reduction factor for CPT failure mode

η_{cp} = non-dimensional group for CPT failure mode

λ_{cp} = non-dimensional group for CPT failure mode

v_{tu} = shear strength of concrete

h = height of stud

b_o = average width of deck trough

h_p = height of steel deck

N_r = number of studs per rib

e_r = distance from center of stud to nearer wall of rib for favourable position studs

T_y = yield tensile strength of stud

f_{cu} = cube strength of concrete

The Johnson and Yuan predicted shear connector strengths are compared with the experimental shear connector resistances in Table 4.3 and Figure 4.13. The shear connector resistance predicted by Johnson and Yuan (1998) method is denoted by $P_{r\text{-}J\&Y}$

in Table 4.3. The mean ratio of the experimental over Johnson and Yuan predicted characteristic resistance is 1.27; the standard deviation is 0.30 and the coefficient of variation is 24%. The minimum and maximum values of the average ratio of experimental over predicted strength are 0.82 and 1.78 respectively. Generally, Johnson and Yuan method gave good estimation of the shear connector resistance. Particularly for push tests without normal load, the results obtained from Johnson and Yuan method were quite reasonable. The strengths predicted by Johnson and Yuan method were predominantly conservative. The strength predictions for push tests with normal load were highly conservative because the theoretical model on which Johnson and Yuan equations are based, does not have any consideration for the normal load.

Table 4.3 Comparison of experimental and Johnson and Yuan predicted strengths

Test Ref.	$f_{cm,cube}$ (MPa)	f_{cm} (MPa)	P_e (kN)	$P_{Rk,e}$ (kN)	$P_{r\text{-}J\&Y}$ (kN)	$P_{Rk,e}$ / $P_{r\text{-}J\&Y}$
PTS 1-1	34.0	25.5	75.7	68.1	69.7	0.98
PTS 1-2	34.0	25.5	78.8	70.9	69.7	1.02
PTS 2-1	27.5	20.6	69.0	62.1	59.6	1.04
PTS 2-2	27.5	20.6	73.8	66.4	59.6	1.11
PTD 1-1	27.9	20.9	52.1	46.9	50.0	0.94
PTD 1-2	27.9	20.9	45.4	40.9	50.0	0.82
PTD 2-1	28.0	21.1	52.2	47.0	50.2	0.94
PTD 2-2	28.0	21.1	47.3	42.6	50.2	0.85
PTSN 1-1	25.4	19.0	97.8	88.0	55.6	1.58
PTSN 1-2	25.4	19.0	98.9	89.0	55.6	1.60
PTSN 2-1	21.2	15.9	90.0	81.0	46.6	1.74
PTSN 2-2	23.2	17.4	81.7	73.5	51.3	1.43
PTDN 1-1	28.2	21.1	61.3	55.2	50.3	1.10
PTDN 1-2	37.0	27.7	67.3	60.6	57.9	1.05
PTDN 2-1	58.8	44.1	91.3	82.2	62.7	1.31
PTDN 2-2	63.2	47.4	93.7	84.3	62.7	1.34
PSNM 1-1	32.8	24.60	113.0	101.7	68.0	1.49
PSNM 1-2	36.1	27.08	138.4	124.6	72.6	1.72
PSNM 2-1	32.3	24.23	127.2	114.5	67.3	1.70
PSNM 2-2	32.7	24.53	134.6	121.1	67.9	1.78
PDNM 1-1	46	34.50	72.7	65.4	61.8	1.06
PDNM 1-2	48.8	36.60	81.8	73.6	62.5	1.18
PDNM 2-1	30.7	23.03	77.3	69.6	52.8	1.32
PDNM 2-2	31.6	23.70	76.8	69.1	53.6	1.29
					Mean	**1.27**
					Standard Deviation (SD)	**0.30**
					Coefficient of Variation (COV)	**24%**

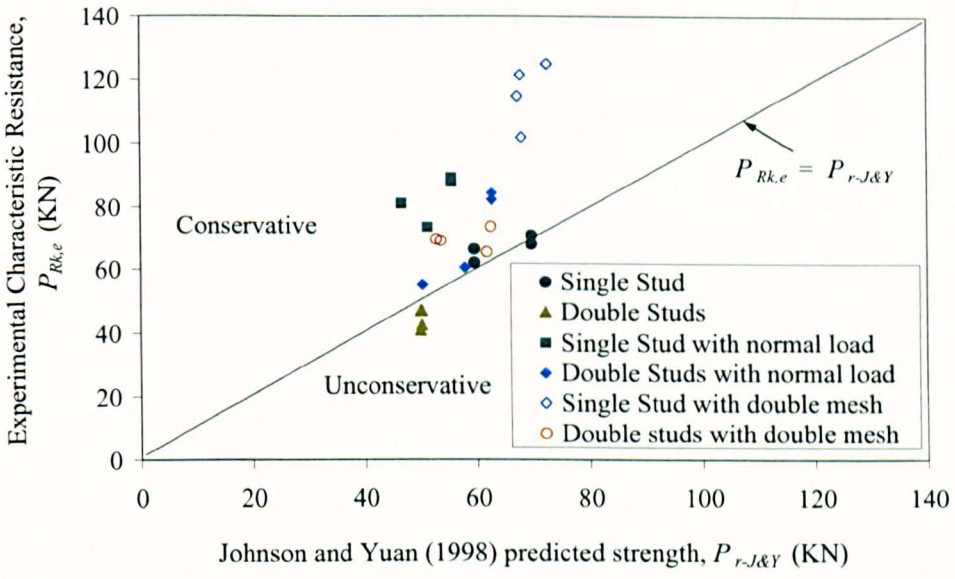

Figure 4.13 Experimental versus Johnson and Yuan predicted characteristic resistances

4.4.3. AISC (2005) Provisions

The shear connector resistances obtained from push tests are compared with the strengths of shear stud calculated using AISC (2005) provisions. This code takes into account different positions of the shear stud namely favourable, central and unfavourable within a sheeting pan and the default value for the shear connector resistance is set equal to the equation for unfavourable position stud. The AISC (2005) code makes no distinction between shear stud strength equations for studs placed in a solid concrete or composite slab and uses a common equation for both types of slabs. According to AISC (2005) provisions, the nominal strength of the shear stud embedded in solid concrete or in a composite slab is given by following equation:

$$Q_n = 0.5 A_{sc} \sqrt{f'_c E_c} \leq R_g R_p A_{sc} F_u \qquad (4.13)$$

where

A_{sc} = cross-sectional area of stud *shear connector*, mm^2

f'_c = specified minimum compressive strength of concrete, MPa

E_c = modulus of elasticity of concrete = $0.043 w_c^{1.5} \sqrt{f'_c}$, MPa

F_u = *specified minimum tensile strength* of a stud shear connector, MPa

R_g = Group effect factor having values equal to 1, 0.85 and 0.7 for one, two and three or more studs welded in a steel deck rib with the deck oriented perpendicular to the steel shape.

R_p = Position effect factor

= 1 for studs embedded in solid concrete slab

= 0.75 for studs welded in *composite* slab with the deck oriented perpendicular to the *beam* and $e_{mid\text{-}ht} \geq 50$ mm (favourable position studs)

= 0.6 for studs welded in *composite* slab with the deck oriented perpendicular to the *beam* and $e_{mid\text{-}ht} < 50$ mm (unfavourable position studs)

$e_{mid\text{-}ht}$ = distance from the edge of stud shank to the steel mid-height of deck web, in the load bearing direction of the stud (in other words, in the direction of maximum moment for a simply supported beam), mm

w_c = weight of concrete per unit volume ($1500 \leq w_c \leq 2500$ kg/m^3)

The shear stud strengths obtained from push test experiments are compared with strengths obtained from AISC (2005) in Table 4.4 and Figure 4.14. The shear connector resistance estimated from AISC (2005) provisions is denoted by $Q_{n\text{-}AISC}$ in Table 4.4. The average ratio of experimental over AISC predicted shear connector strengths is 1.02 with a minimum and maximum value of 0.6 and 1.71 respectively; the standard deviation is 0.32, and the coefficient of variation is 31.2%. Although the mean of the experimental over predicted strength is 1.02, which is close 1 as desired. But, the coefficient of variation is significantly large, which indicates high scatter in the data. Apart from single stud push tests with normal load, the AISC (2005) predicted shear connector strengths were unconservative in all cases as shown in Figure 4.14, which suggests that experimental shear connector resistances are considerably less than the shear stud strengths predicted by AISC (2005) provisions.

Table 4.4 Comparison of experimental and AISC (2005) predicted strengths

Test Ref.	$f_{cm,cube}$ (MPa)	f_{cm} (MPa)	P_e (kN)	$P_{Rk,e}$ (kN)	$Q_{n\text{-}AISC}$ (kN)	$P_{Rk,e}/Q_{n\text{-}AISC}$
PTS 1-1	34.0	25.5	75.7	68.1	86.2	0.79
PTS 1-2	34.0	25.5	78.8	70.9	86.2	0.82
PTS 2-1	27.5	20.6	69.0	62.1	67.5	0.92
PTS 2-2	27.5	20.6	73.8	66.4	67.5	0.98
PTD 1-1	27.9	20.9	52.1	46.9	68.6	0.68
PTD 1-2	27.9	20.9	45.4	40.9	68.6	0.60
PTD 2-1	28.0	21.1	52.2	47.0	69.1	0.68
PTD 2-2	28.0	21.1	47.3	42.6	69.1	0.62
PTSN 1-1	25.4	19.0	97.8	88.0	60.9	1.44
PTSN 1-2	25.4	19.0	98.9	89.0	60.9	1.46
PTSN 2-1	21.2	15.9	90.0	81.0	47.5	1.71
PTSN 2-2	23.2	17.4	81.7	73.5	54.2	1.36
PTDN 1-1	28.2	21.1	61.3	55.2	69.6	0.79
PTDN 1-2	37.0	27.7	67.3	60.6	81.3	0.75
PTDN 2-1	58.8	44.1	91.3	82.2	81.3	1.01
PTDN 2-2	63.2	47.4	93.7	84.3	81.3	1.04
PSNM 1-1	32.8	24.60	113.0	101.7	82.9	1.23
PSNM 1-2	36.1	27.08	138.4	124.6	92.0	1.35
PSNM 2-1	32.3	24.23	127.2	114.5	81.5	1.41
PSNM 2-2	32.7	24.53	134.6	121.1	82.6	1.47
PDNM 1-1	46	34.50	72.7	65.4	81.3	0.80
PDNM 1-2	48.8	36.60	81.8	73.6	81.3	0.90
PDNM 2-1	30.7	23.03	77.3	69.6	76.9	0.90
PDNM 2-2	31.6	23.70	76.8	69.1	79.5	0.87
					Mean	**1.02**
					Standard Deviation (SD)	**0.32**
					Coefficient of Variation (COV)	**31.3%**

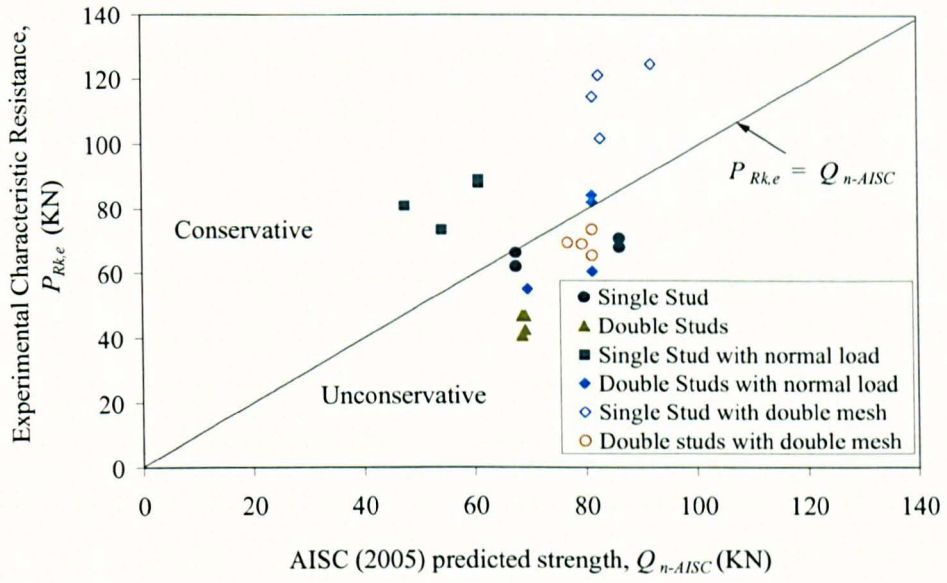

Figure 4.14 Experimental versus AISC (2005) predicted characteristic resistances

It is interesting to note that the shear connector resistance obtained from AISC (2005) equations results in the same shear stud strength for push tests with single or double studs per rib, when the measured compressive cylinder strength, f_{cm} is less than 24 N/mm^2 (f'_c or f_{ck} =16 N/mm^2) because left side of the Equation (4.13) dominates in that case. It is evident from push test results of this study that the strength of stud placed in pairs per rib is approximately 70% of the strength of the stud in push tests with a single stud per trough, when no normal is used. Further, it is widely accepted that the load per stud obtained from push tests with pairs of shear connectors per rib is always less than the one with a single stud per trough. This experimental behaviour where load per stud of the push test with double shear studs per rib being always less than the strength obtained from push tests with a single stud per trough, unless pairs of shear connector are placed sufficiently apart and beyond the practical limits, does not comply with shear stud strength predictions obtained from AISC (2005) provisions.

4.5. Conclusions

The results obtained from 24 push tests have been discussed, and compared with various shear connector strength prediction methods. It was found that the position of the wire mesh within the depth of the concrete slab does not have significant influence on the shear connector resistance. The application of normal load as 10% of the maximum horizontal shear load resulted in almost 40% enhancement in the strength of the shear

connector placed as a single stud per rib and 23% in case of the push test with double studs per rib. However, the application of normal load, in addition to the shear load, did not affect the ductility of the shear connector.

The use of double layers of wire mesh embedded inside the concrete slab resulted in strength improvement of 18% when compared with the push test with a single layer of mesh while keeping all other variables constant. The position of the normal load, placement of high yield reinforcement bar at the bottom trough and the push test arrangement having different configurations such as studs in all ribs, no stud in the first rib, and no stud in the first and last rib, did not have much influence on the behaviour of the shear stud. The shear connector resistances obtained from experimental push tests conducted in this study were compared with the existing strength prediction methods. The Eurocode 4 equations and Johnson and Yuan (1998) method gave good predictions of the shear connector resistance and these predictions were generally conservative. The shear stud strength predictions obtained from AISC (2005) were mostly unconservative except predictions for a push test with a single stud per rib having normal load.

Chapter 5

Development of finite element model

Chapter 5
Development of finite element model

5.1. Introduction

In this chapter, a three-dimensional finite element model is developed using the general purpose finite element program ABAQUS for a push test with profiled sheeting. The main purpose is to attempt different concrete material models, and analysis procedures to facilitate selection of an appropriate modelling technique for the push test with profiled sheeting. The results obtained from the finite element analysis are compared with the experimental results. Discussion of different material models of concrete is also presented. The concrete material model, and analysis procedure that give results which are comparable to the experimental results in terms of shear capacity, load-slip behaviour and failure modes will be considered as the most appropriate combination for modelling the push test with trapezoidal metal decking.

5.2. Summary of experimental investigation

The preliminary finite element model was developed from push tests conducted by Lloyd and Wright (1990) and the results were used to verify the accuracy of the developed finite element model. The general arrangement of the push test consisted of two composite slabs connected to a steel beam with load applied to the top of the beam as shown in Figure 5.1. The push tests conducted by Lloyd and Wright (1990) used 19 × 100 mm long headed shear studs welded through-deck in composite slabs with profiled sheeting. The size of the steel beam was 178×102×19 kg/m UB. A typical slab thickness of 115 mm was used for all push tests. The steel profiled sheeting had a depth of 50 mm, average width of 150 mm and sheeting thickness of 1.2 mm as shown in Figure 5.2, and it was oriented perpendicular to the longitudinal axis of the beam. All dimensions in Figure 5.1 and Figure 5.2 are in mm.

The standard mesh fabric A98, A142 and A193 having diameters equal to 5, 6 and 7 mm respectively with centre to centre spacing of 200 mm both ways were used in different push test specimens. The mesh reinforcement A98 was placed directly on top of the steel deck, while remaining two mesh reinforcements A142 and A193 were placed under the head of the shear stud.

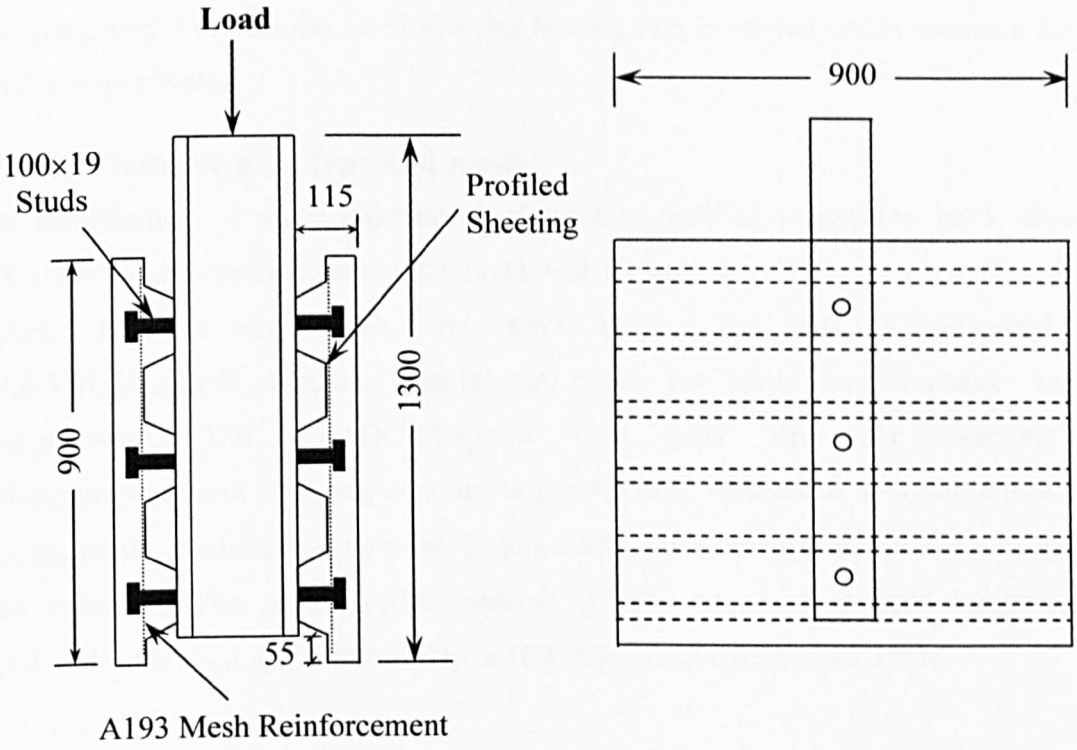

Figure 5.1 General arrangement of the push test (Lloyd and Wright, 1990)

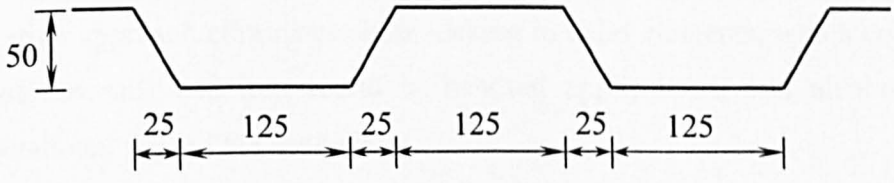

Figure 5.2 Dimensions of the profiled sheeting (Lloyd and Wright,1990)

5.3. Finite element model

The general purpose finite element program ABAQUS/CAE is used to create the geometry of the push test. The finite element model is developed by assuming a quarter symmetry across the centre line of the web of the steel beam. It is assumed that the shear capacity of the stud would be independent of the number of shear studs used in a push test and the load is equally transferred from the steel beam to each shear stud, therefore, only one shear stud is modelled. The steel beam and shear connector are created in the same part with different material properties. The concrete slab, profiled sheeting and welded wire mesh fabric are created as three separate parts. All parts are assembled together to form a complete model for the push test specimen. The

convergence study for the mesh size and loading rate is carried out in section 6.2.3 and 6.2.4 respectively.

5.3.1. Finite element type and mesh

A combination of three-dimensional eight-node reduced integration brick elements (C3D8R) and three-dimensional six-node wedge elements (C3D6) are used to model the shear stud, concrete slab and steel beam. The ABAQUS/Standard and ABAQUS/Explicit element libraries are used for static and dynamic analysis respectively. The ABAQUS/Explicit uses only first-order elements for stress/displacement analyses, contrary to the ABAQUS/Standard in which either linear or quadratic elements can be used. In this study, the linear geometric order is used for all elements. The linear wedge element (C3D6) uses the reduced integration in ABAQUS/Explicit and is referred to as (C3D6R) in all dynamic analyses.

The brick elements give a solution of comparable accuracy at a better rate of convergence and less computational time than the other elements. Therefore, the brick elements are used in most of the regions of the push test and the wedge elements are only used where the geometry of the component necessitated their use. The reduced integration approach eliminates shear locking in solid elements, which could otherwise become too stiff and less useful in bending applications, and also it reduces the computational time of the analysis.

The profiled metal decking is modelled with four-node doubly curved thin shell element with reduced integration (S4R). Generally, this type of element is very useful for thin-walled structures, like profiled sheeting, which undergo large geometrically nonlinear deformation. The welded wire mesh fabric is modelled with a two node three-dimensional truss element (T3D2). The thickness of the head of the stud shear connector is taken as 0.5 times the diameter of the stud and its width is taken as 1.5 times the stud diameter as suggested by Menzies (1971). The complete finite element model is shown in Figure 5.3.

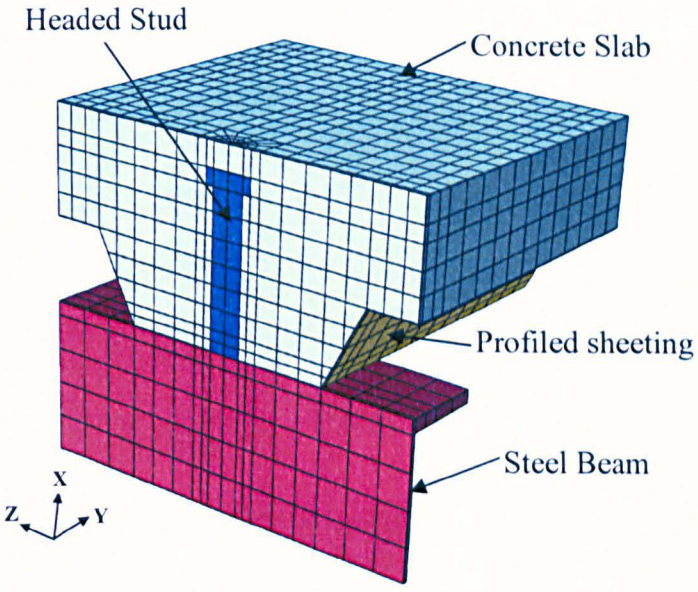

Figure 5.3 The finite element model of the push test

5.3.2. Boundary conditions

All nodes of the steel beam web at its mid depth, indicated by surface 1 in Figure 5.4(a), are restricted from moving in the axis of symmetry X. All nodes of the steel beam, profiled sheeting, concrete slab and headed shear stud which lie on the other symmetry surface, represented by surface 2 in Figure 5.4(b), are restrained from moving in the Y direction due to symmetry. The surface of the concrete slab and profiled sheeting, where it is bedded to the ground, is restrained from translating in the Z direction as indicated by surface 3 in Figure 5.4(c).

In push test experiments, the web and top flange of the profiled sheeting are prevented from deforming by the adjacent concrete slab, which in itself is held in position by headed shear studs. Based on this experimental observation, all profiled sheeting and concrete slab nodes which lie on surface 4 in Figure 5.4(d), are restricted from translating in the Z direction and rotating in the Y direction. As a matter of fact, the application of this boundary condition not only prevents premature concrete cracking in the portion of the concrete slab which rests on the floor but also inhibits any unwanted overturning of the trapezoidal rib. The push test specimen is loaded by applying a

uniform load or displacement on the top surface of the beam, termed as "loading surface" in Figure 5.4(e).

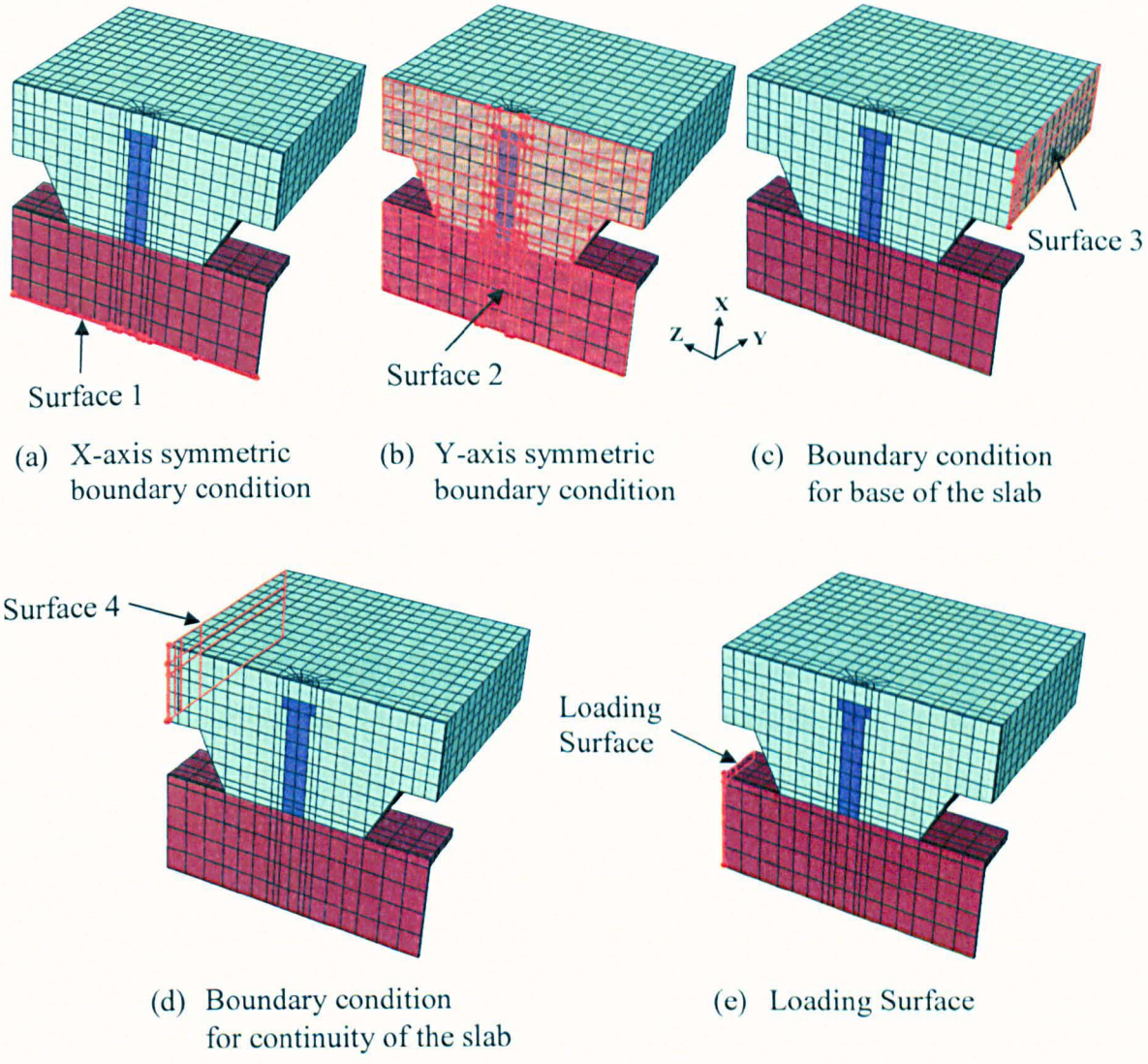

(a) X-axis symmetric boundary condition

(b) Y-axis symmetric boundary condition

(c) Boundary condition for base of the slab

(d) Boundary condition for continuity of the slab

(e) Loading Surface

Figure 5.4 Boundary conditions and loading surface

5.3.3. Constraints and contact interactions

Once all parts of the push test model are positioned together into an assembly, appropriate constraints and contact interactions are applied to various components. To prevent relative slip between the profiled sheeting and shear stud, the nodes of the profiled sheeting around the circumference of the shear stud shaft are tied to the nodes of the shear stud at its base by means of a tie constraint. This is equivalent to the actual push test experiment, where shear stud remains tied to the profiled sheeting by welding.

It has been observed by Jayas and Hosain (1988) that the separation of the concrete behind the shear stud occurs even at very low load levels. Therefore, the nodes behind the shear stud, in the direction of the loading side of the steel beam, are detached from the surrounding concrete nodes. However, all other nodes of the shear stud remain attached to the surrounding concrete slab nodes. This approach has previously been used successfully by El-lobody and Lam (2002); Lam and El-lobody (2005); and El-lobody and Young (2006).

A contact pair algorithm is used to define surface to surface contact between the top of profiled sheeting and the bottom surface of concrete slab. Generally, the harder material is selected as the master surface and the softer material as a slave surface. But the ABAQUS manual suggests that the master and slave surfaces should not be chosen only on the basis of being either soft or hard material, but the stiffness of the material should also be taken into consideration. The profiled metal decking, which is composed of very thin steel sheeting, is less stiff than the concrete slab even though steel is a harder material than the concrete. For this reason, the bottom surface of the concrete slab is taken as a master surface, while the top surface of the steel deck is treated as a slave surface.

The interaction properties between the steel deck and concrete slab surfaces are defined by the behaviour normal and tangential to the surfaces. The default normal behaviour is assumed which consists of a 'hard' contact pressure-over closure relationship. This type of normal behaviour allows minimum penetration of the slave surface into the master surface. The penalty frictional formulation is used, and the coefficient of friction between the steel deck and concrete slab is taken as 0.5 as recommended in Eurocode 4. In order to prevent profiled sheeting nodes from penetrating the steel beam surface, the contact between top of the beam flange and bottom of the profiled sheeting is defined by using default interaction properties.

The wire mesh using a truss element is embedded inside the solid elements of the concrete slab by an embedded constraint. With this constraint, the nodes of a truss element are kinematically constrained to the nodes of the solid element. This means that the displacement of the truss element node is an average value of the displacement of neighbouring nodes of the solid element in which it is embedded. Therefore, the slip and

debonding of the mesh fabric with respect to the concrete slab does not occur and are ignored in this study because they do not influence the results significantly.

5.4. Material models for steel parts

The stress-strain behaviour of the headed shear stud, profiled sheeting and steel beam is similar. They behave as linear elastic materials until yielding, followed by plastic behaviour. The behaviour of the steel beam is of no particular interest in this study; therefore, it is treated as linear elastic, assuming that its modulus of elasticity is 5 times higher than the usual modulus for structural steel. The shear stud and profiled sheeting were treated as elastic perfectly plastic materials. The modulus of elasticity for shear stud and profiled was taken as 200 GPa. The yield stress for profiled sheeting and shear stud was assumed to be 350 MPa and 470 MPa respectively. The material properties for steel parts were obtained from El-lobody and Young (2006) because preliminary finite element model is compared with results obtained from El-lobody and Young (2006). The density of all steel components was taken as 7800 kg/m^3.

5.5. Material models for concrete

The concrete material model is the most important model for the push test simulation. Since, the push test generally fails due to concrete related failure, the selection of a suitable material model for concrete is essential for the accuracy of the finite element analysis. Different concrete material models are presented and discussed together with material properties.

5.5.1. Elastic properties of concrete

The elastic properties of concrete mainly depend on its constituent materials especially the aggregates. The modulus of elasticity of concrete, E_{cm}, for all push test models was calculated using BS EN 1992-1-1 provisions as given in Equation (5.1). Poisson's ratio of concrete was assumed to be 0.2 and normal weight concrete of density 2400 kg/m^3 was assumed for all concrete grades. These elastic properties are common to all material models of concrete used in this study.

$$E_{cm} = 22\left[\frac{f_{cm}}{10}\right]^{0.3} \qquad (f_{cm} \text{ in MPa}) \qquad (5.1)$$

$$f_{cm} = f_{ck} + 8 \qquad \text{(MPa)} \qquad (5.2)$$

where,

f_{cm} = Mean value of concrete cylinder compressive strength

f_{ck} = Characteristic compressive cylinder strength of concrete at 28 days

5.5.2. Elastic-Plastic model

The elastic-plastic model includes the elasticity and plasticity parameters. The elasticity is defined by modulus of elasticity of the material. While, plastic parameters are based on the plasticity theory, conventionally developed to consider the behaviour of ductile metals. The standard plasticity models consist of three essential conditions such as a yield surface, a flow rule and a hardening rule. The yield surface encompasses the elastic region of the material behaviour. All stresses inside this surface are elastic, and stresses which reach this surface become plastic. The yield surface defines when the plastic deformation would begin. A flow rule determines the orientation of the plastic deformation. Particularly, it defines the direction of the plastic strain which may be associated, defined as normal to the yield surface, or non-associated. A hardening rule defines how the yield surface would evolve with the plastic deformation.

The classical plasticity model in ABAQUS uses von Mises yield surface with associated plastic flow, and perfect plasticity or isotropic hardening behaviour. The model can be used in ABAQUS/Standard and ABAQUS/Explicit. The first part of the stress-strain curve ranging up to 40% of the compressive cylinder strength, f_c is linear and material response can be specified by modulus of elasticity. The second part of the curve is nonlinear and ranges from $0.4f_c$ to f_c. The strain corresponding to the maximum compressive strength was calculated using BS EN 1992-1-1 provisions. In case of both static and dynamic analyses, the isotropic hardening rule was used to define yield stress and plastic strain for the push test specimen S_5 of Lloyd and Wright (1990) having cube strength of 43.6 MPa as shown in Table 5.1. The mean compressive cylinder strength of concrete, f_c is assumed to be 80% of the cube strength.

Table 5.1 Material Properties for Elastic-plastic model of concrete

Yield stress	Plastic Strain
$0.4f_c$ = 13.95 MPa	0
f_c = 34.88 MPa	0.00153

5.5.3. Drucker- Prager Hardening model

The Drucker-Prager model is suitable for materials in which the compressive strength is greater than the tensile strength, and pressure dependent materials which become stronger as the pressure increases. This model is often used for concrete, soil or granular materials. It is available in both ABAQUS/Standard and ABAQUS/Explicit. The model uses Drucker-Prager yield surface, and is commonly used for concrete where failure is determined by normal and shear stresses. The linear Drucker-Prager with associated plastic flow is used for this study. This model also allows for volume change in the inelastic range.

The material properties of the concrete are specified in two parts. Firstly, the linear elastic properties are defined by Young's modulus of elasticity of the concrete. Secondly, the nonlinear part of the stress-strain curve of concrete is specified by "Drucker-Prager Hardening" sub-option of the Drucker-Prager model. The response of the concrete material is considered elastic up to $0.4f_c$, followed by the hardening behaviour with a maximum compressive strength of f_c and finally, the softening response is defined. The stress-strain response of concrete is determined from BS EN 1992-1-1 provisions as shown in Table 5.2. The parameters for linear yield surface of the Drucker-Prager model (β and K) are obtained from Hu et al (2003). The angle of internal friction (β) is taken as 20° and the ratio of flow stress in triaxial tension to that in compression (K) is taken as 0.8.

Table 5.2 Material Properties for Drucker-Prager Hardening model

Yield stress (MPa)	**Absolute Plastic Strain**
$0.4f_c = 13.95$	0
$f_c = 34.88$	0.00153
20.2	0.00303

5.5.4. Concrete Smeared Cracking model

The Concrete Smeared Cracking model in ABAQUS/Standard is intended for applications in which concrete is subjected to essentially monotonic straining and the material exhibits either tensile cracking or compressive crushing. Primarily, it is designed for reinforced concrete structures, but it can be used for plain concrete as well.

The compressive plastic straining in this model is controlled by a compression yield surface.

Cracking is the most important feature of this model, which is assumed to occur when the stress reaches a failure surface termed as "crack detection surface". The direction of the crack is stored for subsequent calculations, once a crack has been detected. Subsequent cracking at the same point is restricted to the direction perpendicular to the stored direction. One of the limitations of this model is that the cracks are irrecoverable and no more than three cracks can occur at a single point. The model is called smeared crack model because it does not track individual "macro" cracks.

The compressive stress and plastic strain values are calculated in the same way as that for the elastic-plastic model. The effect of interaction between the mesh reinforcement and concrete is modeled by introducing tension stiffening in the model. The tension stiffening can be specified by means of either post failure stress-strain curve or by applying a fracture energy cracking criterion. In this model, the tension stiffening is specified using a fracture energy criterion by assuming a linear decrease of the tensile stress to zero stress, at a displacement of 1.2mm. In this model, only linear loss of strength after cracking can be used. Further detail about tensile behaviour of concrete is given in section 5.5.5.3. The shape of the failure surface for the Concrete Smeared Cracking model is defined using four failure ratios. The default values given in ABAQUS are used for failure ratios as shown in Table 5.3.

Table 5.3 Failure ratios for Concrete Smeared Cracking model

Ratio 1	Ratio 2	Ratio 3	Ratio 4
1.16	0.09	1.28	0.3333

where,

Ratio 1 is ratio of the ultimate biaxial compressive stress to the uniaxial compressive ultimate stress.

Ratio 2 is absolute value of the ratio of uniaxial tensile stress at failure to the uniaxial compressive stress at failure.

Ratio 3 is ratio of the magnitude of a principal component of plastic strain at ultimate stress in biaxial compression to the plastic strain at ultimate stress in uniaxial compression.

Ratio 4 is ratio of the tensile principal stress value at cracking in plane stress, when the other nonzero principal stress component is at the ultimate compressive stress value, to the tensile cracking stress under uniaxial tension.

5.5.5. Concrete Damaged Plasticity model

The Concrete Damaged Plasticity model in the ABAQUS/Standard and ABAQUS/Explicit is capable of modelling concrete and other quasi-brittle materials in a variety of structures. This model uses the concepts of isotropic damaged elasticity together with isotropic tensile and compressive plasticity to model the inelastic behaviour of concrete. It is intended for applications in which concrete is subjected to arbitrary loading conditions, including cyclic loading. The model takes into consideration the degradation of the elastic stiffness induced by plastic straining both in tension and compression. It also accounts for stiffness recovery effects under cyclic loading.

Concrete damaged plasticity model is based on two main failure mechanisms namely tensile cracking and compressive crushing of concrete. The evolution of the yield surface is controlled by two hardening variables, which cause failure under tensile and compressive loading. The post-failure behaviour under compression is defined by a softening stress-strain response. The strain softening behaviour of the cracked concrete in tension is specified by the tension stiffening in terms of either post-failure stress-strain behaviour in tension or a fracture energy cracking criterion.

5.5.5.1 Plasticity Parameters

The concrete damaged plasticity model follows a non-associated plasticity flow rule, whereby the plastic potential function and yield surface do not coincide with each other. Concrete can show a significant volume change, commonly referred to as dilation, when subjected to severe inelastic stress states. The dilation can be represented by an appropriate plastic potential function. Conversely, the yield surface can be defined by

the hardening rule. In this study, the dilation angle was taken as 40°, while default values were assumed for all other plasticity parameters as shown in Table 5.4.

Table 5.4 Plasticity parameters for Concrete Damaged Plasticity model

Dilation Angle, ψ	**Eccentricity,** ε	f_{b0}/f_{c0}	K	**Viscosity Parameter,** μ
40°	0.1	1.16	2/3	0

where,

Dilation Angle, ψ is defined in the p-q plane and value is entered in degrees.

Eccentricity, ε is flow potential eccentricity is a small positive number that defines the rate at which the hyperbolic flow potential approaches its asymptote.

f_{b0}/f_{c0} σ_{b0}/σ_{c0} is the ratio of initial equi-biaxial compressive yield stress to initial uniaxial compressive yield stress.

K K_c is the ratio of the second stress invariant on the tensile meridian, q(TM), to that on the compressive meridian, q(CM), at initial yield for any given value of the pressure invariant p such that the maximum principal stress is negative, $\hat{\sigma}_{max} < 0$. It must satisfy the condition $0.5 < K_c \leq 1.0$.

Viscosity Parameter is used for the visco-plastic regularization of the concrete constitutive equations in Abaqus/Standard analyses. This parameter is ignored in Abaqus/Explicit.

5.5.5.2 Compressive behaviour

The stress-strain behaviour of plain concrete in uniaxial compression was determined from Equation (5.3), given by BS EN 1992-1-1. The schematic diagram of the stress-strain relationship for nonlinear structural analysis of concrete is shown in Figure 5.5.

$$\frac{\sigma_c}{f_{cm}} = \frac{k\eta - \eta^2}{1 + (k-2)\eta} \tag{5.3}$$

where,

σ_c = Compressive stress in the concrete

η = $\dfrac{\varepsilon_c}{\varepsilon_{c1}}$

ε_c = Compressive strain in the concrete

ε_{c1} = Compressive strain in the concrete at the peak stress f_c,

$$\varepsilon_{c1} = 0.7 f_{cm}{}^{0.31} \leq 2.8$$

k = $\dfrac{1.05 E_{cm} \times |\varepsilon_{c1}|}{f_{cm}}$

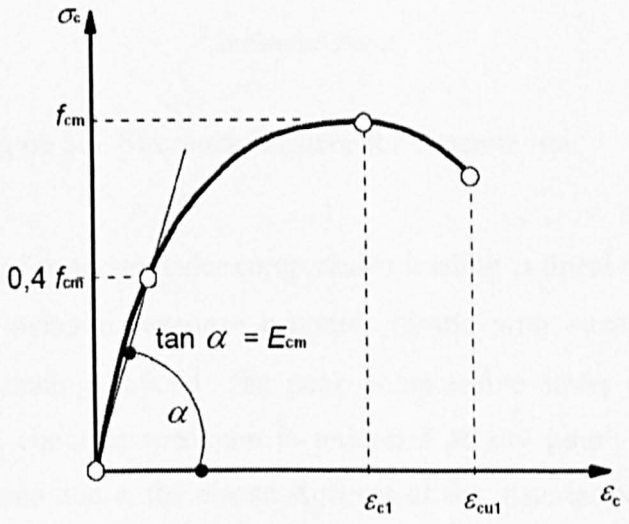

Figure 5.5 Schematic representation of the stress-strain relation for structural analysis of concrete material (BS EN 1992-1-1)

Expression (5.3) is valid for $0 < |\varepsilon_c| < |\varepsilon_{cu1}|$ where ε_{cu1} is the nominal ultimate strain.

According to BS EN 1992-1-1, the nominal ultimate strain, ε_{cu1} for concrete characteristic compressive cylinder strength, f_{ck} of 12 to 50 MPa can be taken as 0.0035. For the characteristic compressive strength, f_{ck} greater than 50 MPa, the ultimate compressive strain, ε_{cu1} can be calculated from Equation 5.4. The uniaxial compressive stress versus inelastic strain curve for the push test specimen having a mean compressive cylinder strength, f_{cm} of 34.9 MPa is shown in Figure 5.6.

$$\varepsilon_{cu1} = 2.8 + 27\left[\frac{(98 - f_{cm})}{100}\right]^4 \qquad (5.4)$$

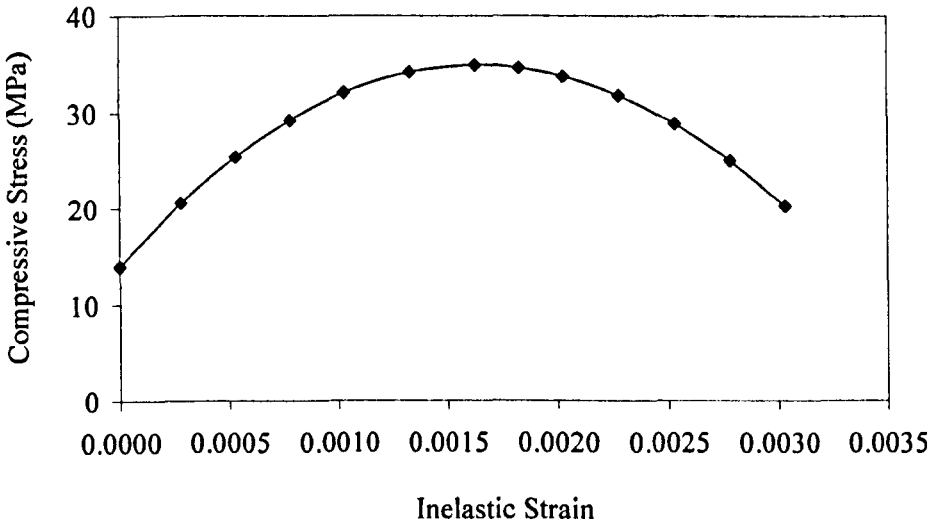

Figure 5.6 Stress-strain curve for concrete slab

The uniaxial resposne of concrete under compressive loading is linear up to initial yield stress, σ_{c0}. Then, the material response becomes plastic with stress hardening and followed by strain softening beyond the peak compressive stress σ_{cu} as shown in Figure 5.7. When the concrete specimen is unloaded at any point on the softening branch of the stress strain curve, the elastic stiffness of the material becomes degraded and is characteristed by the compressive damage variable, d_c. The zero value of the compressive damage variable respresents undamaged material and value equal to one denotes total loss of the compressive strength.

If E_0 is the elastic stiffness of the undamaged material and ε_c is the total compressive strain, the stress-strain relation can be computed from Equation (5.5). In this study, the stress-strain curve and elastic stiffness were determined as per BS EN 1992-1-1 provisions, therefore, the compressive damage variable, d_c was calculated from Equation (5.5) as given in the ABAQUS manual.

$$\sigma_c = (1 - d_c) E_o (\varepsilon_c - \tilde{\varepsilon}_c^{pl}) \qquad (5.5)$$

where, $\tilde{\varepsilon}_c^{pl}$ = Compressive equivalent plastic strain.

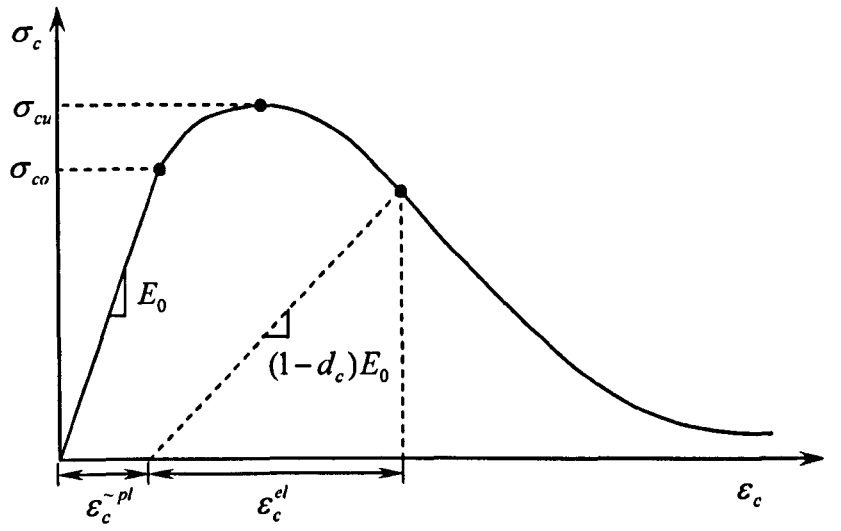

Figure 5.7 Response of concrete to uniaxial loading in compression (ABAQUS manual)

The Concrete Damaged Plasticity model in ABAQUS requires the yield stress versus inelastic strain curve and the damage parameter versus inelastic strain curve to define the compressive behaviour and concrete compression damage respectively. The compressive inelastic (or crushing) strain, $\tilde{\varepsilon}_c^{in}$ is calculated from Equation (5.6) as suggested in the ABAQUS manual.

$$\tilde{\varepsilon}_c^{in} = \tilde{\varepsilon}_c^{pl} + \frac{d_c}{1-d_c}\frac{\sigma_c}{E_0} \tag{5.6}$$

5.5.5.3 Tensile behaviour

The ABAQUS manual suggests the use of a tension stiffening approach for problems with no or little reinforcement in the significant regions of the model. For unreinforced or lightly reinforced concrete problems, it is appropriate to express the brittle behaviour of concrete in terms of fracture energy rather than specifying a stress-strain relation in tension. According to Hillerborg *et al* (1976), the fracture energy G_f, can be defined as the energy required to develop a unit area of crack, in order to obtain a stress-free crack. The area under the unloading part of the stress-crack opening curve represents the fracture energy of a particular concrete grade.

The softening response of concrete using the fracture energy concept can be defined in a number of ways. The most convenient way is to define tensile cracking by a linear approximation, in which the linear loss of strength takes place after cracking as shown

in Figure 5.8(a). Although, reasonably accurate results could be obtained using linear softening approach, but the material response tends to be too stiff. Softening behaviour of concrete in tension can be specified in more detail using a bilinear function, derived by Hillerborg (1985) and is presented in Figure 5.8(b). A more realistic method of defining tension softening is to use an exponential expression, which is experimentally derived by Cornelissen *et al* (1986) and is illustrated in Figure 5.8(c). In this study, the post-failure tensile behaviour is defined with the help of an exponential function as proposed by Cornelissen *et al* (1986).

The axial tensile strength of the concrete is calculated using BS EN 1992-1-1 provisions and it is multiplied by a dynamic amplification factor of 1.2 to account for the rate effects. This approach is suggested in the ABAQUS Example problem manual. Furthermore, it is assumed that stress can no longer be transferred beyond 10% of the axial tensile strength. The tensile stress and the cracking displacement have been obtained from Equation (5.7), and are plotted in Figure 5.9. The tensile damage variable, d_t is obtained from equation $d_t = 1-\sigma_t / f_t$. The tensile damage parameter versus cracking displacement curve for the push test is shown in Figure 5.10. The fracture energy G_f is determined from the expression $G_f = G_{fo}\,(f_{cm}/f_{cmo})^{0.7}$ as per MC 90 CEB-FIP design code, where f_{cmo} is the base value of mean compressive cylinder strength having a constant value of 10 MPa and G_{fo} is the base value of the fracture energy, which depends on the maximum size of the aggregate.

$$\frac{\sigma_t}{f_t} = f(w) - \frac{w}{w_c} f(w_c) \tag{5.7}$$

$$f(w) = \left[1 + \left(\frac{c_1 w}{w_c}\right)^3\right] \exp\left(-\frac{c_2 w}{w_c}\right) \tag{5.8}$$

where,

w is the crack opening displacement

w_c is the crack opening displacement at which stress can no longer be transferred
$w_c = 5.14\, G_f / f_t$ for normal weight concrete

c_1 is a material constant and $c_1 = 3.0$ for normal density concrete

c_2 is a material constant and $c_2 = 6.93$ for normal density concrete

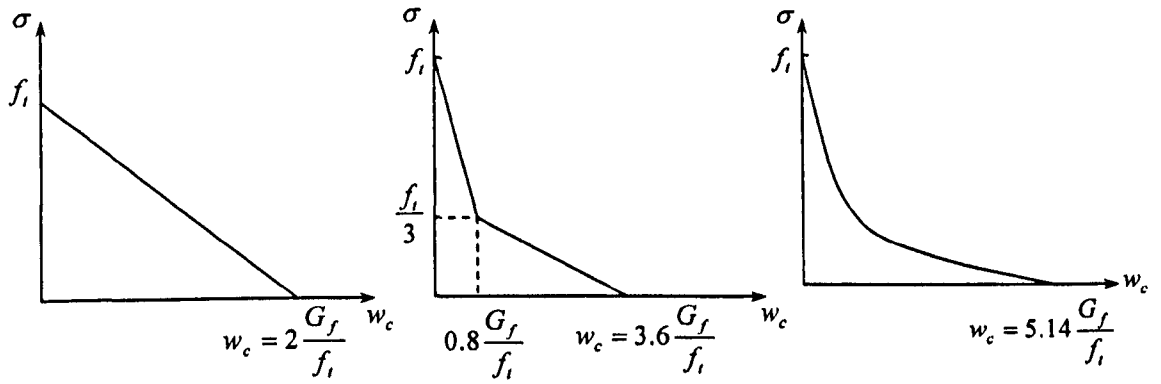

(a) Linear function (b) Bilinear function (c) Exponential function

Figure 5.8 Linear (ABAQUS manual), Bilinear (Hillerborg, 1985) and exponential (Cornelissen *et al*, 1986) tension softening model

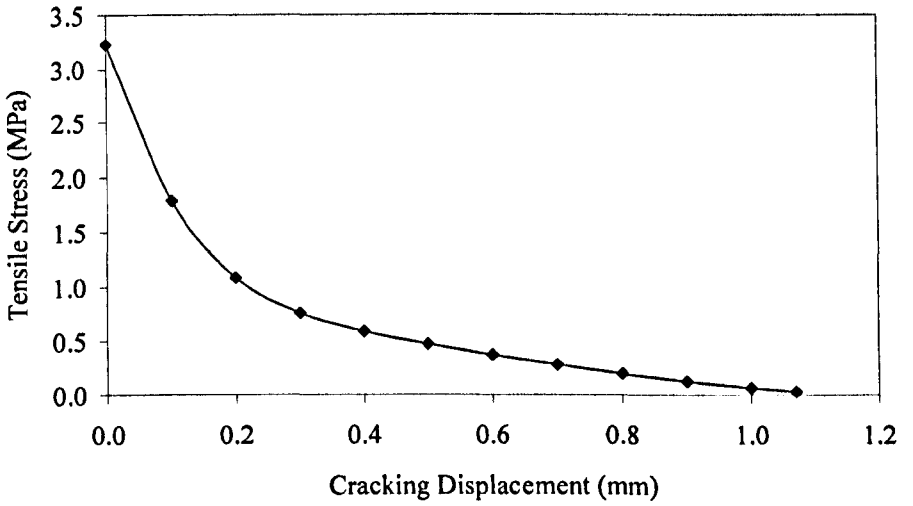

Figure 5.9 Tensile stress versus cracking displacement curve

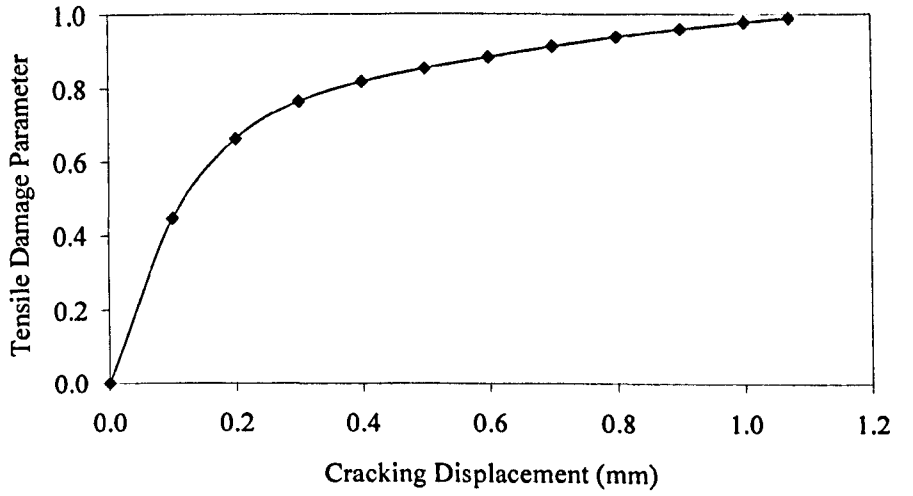

Figure 5.10 Tensile damage parameter versus cracking displacement curve

5.5.6. Brittle Cracking model

The Brittle Cracking model for concrete is only available in the ABAQUS/Explicit. The model is intended for applications where the material behaviour is dominated by tensile cracking. It assumes that the compressive behaviour of concrete is linear elastic, which does not represent the real behaviour of concrete material and is a major drawback of this model. It is most suitable for applications where predominant material behaviour is brittle cracking so that the assumption that the compressive behaviour is always linear elastic is reasonable. A simple brittle failure criterion allows the removal of elements from a mesh, which helps in avoiding large distortion of the elements. Though primarily intended for the analysis of reinforced concrete structures, this model can also be used for modelling other materials such as ceramics or brittle rocks.

Defining post failure stress-strain behaviour in tension introduces unreasonable mesh sensitivity in the results when there is very little or no reinforcement in the significant regions of the finite element model. In that case, the mesh refinement leads to narrower crack bands rather than a converged solution. Thus, the post-failure tensile behaviour in the Brittle Cracking model was specified by the tensile stress versus displacement curve as shown in Figure 5.9 instead of a stress-strain relation.

The ABAQUS/Explicit describes the brittle failure criterion as a crude way of modelling failure. This should be used in a situation, where not removing the elements that can no longer carry tensile stress, can cause excessive distortion of the elements and subsequent termination of the analysis. However, just because an element loses its ability to carry tensile stress does not mean it cannot carry compressive loads. Therefore, it is not appropriate to use the *BRITTLE FAILURE option, pertaining to removal of cracked elements, in this analysis as it can lead to inaccurate results when the material is expected to carry compressive loads after it fails in tension.

The Brittle Cracking model uses shear retention model that must be specified to define post-cracking shear behaviour. The post-cracked shear modulus is reduced as the crack opens, and is a function of the opening strain across the crack and uncracked shear modulus. Shear retention can be defined in terms of power law or piecewise linear form. In this study, the shear retention behaviour is specified in the power law form which is given by Equation (5.9) and is graphically represented in Figure 5.11.

$$\rho(e_{nn}^{ck}) = \left(1 - \frac{e_{nn}^{ck}}{e_{\max}^{ck}}\right)^{p} \tag{5.9}$$

where, ρ is the shear retention factor, e^{ck}_{max} is the crack opening strain at which the post-cracking shear modulus is equal to zero and complete loss of aggregate interlock occurs. The exponent p equivalent to one represents the linear loss and having a value greater than one indicates the exponential loss of the shear stiffness.

In the absence of combined tension and shear experiments, which are difficult to perform, to calibrate the post-cracking shear behaviour, the ABAQUS manual suggests testing different values for material parameters p and e^{ck}_{max}. The values of material properties tried in this study for the Brittle Cracking model are 0.005, 0.01 and 0.04 for e^{ck}_{max}, and 1 and 5 for exponent p. The analysis terminated due to excessive distortion of elements for all the values except for the combination $e^{ck}_{max} = 0.04$ and $p = 1$.

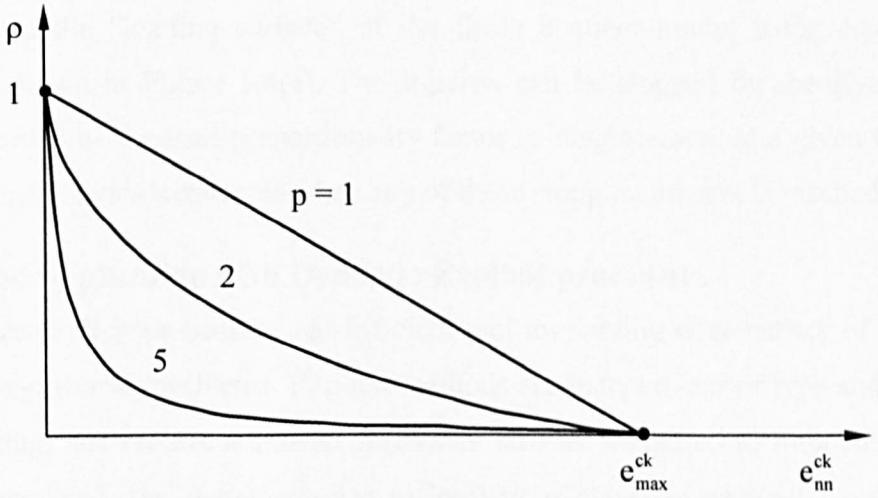

Figure 5.11 Power law form of the shear retention model

5.6. Load application and analysis procedure

The push test can be analysed using traditional nonlinear static implicit procedures or dynamic explicit procedures with slow load application. The load in the finite element model can be applied under load or displacement control, in the same way as it is applied in the experiments. In all static analyses, the load is applied to the model in increments using static RIKS procedure. In contrast, the push test specimen is loaded by applying a uniform displacement to the loading surface of the beam in case of all dynamic explicit analyses. This section explains load application using two analysis

procedures namely static RIKS and dynamic Explicit, and their suitability for a particular type of analysis.

5.6.1. Load application with Static RIKS procedure

The static RIKS method is suitable for geometrically and materially nonlinear static problems involving buckling and collapse behaviour, where load-displacement response shows a negative stiffness. It uses the load as an additional unknown and solves simultaneously for loads and displacements. Therefore, another quantity must be used to observe the progress of the analysis for obtaining a converged solution. The ABAQUS uses the arc length along the static equilibrium path in the load–displacement space, which means it performs the iterations until equilibrium is reached. This approach gives solution irrespective of the stable or unstable response of the structure.

The analysis is started by specifying initial arc length increment. This increment is adjusted if the solution fails to converge. The static uniform load is applied in increments to the "loading surface" of the finite element model using static RIKS method as shown in Figure 5.4(e). The solution can be stopped by specifying either maximum value of the load proportionality factor or displacement at a given degree of freedom. The analysis terminates when any of these stopping criteria is reached.

5.6.2. Load application with Dynamic Explicit procedure

The dynamic explicit procedure is an efficient tool for solving wide variety of nonlinear structural engineering problems. Explicit methods are independent of type and duration of the loading, and require a smaller increment size as compared to implicit methods. On the other hand, the increment size in implicit methods is generally governed by accuracy and convergence considerations. Therefore, the computational cost per increment in explicit methods is relatively smaller than implicit methods.

The ABAQUS/Explicit is especially well suited for problems involving complex contact interactions and post-buckling behaviour, highly nonlinear quasi-static problems and problems having materials with degradation and failure. In explicit methods, contact interactions are formulated with greater ease than implicit procedures. The ABAQUS/Explicit is particularly suitable for structures which undergo complex contact interactions as the load is applied. The ABAQUS/Explicit is also very effective in solving unstable post-buckling problems, where the stiffness of the structure varies

drastically with the application of loads and it is very efficient for solving quasi-static problems involving complicated contact interactions as well. The ABAQUS/Explicit can solve quasi-static problems quicker than the ABAQUS/Standard. The explicit procedure requires fewer system resources and resolves complex contact problems more easily than the implicit procedure. The ABAQUS/Explicit is also well-suited for modelling materials involving stiffness degradation and failure, which often cause severe convergence issues in implicit procedures.

Push tests have conventionally been modelled using well-established nonlinear static implicit procedures even though they are not entirely suitable for use in the post-failure range and complex contact interactions. Since the push test with profiled sheeting is a quasi-static problem involving complicated contact interactions, post-buckling behaviour and material degradation, the use of dynamic explicit procedure will not only be appropriate for such kind of problem but will also lead to a computationally efficient solution. The quasi-static solution is required for a push test, which is ensured in the explicit dynamic program ABAQUS/Explicit by slow load application in order to keep inertia forces to a minimum level. The dynamic explicit method is especially useful for modelling brittle materials like concrete, which fail by sudden drop of the load carrying capacity, and as a result, the kinetic energy of the system is increased significantly.

In the dynamic explicit analysis, the top surface of the beam is displaced by applying a uniform velocity to the "loading surface" with the help of a smooth amplitude function to ensure a quasi-static solution as shown in Figure 5.4(e). Mainly, the quasi-static solution limits the kinetic energy of the push test to a small value throughout the analysis. Different loading rates have been tried and the optimum rate is found out to be 0.25 mm/sec. The total force applied to the specimen is calculated by summing up the reaction force on the loading surface.

The computational efficiency in the quasi-static analysis using dynamic explicit procedure is ensured by either increasing the time increment or by introducing mass scaling in the model. In either case the ratio of the kinetic energy to the internal energy (ALLKE/ALLIE) must always be checked and should be less than 10%. The mass scaling is used to increase the mass of the model artificially without compromising on the adequate level of accuracy of the simulation. Therefore, the mass scaling equal to

1000, 100 and 10 is applied to the entire model in all dynamic explicit analyses while monitoring the ratio ALLKE/ALLIE. A mass scaling of 10 is found to be the most appropriate for the finite element model of the push test and the ratio of the kinetic energy to the internal energy is less than 1% which is within acceptable limit of 10% as shown in Figure 5.12.

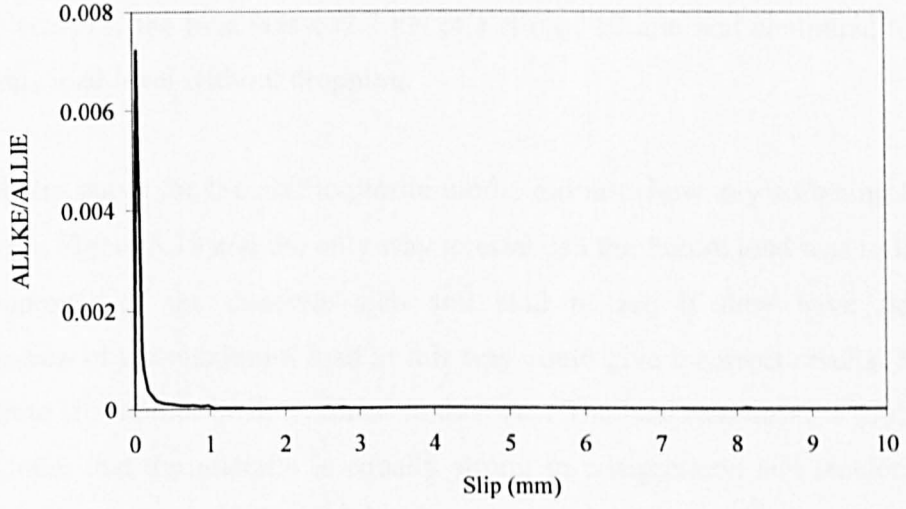

Figure 5.12 The ratio of kinetic over internal energy versus slip for dynamic analysis

5.7. Comparison of different material models and analysis procedures

The static and dynamic analysis have been performed using different concrete material models to facilitate the selection of an appropriate concrete model and analysis procedure for the push test with profiled sheeting. The concrete material model plays an important role in the accurate prediction of the behaviour of the push test which predominantly fails by formation of concrete failure cones around the shear stud. Static and dynamic analyses are carried out using the Elastic-Plastic (EP), Drucker-Prager (DP) and Concrete Damaged Plasticity (CDP) models. The Concrete Smeared Cracking (CSC) and Brittle Cracking (BC) models are used to perform static and dynamic analysis respectively.

The comparison of different concrete material models and analysis procedures in terms of the load per stud versus slip is shown in Figure 5.13. Initially, the results from the elastic-plastic model are compared with the experiment. The elastic-plastic model for concrete has previously been used by Lam and El-lobody (2005) to model the push test

with solid slab and their results have shown close agreement with experiments. It is evident from Figure 5.13 that the load-slip behaviour of the elastic-plastic model for both static and dynamic analysis follow the same trend, except that the dynamic analysis continued until the end of the analysis and the static analysis terminated due to convergence difficulties. For the elastic-plastic model using static procedure, the analysis stopped at a load per stud of 123 kN with a slip of about 6 mm. In case of the dynamic analysis, the load was 132.7 kN at a slip of 10 mm and continued to increase beyond this load level without dropping.

The load-slip curve for the elastic-plastic model did not show any softening behaviour as shown in Figure 5.13 and the only way to establish the failure load was to look at the stress contours of the concrete slab and stud to see if they have failed. The determination of the maximum load in this way could give incorrect results. Moreover, the accurate slip cannot be determined in this way. The basic assumption of the elastic-plastic model that the material is equally strong in compression and tension does not seem to hold true for modelling of the concrete slab in a push test. For this reason, the load per stud obtained from the finite element analysis is greater than that observed in the experiment, although the initial stiffness of the load-slip behaviour of the finite element model matched well with the experiment. Therefore, the Elastic-Plastic model is not appropriate for modelling the composite slab in a push test.

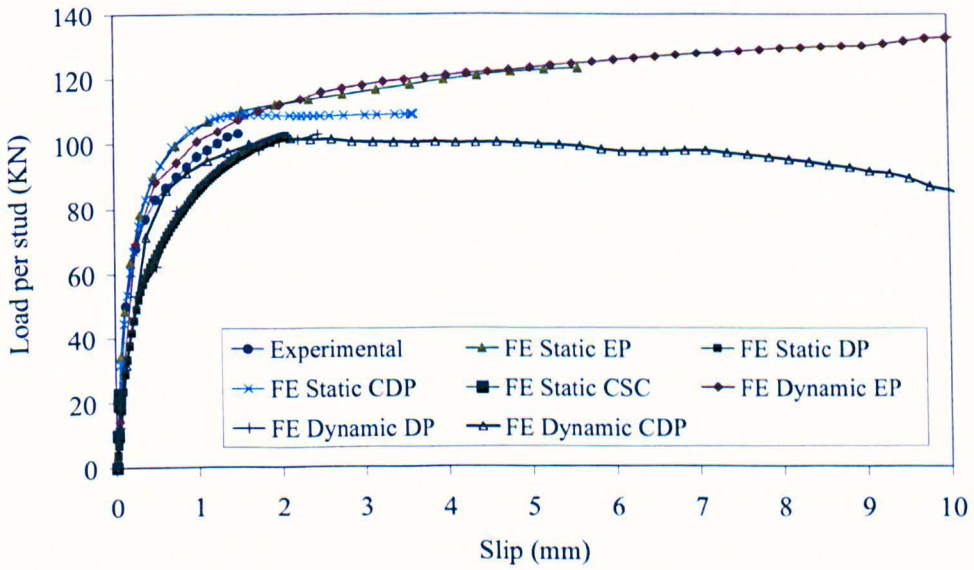

Figure 5.13 Comparison of different material models and analysis procedures with push test experiment

The Drucker-Prager model gave reasonable results. The load per studs for the static analysis was 102.4 kN at a slip of 2.06 mm and for the dynamic analysis it was 102.6 kN with a slip of 2.45 mm. The results of the static and dynamic analysis were about the same. It was difficult to distinguish between load-slip curves obtained from the static and dynamic analysis as shown in Figure 5.13. The shape of the load-slip curve in case of the Drucker-Prager model is also similar to the experimental load-slip behaviour with slightly lower stiffness in case of the finite element analysis. The load-slip behaviour did not exhibit softening once it reached a certain load level and it was not clear that whether the analysis stopped because of convergence issues or material failure. However, the results obtained from the Drucker-Prager model were quite close to the experiment and the model could be used for modelling the push test with steel deck. However, the accurate determination of the slip at failure would be difficult in case of the Drucker-Prager model.

The static analysis using the Concrete Smeared Cracking model resulted in an extremely low load per stud and slip; and the load-slip curve is hardly visible in Figure 5.13. The analysis terminated prematurely at a load of 27.7 kN and a slip of 0.042 mm. The reason for early termination of the analysis is that the model does not allow the element to be cracked further in the same direction, and the number of cracks in an element is restricted to only three. Hence, the Concrete Smeared Cracking model is not suitable for modelling the push test with profiled sheeting.

The Brittle Cracking model, only available in the ABAQUS/Explicit, gave very high load per stud of 238.8 kN, which is far beyond the experimental load per stud of 103 kN, and the slip at failure was 3.5 mm. Due to unreasonably high load per stud, the results from the Brittle Cracking model are not presented in Figure 5.13 in order to make better comparison of other material models with experimental results. Although, the Brittle Cracking model showed softening behaviour in the load-slip curve, which helped in determination of the slip, the failure load was extremely high. The assumption related to a linear elastic compressive behaviour, and the high value for the crack opening strain of 0.04 could be the reasons for such a high load per stud achieved in this model. However, this was the only way to perform the analysis as it terminated prematurely at other crack opening strains of 0.0005 and 0.01. Based on the

unreasonably high load, it is concluded that the Brittle Cracking model cannot be used for modelling the push test with profiled sheeting.

The Concrete Damaged Plasticity model using a static procedure showed a similar trend to that of the experiment in terms of the load-slip behaviour with slightly high stiffness in case of the numerical model. After reaching the maximum load, the load-slip curve became almost flat and the analysis stopped probably because of complex contact interactions between the concrete slab and steel deck. The load per stud obtained from this model with static procedure was 108.8 kN at a slip of 3.6 mm, which is higher than the experimental failure load of 103.0 kN. As the load-slip behaviour does not exhibit softening, the exact determination of slip cannot be obtained by using this method. It is observed that the Concrete Damaged Plasticity model with static procedure experiences convergence difficulties on account of complex contact interactions in a push test.

The load-slip behaviour obtained from dynamic explicit analysis of the push test using the Concrete Damaged Plasticity model compared very well with the experimental load-slip curve as shown in Figure 5.13. The model resulted in a load per stud of 101.4 kN at a slip of 2.12 mm, which is very close to the experimental load per stud of 103.0 kN with a slip of 1.50 mm. The load-slip behaviour showed softening response, which is essential for accurate determination of the slip at failure. The post-failure behaviour of the push test was also appropriately modelled by using this material model with dynamic explicit procedure. In addition, the modelling of the post-failure behaviour also enabled correct identification of failure modes in a push test.

The results obtained from the Concrete Damaged Plasticity with dynamic explicit procedure resembled more closely to the experimental results as compared to all other material models used for concrete in this study. It is concluded that the Concrete Damaged Plasticity model accurately predicts the shear connector resistance, load-slip behaviour and failure modes in a push test with trapezoidal metal decking. Based on the analyses conducted so far, the Drucker-Prager model with static procedure and the Concrete Damaged Plasticity model with dynamic explicit procedure have been selected for validation against several push test experiments.

The finite element model developed in this study is verified against push test experiments conducted by Lloyd and Wright (1990). The shear capacity, load-slip behaviour of the headed stud and failure modes have been investigated. Details of the concrete slab width and depth, concrete cube strength, size of wire mesh and the experimental shear connector resistance obtained from Lloyd and Wright (1990) are presented in Table 5.5

The results obtained from finite element analysis and El-lobody and Young (2006) are compared with experimental push tests conducted by Lloyd and Wright (1990) as shown in Table 5.6. The experimental shear connector resistance is denoted by P_{TEST}. The capacity of the shear connector obtained from the static analysis using the Drucker-Prager model, the ABAQUS Explicit dynamic analysis using the Concrete Damaged Plasticity model and the analysis conducted by El-lobody and Young (2006) are abbreviated as $P_{FE\text{-}DP\text{-}S}$, $P_{FE\text{-}CDP\text{-}D}$ and $P_{FE\text{-}E\&Y}$ respectively.

Table 5.5 Details of push test and strength of stud (Lloyd And Wright, 1990)

Test Ref.	Slab Size		Mesh size	Experimental load per stud (kN)			P_{TEST}, Average Exp. Load (kN)
	B (mm)	D (mm)		Test 1	Test 2	Test 3	
S_1	450	115	A98	96.3	96.2	93.3	95.3
S_2	675	115	A98	83.3	83.8	78.3	81.8
S_3	900	115	A98	79.2	100	90.5	89.9
S_4	1125	115	A98	95.8	91.7	100	95.8
S_5	1350	115	A98	100.2	108.5	100	102.9
S_6	900	115	A193	97.3	101	98	98.8
S_7	900	115	A142	100.5	95	89.2	94.9
S_8	900	115	A142	76.5	94	91.3	87.3
S_9	600	115	A142	85.7	90.7	88.7	88.4

Table 5.6 Comparison of shear connector capacity between FE analysis and experiment

Test Ref.	f_{cu} (MPa)	P_{TEST} (kN)	$P_{FE\text{-}CDP\text{-}D}$ (kN)	$P_{FE\text{-}DP\text{-}S}$ (kN)	$^{1}P_{FE\text{-}E\&Y}$ (kN)	$P_{TEST}/P_{FE\text{-}CDP\text{-}D}$	$P_{TEST}/P_{FE\text{-}DP\text{-}S}$	$P_{TEST}/{}^{1}P_{FE\text{-}E\&Y}$
S_1	44.8	95.3	102.6	103.3	94.0	0.93	0.92	1.01
S_2	35.3	81.8	90.5	91.0	88.1	0.90	0.90	0.93
S_3	39.5	89.9	96.4	96.7	93.2	0.93	0.93	0.96
S_4	46.3	95.8	104.0	105.0	94.1	0.92	0.91	1.02
S_5	43.6	102.9	101.4	102.4	97.3	1.01	1.01	1.06
S_6	43.8	98.8	101.6	102.8	94.0	0.97	0.96	1.05
S_7	37.3	94.9	95.2	96.0	92.0	1.00	0.99	1.03
S_8	39.6	87.3	96.5	96.7	93.2	0.90	0.90	0.94
S_9	39.8	88.4	96.6	96.8	93.3	0.92	0.91	0.95
Mean			---			0.94	0.94	0.99
SD			---			0.039	0.036	0.047
COV(SD/Mean)			---			0.041	0.039	0.048

[1] Finite element analysis shear connector resistance obtained from El-lobody and Young (2006)

The results obtained from the finite element analysis using both static analysis with Drucker-Prager model and dynamic analysis with Concrete Damaged Plasticity model showed close agreement with the experimental results in terms of shear connector capacities as shown in Table 5.6. A maximum difference of 10% was observed between the numerical and experimental results. The mean of the experimental load over numerical load was 0.94 for both static and dynamic analysis. The coefficient of variation (COV) for $P_{TEST}/P_{FE\text{-}DP\text{-}S}$ and $P_{TEST}/P_{FE\text{-}CDP\text{-}D}$ was 0.039 and 0.041 respectively. These results suggest that the shear connector strength predictions obtained from the finite element analysis using both static analysis with Drucker-Prager model and dynamic explicit analysis with Concrete Damaged Plasticity model are quite reasonable. However, it is difficult to accurately estimate the slip at failure in case of the static analysis using Drucker-Prager model, which terminates after reaching a certain load level and it does not exhibit any softening behaviour.

It is clear from the results of the finite element analysis that the shear connector resistance is largely dependent on the concrete strength. In Table 5.5 and 5.6, the slab dimensions and concrete strength for the push test specimens S_5 and S_6 were almost the same with slight difference in the concrete strength. The failure loads obtained by El-lobody and Young (2006) for tests S_5 and S_6 were 97.3 kN and 94 kN respectively

with corresponding concrete cube strengths of 43.6 MPa and 43.8 MPa. The results by El-lobody and Young (2006) showed that the concrete strength reduced but the shear connector capacity increased which can be difficult to justify in the case of the numerical modelling even though it can happen in experiments as the actual concrete strength in the slabs may be different to that of the cube strength. The discrepancy could be due to the way the maximum load was determined manually in the static analysis.

The failure mode of the push test was also investigated. In experiments, it has been observed that the push test usually fails due to concrete cone failure, where the tensile force acting on the stud forces the concrete slab to move up leaving behind a cone of concrete. The finite element analysis confirmed this failure mode as indicated by stress contours at failure for specimen S_5 in case of both static analysis with Drucker-Prager model and dynamic explicit analysis with Concrete Damaged Plasticity as shown in Figure 5.14. It can be observed that the maximum stresses in the concrete are at the bottom half of the stud, which suggests concrete crushing behind the stud.

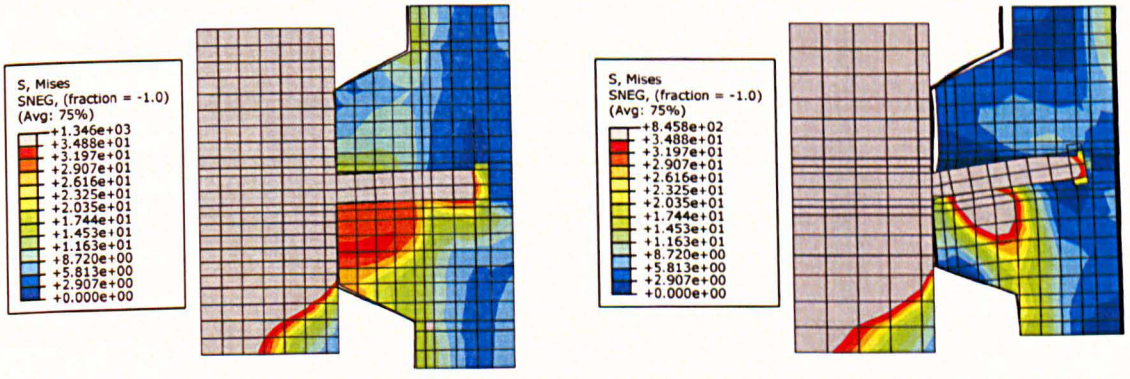

(a) Static analysis with Drucker-Prager model

(b) Dynamic analysis with Concrete Damaged Plasticity model

Figure 5.14 Stress Contours for push test specimen S_5 at failure

The deformed shape of the specimen S_5 at the end of the dynamic analysis is shown in Figure 5.15. It can be observed that as the load increases, the steel deck tends to separate from the concrete slab. Eventually, the bond between the steel deck and the concrete slab breaks, and the concrete slab is delaminated from the steel deck and as a result the concrete slab tries to move up, and ride over the steel deck as shown in Figure 5.15. This phenomenon observed during the dynamic analysis of the push test exactly resembles the experimental behaviour of the push test with profiled sheeting.

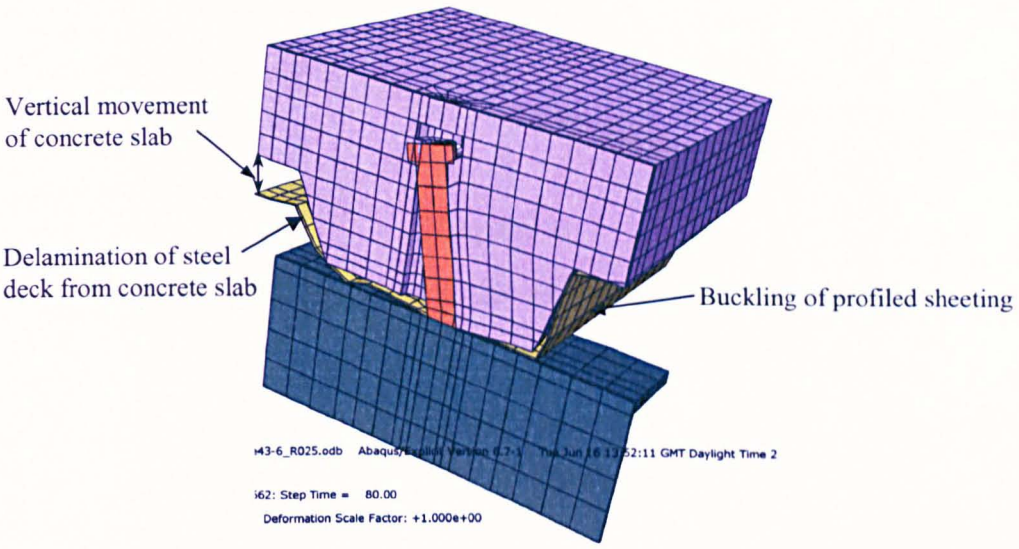

Figure 5.15 Post-failure behaviour of push test S_5

5.8. Summary and conclusions

The analysis of the push test with profiled sheeting was performed using different concrete material models and analysis procedures. The main purpose of this chapter was to develop a three-dimensional finite element model and to facilitate the selection of an appropriate concrete material model and analysis procedure for push test with profiled metal decking. Static and dynamic explicit procedures were tried using the Elastic-Plastic, Drucker-Prager and Concrete Damaged Plasticity models. Concrete Smeared Cracking and Brittle Cracking models were used to carry out static and dynamic analysis respectively. The results obtained from the Drucker-Prager model and Concrete Damaged Plasticity model showed good agreement with experimental results. All other material models failed to capture the behaviour of the push test properly.

Although, the Drucker-Prager model gave reasonable results in terms of the shear capacity, the post-failure behaviour, which is crucial for exact determination of the slip and correct identification of the failure mode in a push test, could not be obtained from this model. The Concrete Damaged Plasticity model using dynamic explicit procedure accurately predicted the shear connector resistance, load-slip behaviour and failure modes of the push test with profiled sheeting. However, before this model could be used for a parametric study, it should be validated against a variety of push test experiments having different stud positions, profiled sheetings, sizes of the stud, number of studs in a trough and concrete strengths.

Chapter 6

Validation of finite element model

Chapter 6
Validation of finite element model

6.1. Introduction

This chapter deals with validation of the finite element model developed in Chapter 5 against push test experiments conducted in this research and previous experimental studies undertaken by other authors. The convergence study for the mesh size and loading rate is also carried out to select the reasonable mesh size and loading rate. It is evident from the preliminary verification of the finite element model in Chapter 5 that the three-dimensional finite element model of the push test with profiled metal decking using the Concrete Damaged Plasticity material model and the dynamic explicit analysis procedure gives results that are comparable to the push test experiment. To assess the accuracy and reliability of the developed finite element model, it is validated against a variety of push test experiments with different steel decks and shear stud dimensions, positions of shear stud within a rib and push test arrangements. Once validated properly, the finite element model will be considered suitable for predicting the strength and ductility of the shear connector embedded in a composite slab with profiled sheeting and will also be used to conduct a parametric study in the next chapter.

6.2. Finite element model of the push test

Push test experiments explained in Chapter 3 are used to create the finite element model. It is decided to use the full scale model of the push test by assuming a half or quarter symmetry, wherever possible, rather than the model with just one sheeting rib used in Chapter 5. Modelling all troughs gives better estimation of the shear connector behaviour, particularly failure modes and slip at the steel-concrete interface, as compared to using only one sheeting rib.

The geometry of horizontal push tests conducted in this study is created by assuming a half symmetry along the longitudinal centre line of the steel beam. Complete finite element models for push tests with single and double studs per tough are shown in Figure 6.1 and Figure 6.2 respectively. To view the steel deck, shear studs and wire mesh clearly, the concrete slab is raised slightly, which rests directly on top of the profiled sheeting in the actual model.

Since the behaviour of the push test remains unaffected by the geometry of the steel beam, the modelling of the beam web is ignored and only top flange of the steel beam, which is connected to shear studs, is modelled. The concrete slab and profiled sheeting are modelled as separate parts. The steel beam flange and shear studs are created in the same part. All parts are assembled together to form a complete model for the horizontal push test specimen. All parts are meshed with the same element types as that of the finite element model developed in Chapter 5.

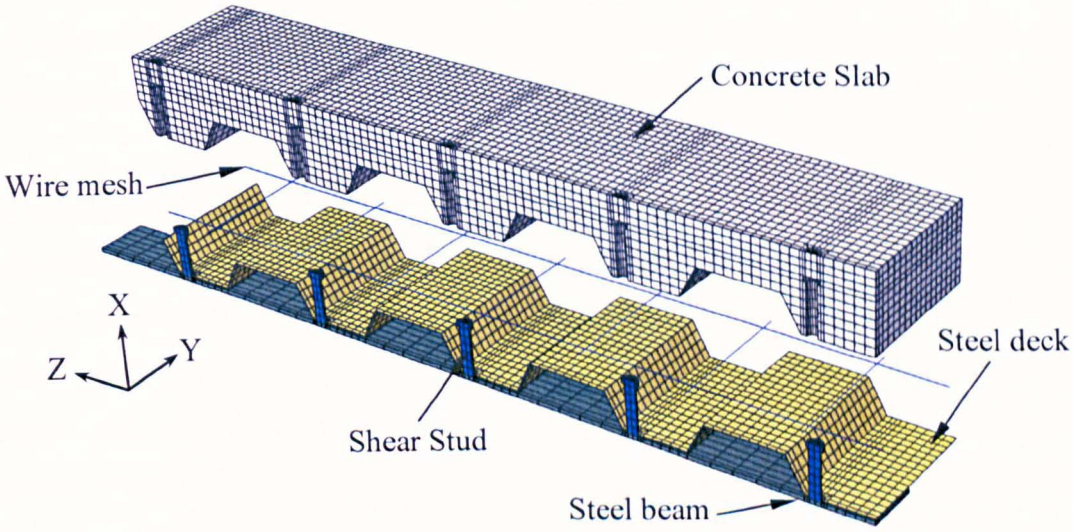

Figure 6.1 Finite element model for the push test with a single stud per rib

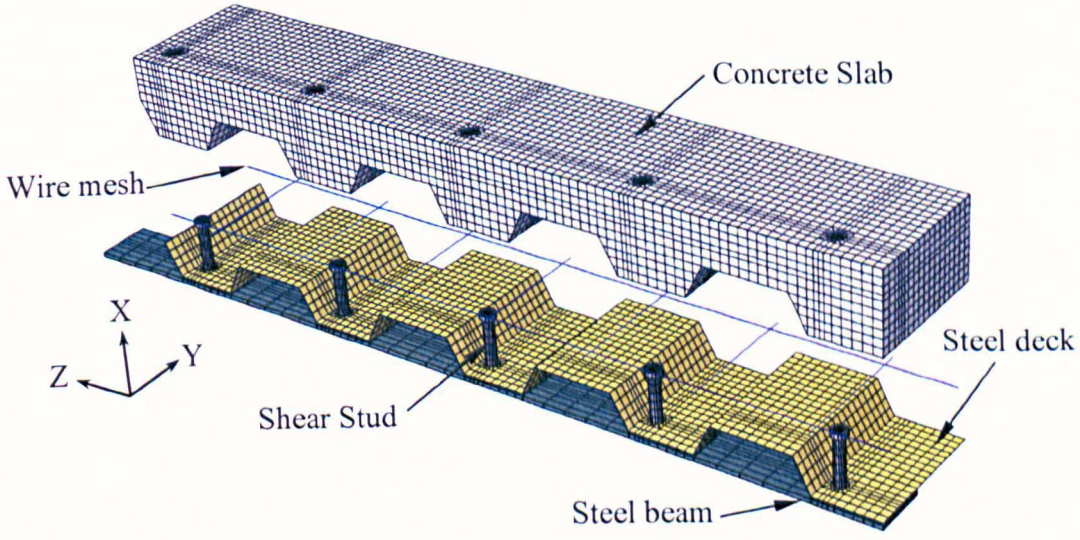

Figure 6.2 Finite element model for the push test with double studs per rib

6.2.1. Boundary conditions and load application

The boundary conditions and loading surfaces of push tests with single and double shear connectors per rib are shown in Figure 6.3 and Figure 6.4 respectively. The bottom surface of the steel beam flange, designated as surface 1 in Figure 6.3(a) and Figure 6.4(a), is restrained from moving in all three directions. The symmetry boundary condition is applied to the surface, which lies on the symmetric plane of the horizontal push test specimen as identified by surface 2 in Figure 6.3(b) and Figure 6.4(b). Surface 2 is considered to be symmetric in the Y direction, which means that all of the steel beam flange, profiled sheeting and concrete nodes, which lie on this surface, are prevented from translating in the Y direction, and rotating in the X and Z direction.

The surface on which the horizontal shear loading is applied to the finite element model is identified by "Loading surface" as shown in Figure 6.3(c) and Figure 6.4(c). Some of push test experiments conducted in this study had normal load applied to the top surface of the concrete slab in the direction parallel to the axis of the beam. The surface of the concrete slab on which the normal load is applied in a push test with the help of spreader beams is represented by "Normal loading surface" in the finite element model as shown in Figure 6.3(d) and Figure 6.4(d).

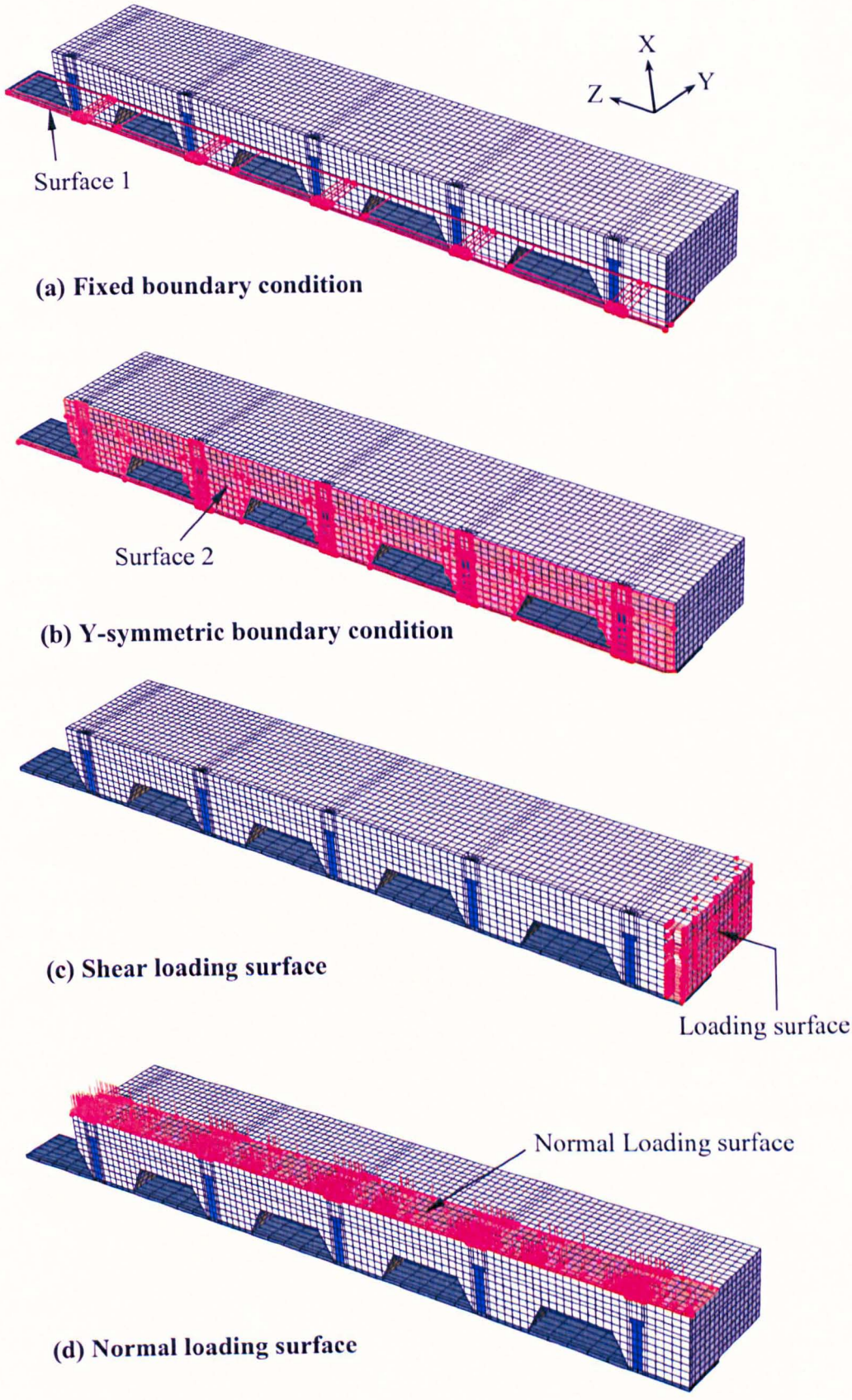

Figure 6.3 Boundary conditions and loading surfaces for the push test with a single stud per rib

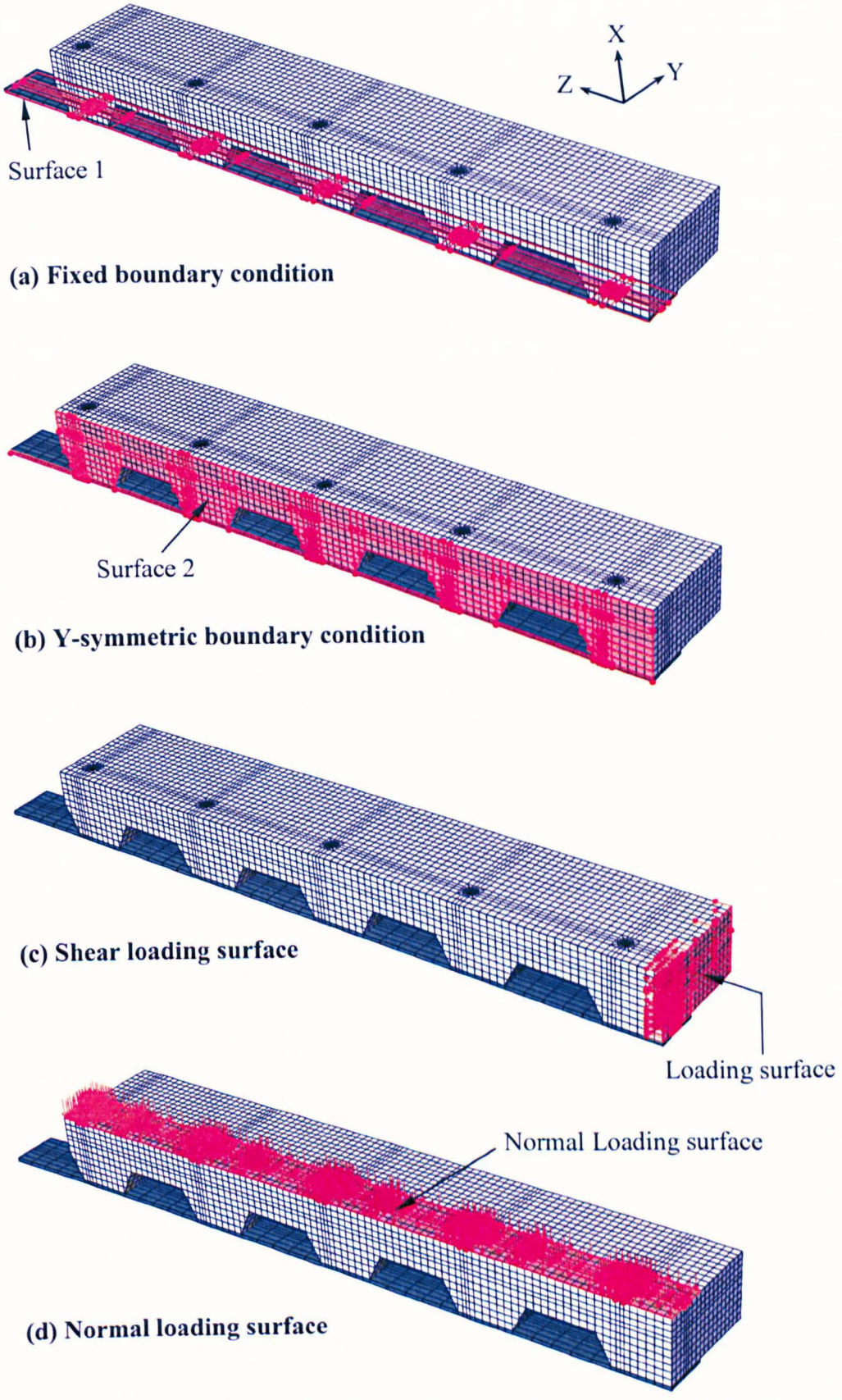

Figure 6.4 Boundary conditions and loading surfaces for the push test with double studs per rib

6.2.2. Constraints and contact interactions

All parts are positioned together to form an assembly, and appropriate constraints and contact interactions are defined between them. In push test experiments, shear studs are welded through the sheeting to the steel beam flange. This process is implemented in the finite element model by tying the nodes of the profiled sheeting around the circumference of the stud shaft to the nodes of the shear stud at its base, and creating the shear stud and the steel beam flange in the same part assuming that the shear stud remains tied to the beam all the time until the material of the shear stud fails.

A contact pair algorithm was used to define surface to surface contact between the steel deck and concrete slab, and between the stud shaft and surrounding concrete. The general contact algorithm was used to specify the contact between bottom of the profiled sheeting and top of the steel beam, primarily because of the discontinuous surface of the bottom of the trapezoidal shaped steel deck. The penalty frictional formulation with a coefficient of friction equal to 0.5 was used for all contact interactions except for beam-deck contact which was assumed to be frictionless. The default normal behaviour was assumed for all interactions. The wire mesh was embedded inside the concrete slab by means of an embedded constraint, neglecting the effect of relative slip and debonding of the mesh with respect to the concrete.

6.2.3. Convergence study for mesh size

The mesh sensitivity analysis is carried out to select a suitable mesh size for the push test model based on the comparison with experimental results, and reasonable computational efficiency. The mesh configuration of the shear stud and its surrounding area is the most important because mostly failure occurs in the vicinity of this region. Same mesh size is used for the contacting surfaces of the profile sheeting, concrete slab, shear stud and steel beam to make sure that the contact interaction between them is modelled accurately. Three different mesh sizes namely coarse mesh having 20 × 20 mm elements, medium mesh having 15 × 15 mm elements and fine mesh with 10 × 10 mm elements have been tried for push tests with single and double studs per rib as shown in Figure 6.5 and Figure 6.6 respectively.

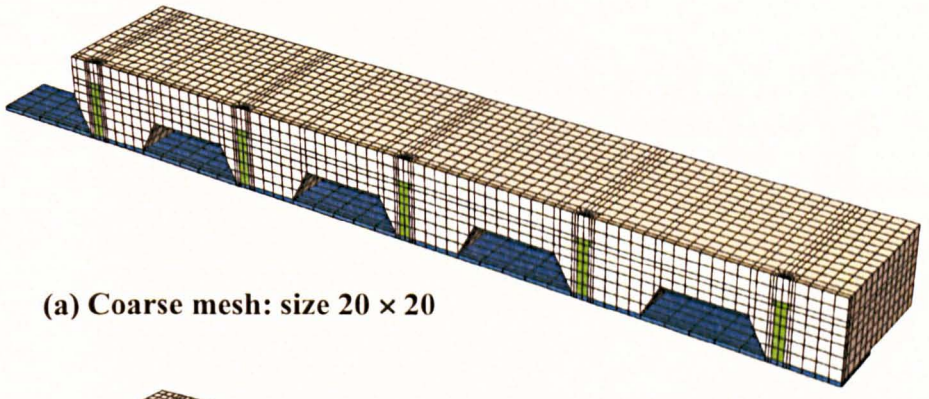

(a) Coarse mesh: size 20 × 20

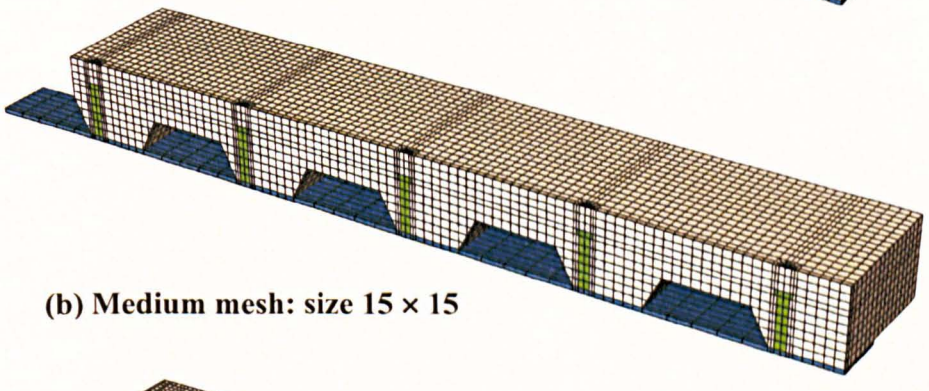

(b) Medium mesh: size 15 × 15

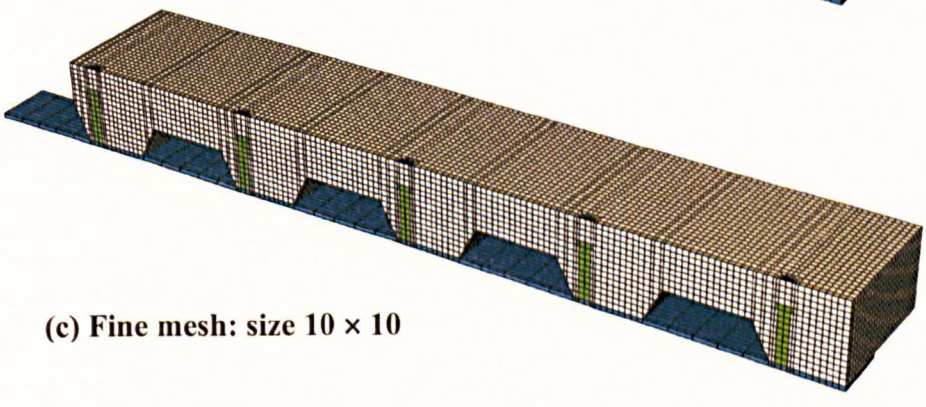

(c) Fine mesh: size 10 × 10

Figure 6.5 Mesh sensitivity for the push test with a single stud per rib

The results of the mesh sensitivity analysis are compared with single and double studs per rib experimental push tests PTS1 and PTD1, which are explained in detail in Chapter 3, and error percentage for each test is computed as shown in Table 6.1. Initial loading rate of 0.5 mm/sec is used for all analysis in this convergence study, which will later be tested in a separate convergence study for the loading rate once an appropriate mesh size is selected. The experimental and numerical load per stud is denoted by P_{Test} and P_{FE} respectively. The error percentage is the absolute value of P_{Test} over P_{FE} minus one. The error percentages computed for coarse, medium and fine mesh sizes were 9.3%, 5.5% and 4.3% respectively.

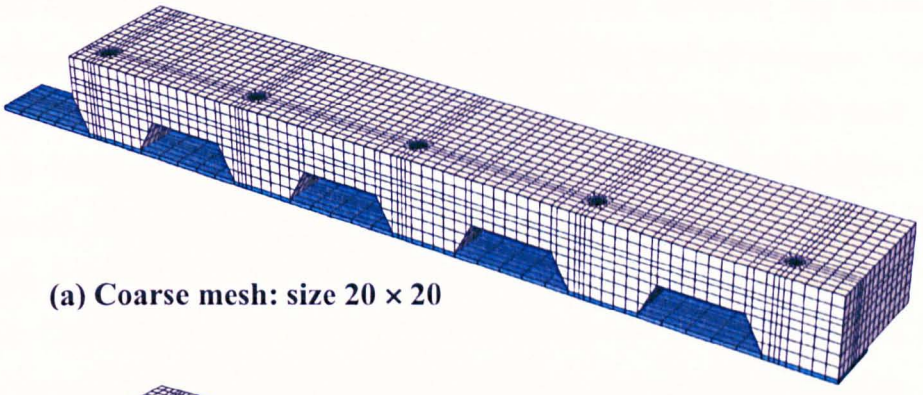

(a) Coarse mesh: size 20 × 20

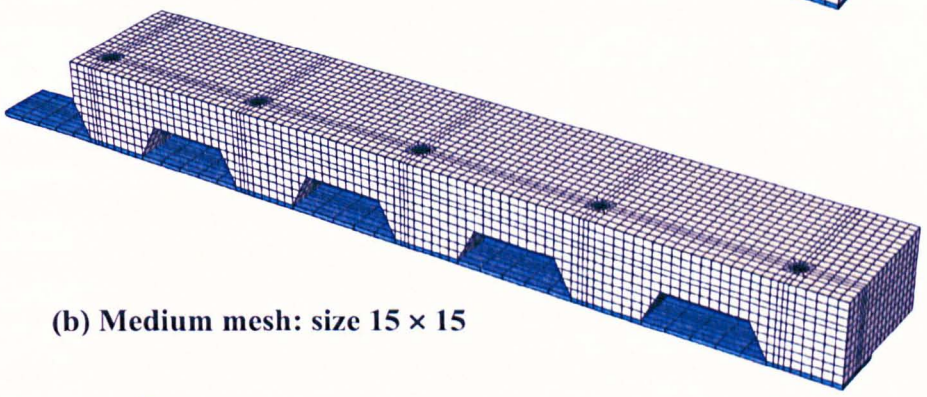

(b) Medium mesh: size 15 × 15

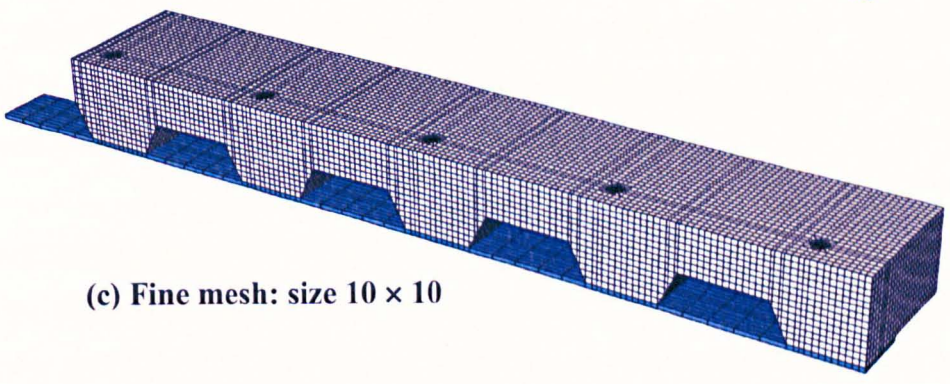

(c) Fine mesh: size 10 × 10

Figure 6.6 Mesh sensitivity for the push test with double studs

Table 6.1 Convergence study for different mesh sizes

Test Ref.	P_{Test}	Coarse Mesh size: 20 × 20		Medium Mesh size: 15 × 15		Fine Mesh size: 10 × 10	
		P_{FE}	% Error	P_{FE}	% Error	P_{FE}	% Error
PTS 1-1	75.7	83.8	9.7%	80.4	5.8%	78.0	2.9%
PTS 1-2	78.8	83.8	6.0%	80.4	2.0%	78.0	1.0%
PTD 1-1	52.1	54.6	4.6%	52.5	0.8%	50.9	2.4%
PTD 1-2	45.4	54.6	16.8%	52.5	13.5%	50.9	10.8%
Average % Error			**9.3%**		**5.5%**		**4.3%**

In the finite element analysis, the mesh size requiring less computer time to run should be used without necessarily compromising on reasonable level of accuracy. The coarse mesh resulted in a bit larger error percentage than the medium and fine mesh sizes as indicated in Table 6.1. The slight differences in error percentages among three different mesh sizes are within the margin of error expected of a push test simulation. The error percentages obtained from medium and fine mesh sizes were not much different from each other. Therefore, the medium mesh size is selected for further analysis of the push test, considering the computational efficiency and accuracy of the numerical simulation.

6.2.4. Convergence study for loading rate

The appropriate loading rate that can ensure a quasi-static solution of the push test simulation is very important, especially when analysis involves the dynamic explicit procedure and material damage. Generally, a slow loading rate helps reduce the noise in the load-slip curve of the push test. However, a compromise is to use such a loading rate which gives accurate results in the reasonable computational time. The appropriate mesh of medium size determined from previous section is used for the analysis of all push tests in the convergence study for the loading rate.

Different loading rates of 0.05, 0.075, 0.1, 0.25, 0.5, 0.75 and 1 mm /sec are used to study the effect loading rate on the finite element analysis results. The results of the sensitivity analysis for the loading rate with error percentages are tabulated in Table 6.2. The error percentages calculated are 4.2%, 4.3%, 4.6%, 4.9%, 5.5%, 6.2% and 6.7% for loading rates of 0.05, 0.075, 0.1, 0.25, 0.5, 0.75 and 1 mm /sec respectively. It can be observed that there is a very little change in error percentages when the loading rate is decreased from 0.25 mm/sec to 0.05 mm/sec. Based on the computational time and accuracy of the analysis results, a loading rate of 0.25 mm/sec was found to be the optimum loading rate for the numerical simulation of the push test.

Table 6.2 Convergence study for loading rate

Test Ref	P_{TEST} (kN)	Loading Rate							Loading Rate						
		0.05	0.075	0.1	0.25	0.5	0.75	1	0.05	0.075	0.1	0.25	0.5	0.75	1
		P_{FE} (kN)	P_{FE} (kN)	P_{FE} (kN)	P_{FE} (kN)	P_{FE} (kN)	P_{FE} (kN)	P_{FE} (kN)	% Error	% Error	% Error	% Error	% Error	% Error	% Error
PTS 1-1	75.7	78.6	79	79.4	79.7	80.4	80.9	81.3	3.7%	4.2%	4.7%	5.0%	5.8%	6.4%	6.9%
PTS 1-2	78.8	78.6	79	79.4	79.7	80.4	80.9	81.3	0.3%	0.3%	0.8%	1.1%	2.0%	2.6%	3.1%
PTD 1-1	52.1	51.7	51.9	52.1	52.3	52.5	52.9	53.2	0.8%	0.4%	0.0%	0.4%	0.8%	1.5%	2.1%
PTD 1-2	45.4	51.7	51.9	52.1	52.3	52.5	52.9	53.2	12.2%	12.5%	12.9%	13.2%	13.5%	14.2%	14.7%
Average % Error									4.2%	4.3%	4.6%	4.9%	5.5%	6.2%	6.7%

Note: All loading rates are in mm/sec

6.3. Validation against push tests conducted in this study

After selection of the appropriate mesh size and loading rate through convergence studies, the developed finite element model is used to carry out numerical analysis of push test experiments conducted in this study. The load-slip behaviour, shear connector capacity and failure modes obtained from the finite element analysis are compared with experimental push tests conducted in Chapter 3. In experiments, each push test was repeated twice with the same configuration to ensure statistical acceptance of the test results. The results obtained from the finite element analysis are compared with both push test specimens.

6.3.1. Test PTS 1

The push test had a single stud per rib with the wire mesh positioned on top of the steel deck and concrete cube strength of 34 N/mm^2. The comparison of the experimental versus numerical load-slip behaviour is shown in Figure 6.7. The slip in the finite element model was measured at the back of the test slab, which was the same point where LVDTs were located in the experimental push test. The maximum load observed in the finite element analysis was 79.7 kN compared with 75.7 kN and 78.8 kN observed in push test specimens PTS 1-1 and PTS 1-2 respectively. The push test specimens PTS 1-1 and PTS 1-2 failed at slips of 0.6 mm and 0.7 mm respectively, while slip at the maximum load in case of the finite element analysis was 1.2 mm. The load-slip behaviour of the experimental push test and finite element analysis matched well. Although, the load-slip curve in the finite element analysis followed a similar trend as that of the experimental curve, the former had a slightly higher post-failure region than the latter.

The difference between experimental and numerical load–slip curve in the post-failure range in Figure 6.7 could be due to two reasons. First, the push test specimen was loaded under load control in the experiment, which meant that as soon as the failure load was reached, there was always a slight tendency of overloading the specimen leading to a rapid drop in the load–slip curve. On the contrary, in the finite element analysis the model was loaded very slowly under displacement control by applying small velocity in increments. The way the load was applied to the specimen in the

experiment and numerical model could be the reason for slight variation in the load–slip behaviour in the post-failure range. Second, the concrete compressive strength is modelled in accordance with BS EN 1992-1-1 which might have a slight variation to the actual stress–strain characteristic of the concrete used in the experiment. Yet, in general, the finite element model effectively captured the load–slip behaviour of the push test experiment.

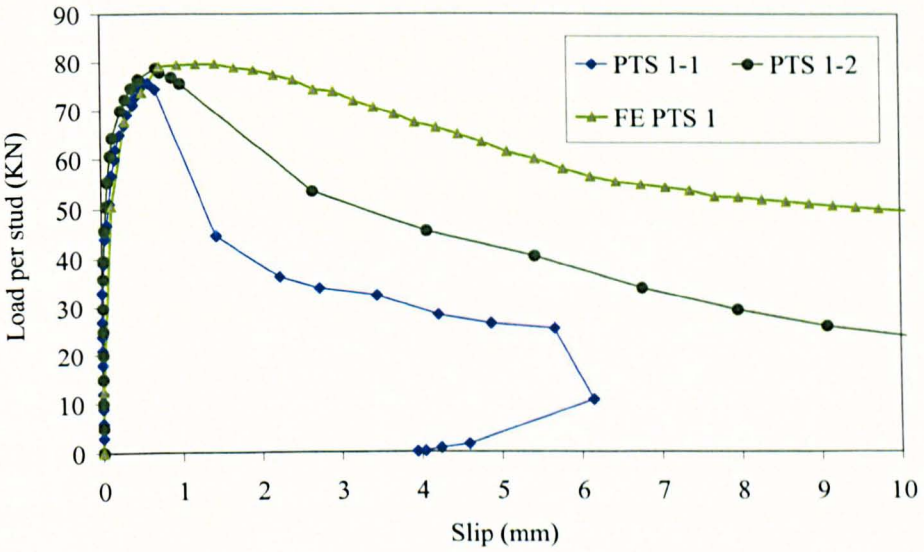

Figure 6.7 Comparison of experimental and numerical load-slip behaviour for push test PTS 1

The comparison of the failure mode in the finite element analysis and experiment for the push test PTS 1 is shown in Figure 6.8. In the experiment, the push test specimen failed by formation of concrete cones around shear studs along with rotation of the last studded rib. The cracking of the concrete slab is represented by the tensile damage variable, *dt* in the finite element model. The value of the tensile damage variable equal to one indicates complete tensile failure of the material and zero represents no tensile damage. It can be observed that cracking in the finite element model and experiment occurred at the same location. The last studded rib in the finite element model rotated in the same way as in the experiment, and the portion of the concrete slab above the top flange of the steel deck close to the last studded rib in the numerical model and experiment failed by excessive cracking across the entire length of the rib as shown in Figure 6.8.

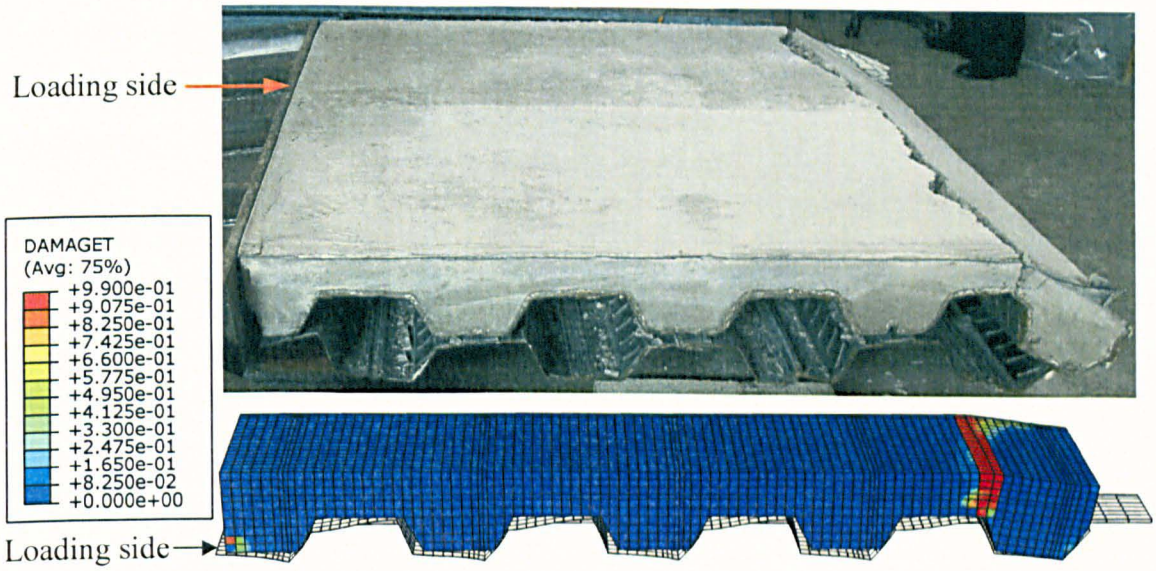

Figure 6.8 Comparison of experimental and numerical failure modes for push test PTS 1

It is evident from Figure 6.8 that the concrete slab in the experiment rides over the steel deck, and the last studded rib rotates more in the experiment than the finite element model. It can be explained by the fact that the push test specimen was loaded until the concrete slab completely lost its shear connection with the steel deck and shear connectors; and the finite element model was loaded until a slip of 20 mm was reached at the steel-concrete interface. However, the way the concrete slab rode over the steel deck exactly matched with the behaviour observed in the finite element analysis.

The buckling behaviour and stress contours of the profiled sheeting for the push test PTS 1 are shown in Figure 6.9. When the load applied to the push test approaches failure load, the steel deck deformations become more prominent resulting in buckling of the steel deck. The top and bottom corner of the profiled sheeting behind the shear stud, where the concrete slab pushes the steel deck to ride over it, experience the maximum stress as indicated by stress contours in Figure 6.9.

The shear stud and steel deck deformations for the push test PTS 1 are shown in Figure 6.10. Similar to the push test experiment, shear studs bent in the direction of the applied shear loading in the finite element model. The point, where the top flange and web of the steel deck meet, depresses down when the concrete slab tends to ride over the profiled sheeting. As a result, some lifting is observed on the other side of the

bottom flange of the steel deck which is not attached to the shear stud as shown in Figure 6.10. The shear stud and steel deck deformations observed in the finite element analysis showed close agreement with the deformations observed in the push test experiment.

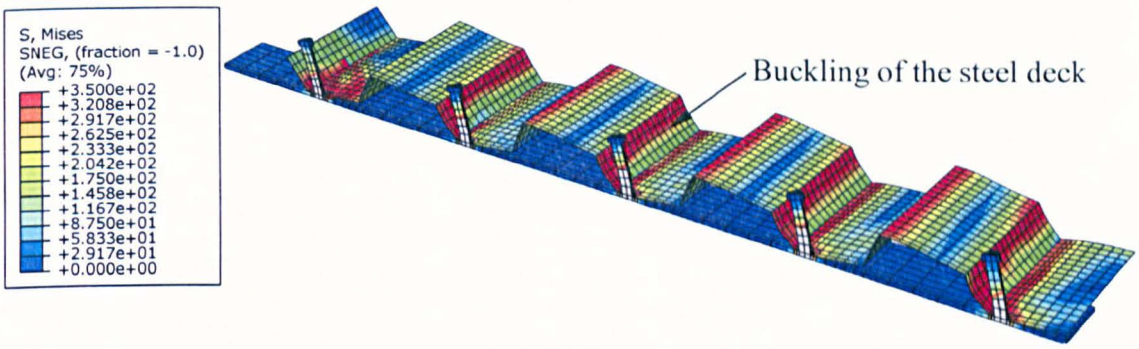

Figure 6.9 Buckling behaviour and stress contours of the steel deck for push test PTS 1

The comparison of concrete failure cones in case of the experiment and finite element model for the push test PTS 1 is shown in Figure 6.11. Concrete failure cones in the finite element model are shown by tensile cracking of the concrete material characterised by the tensile damage variable. The push test PTS1 failed by formation of concrete failure cones around the shear stud; and the size of failure cone in middle three sheeting ribs was larger than the first and last rib. In order to view failure cones clearly, the portion of the concrete slab above the top flange of the steel deck has been removed in Figure 6.11. It can be observed that the size and shape of concrete failure cones in the finite element model are similar to the push test experiment.

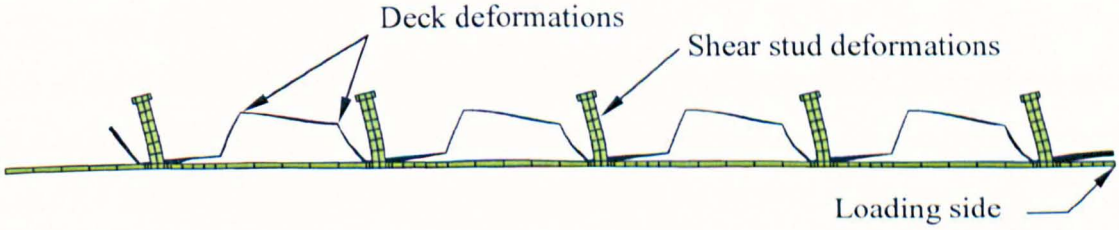

Figure 6.10 Shear stud and steel deck deformations for push test PTS 1

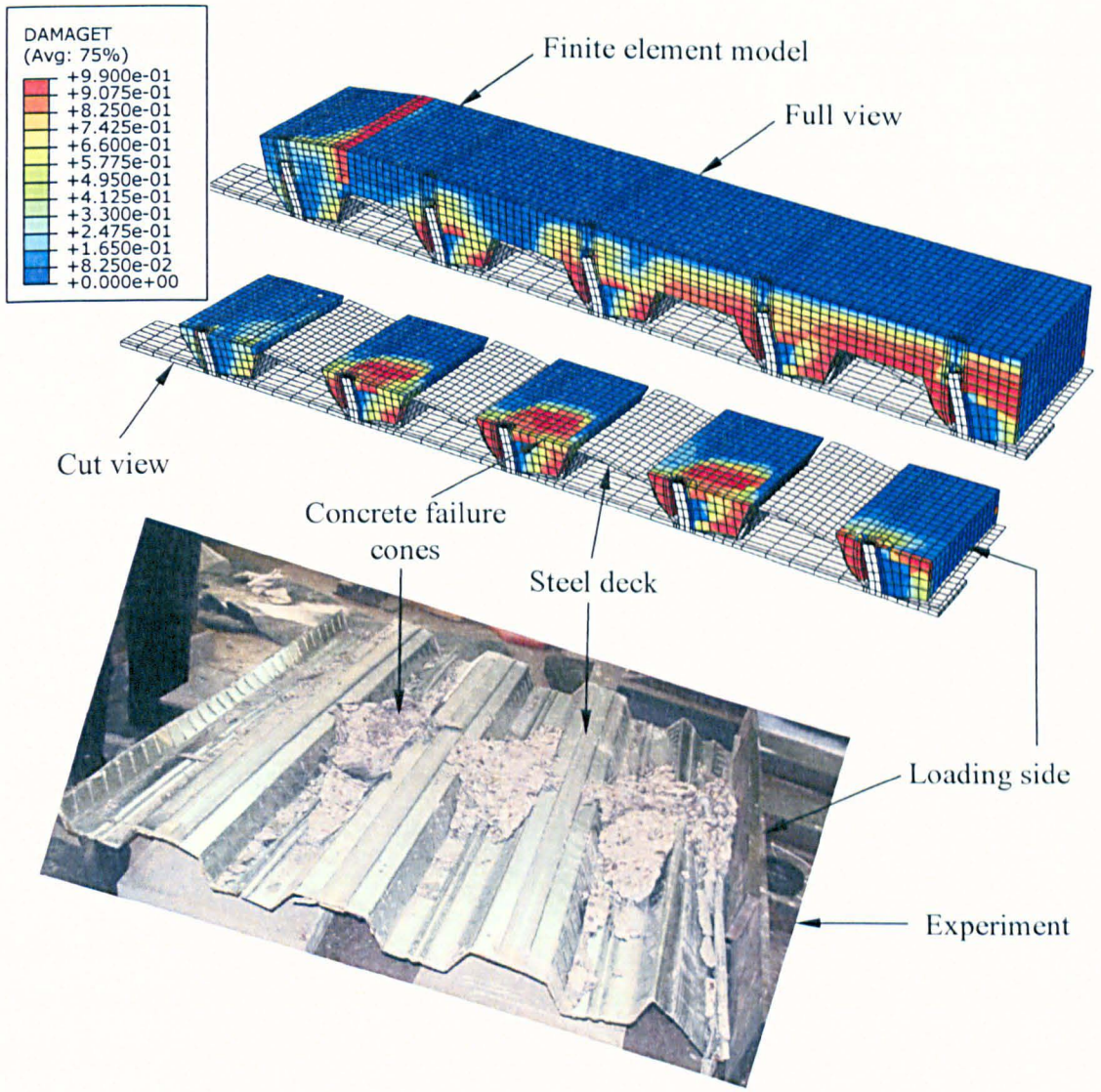

Figure 6.11 Comparison of experimental and numerical concrete failure cones for push test PTS 1

6.3.2. Test PTS 2

The position of the wire mesh was raised above the steel deck with a concrete cover of 30 mm from top surface of the concrete slab in this push test, and concrete cube strength was 27.5 N/mm^2. The other properties remained same as that of the push test PTS 1. The load versus slip curves obtained from the finite element analysis and push test experiments are plotted in Figure 6.12. The maximum load recorded in the experimental push test was 69.0 kN and 73.8 kN for specimens PTS 2-1 and PTS 2-2 respectively as against a peak load of 73.0 kN obtained from the finite element analysis. The slip at failure was 1.5 mm in case of the finite element analysis compared with 1.7 mm and 1.4 mm obtained from push test experiments PTS 2-1 and PTS 2-2 respectively. The

concrete failure cones, steel deck and shear stud deformations in the finite element model were similar to that of FE model of the push test PTS 1.

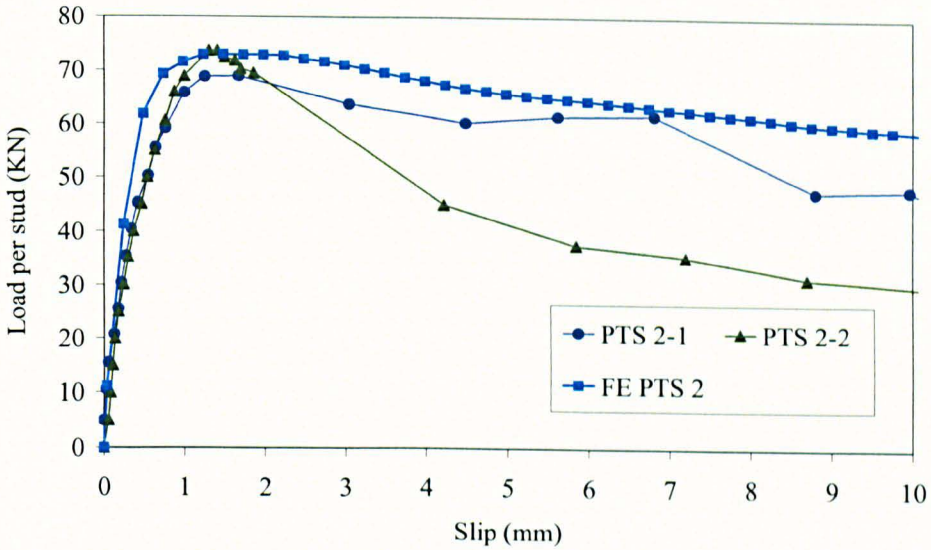

Figure 6.12 Comparison of experimental and numerical load-slip behaviour for push test PTS 2

6.3.3. Test PTD 1

This push test used double studs per rib with raised mesh and concrete cube strength of 27.85 N/mm^2. The load-slip behaviour obtained from the experiment and finite element analysis is presented in Figure 6.13. The maximum load obtained from push test specimens PTD 1-1 and PTD 1-2 was 52.1 kN and 45.4 kN with corresponding slips of 1.00 mm and 0.94 mm respectively. The ultimate load obtained from the finite element analysis was 52.3 kN at a slip of 1.22 mm.

The failure modes of the push test PTD 1 were also investigated in the finite element model. In the experiment, the push test specimen failed on account of a combination of concrete conical failure and rotation of the last studded rib, commonly described as 'back-breaking', at the free end. The comparison of failure patterns in the experiment and finite element model for the push test PTD 1 is presented in Figure 6.14. It is clear that the last rib in the finite element model rotates in the same way as in the experiment, forcing the weakest part of the concrete slab above the steel deck flange to crack as shown by the tensile damage variable, d_t in the finite element model.

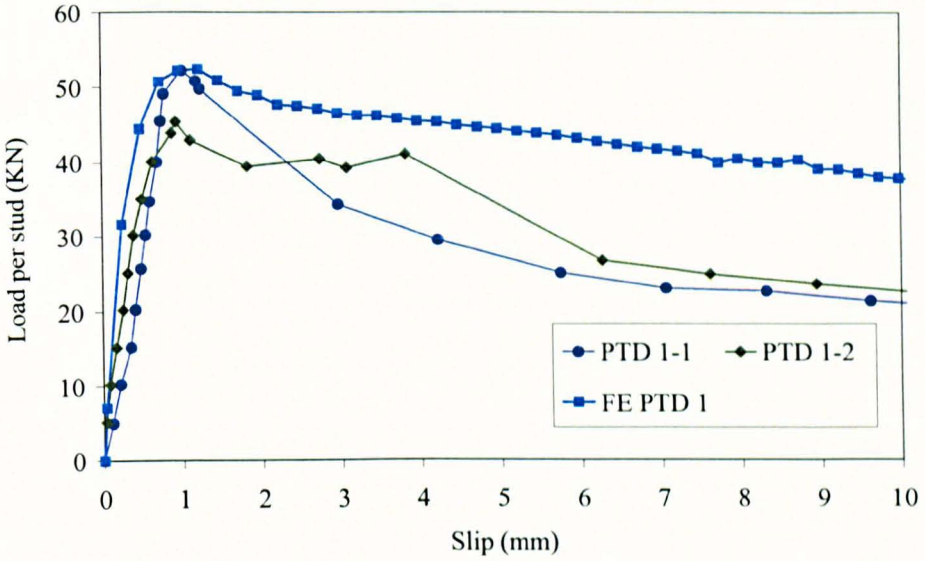

Figure 6.13 Comparison of experimental and numerical load-slip behaviour for push test PTD 1

When the failure load is reached, deformations in the steel deck become more prominent, resulting in buckling of the steel deck. The top and bottom corner of the profiled sheeting rib, where it meets the concrete slab, experience the maximum stress, as it is evident from the stress contour plot of the steel deck in Figure 6.15. It is important to note that the steel deck deformations in the finite element model are similar to the ones observed in the push test.

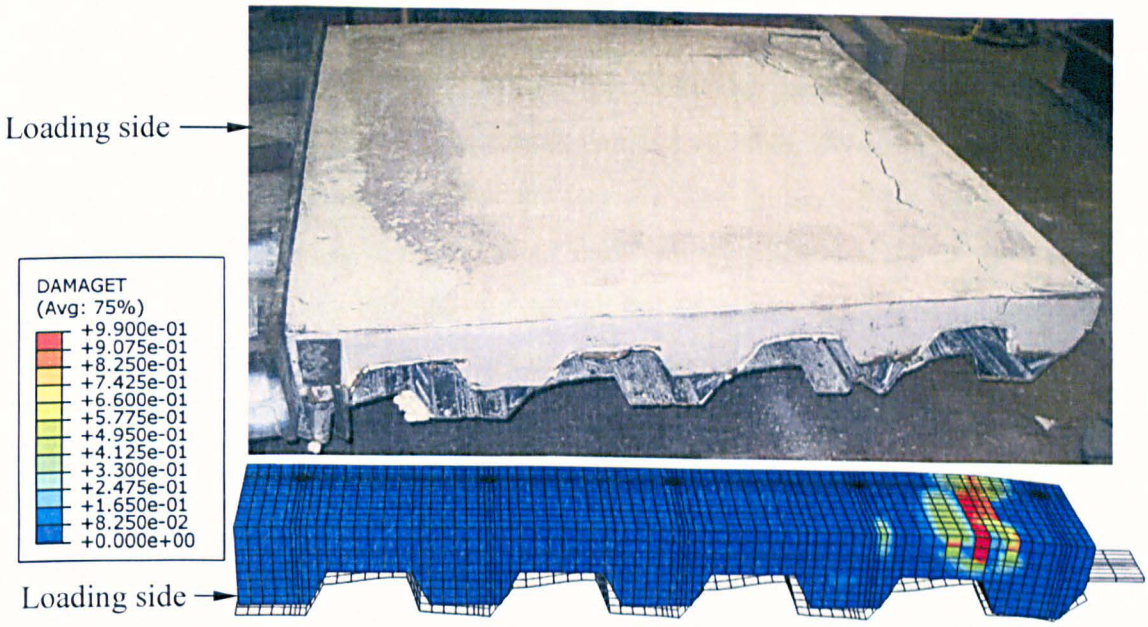

Figure 6.14 Comparison of experimental and numerical failure modes for push test PTD 1

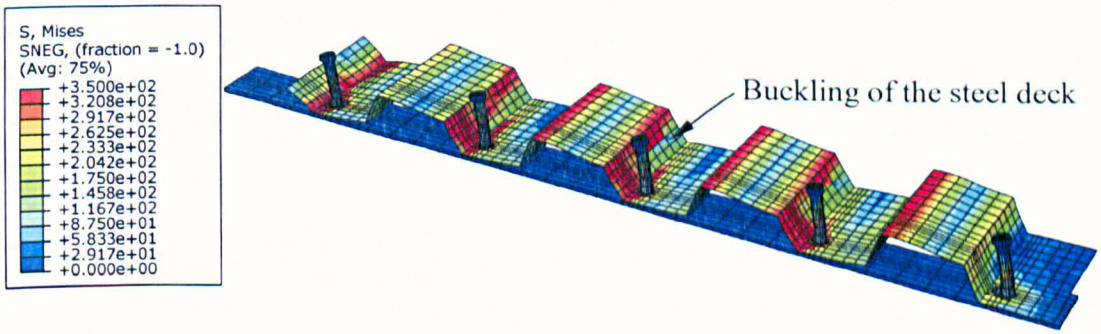

Figure 6.15 Buckling behaviour and stress contours of the steel deck for push test PTD 1

The push test specimen failed by concrete conical failure, thus leaving behind a cone of concrete in case of the push test experiment. In order to see concrete failure cones clearly, the finite element model is cut horizontally just above the top flanges of the steel deck. The contour plot of the tensile damage variable for full as well as cut view of the finite element model for the push test PTD1 is shown in Figure 6.16. When the load is increased, the steel deck tends to separate from the concrete slab, and eventually, delaminates from it.

At failure, it can be observed in Figure 6.16 that large concrete failure cones develop in the middle three rib of the profiled sheeting; while the last rib does not have much tensile cracking as indicated by the tensile damage variable. However, the first deck rib had slightly larger failure cone than the last rib. The failure of the push test PD1 by formation of concrete cones around shear studs exactly resembled the failure patterns in the finite element model. Thus, the actual failure mode has been predicted in the numerical model, which is crucial for understanding the true behaviour of the push test.

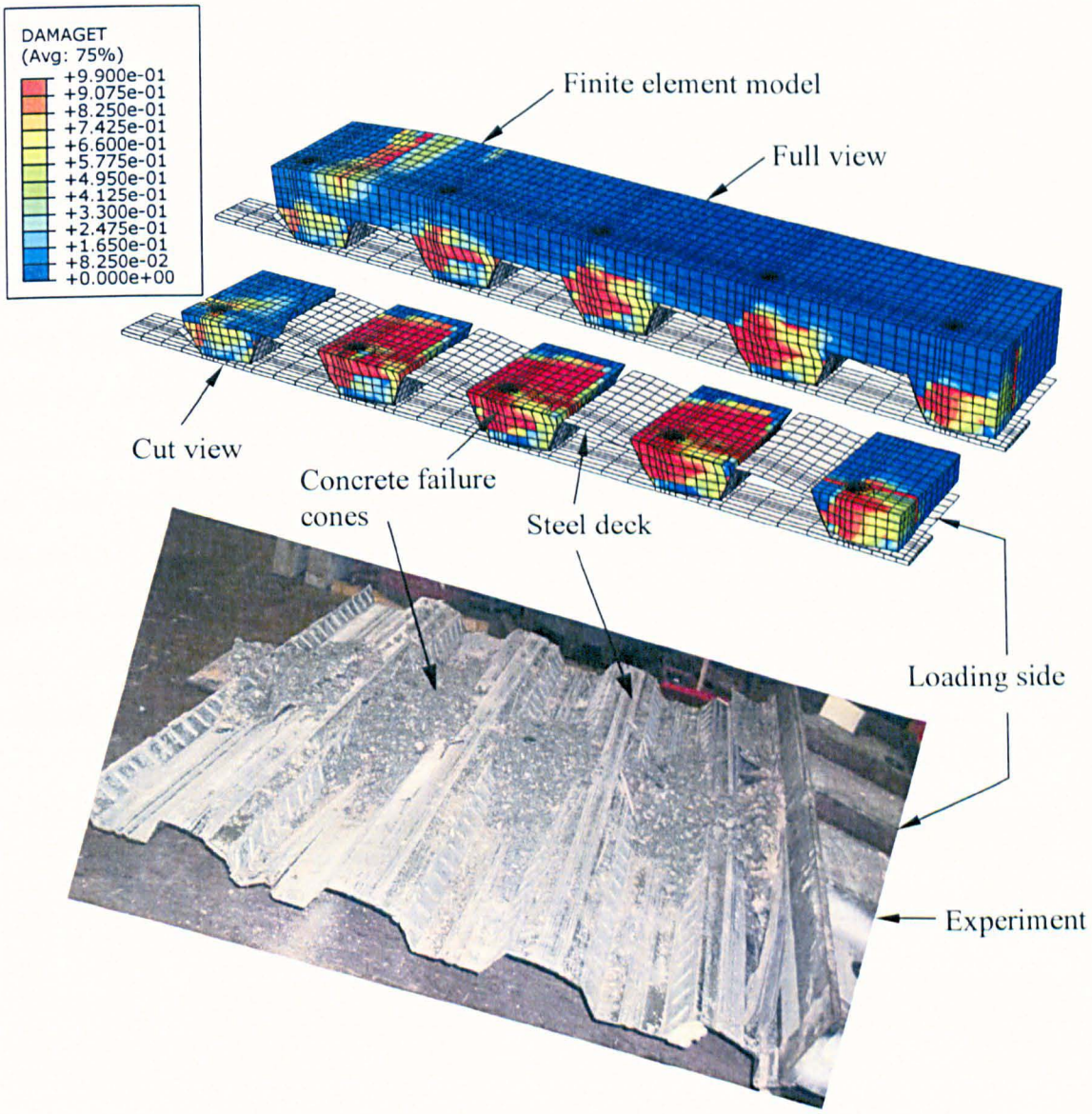

Figure 6.16 Comparison of experimental and numerical concrete failure cones for push test PTD 1

The development of the tensile damage and scalar stiffness degradation at different stages of loading for the push test PTD 1 are illustrated in Figure 6.17 and Figure 6.18

respectively, showing the contour plot of the tensile damage variable, DAMAGET (or d_t) and the scalar stiffness degradation variable, SDEG (or d). The tensile damage is initiated when the concrete material starts to crack, which keeps on increasing continuously, until the material completely fails in tension. While, the scalar stiffness degradation variable can increase or decrease exhibiting the stiffness recovery effects linked to opening or closing of cracks. Any value greater than zero for both the tensile damage parameter and stiffness degradation variable at a given point represents an open crack. Conversely, a closed crack is characterised by concrete damage parameter greater than zero and stiffness degradation variable equal to zero.

At failure, tensile cracks are formed in the concrete slab around shear studs, mainly, in the middle three sheeting ribs. The damage as well as stiffness degradation are greater than zero indicating crack openings at this position as shown in Figure 6.17(a) and Figure 6.18(a). At a load drop of 35 kN with a corresponding slip of 10 mm, the tensile cracks become more prominent in the first and last rib, and propagate further in middle three ribs as shown in Figure 6.17(b). The tensile damage is also observed at top of the concrete slab in the last studded rib. Eventually, the entire portion of concrete around the shear stud is damaged followed by rotation of the last rib as illustrated in Figure 6.17(c). Some cracks in the concrete slab at bottom right corner of the rib are closed as indicated by zero value of the stiffness degradation variable in Figure 6.18(c). These cracks are closed on account of compressive stresses in that region, which indicates that some of the stiffness in that zone has been recovered.

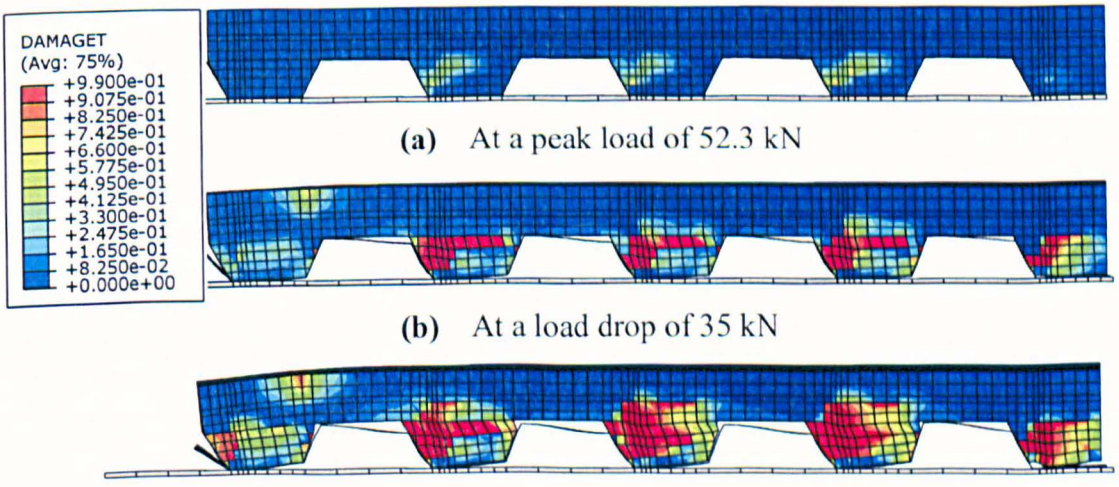

(a) At a peak load of 52.3 kN

(b) At a load drop of 35 kN

(c) At the end of analysis

Figure 6.17 Tensile damage at different stages of loading for push test PTD 1

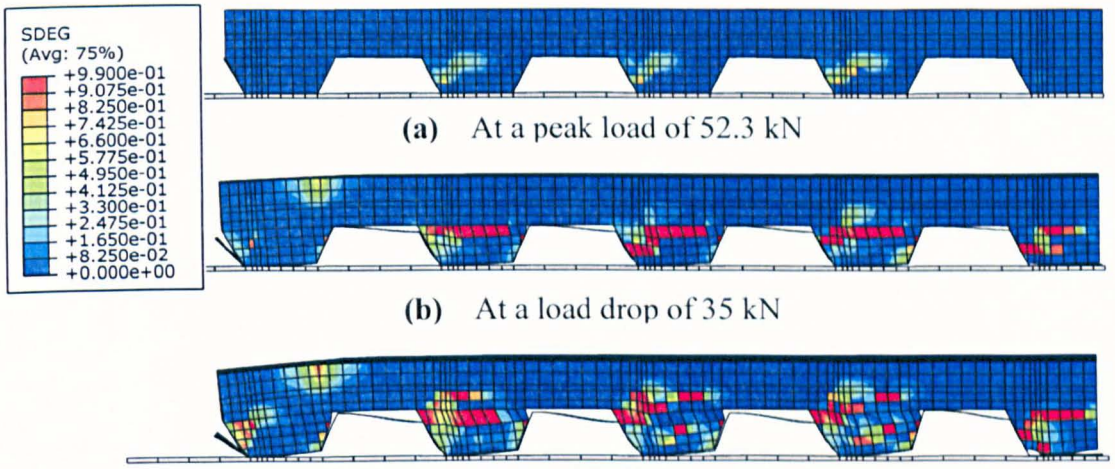

(a) At a peak load of 52.3 kN

(b) At a load drop of 35 kN

(c) At the end of analysis

Figure 6.18 Scalar stiffness degradation at different stages of loading for push test PTD 1

6.3.4. Test PTD 2

This push test had a high yield T16 bar at each bottom flange of the profiled sheeting, and everything else was exactly the same as that of the push test PTD 1 with marginally different concrete cube strength of 28 N/mm^2. The load-slip curves obtained from the finite element analysis and experiment are shown in Figure 6.19. In the experiment, the push test specimens PTD 2-1 and PTD 2-2 started to fail at a load of 52.2 kN and 47.3 kN with a slip of 1.2 mm and 0.95 mm respectively. While, in the finite element analysis, the push test began to fail at a load of 52.3 kN with a slip 1.5 mm at the steel-concrete interface. The steel deck deformations and formation of concrete failure cones in the finite element model of PTD 2 matched with the experiment, and were not much different from failure modes observed in the finite element model of PTD 1.

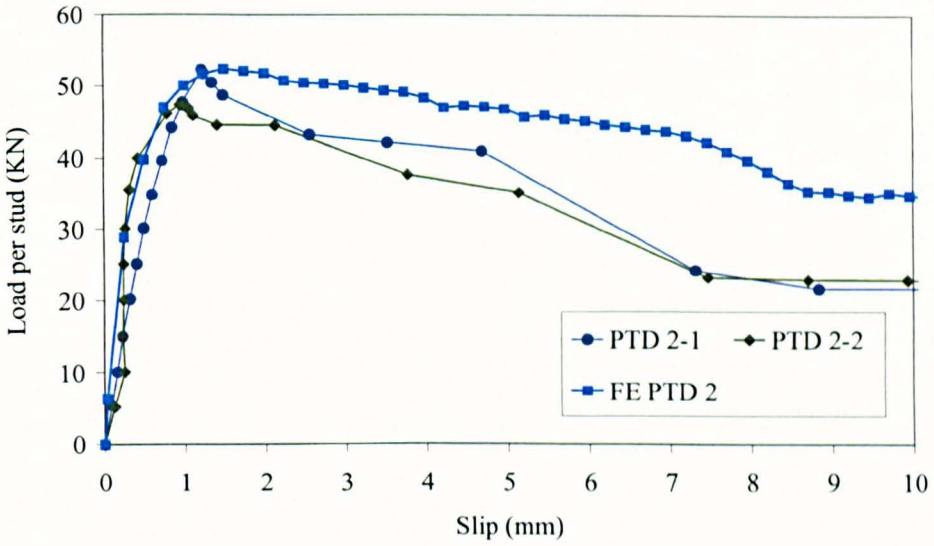

Figure 6.19 Comparison of experimental and numerical load-slip behaviour for push test PTD 2

6.3.5. Test PTSN 1

The push test PTSN 1 had the wire mesh placed directly on top of the steel deck, and the normal load was also applied to this push test, besides conventional shear load. The concrete cube strength was 25.4 N/mm^2. The comparison of the numerical versus experimental load-slip behaviour is presented in Figure 6.20. The maximum load per studs in case of experiments PTSN 1-1 and PTSN 1-2 was 97.8 kN and 98.9 kN with corresponding slips of 2.52 mm and 2.45 mm respectively. While, in case of the finite element model the maximum load per stud was 99.2 kN at a slip of 2.86 mm. It can be observed that the load-slip curve obtained from the finite element model followed a similar pattern as that of the experimental load-slip curve.

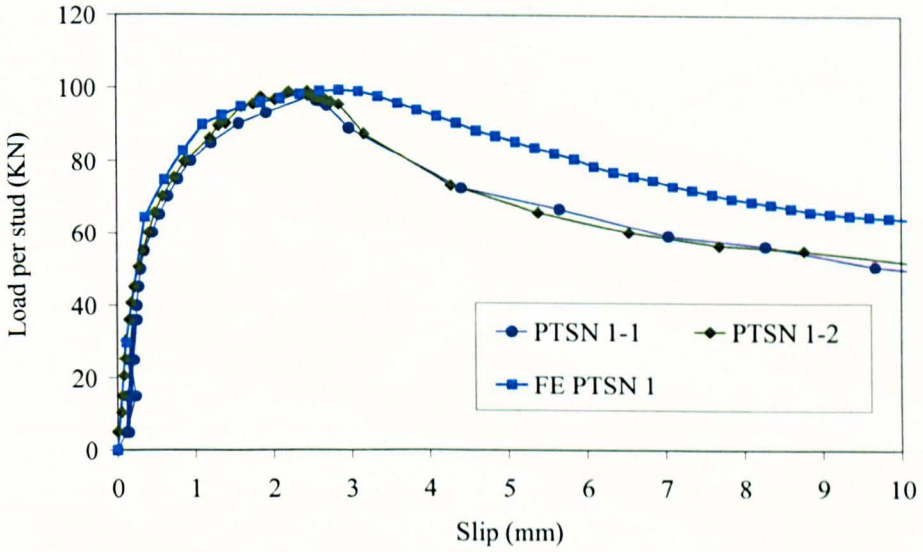

Figure 6.20 Comparison of experimental and numerical load-slip behaviour for push test PTSN 1

The comparison of concrete failure cones in the finite element model and push test PTSN 1 is given in Figure 6.21. The concrete failure cones in the push test PTSN 1 formed in the same way as in push tests having a single stud per tough with no normal load. The formation of concrete failure cones in the finite element model is indicated by the tensile damage variable. It can be observed in the experiment that shear studs bent in the direction of the applied shear loading and the application of normal load increased this bending. The reason for more bending of shear studs in the experiment than the finite element model is that the numerical model is loaded up to a slip of 20 mm at the steel-concrete interface; while in the experiment the load was continued until complete loss of shear connection occurred among the concrete slab, steel deck and shear studs. It can also be noticed that the failure cones are more prominent in the middle three sheeting pans as compared with the first and last rib. The finite element model also indicates that the size of failure cones in middle three ribs is larger than the first and last rib. Generally, the failure patterns observed in the finite element model of the push test PTSN 1 matched with the experimental failure modes.

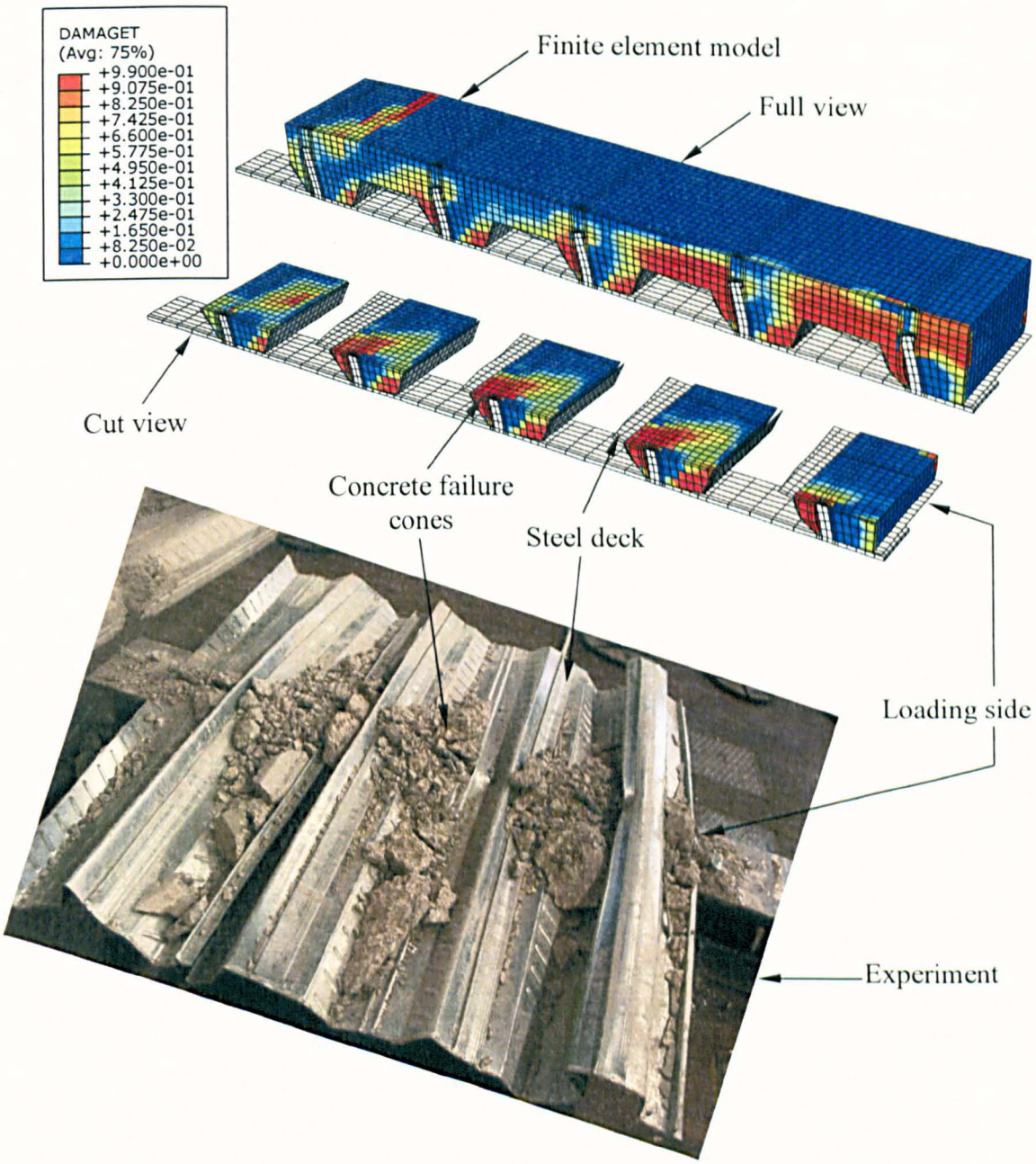

Figure 6.21 Comparison of experimental and numerical concrete failure cones for push test PTSN 1

6.3.6. Test PTSN 2

This push test had the wire mesh placed at a distance of 30 mm from the top surface of the concrete slab with average cube strength of 22.2 N/mm^2. The comparison of the experimental versus numerical load-slip behaviour for the push test PTSN 2 is presented in Figure 6.22. The push test specimen PTSN 2-1 failed at a load per stud of 90 kN with a corresponding slip of 1.36 mm; while the maximum failure load per stud obtained in case of the specimen PTSN 2-2 was 81.7 kN with a slip of 1.61 mm at the steel-concrete

interface. The maximum load per stud in case of the finite element model was 88.6 kN with a slip of 1.72 mm. The load-slip curve of the push test specimen PTSN 2-1 showed close agreement with the load-slip curve obtained from the finite element analysis. However, the maximum load per stud obtained from the push test specimen PTSN 2-2 was lower than the load per stud obtained from the finite element analysis because of the cyclic loading applied to the push test experiment. The failure modes observed in this push test also showed close resemblance with the finite element model.

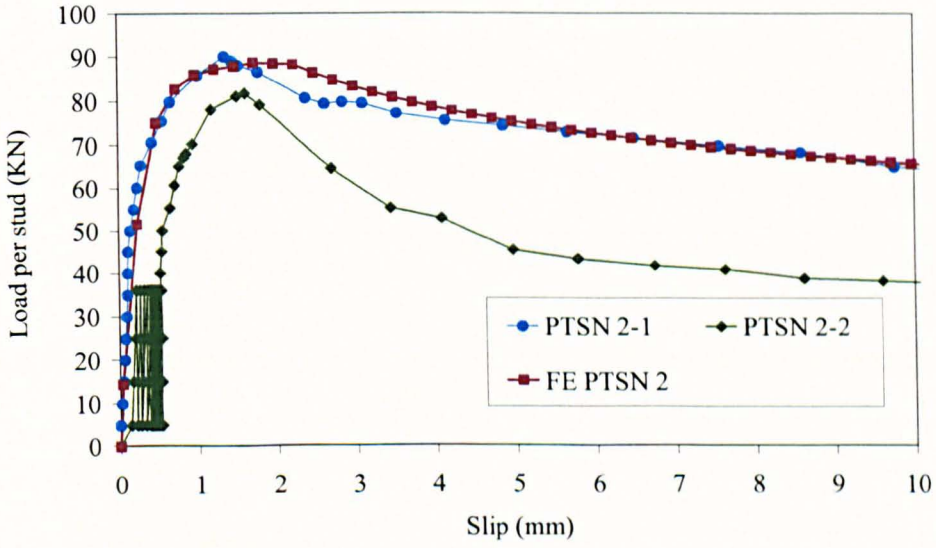

Figure 6.22 Comparison of experimental and numerical load-slip behaviour for push test PTSN 2

6.3.7. Test PTDN 1

The push test PTDN1 consists of double studs per sheeting pan with 10% normal load in addition to the shear loading. The push test specimens PTDN 1-1 and PTDN 1-2 were tested on different days with concrete cube strengths of 28.2 N/mm^2 and 37 N/mm^2 respectively. The load-slip curve for the push test specimen PTDN 1-1 is plotted in Figure 6.23. The experimental maximum load per stud for PTDN 1-1 was 61.3 kN compared with 59.2 kN per stud obtained from the finite element analysis. The slip at failure was 1.4 mm in case of both experimental and numerical push tests. The experimental and numerical load-slip behaviour of the push test specimen PTDN 1-2 is shown in Figure 6.24. The maximum failure load per stud was 67.3 kN as against 67 kN observed in the finite element analysis. The slip at failure was 1.2 mm for both

experimental push test and finite element analysis. The formation of failure cones in the finite element model of PTDN 1 was almost similar to the one observed in the numerical model of the push test with double studs without normal load.

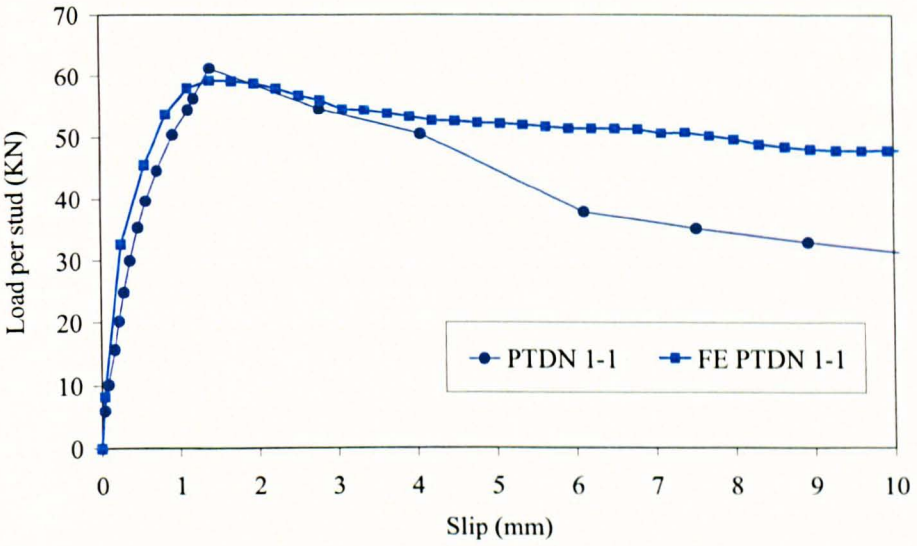

Figure 6.23 Comparison of experimental and numerical load-slip behaviour for push test PTDN 1-1

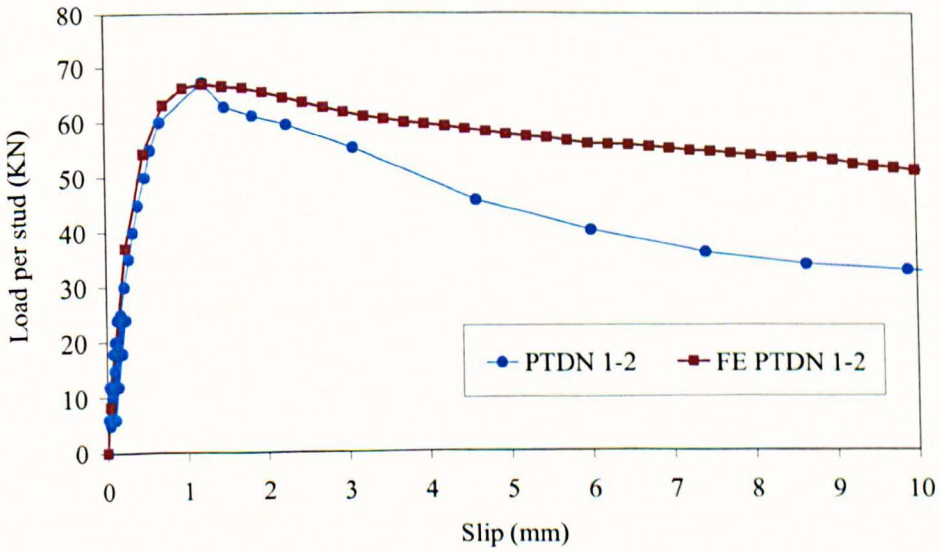

Figure 6.24 Comparison of experimental and numerical load-slip behaviour for push test PTDN 1-2

6.3.8. Test PTDN 2

This push test had double studs per rib with no studs in the last trough close to the free end. The reason for not using shear studs in the last rib was to prevent rotation of the last rib. The concrete grade of C40/50 was used which was higher than other tests. At the time of testing, the average cube strength for both push test specimens was 61 N/mm^2. The comparison of the experimental and numerical load-slip behaviour for the push test PTDN 2 is presented in Figure 6.25. The maximum load per stud obtained from the finite element analysis was 93.6 kN with a slip of 1.5 mm. While, the load per stud at failure in case of the push test specimen PTDN 2-1 and PTDN 2-2 was 91.3 kN and 93.7 kN with a slip of 1.11 mm and 1.4 mm respectively.

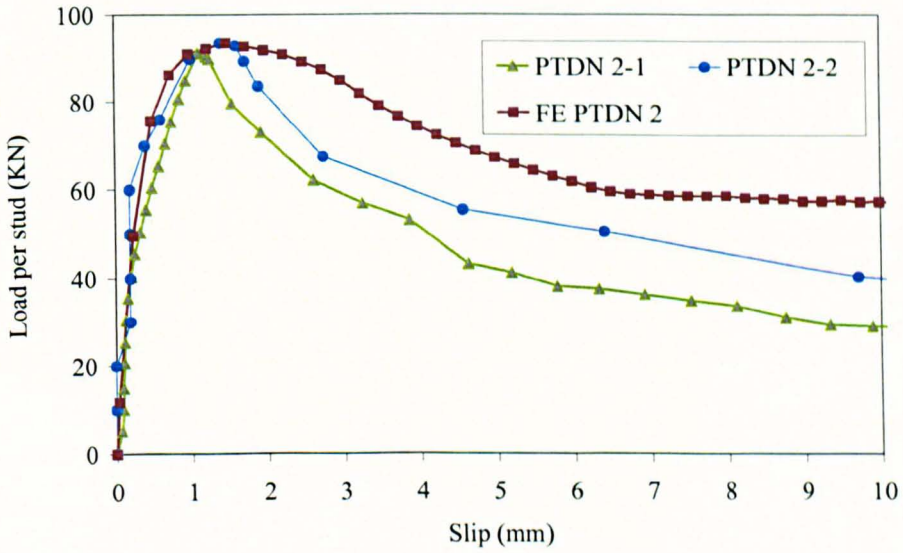

Figure 6.25 Comparison of experimental and numerical load-slip behaviour for push test PTDN 2

The comparison of concrete failure cones in case of both experiment and finite element analysis is shown in Figure 6.26. Last three sheeting pans had larger concrete failure cones as compared with the first one; and the formation of failure cones in the finite element model matched with the push test experiment. As the last sheeting pan did not have any shear stud, therefore, no failure cone formed there as indicated in the experiment and finite element model.

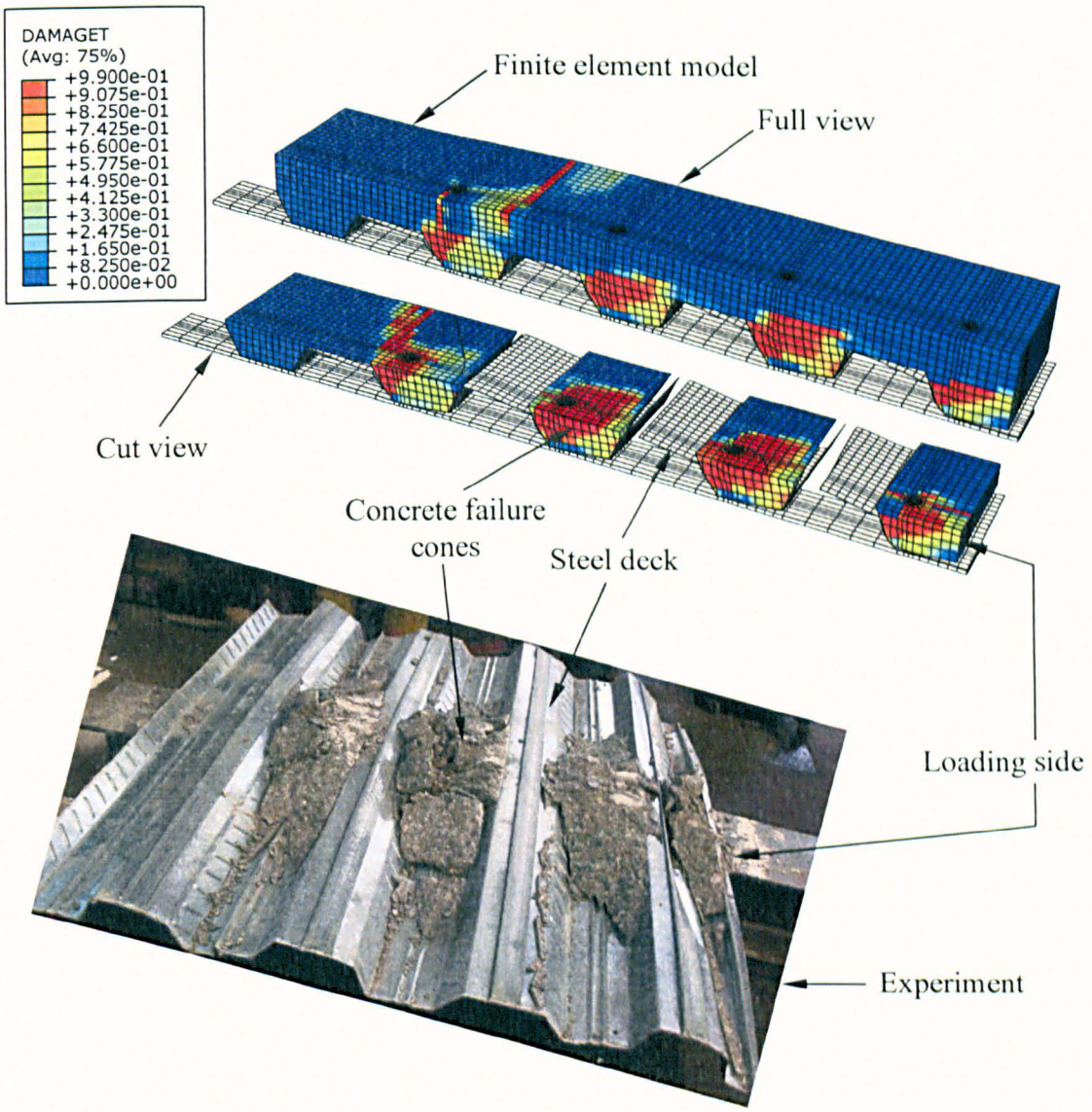

Figure 6.26 Comparison of experimental and numerical concrete failure cones for push test PTDN 2

6.3.9. Test PSNM 1

The push test PSNM 1 had double layers of wire mesh with one directly on top of the steel deck and the other at a distance of 30 mm from top surface of the concrete slab. The test used a single stud per rib with no stud in the last rib; and had concrete cube strength of 32.7 N/mm^2 and 36.1 N/mm^2 for specimens PSNM 1-1 and PSNM 1-2 respectively. The comparison of load-slip curves obtained from the experiment and the finite element model for push test specimens PSNM 1-1 and PSNM 1-2 is shown in Figure 6.27 and Figure 6.28 respectively. The maximum load per stud in case of the specimen PSNM 1-1 was 113 kN at a slip of 2.71 mm as against a load per stud of

120.4 kN with a corresponding slip of 2.98 mm observed in the finite element model. The maximum load per stud of 138.4 kN at a slip of 2.44 mm was observed in the specimen PSNM 1-2; while the maximum load in case of the numerical model was 130.6 kN with a slip of 2.98 mm for the same push test. The numerical load-slip curves showed a similar trend to that of the experiment for the push test PSNM 1.

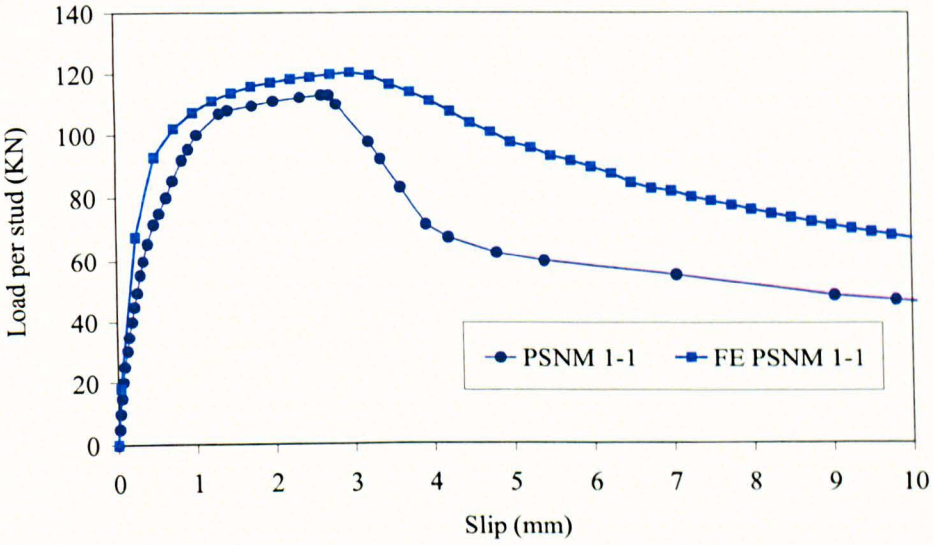

Figure 6.27 Comparison of experimental and numerical load-slip behaviour for push test PSNM 1-1

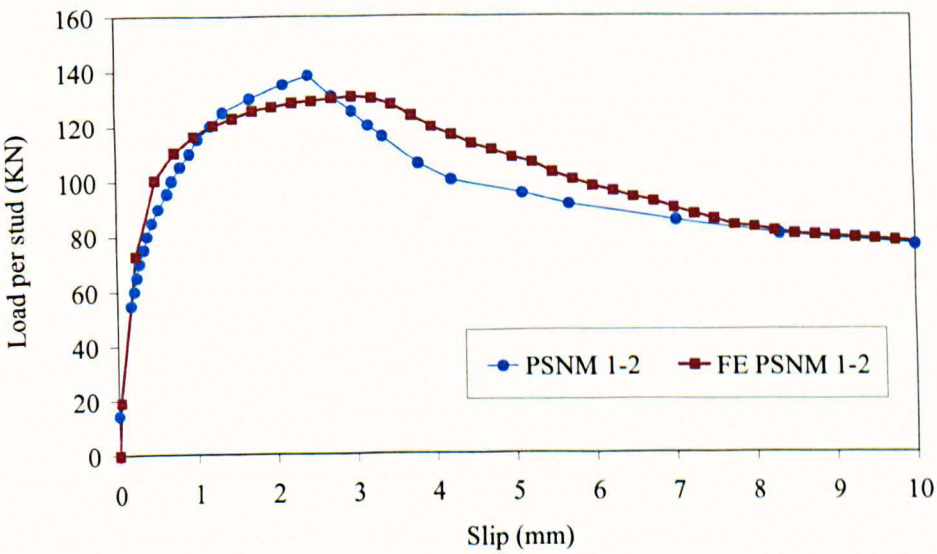

Figure 6.28 Comparison of experimental and numerical load-slip behaviour for push test PSNM 1-2

6.3.10. Test PSNM 2

This push test had a single stud per trough with normal load applied on the first sheeting rib perpendicular to the longitudinal axis of the beam. The average concrete cube strength was 32.5 N/mm^2. The load-slip curves obtained from the experiment and finite element analysis for the push test PSNM 2 are presented in Figure 6.29. The maximum strength in case of specimens PSNM 2-1 and PSNM 2-2 was 127.2 kN with a slip of 2.3 mm and 134.6 kN at a slip of 1.38 mm respectively. The maximum load per stud in case of the finite element analysis was 127.6 kN with a slip of 2.74 mm. The load-slip behaviour obtained from the finite element analysis agreed well with experimental results.

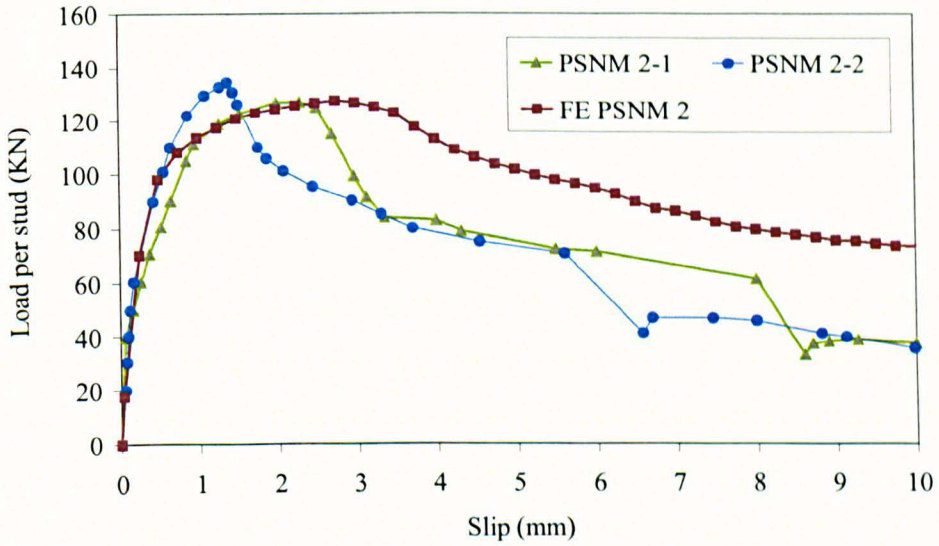

Figure 6.29 Comparison of experimental and numerical load-slip behaviour for push test PSNM 2

6.3.11. Test PDNM 1

This push test contained double layers of wire mesh with double studs per rib along with the normal load application in addition to the shear load. The average concrete cube strength was 47 N/mm^2. The comparison of the experimental versus numerical load-slip behaviour for the push test PDNM 1 is presented in Figure 6.30. The shear connector resistance obtained from push test specimens PDNM 1-1 and PDNM 1-2 was 72.7 kN and 81.8 kN with slips of 3.18 mm and 1.39 mm respectively. The maximum load per stud in case of the finite element analysis was 79.7 kN at a slip of 2.23 mm.

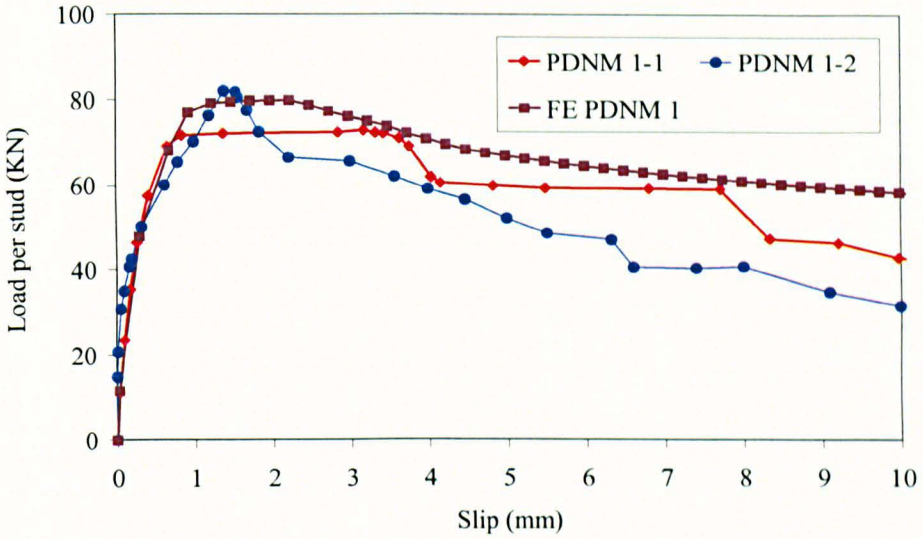

Figure 6.30 Comparison of experimental and numerical load-slip behaviour for push test PDNM 1

6.3.12. Test PDNM 2

The push test PDNM 2 used double studs per rib and had no studs in the first and last rib. The average concrete cube strength was 31 N/mm^2. The comparison of load-slip curves obtained from the finite element analysis and the push test experiment PDNM 2 is given in Figure 6.31. Push test specimens PDNM 2-1 and PDNM 2-2 failed at a load per stud of 77.3 kN and 76.8 kN respectively. The corresponding slip at failure was 0.84 mm and 1.32 mm for specimens PDNM 2-1 and PDNM 2-2 respectively. The failure in the finite element model occurred at a load per stud of 75.6 kN with a slip of 1.82 mm.

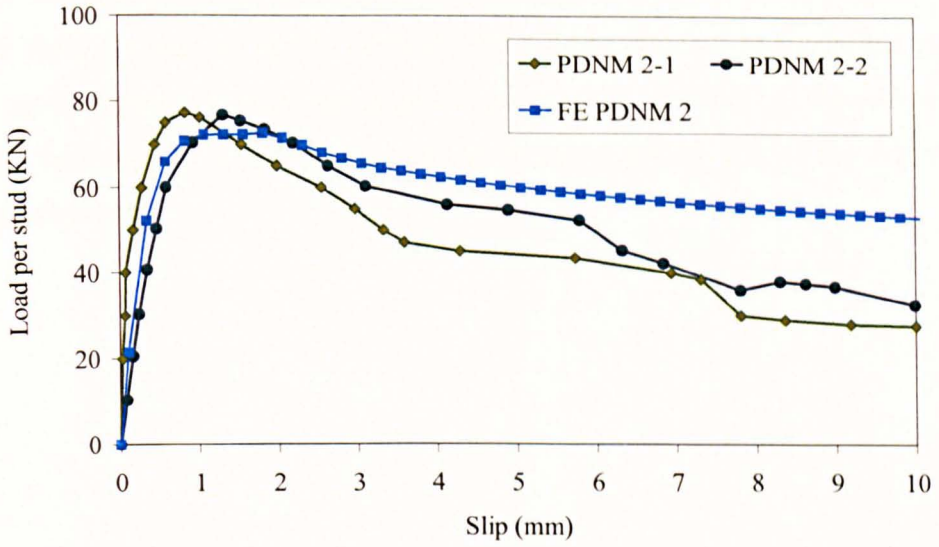

Figure 6.31 Comparison of experimental and numerical load-slip behaviour for push test PDNM 2

6.3.13. Summary

The developed three-dimensional finite element model have been validated against push tests conducted in this study with different mesh layers, mesh positions, load applications, number of shear studs per rib, concrete strengths and push testing arrangements. The summary of comparison of the shear connector strength and slip obtained from push test experiments conducted in this study and finite element analysis is presented in Table 6.3. The mean value of the experimental over finite element load per stud is 0.99 with a coefficient of variation of 5.3% and the mean value of experimental over numerical slip is 0.82 with corresponding coefficient of variation of 26.3%. It can be observed in Table 6.3 that a very close correlation has been achieved between the experimental and numerical shear connector resistance. The load per stud obtained from the finite element analysis is within 10% of the experimental shear connector strength.

There is a large variation between the numerical and the experimental results in terms of ductility of the shear connector. The post-failure load-slip behaviour of the push test is dependent upon the position of wire mesh with respect to the shear connector and aggregate interlock of the concrete mix used. Sometimes two push test specimens with same material properties result in different slip at failure, as it is not always possible to

locate the wire mesh in two separate specimens precisely at the same position. Except few push tests, the slip at failure obtained from finite element analysis has generally showed good agreement with the experimental results. Moreover, the shape of the numerical load-slip curve mostly follows the similar trend as that of the experimental load-slip behaviour.

Table 6.3 Comparison of shear connector strength and slip obtained from push tests conducted in this study and finite element analysis

S. No.	Test Ref.	Concrete Cube Strength, f_{cu} (MPa)	No. of Studs per rib, Nr	Total No. of studs	Mesh Position	No. of Mesh layers	Extra Reinforcement	Experimental Load, P_{test} (kN)	Load per stud from FEA, P_{FEA} (kN)	Slip, δ_{test} (mm)	Slip, δ_{FEA} (mm)	P_{test} / P_{FEA}	δ_{test} /δ_{FEA}
1	PTS 1-1	34.00	1	5	Low	single	--	75.7	79.7	0.6	1.2	0.95	0.50
2	PTS 1-2	34.00	1	5	Low	single	--	78.8	79.7	0.7	1.2	0.99	0.58
3	PTS 2-1	27.50	1	5	High	single	--	69.0	73.0	1.7	1.5	0.95	1.13
4	PTS 2-2	27.50	1	5	High	single	--	73.8	73.0	1.4	1.5	1.01	0.93
5	PTD 1-1	27.85	2	10	High	single	--	52.1	52.3	1.0	1.2	1.00	0.83
6	PTD 1-2	27.85	2	10	High	single	--	45.4	52.3	0.9	1.2	0.87	0.75
7	PTD 2-1	28.04	2	10	High	single	T16	52.2	52.3	1.2	1.5	1.00	0.80
8	PTD 2-2	28.04	2	10	High	single	T16	47.3	52.3	1.0	1.5	0.90	0.67
9	PTSN 1-1	25.35	1	5	Low	single	--	97.8	99.2	2.5	2.9	0.99	0.86
10	PTSN 1-2	25.35	1	5	Low	single	--	98.9	99.2	2.5	2.9	1.00	0.86
11	PTSN 2-1	21.19	1	5	High	single	--	90.0	88.6	1.4	1.7	1.02	0.82
12	PTSN 2-2	23.24	1	5	High	single	--	81.7	88.6	1.6	1.7	0.92	0.94
13	PTDN 1-1	28.19	2	10	High	single	--	61.3	59.2	1.4	1.4	1.04	1.00
14	PTDN 1-2	36.97	2	10	High	single	--	67.3	67.0	1.2	1.2	1.00	1.00
15	PTDN 2-1	58.82	2	8	High	single	--	91.3	93.6	1.1	1.5	0.98	0.73
16	PTDN 2-2	63.17	2	8	High	single	--	93.7	93.6	1.4	1.5	1.00	0.93

S. No.	Test Ref.	Concrete Cube Strength, f_{cu} (MPa)	No. of Studs per rib, Nr	Total No. of studs	Mesh Position	No. of Mesh layers	Extra Reinforcement	Experimental Load, P_{test} (kN)	Load per stud from FEA, P_{FEA} (kN)	Slip, δ_{test} (mm)	Slip, δ_{FEA} (mm)	P_{test} / P_{FEA}	δ_{test} /δ_{FEA}
17	PSNM 1-1	32.8	1	4	Low & High	double	--	113.0	120.4	2.7	3	0.94	0.90
18	PSNM 1-2	36.1	1	4	Low & High	double	--	138.4	130.6	2.4	3	1.06	0.80
19	PSNM 2-1	32.3	1	4	Low & High	double	--	127.2	127.6	2.3	2.7	1.00	0.85
20	PSNM 2-2	32.7	1	4	Low & High	double	--	134.6	127.6	1.4	2.7	1.05	0.52
21	PDNM 1-1	46.0	2	8	Low & High	double	--	72.7	79.7	3.2	2.2	0.91	1.45
22	PDNM 1-2	48.8	2	8	Low & High	double	--	81.8	79.7	1.4	2.2	1.03	0.64
23	PDNM 2-1	30.7	2	6	Low & High	double	--	77.3	72.6	0.84	1.8	1.06	0.47
24	PDNM 2-2	31.6	2	6	Low & High	double	--	76.8	72.6	1.3	1.8	1.06	0.72
											Mean	**0.99**	**0.82**
											COV	**5.3%**	**26.3%**

Note: Mesh located at low position is resting on top of the steel deck and at high location is 30 mm from top of the concrete slab. T16 bar is placed at the bottom trough of the sheeting.

6.4. Validation against push tests conducted by other authors

Push tests conducted in this study used 19 × 100 mm long shear studs and 60 mm high steel deck; and shear studs were located on the favourable side of the sheeting pan only. In order to ensure the reliability of the finite element model developed in this study, various numerical models have been prepared using experimental studies conducted by different authors in the past and the results from the finite element analysis are verified against these experiments. The comparison of the strength and ductility of the shear connector obtained from experimental push tests conducted by various authors and the finite element analysis is presented in Table 6.4. Push tests with different shear stud locations, sheeting thicknesses, sizes of the shear connector, steel deck heights and push testing arrangements have been used in this validation study to make absolutely sure that the finite element model developed in this study is suitable for modelling the behaviour of the headed shear connector in steel-concrete composite beams with transversely placed profiled sheeting under all possible situations. The mean value of the experimental over numerical load per stud is 1.03 with a coefficient of variation of 4.7% and the mean value of the experimental over numerical slip is 0.99 with a corresponding coefficient of variation of 11.1%. Generally, the results obtained from the finite element analysis matched very well the experimental results.

Table 6.4 Comparison of shear connector strength and slip obtained from push tests conducted by other authors and finite element analysis

S. No.	Test Ref.	Concrete Cube Strength, f_{cu} (MPa)	Stud Details			Deck details			Experimental Load, P_{test} (kN)	Load per stud from FEA, P_{FEA} (kN)	Slip, δ_{test} (mm)	Slip, δ_{FEA} (mm)	P_{test} / P_{FEA}	δ_{test} /δ_{FEA}	Tested by
			Position	Size $d \times h_{sc}$ (mm × mm)	Transverse spacing (mm)	Height, h_p (mm)	Average rib width, b_o (mm)	Thickness, t (mm)							
1	G1F	35.0	F	19 × 125	--	80	140	1.2	91.9	86.8	3.8	4.0	1.06	0.95	Johnson & Yuan (1998)
2	G2C	27.3	C	19 × 125	--	55	162	0.9	88.4	87.3	15	14.0	1.01	1.07	
3	G5U	35.0	U	19 × 125	--	80	140	1.2	69.2	69.5	8	9.2	1.00	0.87	
4	G6U	27.3	U	19 × 95	--	60	113	0.9	52.6	55.2	16	17.2	0.95	0.93	
5	G7S	24.2	F & U	19 × 95	53	60	113	0.9	50.7	47.0	4.9	5.0	1.08	0.98	
6	G8S	24.2	F & U	19 × 125	65	80	140	1.2	60.8	55.7	4.5	4.7	1.09	0.96	
7	JDT-4	34.5	C	16×76	76	38	91.8	0.9	54	50	3.0	2.7	1.08	1.11	Jayas & Hosain (1988)
8	JDT-5	34.5	C	16×76	76	38	60.6	0.9	44.8	44.4	2.2	2.1	1.01	1.05	
9	JDT-7	24.4	F	19×127	90	76	152.5	1.2	46	44	3.2	2.8	1.05	1.14	
10	R30-1-U	31.6	U	19 × 95	--	60	170	1.2	72.3	70.2	7	7.7	1.03	0.91	Mottram & Johnson (1990)
11	R30-1-UD	34.6	U	19 × 120	--	60	170	1.2	89.3	91.7	7	8.1	0.97	0.86	
12	--	20.4	F	19 × 100	76	60	150	0.9	51.2	51.6	2.5	2.1	0.99	1.19	Hicks (2007)
13	--	20.4	F	19 × 100	--	60	150	0.9	84.7	76.3	2.0	2.3	1.11	0.87	
												Mean	**1.03**	**0.99**	
												COV	**4.7%**	**11.1%**	

6.5. Conclusion

The developed finite element model has been verified in this chapter against a variety of push tests conducted in this study and experimental studies performed previously by other authors. The sensitivity of the finite element model to the mesh size and loading rate is also tested; and appropriate mesh size and loading rate have been selected. The results obtained from the finite element analysis not only compared well with experimental studies in terms of the strength and ductility of the shear connector but the failure patterns of the numerical model also matched with the experiments.

The experimental studies selected for the validation study had different shear stud positions, shear stud dimensions, sheeting dimensions, transverse spacings, number of shear studs, wire mesh positions, loading arrangements and push testing arrangements. The finite element model predicted the behaviour of the push test accurately comparable with these experimental studies. It is concluded that the three-dimensional finite element model developed in this study is reliable enough for modelling the push test with trapezoidal steel deck and is suitable for performing a parametric study.

Chapter 7
Parametric study

Chapter 7
Parametric study

7.1. Introduction

This chapter presents the results and discussions of an extensive parametric study conducted after development and validation of the three-dimensional finite element model for the push test with steel deck in Chapter 5 and 6 respectively. The parametric study is divided into two parts. The first part considers the effect of transverse spacing of pairs of shear connecters placed in the favourable position or staggered by placing one each in the favourable and unfavourable position on the performance of the headed shear stud. The second part deals with the influence of steel deck thickness and shear stud position on the strength, ductility and failure mechanisms of the headed shear stud in steel-concrete composite beams. The behaviour of the push test with profiled sheeting having different sheeting thicknesses, shear connector layouts and positions, number of shear studs in a rib and concrete strengths is discussed; and shear stud strength prediction equations have been proposed and verified. The dimensions of the shear stud, concrete slab, and welded wire mesh are kept constant throughout this investigation.

7.2. Summary of push test set up

The parametric study conducted in this study necessitated the use of the finite element model with full width of the concrete slab, in particular for the staggered positioned stud layout, where the symmetry across the longitudinal centre line of the beam flange cannot be utilized. However, the symmetry has been used wherever possible. If the full scale finite element model of the horizontal push tests, conducted in this study, were used for the parametric study, it would be very intensive in terms of computational time. As, the material models and analysis procedure employed in this study have matched very well with experimental studies, the standard push test arrangement with profiled sheeting suggested by Hicks (2007) is adopted for the parametric study as shown in Figure 1.1, which is shorter than the push tests conducted in this research. The dimensions of the shear stud, profiled sheeting and wire mesh are same as that of push tests conducted in this study. The depth of the concrete slab was changed from 150 mm, as used by Hicks (2007), to 140 mm to make it consistent with the push tests conducted in this study.

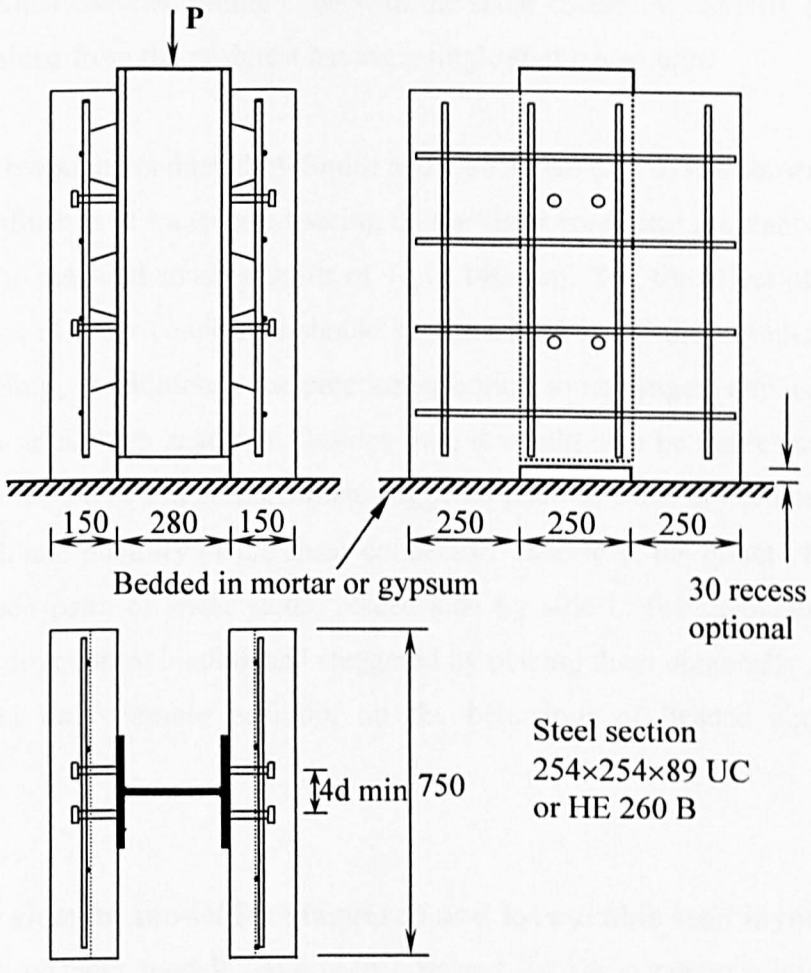

Figure 7.1 Standard push test arrangement with profiled sheeting (Hicks, 2007)

7.3. Effect of shear connector spacing and layout

It is widely accepted that failure in the push test with metal deck is predominantly controlled by failure of concrete around shear connectors. For a single stud, a cone-shaped failure surface is formed starting from the underside of the head of the shear stud, while progressing towards the flanges of the profiled sheeting. In case of double studs per trough, failure cones around each stud are joined to form a wedge-shaped failure surface, thus some of the area of the failure surface is duplicated between two studs. For this reason, the load per stud obtained from the push test with double studs per trough is always less than that from the push test with a single stud per trough, if the spacing between studs is within the practical limits of 80-100 mm. However, if the spacing between shear studs is increased significantly, it is expected that each shear connector would be independent of each other and would have sufficient space to

develop individual concrete failure cone with the shear connector capacity comparable to the one obtained from the push test having a single stud per trough.

Although, the research conducted by Smith and Couchman (2010) has shown that there is very little influence of transverse spacing on the shear connector resistance of double studs within the practical spacing limits of 75 to 140 mm. Yet, the effect of transverse spacing of pairs of shear connectors should be extended beyond these limits to include the larger spacings, in addition to the practical spacings, to investigate any likely benefit of using larger transverse spacings. Besides this, it would also be interesting to see if there is any influence of staggering, when staggered pairs of shear connectors are used, on the strength and ductility of the shear connector. Therefore, the effect of transverse spacing between pairs of shear studs, placed side by side in the favourable position parallel to the direction of loading and staggered by placing them diagonally apart in the favourable and unfavourable position, on the behaviour of headed shear stud is investigated.

7.3.1. Finite element model for staggered and favourable stud layout

Separate finite element models have been prepared for the parametric study using a push test with staggered and favourable positioned studs as shown in Figure 7.2 and Figure 7.3 respectively. The geometry of the push test was created by assuming half symmetry along the web of the steel beam. In finite element model, the beam flanges have been widened to accommodate larger spacings between the shear connectors. All parts were meshed with the same element types as that of the validated model.

The bottom of the beam flange was taken as symmetric in the X direction. The surface of the concrete slab and steel deck, where it was bedded to the ground which was on the opposite side of the applied shear loading on the steel beam in this case, was restrained from translating in the Z direction. Four corner nodes of the concrete slab, steel deck and beam were restricted from moving in the Y direction to prevent the free body motion of the model. The constraints, contact interaction and material properties of all steel components remained same as that of the validated model. The concrete properties consisting of characteristic compressive strength, f_{ck}, mean compressive strength, f_{cm}, mean tensile strength, f_{ctm} and elastic modulus, E_{cm} were calculated as per Eurocode 2 provisions as shown in Table 7.1.

Table 7.1 Concrete material properties for parametric study

Concrete Property	Concrete Grade			
	C12	C20	C30	C40
f_{ck} (MPa)	12	20	30	40
f_{cm} (MPa)	20	28	38	48
f_{ctm} (MPa)	1.6	2.2	2.9	3.5
E_{cm} (GPa)	27	30	33	35

7.3.2. Results and discussion

In total 64 push tests with different transverse spacings and stud layouts, and 4 push tests with a single stud in the favourable location have been analysed. The push test specimens have been divided into 8 groups as shown in Table 7.2. The first 4 groups consist of specimens with double studs placed in favourable positions, while the rest of the groups contain diagonally placed studs each in the favourable and unfavourable position. Each group contains 8 push test specimens with transverse spacing of 40, 60, 80, 100, 150, 200, 300 and 400 mm. Group 1 to 4 had the same geometry but with different concrete grades of C12, C20, C30 and C40. Similarly, group 5 to 8 had the same dimensions but with different concrete grades of C12, C20, C30 and C40.

The results of the parametric study for the effect of the shear connector spacing and layout have been summarised in Table 7.2. In this Table, the load per stud obtained from the finite element analysis for double studs is denoted by P_{FE}, the numerical load per stud for staggered positioned studs and single stud is indentified by $P_{FE\text{-}Stagg}$ and $P_{FE\text{-}Single}$ respectively. The strength of the shear connector obtained from eight groups having double studs in the sheeting pan is compared with the resistance of a single shear stud per trough. The shear connector resistance of double studs placed in the favourable position is also compared with the strength of staggered shear connectors. In addition, the failure modes for each push test have also been predicted in Table 7.2.

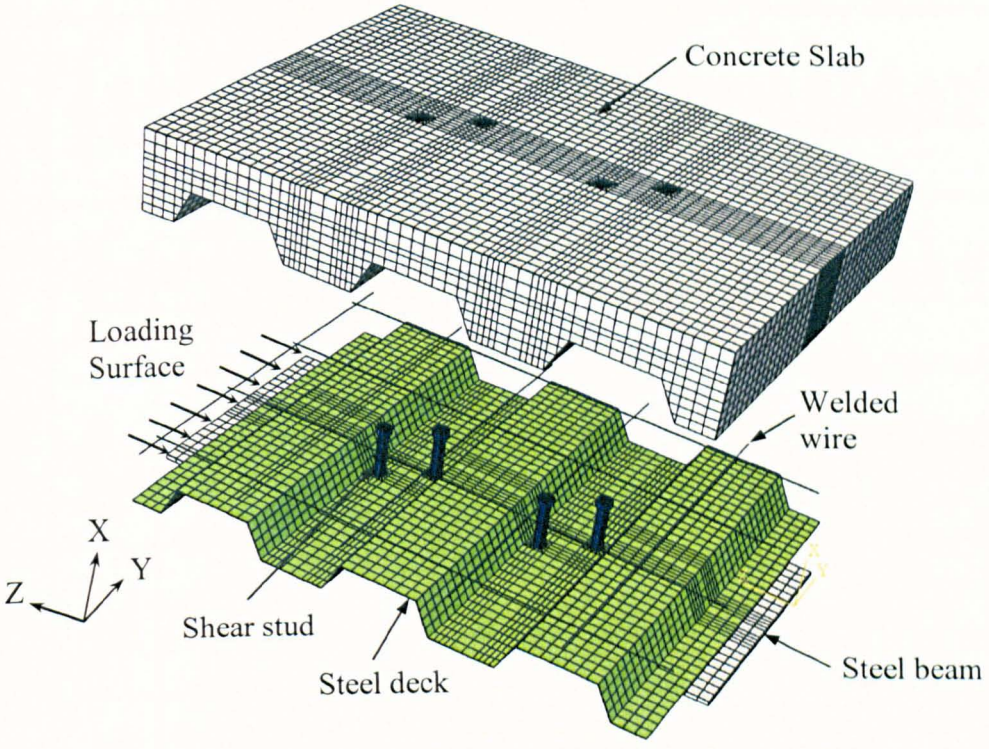

Figure 7.2 Finite element model used for parametric study of staggered positioned studs

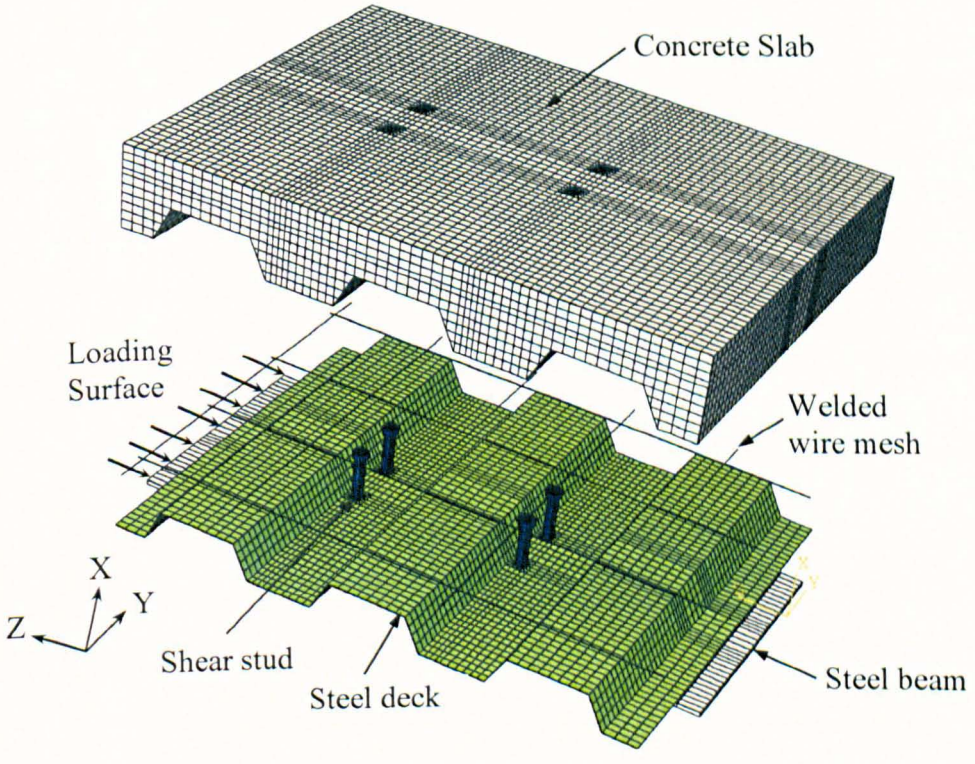

Figure 7.3 Finite element model used for parametric study of favourable positioned studs

Table 7.2 Results of parametric study for shear connector spacing and layout

Group	Test Ref	Concrete Grade	Stud position	Stud layout	Transverse spacing, (mm)	P_{FE}, (kN)	$P_{FE\text{-}Single}$, (kN)	$P_{FE}/P_{FE\text{-}Single}$	$P_{FE}/P_{FE\text{-}Stagg}$	Failure Mode
G1	G1-1	C12	F	in line	40	49.8	72.6	0.69	1.00	CCF
	G1-2				60	49.9		0.69	1.00	CCF
	G1-3				80	51.6		0.71	1.00	CCF
	G1-4				100	53.5		0.74	1.00	CCF
	G1-5				150	59.8		0.82	1.01	CCF
	G1-6				200	66.0		0.91	1.04	CCF
	G1-7				300	66.3		0.91	1.05	CCF
	G1-8				400	66.7		0.92	1.05	CCF
G2	G2-1	C20	F	in line	40	62.4	90.9	0.69	1.01	CCF
	G2-2				60	62.6		0.69	1.01	CCF
	G2-3				80	64.4		0.71	1.01	CCF
	G2-4				100	68.2		0.75	1.00	CCF
	G2-5				150	76.1		0.84	1.03	CCF
	G2-6				200	84.0		0.92	1.07	CCF
	G2-7				300	84.4		0.93	1.07	CCF
	G2-8				400	84.9		0.93	1.08	CCF
G3	G3-1	C30	F	in line	40	78.0	110.5	0.71	1.01	CCF
	G3-2				60	78.2		0.71	1.01	CCF
	G3-3				80	80.4		0.73	1.01	CCF
	G3-4				100	85.0		0.77	1.00	CCF
	G3-5				150	94.0		0.85	1.04	CCF
	G3-6				200	104.0		0.94	1.09	CCF
	G3-7				300	104.5		0.95	1.10	CCF
	G3-8				400	105.0		0.95	1.11	CCF

Group	Test Ref	Concrete Grade	Stud position	Stud layout	Transverse spacing, (mm)	P_{FE}, (kN)	$P_{FE\text{-}Single}$, (kN)	$P_{FE}/P_{FE\text{-}Single}$	$P_{FE}/P_{FE\text{-}Stagg}$	Failure Mode
G4	G4-1	C40	F	in line	40	89.3	127.5	0.70	1.02	CCF
	G4-2				60	89.5		0.70	1.02	CCF
	G4-3				80	94.0		0.74	1.02	CCF
	G4-4				100	99.3		0.78	1.02	CCF
	G4-5				150	110.0		0.86	1.08	CCF
	G4-6				200	121.4		0.95	1.12	CCF
	G4-7				300	122.0		0.96	1.12	CCF
	G4-8				400	122.6		0.96	1.12	CCF
G5	G5-1	C12	F & U	Staggered	40	49.7	72.6	0.68	1.00	CCF
	G5-2				60	49.8		0.69	1.00	CCF
	G5-3				80	51.4		0.71	1.00	CCF
	G5-4				100	53.4		0.74	1.00	CCF
	G5-5				150	59.1		0.81	1.00	CCF
	G5-6				200	63.3		0.87	1.00	CCF
	G5-7				300	63.3		0.87	1.00	CCF
	G5-8				400	63.5		0.87	1.00	CCF
G6	G6-1	C20	F & U	Staggered	40	61.5	90.9	0.68	1.00	CCF
	G6-2				60	61.7		0.68	1.00	CCF
	G6-3				80	63.5		0.70	1.00	CCF
	G6-4				100	68.2		0.75	1.00	CCF
	G6-5				150	74.2		0.82	1.00	CCF
	G6-6				200	78.6		0.86	1.00	CCF
	G6-7				300	78.6		0.86	1.00	CCF
	G6-8				400	78.8		0.87	1.00	CCF

Group	Test Ref	Concrete Grade	Stud position	Stud layout	Transverse spacing, (mm)	P_{FE}, (kN)	$P_{FE\text{-}Single}$, (kN)	$P_{FE}/P_{FE\text{-}Single}$	$P_{FE}/P_{FE\text{-}Stagg}$	Failure Mode
G7	G7-1	C30	F & U	Staggered	40	76.9	110.5	0.70	1.00	CCF
	G7-2				60	77.1		0.70	1.00	CCF
	G7-3				80	79.3		0.72	1.00	CCF
	G7-4				100	85.2		0.77	1.00	CCF
	G7-5				150	90.6		0.82	1.00	CCF
	G7-6				200	95.2		0.86	1.00	CCF
	G7-7				300	95.2		0.86	1.00	CCF
	G7-8				400	95.0		0.86	1.00	CCF
G8	G8-1	C40	F & U	Staggered	40	87.8	127.5	0.69	1.00	CCF
	G8-2				60	88.0		0.69	1.00	CCF
	G8-3				80	92.0		0.72	1.00	CCF
	G8-4				100	97.7		0.77	1.00	CCF
	G8-5				150	102.3		0.80	1.00	CCF-SS
	G8-6				200	108.8		0.85	1.00	CCF-SS
	G8-7				300	108.8		0.85	1.00	CCF-SS
	G8-8				400	109.5		0.86	1.00	CCF-SS

"CCF" indicates concrete cone failure, and "CCF-SS" stands for combined concrete cone and stud shearing failure.

To investigate any benefit of using a large spacing between studs, the load per stud versus transverse spacing and load per stud versus staggered spacing curves for different concrete grades are plotted in Figure 7.4 and Figure 7.5 respectively. The results indicate that there is very little change in the shear connector resistance for spacing equal to or less than 80 mm. This suggests that placing shear studs less than 80 mm apart does not give any benefit in terms of an increase in the shear connector resistance. The strength increases in a straight line beyond transverse and staggered spacings of 100 mm and continues to enhance until 200 mm spacing is reached.

Although, very large spacings of up to 400 mm were tried, no improvement in the shear connector resistance was observed past 200 mm spacing. It suggests that using transverse and staggered spacings beyond 200 mm does not give any particular advantage, and the shear connector strength remains almost unchanged as indicated by horizontal line in load versus transverse spacing and load versus staggered spacing curves. It is clear from Figure 7.4 and Figure 7.5 that the most crucial spacing limit is between 100 and 200 mm, whereby the shear connector resistance increases significantly.

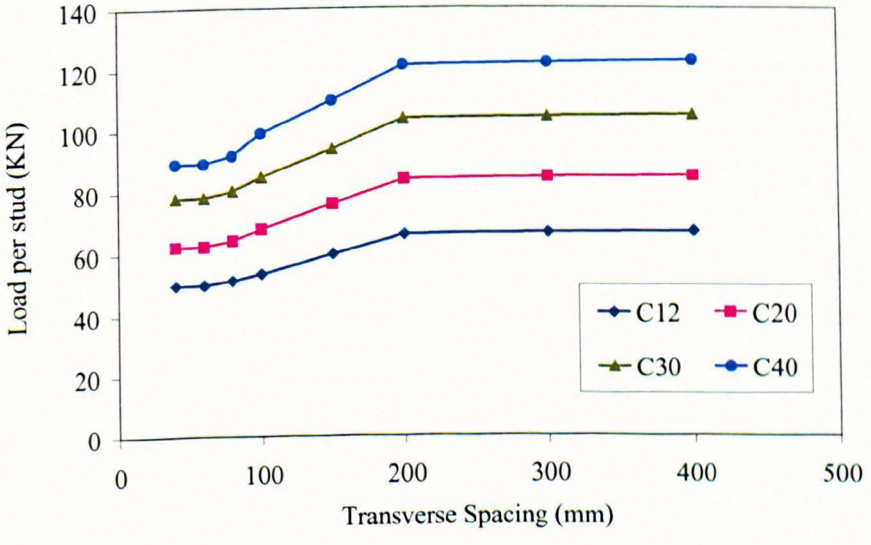

Figure 7.4 Load versus transverse spacing curve for favourable positioned studs

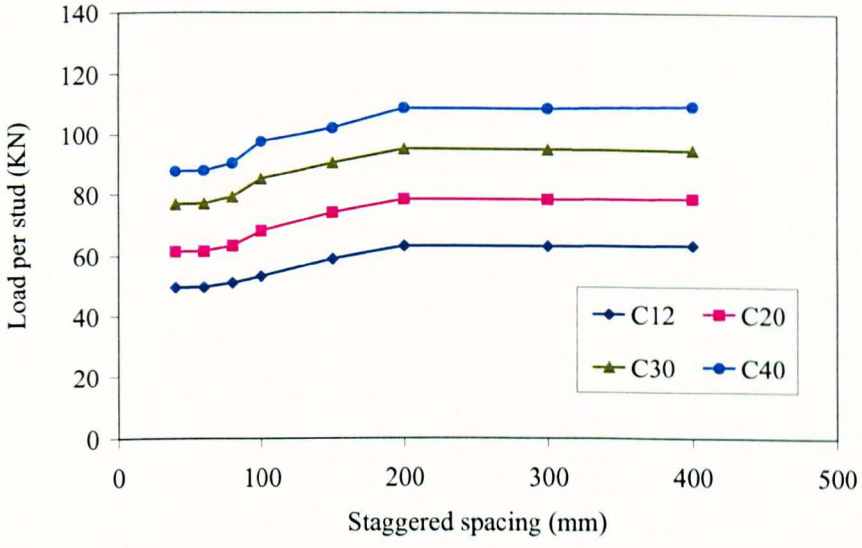

Figure 7.5 Load versus staggered spacing curve for staggered stud layout

According to the strength reduction factor approach of Eurocode 4 for calculating the shear capacity of the stud in a composite beam with profiled sheeting, the resistance per stud when used as double studs per trough should be 71% of the single shear stud resistance. The factor $P_{FE}/P_{FE\text{-}Single}$ for 80 mm transverse and staggered spacing is 0.71 in case of C12 and C20 concrete. For higher concrete strengths, this factor increases to 0.72 and 0.74 in case of staggered and transverse spacings respectively. The Eurocode 4 requires that the spacing of shear studs in the direction transverse to the shear force should not be less than 4 times the diameter of the stud shaft, which comes out to be 76 mm for 19 mm dia studs. The results of the finite element analysis suggested that the Eurocode 4 provision of the strength of double studs being 71% of the resistance of a single stud holds true if the transverse spacing is not more than 80 mm. For spacings larger than 80 mm, higher shear connector resistances can be obtained.

The strength of double studs, placed in favourable and staggered positions, and single stud for C12 concrete is compared in Figure 7.6. The resistance of double studs is 0.91 of the single stud, when the transverse spacing between studs is 200 mm or higher. For staggered positioned studs, when the staggered spacing is 200 mm, the shear connector resistance of double studs is 0.87 times the shear connector resistance of a single stud per rib. Apparently, there is no difference in shear connector resistances between staggered and favourable double studs when the spacing is less than 150 mm. At 200

mm spacing, the strength of transverse positioned studs is 4% more than the staggered positioned studs for a concrete grade of C12.

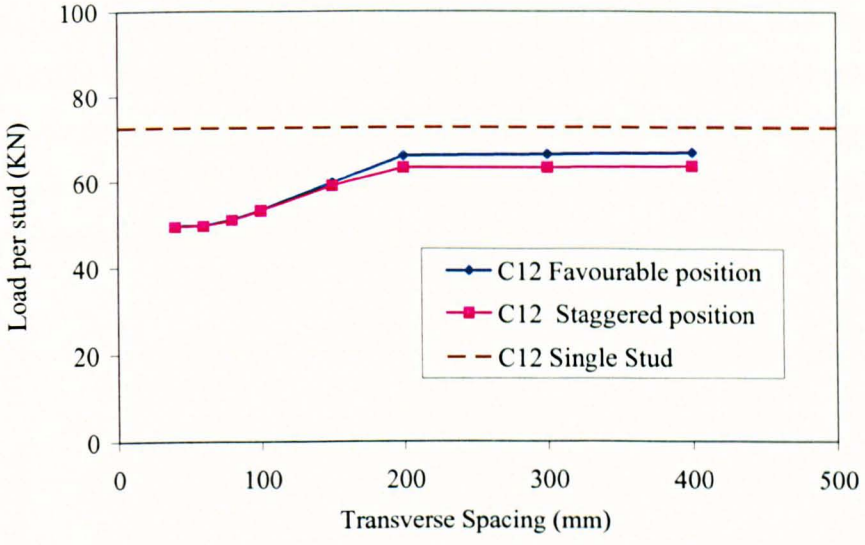

Figure 7.6 Shear connector resistance of single and double studs for C12 concrete

The shear connector resistance of double and single studs per rib with C20 concrete grade is plotted in Figure 7.7. The strength of double studs in a favourable position is 0.92 of the single stud, while the strength of staggered double studs is 0.86 of the single stud for 200 mm spacing. The shear connector resistance of favourable double studs is 7% more than the staggered positioned double studs for C20 concrete grade.

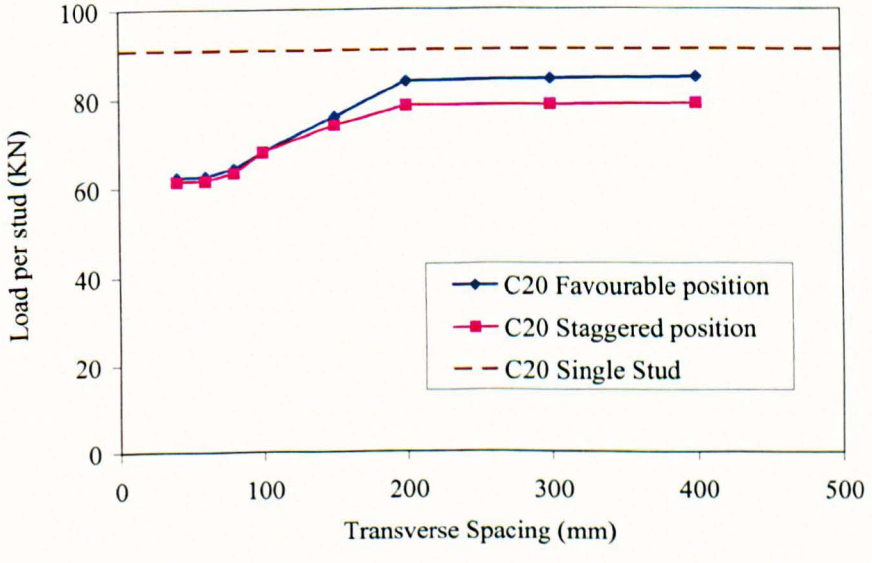

Figure 7.7 Shear connector resistance of single and double studs for C20 concrete

The shear connector strength of double and single studs per rib for C30 concrete is presented in Figure 7.8. The strength of double studs placed in favourable and staggered positions is 0.94 and 0.86 of the single stud respectively. At 200 mm transverse spacing, the resistance of double studs in a favourable position is 9% more than the staggered positioned studs. The shear connector resistance of double and single studs for C40 concrete grade is presented in Figure 7.9. The strength of double studs placed in the favourable position is 0.95 of the single stud for 200 mm transverse spacing. The resistance of double studs is 12% more than staggered studs for C40 concrete grade.

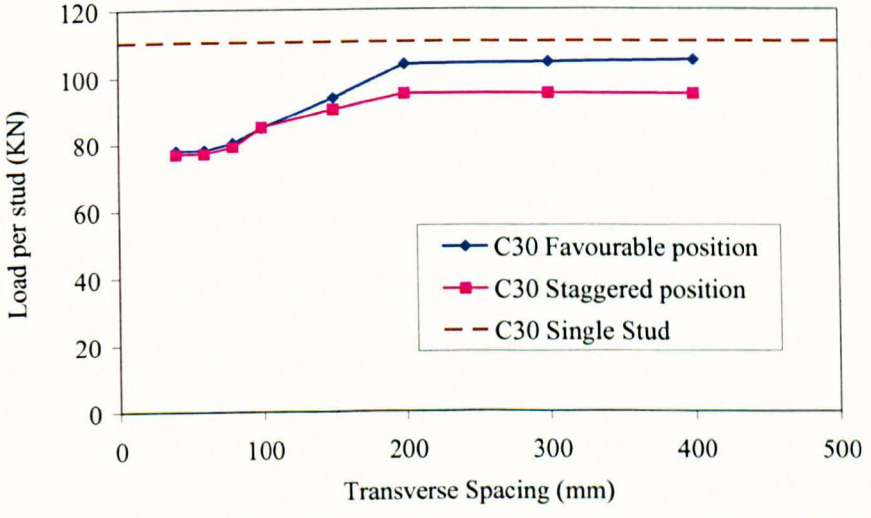

Figure 7.8 Shear connector resistance of single and double studs for C30 concrete

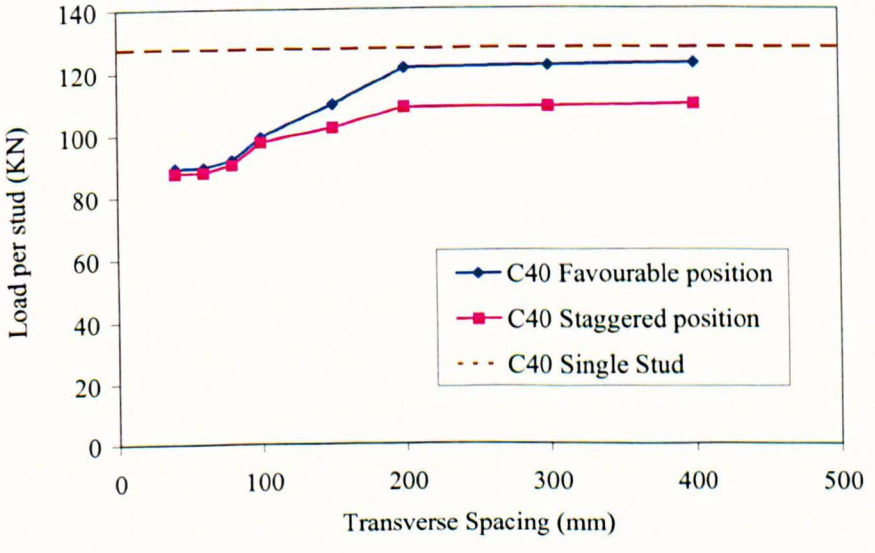

Figure 7.9 Shear connector resistance of single and double studs for C40 concrete

Mainly, the strength of double shear studs placed in a favourable position is more than the strength of staggered positioned studs. In the staggered layout, one stud is placed in the favourable location, while the other is placed on the unfavourable side. Concrete failure surfaces primarily develop around the shear stud placed on the favourable side; and the unfavourable side stud does not form much of a failure cone. Contrary to that, when the shear studs are considerably far apart, double studs in a favourable position develop individual failure cones, which could be independent of each other. Thus, the area of the failure surface is larger in double studs placed on the favourable side than the failure surface area of staggered pairs of shear connectors. This is the reason that the resistance of staggered pairs is less than the double studs in a favourable location.

7.3.3. Load-slip behaviour

The position of the shear connector within a sheeting pan affects the load-slip behaviour of a push test. Push tests with favourable studs are as generally considered to fail at a lower slip than the push tests with unfavourable studs. In order to understand the effect of transverse spacing on the load-slip behaviour of a push test, load versus slip curves are plotted for push tests with favourable studs and staggered positioned studs.

The load versus slip curve for push tests with favourable double studs having different transverse spacings, and a concrete grade of C12 is plotted in Figure 7.10. As all push tests with favourable studs exhibited almost similar load-slip behaviour for a particular concrete grade, only transverse spacings of 100, 150, 200 and 300 mm are used in the load-slip plot. It can be observed that an average slip of not more than 1.5 mm is observed in all push tests with favourable double studs having a concrete grade of C12. It has, however, increased to 2, 2.5 and 3 mm for concrete grades of C20, C30 and C40 respectively as shown in Table 7.3.

The load-slip curve for the push test with staggered positioned studs having a transverse spacing of 100 mm is plotted in Figure 7.11. It is evident that the slips in the range of 6-9 mm are observed when the shear studs are staggered with a spacing of 100 mm. The staggered layout consists of both favourable and unfavourable studs placed within one sheeting rib. The behaviour of the unfavourable stud is more ductile than the favourable stud because the former depends on properties of the steel deck rather than the concrete strength, which results in greater slip at the steel-concrete interface.

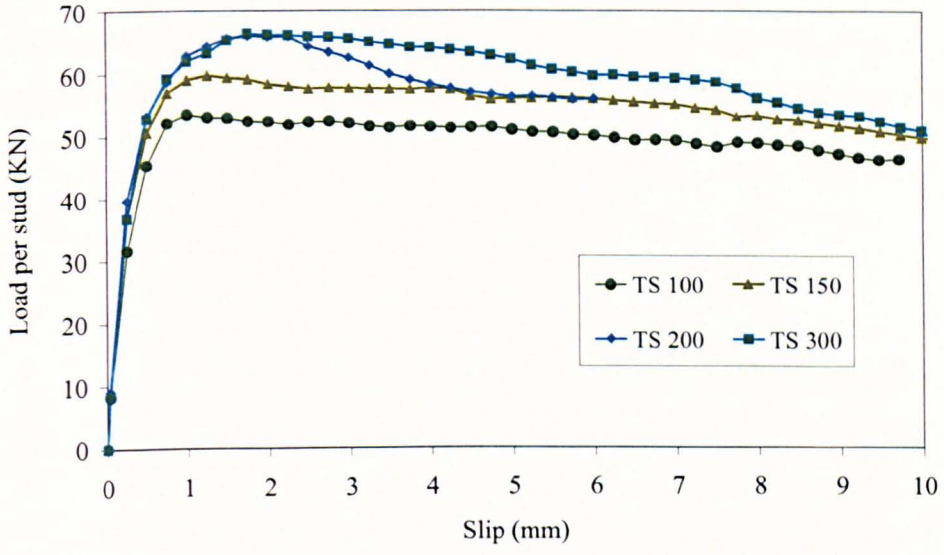

Figure 7.10 Load-slip curve for push tests with favourable double studs having different transverse spacings and C12 concrete grade

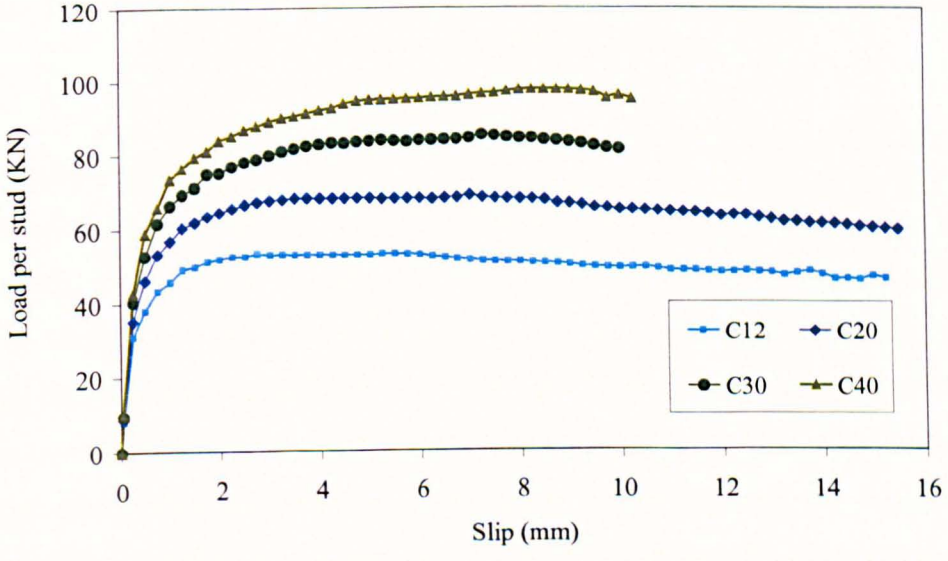

Figure 7.11 Load-slip curve for the push test with staggered positioned studs having a transverse spacing of 100 mm

The load versus slip curve for the push test with staggered positioned studs having a transverse spacing of 200 mm is plotted in Figure 7.12. Similar to the push test with a staggered spacing of 100 mm, slips in the range of 6-9 mm are observed in the load-slip plot for different concrete grades. All push tests having staggered spacing of 200 mm with different concrete grades behaved in more or less similar manner apart from the

test with C40 concrete grade in which the load-slip curve plunged down as soon as one of the favourable shear studs failed. This type of behaviour was observed in all push tests having a staggered spacing of 150 mm or more with a concrete grade of C40.

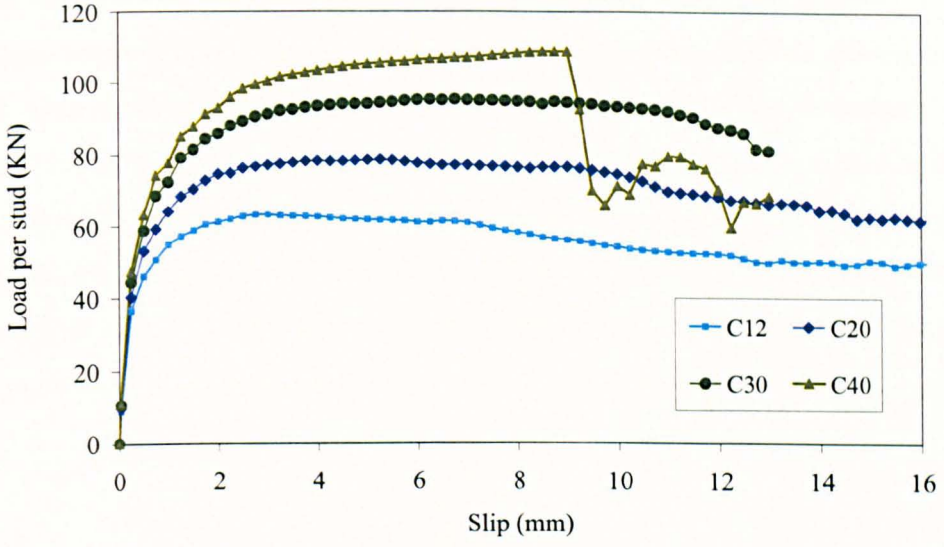

Figure 7.12 Load-slip curve for push test with staggered positioned studs having a transverse spacing of 200 mm

7.3.4. Failure modes

The failure mode of a push test depends on the position and layout of the shear stud in a sheeting rib, and concrete strength. Conventionally, the concrete cone failure, where cones or wedges of concrete are formed around the shear connector, has been the principal failure mode in a push test with trapezoidal metal floor decking. Therefore, the shear connector resistance has been largely dependent on the failure of concrete around the shear stud, rather than failure of the shear connector itself. In this study, for understanding the failure mechanism in a push test with trapezoidal profiled sheeting having different transverse spacings and shear connector layouts, the tensile damage variable, characterised by tensile cracking of the material, is plotted. The concrete slab above the top flange of the steel deck is removed to view the development of concrete failure cones properly. In all push tests, the sheeting rib closer to the load bearing direction of stud is termed as "first rib" and rib away from it is referenced as "second rib" as shown in Figure 7.13.

The tensile damage variable for the push test with double studs in the favourable position spaced at 60 mm and 400 mm having a concrete grade of C12 is plotted in Figure 7.13. It can be observed that due to a limited space available for concrete failure cones to be formed completely independently in case of transverse spacing of 60 mm, the failure cones around the shear connector are joined together as shown in Figure 7.13(a). This is the reason that the resistance of double studs in the favourable position is about 70% of the shear connector resistance of a single stud per tough. On the other hand, individual failure cones are formed around shear studs when they are 400 mm apart as shown in Figure 7.13(b). Because of independent concrete failure cones around shear studs in case of double studs spaced at 400 mm, the shear connector resistance is approximately 94% of the resistance obtained from a single stud per trough.

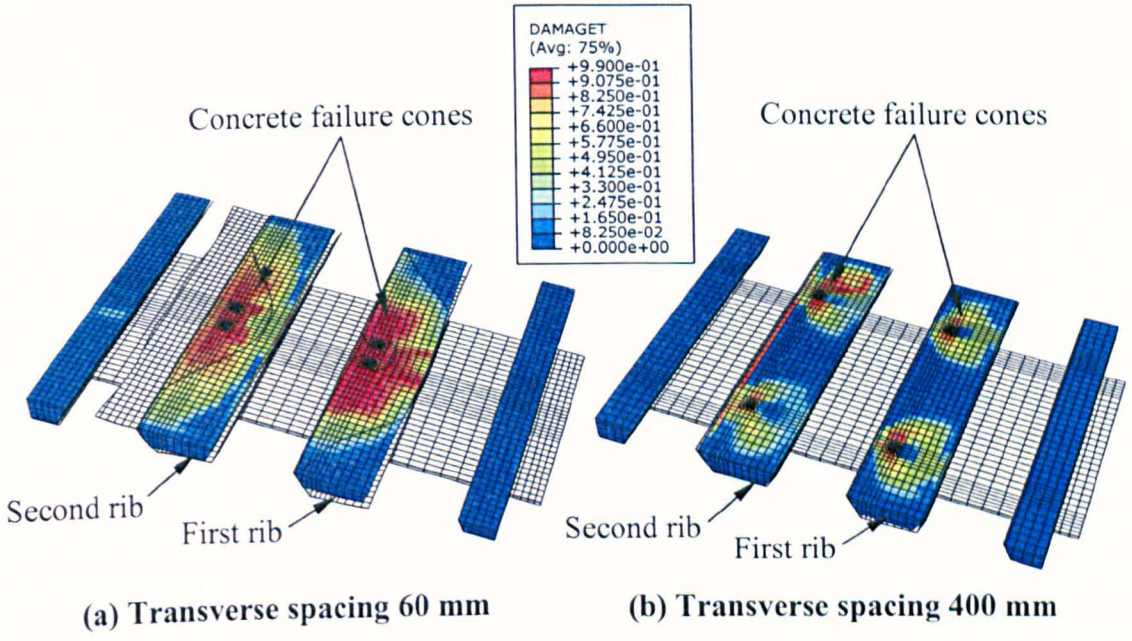

(a) Transverse spacing 60 mm **(b) Transverse spacing 400 mm**

Figure 7.13 Development of concrete failure cones in push tests with transverse spacings of 60 mm and 400 mm and C12 concrete

The comparison of concrete failure cones for push tests with favourable and staggered positioned studs having a transverse spacing of 100 mm and a concrete grade of C12 is shown in Figure 7.14. In case of favourable positioned double studs, failure cones are formed around shear studs while joining together at the zone of concrete between two studs as shown in Figure 7.14(a) and it can also be observed that failure cones are more prominent in the sheeting rib closer to the load bearing direction. For staggered studs, one stud is in the favourable position and other is in the unfavourable position; the favourable stud had a large failure cone formed around its shaft, while no visible failure

cone developed around the unfavourable stud as shown in Figure 7.14(b). The size of the failure cone was larger in the first rib as compared to the second rib. The failure patterns of push tests with concrete grades of C20, C30 and C40 were almost similar to the push test with C12 concrete and a transverse spacing of 100 mm.

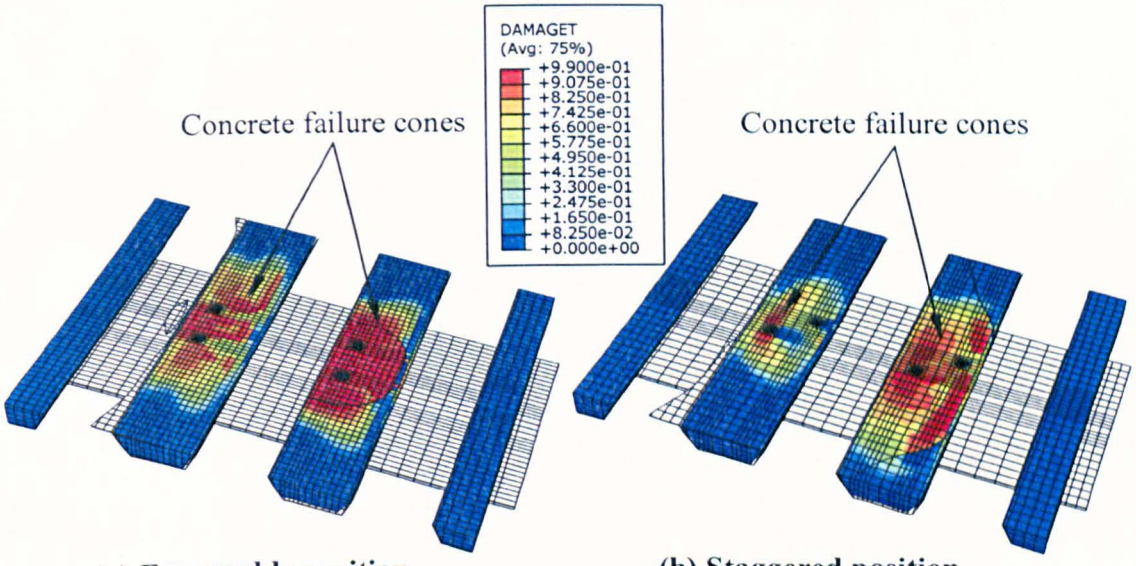

(a) Favourable position **(b) Staggered position**

Figure 7.14 Development of concrete failure cones in push tests with a transverse spacing of 100 mm and C12 concrete

The formation of failure cones for a push test with a transverse spacing of 150 mm and a concrete grade of C12 is shown in Figure 7.15. The size of concrete failure cones becomes larger when the transverse spacing is increased from 100 mm to 150 mm as indicated by more tensile damage in Figure 7.15 compared to Figure 7.14. The failure surfaces around the favourable stud in the first rib for the staggered position were grown to be bigger; and failure surfaces were not formed around the unfavourable stud. All other push tests with a transverse spacing of 150 mm and C20, C30 and C40 concrete grades failed by concrete cone failure except the push test with a staggered spacing of 150 mm having C40 concrete grade which failed by a combination of concrete cone failure and stud shearing failure. As, the staggered positioned layout had one stud in the favourable and other stud in the unfavourable side of the trough, there was a large volume of concrete in front of the favourable stud when spacing was equal to 150 mm. A large volume of strong concrete pushed the stud, and as a result, a combination of stud shearing and concrete conical failure occurred. The stud shearing failure in the

push test with a staggered spacing of 150 mm having C40 concrete grade is shown in Figure 7.16.

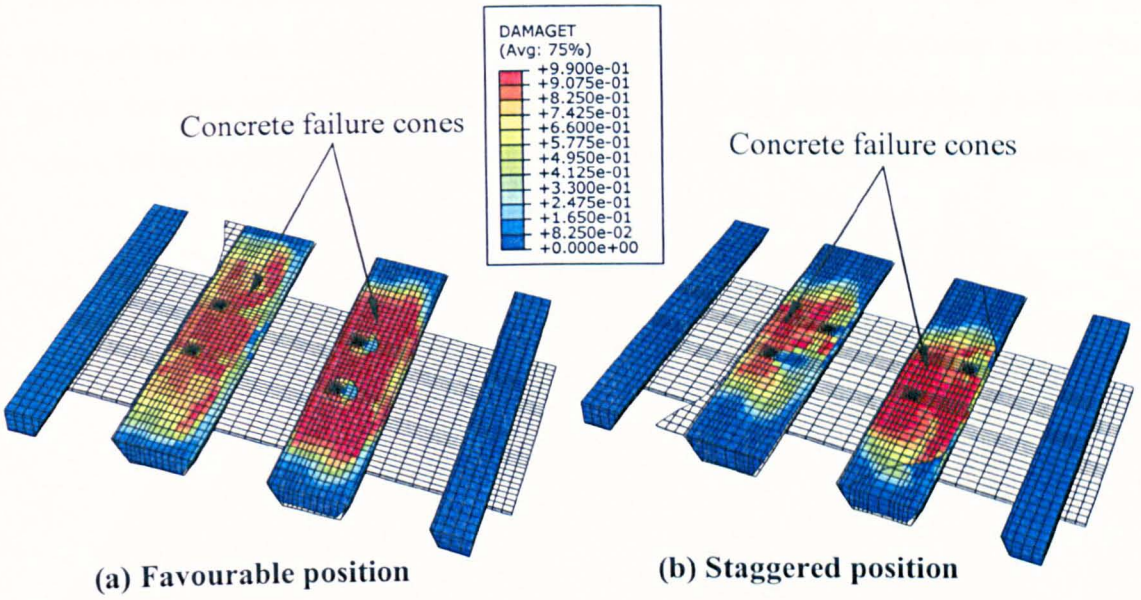

Figure 7.15 Development of concrete failure cones in push tests with a transverse spacing of 150 mm and C12 concrete

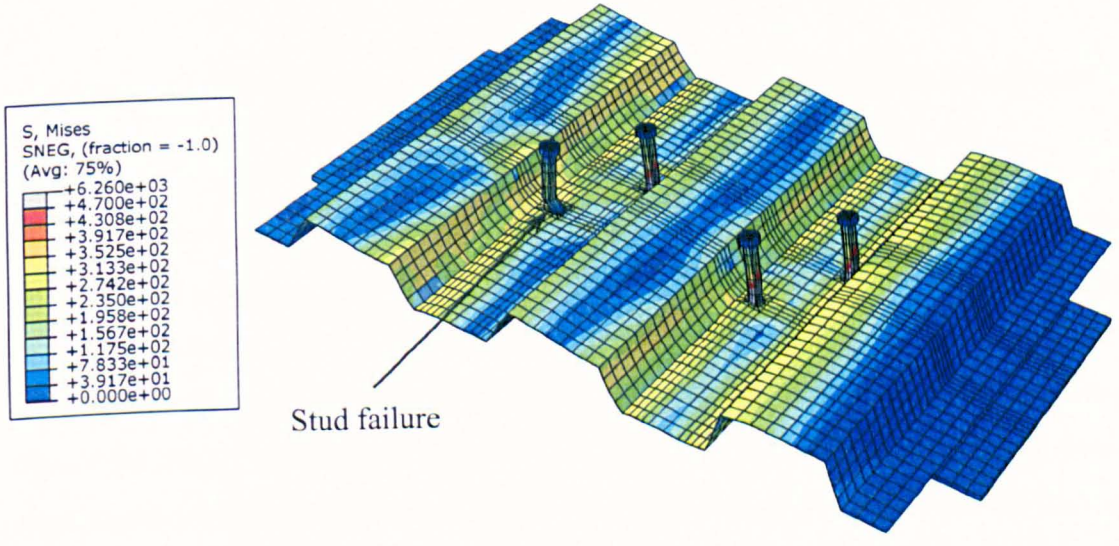

Figure 7.16 Stud shearing failure with a staggered spacing of 150mm & C40 concrete grade

The failure patterns of the push test with a transverse spacing of 200 mm and a concrete grade of C12 are shown in Figure 7.17. It can be observed that in case of favourable double studs, the size of failure cone grows in diameter in both sheeting ribs. In case of

the staggered position, the failure cone only developed around the favourable stud rather than the unfavourable stud. The size of failure cones with a transverse spacing of 200 mm was larger than the size of failure cones with a transverse spacing of 150 mm. All push tests with concrete grades of C20, C30, C40 failed by concrete cone failure except the push test with a staggered spacing of 200 mm and a concrete grade of C40 where failure occurred due to formation of concrete failure cones and stud shearing.

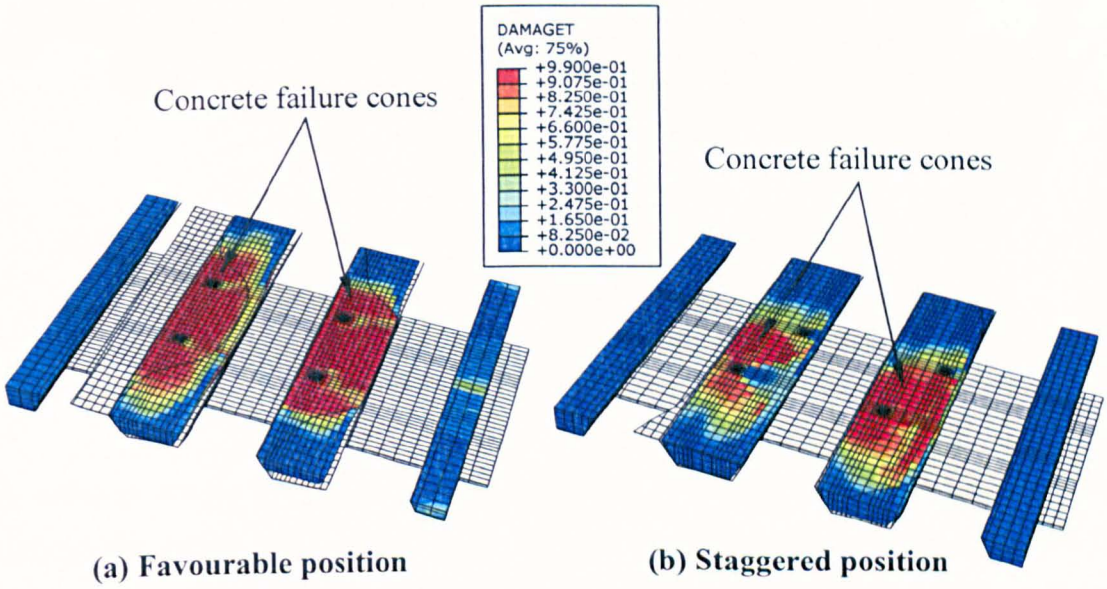

Figure 7.17 Development of concrete failure cones in push tests with a transverse spacing of 200 mm and C12 concrete

The failure modes of push tests with a transverse spacing of 300 mm and a concrete grade of C12 are shown in Figure 7.18. In case of favourable double studs, individual failure cones formed around shear studs in the first sheeting rib; and in the second rib some portion of the failure cone still remained joined with each other. However, overall size of the concrete failure surfaces was almost equal to each other in case of double studs in the favourable position with transverse spacings of 200, 300 and 400 mm and that was the reason the shear connector resistance with these transverse spacings was nearly equal to the resistance obtained from a single shear connector per trough. All push tests with a transverse spacing of 200 mm failed by the concrete cone failure except the push test with a staggered spacing of 200 mm having a concrete grade of C40 which failed by a combination of stud shearing and concrete cone failure.

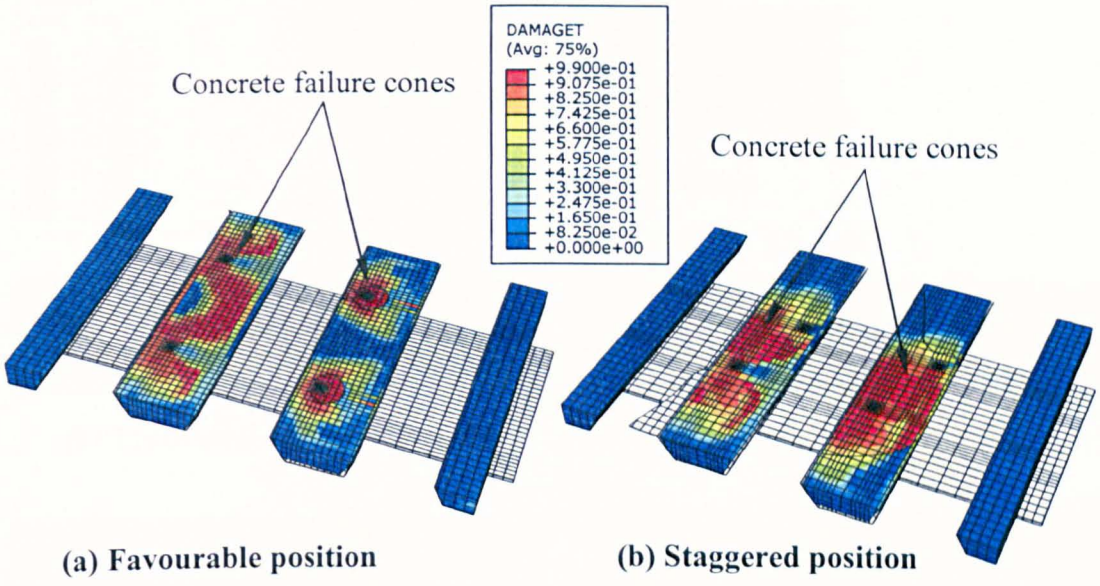

Figure 7.18 Development of concrete failure cones in push tests with a transverse spacing of 300 mm and C12 concrete

In order to see the formation of concrete failure cones more clearly, a section is cut through the length of the sheeting rib and the tensile damage variable is plotted for various push tests with double studs in the favourable position having different transverse spacings as shown in Figure 7.19. Shear studs and steel beam have been removed for clarity. It can be observed that for a transverse spacing of 60 mm, the failure cones are connected with a straight line in the region between two shear studs, thus resembling a wedge shape. As the transverse spacing is increased to 100 mm, failure cones tend to separate from each other and are joined together with a concave curve in the space between two shear connectors. At the same time, failure surfaces are spreading sideways as well. Somewhat separate failure cones are formed around both shear studs when the transverse spacing is changed to 150 mm, however, they still remain connected below the mid-height of the shear connector. At 200 mm transverse spacing, two concrete failure cones form around shear studs with some failure surfaces being connected to each other close to the lower half of the shear stud. The failure cones become completely independent of each other when the transverse spacing is 300 mm or above.

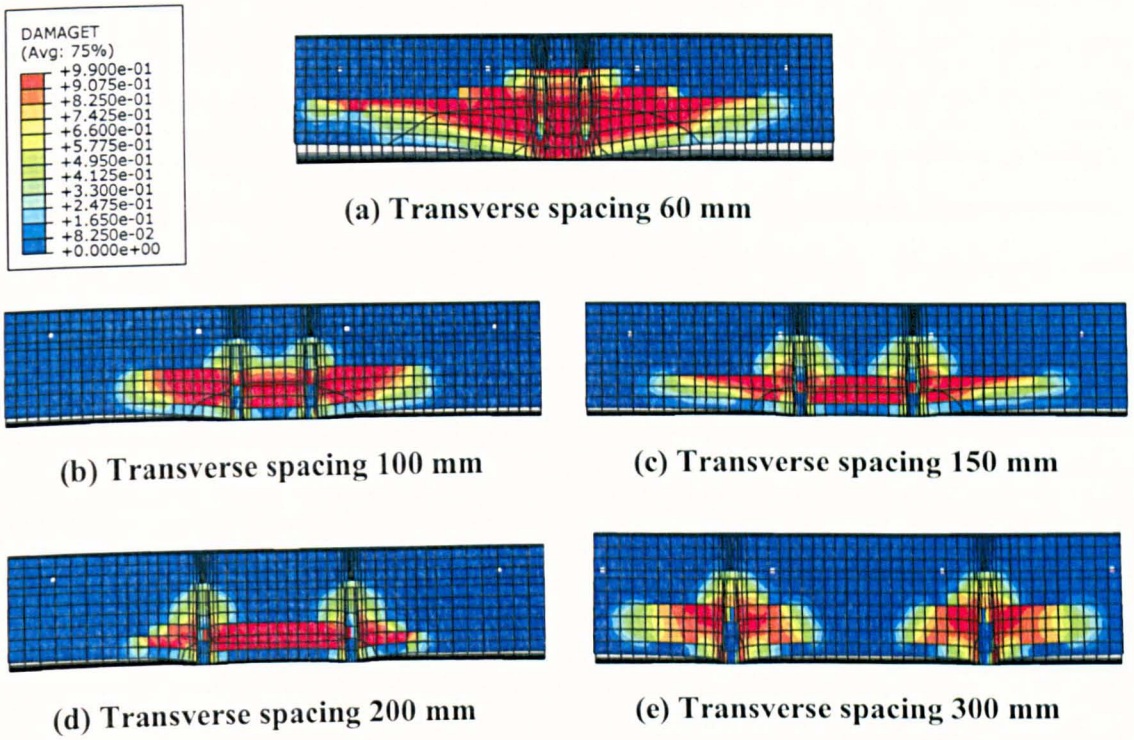

Figure 7.19 Formation of concrete failure cones around shear stud for push test with double studs placed in the favourable position

Typical deformations of the steel deck and shear stud for push tests with double studs in the favourable position are shown in Figure 7.20. The shear studs are bent in the direction of the applied shear loading when the load is increased on the push test. When failure occurs, the bond between the steel deck and the concrete slab breaks, and the concrete slab tends to move up and ride over the profiled sheeting. As a result, the top flange and web of the steel deck opposite to the load bearing direction of the shear stud tends to depress down, and the bottom flange of the steel deck lifts up. Significant uplift of the steel deck and concrete slab is observed at the surface where the concrete slab is bedded to the ground.

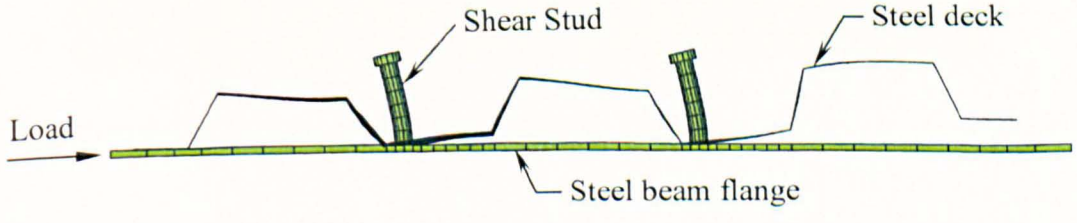

Figure 7.20 Typical deformations of the steel deck and the shear stud in push test with favourable positioned studs

Typical steel deck and shear stud deformations of the push test with staggered positioned double studs are shown in Figure 7.21. Both unfavourable and favourable shear studs bent in the direction of the applied shear loading when the load was increased. On account of placing one shear stud in the unfavourable position, no lifting of the bottom flange of the steel deck was observed. The unfavourable shear connector punched through the adjacent web of the steel deck marked by rib punching, and buckling of the steel deck web also occurred close to the favourable shear stud as shown in Figure 7.22. Therefore, the failure mode of the push test with staggered positioned double studs is not only characterised by concrete cone failure but rib punching as well.

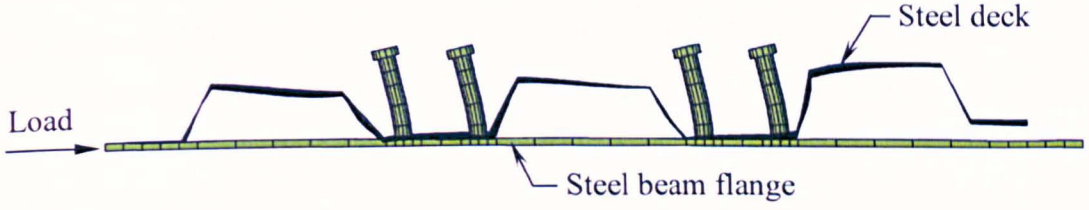

Figure 7.21 Typical deformations of the steel deck and the shear stud in push tests with staggered positioned double studs

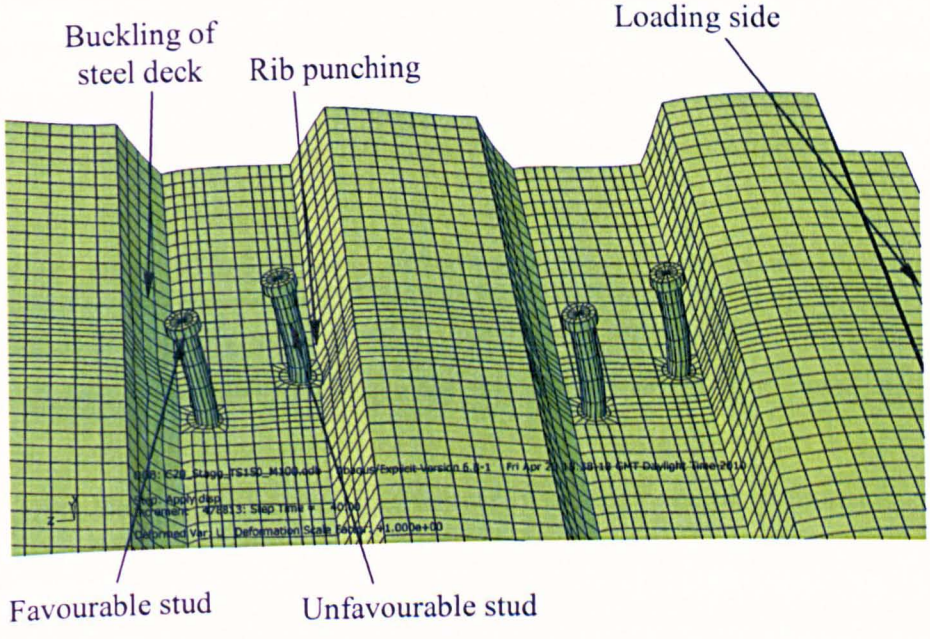

Figure 7.22 Buckling and rib punching of the steel deck for push tests with staggered positioned double studs

7.3.5. Summary and conclusions

The validated three-dimensional finite element model is used to conduct a parametric study involving 64 double stud push tests with studs placed next to each other in the favourable position and staggered by placing each of them in the favourable and unfavourable location. Four single stud push tests were also analysed for comparison of results with double studs. The main variables in the parametric study were the effect of transverse spacing, shear connector layout and concrete strength. Transverse spacings of 40 to 400 mm were tried. It was found that the shear connector resistance remained unchanged for transverse spacings of less than 80 mm and more than 200 mm. The Eurocode 4 relation for the strength of the push test with double studs per rib being 71% of the resistance of the push test with a single stud per rib was found to be valid for spacings of 80 mm or lower.

All push tests failed by the concrete conical failure except push tests with C40 concrete grade having staggered pairs of connectors beyond 150 mm spacing, which failed by a combination of concrete cone and stud shearing failure. It is concluded that the resistance of pairs of shear connectors placed in the favourable position is 94% of the strength of a single shear stud on average, when the transverse spacing between studs is 200 mm or more. On the other hand, the resistance of staggered pairs of studs was only 86% of the strength of a single stud. The strength of double shear studs in a favourable position was generally more than the staggered pairs of shear connectors.

7.4. Effect of profiled sheeting thickness and shear stud position

The presence of a small central stiffening rib at the bottom of the trough in the modern profiled sheeting has led to a change in the position of the shear stud, either in the favourable or unfavourable side of the trough. The shear stud is considered to be strong in the favourable position and weak in the unfavourable position, primarily because of a larger zone of concrete under compression in front of the favourable stud in its load bearing direction than the compressive zone behind it. In a beam, the stud placed on the side of the stiffener away form the mid span is in the favourable position, while the stud placed closest to the location of the maximum moment for a simply supported beam is in the unfavourable position. Many researchers and design codes recommend that studs

be placed in the favourable position. However, it is not practically possible to make sure that shear connectors are always placed on the favourable side of the trough.

The thickness of the profiled sheeting affects the strength and ductility of the shear connector, in particular when it is placed in the unfavourable positions. Generally, it is believed that the strength of the unfavourable stud is dependent on the strength of the steel deck rather than the concrete strength. The shear studs placed in the unfavourable position usually fail by punching through the adjacent web of the steel deck without actually developing concrete failure cones and that is why the thickness of the profiled sheeting can significantly influence the performance of the headed shear connector placed in the unfavourable position.

The main objective of the parametric study in this section is to investigate the effect of profiled sheeting thickness and shear stud position on the strength, ductility and failure modes of the headed shear connector in steel-concrete composite beams. Different profiled sheeting thicknesses with shear studs placed as single and double studs per rib in the favourable, central and unfavourable positions were studied. The other variables include concrete strength and transverse spacing of shear studs. The validated finite element model is used in the parametric study to investigate the effect of these variables. The size of the shear stud, concrete slab and wire mesh fabric, and geometry of the steel deck were kept constant throughout the analysis.

7.4.1. Finite element model

The geometry of the push test is created by assuming a quarter symmetry at the centre line of the steel beam web for the parametric study of the effect of the sheeting thickness and shear stud position as shown in Figure 7.23. Since the behaviour of the push test is unaffected by the steel beam, modelling of the beam web is ignored and only flange of the beam is modelled. This model is meshed with the same elements as that for the validated model.

The boundary conditions and loading surface of the model used for the parametric study in this section are shown in Figure 7.24. The bottom of the steel beam flange, designated as surface 1, was treated as symmetric in the X direction. The nodes of the profiled sheeting, concrete slab and steel beam that lie on the other symmetry plane denoted by surface 2 were assumed to be symmetric in the Y direction. The surface of

the concrete slab and profiled sheeting designated by surface 3, where it was bedded to the ground, was restrained from translating in the Z direction. The material properties, constraints and contact interactions are similar to the validated model.

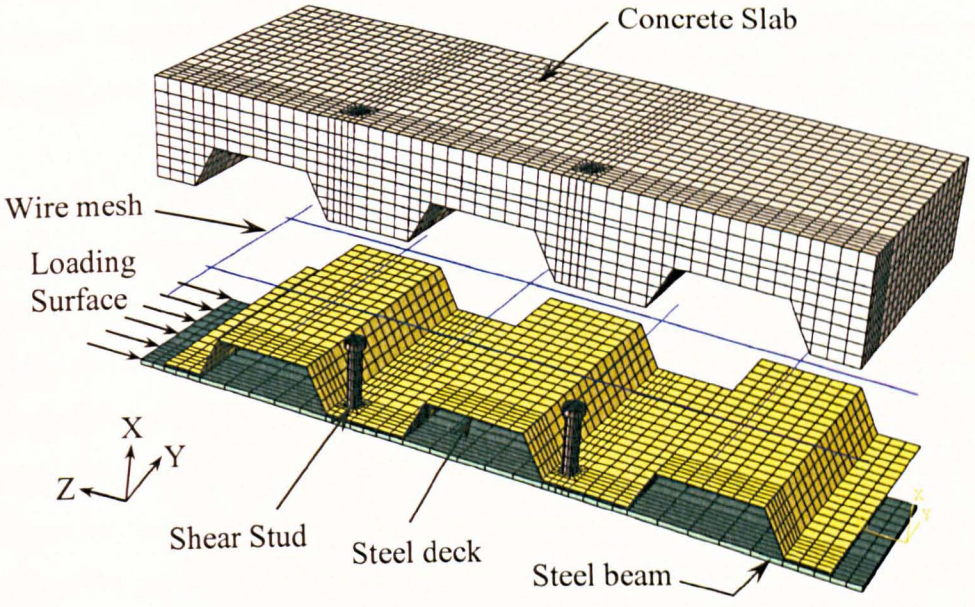

Figure 7.23 Finite element model to study the effect of shear stud position and profiled sheeting thickness

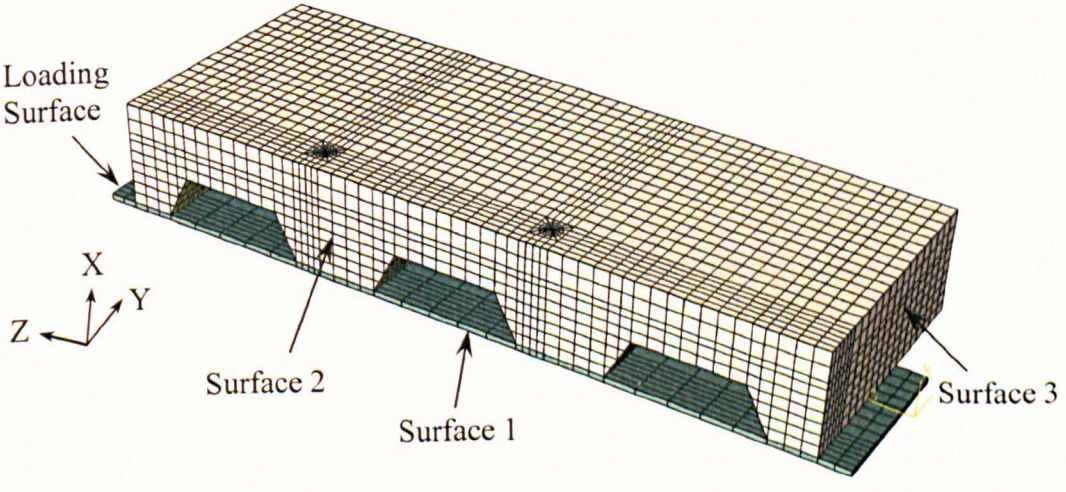

Figure 7.24 Boundary conditions for the model used for a parametric study of shear stud position and profiled sheeting thickness

7.4.2. Results of parametric study for sheeting thickness and stud position

The position of the shear connector within a profiled sheeting trough affects the strength and ductility of the headed shear stud. The shear connector behaviour is also influenced

by the thickness of the profiled sheeting, particularly when the shear stud is positioned in the unfavourable position. Therefore, the validated finite element model was used to conduct a parametric study to investigate the effect of the profiled sheeting thickness and shear stud position on the shear resistance and slip capacity of the headed shear connector. Besides these key variables, the effect of concrete strength and transverse spacing of shear studs was also studied.

The parametric study was divided into 16 groups. Each group consisted of favourable, central and unfavourable stud positions using both single and double studs per trough. In total 240 push tests were investigated including 192 analyses for double studs and 48 analyses for a single stud per trough. The sheeting thickness of 0.9, 1.2, 1.5 and 2 mm were used for groups 1-4, 5-8, 9-12 and 13-16 respectively. The reason for using higher sheeting thicknesses beyond the practical limit of 1.2 mm was to assess the validity and accuracy of the developed model and proposed strength prediction equations. The results of the parametric study in section 7.3 suggest that the shear connector resistance remains unaffected for transverse spacings less than 80 mm and more than 200 mm. On the basis of this conclusion, it was decided to use transverse spacings of 80, 100, 150 and 200 mm for each group. Each 4 groups had concrete grades of C12, C20, C30 and C40. The results of the parametric study consisting of shear connector resistances and slips at the steel-concrete interface obtained from the finite element analysis of the 240 push tests are presented in Table 7.3.

Table 7.3 Results of parametric study to study the effect of profiled sheeting thickness and shear stud position

Group	Test Ref	Sheeting thickness, t (mm)	Concrete Grade	Transverse spacing (mm)	Double Studs								Single Stud							
					F	C	U						F	C	U					
					P_F	P_C	P_U	P_U/P_F	P_C/P_F	δ_F	δ_U	δ_U/δ_F	P_F	P_C	P_U	P_U/P_F	P_C/P_F	δ_F	δ_U	δ_U/δ_F
G1	G1-1	0.9	C12	80	51.6	51.5	49.3	0.96	1.00	1.5	3.5	2.3	72.6	70.5	61.5	0.85	0.97	3.0	8.5	2.8
	G1-2			100	53.5	53.2	51.1	0.96	0.99	1.5	4.0	2.7								
	G1-3			150	59.8	58.8	55.1	0.92	0.98	1.5	4.0	2.7								
	G1-4			200	66.0	63.6	58.0	0.88	0.96	1.8	5.0	2.9								
G2	G2-1		C20	80	64.4	63.1	57.4	0.89	0.98	1.8	4.5	2.6	90.9	85.8	73.4	0.81	0.94	3.0	10.0	3.3
	G2-2			100	68.2	66.9	60.0	0.88	0.98	2.0	5.0	2.5								
	G2-3			150	76.1	73.4	65.0	0.85	0.97	2.0	5.0	2.5								
	G2-4			200	84.0	77.2	69.3	0.82	0.92	2.0	6.0	3.0								
G3	G3-1		C30	80	80.4	73.4	65.0	0.81	0.91	2.5	4.5	1.8	110.5	99.4	84.1	0.76	0.90	3.3	11.0	3.4
	G3-2			100	85.0	77.6	68.0	0.80	0.91	2.5	5.5	2.2								
	G3-3			150	94.0	85.0	74.2	0.79	0.90	2.5	6.0	2.4								
	G3-4			200	104.0	91.7	80.0	0.77	0.88	2.5	6.3	2.5								
G4	G4-1		C40	80	92.0	83.6	72.5	0.79	0.91	3.0	5.0	1.7	127.5	109.8	93.5	0.73	0.86	3.8	13.0	3.5
	G4-2			100	99.3	90.2	77.0	0.78	0.91	3.0	6.0	2.0								
	G4-3			150	110.0	96.0	83.0	0.75	0.87	3.0	6.3	2.1								
	G4-4			200	121.4	101.3	89.0	0.73	0.83	3.3	6.8	2.1								

Group	Test Ref	Sheeting thickness, t (mm)	Concrete Grade	Transverse spacing (mm)	Double Studs								Single Stud							
					F	C	U						F	C	U					
					P_F	P_C	P_U	P_U/P_F	P_C/P_F	δ_F	δ_U	δ_U/δ_F	P_F	P_C	P_U	P_U/P_F	P_C/P_F	δ_F	δ_U	δ_U/δ_F
G5	G5-1	1.2	C12	80	53.0	53.8	57.0	1.07	1.01	1.5	4.8	3.2	77.0	75.2	70.0	0.91	0.98	3.0	10.0	3.3
	G5-2			100	55.0	55.6	58.0	1.05	1.01	1.5	5.5	3.7								
	G5-3			150	61.5	61.5	60.7	0.99	1.00	1.5	6.5	4.3								
	G5-4			200	67.8	66.4	62.5	0.92	0.98	1.8	7.5	4.3								
G6	G6-1		C20	80	66.2	66.0	65.4	0.99	1.00	2.0	4.8	2.4	95.0	93.0	82.0	0.86	0.98	3.0	11.5	3.8
	G6-2			100	70.1	69.9	68.0	0.97	1.00	2.0	6.0	3.0								
	G6-3			150	78.2	76.7	72.4	0.93	0.98	2.0	7.8	3.9								
	G6-4			200	86.3	83.2	76.5	0.89	0.96	2.0	8.3	4.1								
G7	G7-1		C30	80	82.6	79.7	73.5	0.89	0.96	2.5	5.3	2.1	116.0	109.5	94.0	0.81	0.94	3.2	12.0	3.8
	G7-2			100	87.4	84.0	76.5	0.88	0.96	2.5	6.3	2.5								
	G7-3			150	96.6	92.0	83.0	0.86	0.95	2.5	7.5	3.0								
	G7-4			200	106.9	98.2	89.2	0.83	0.92	2.5	8.3	3.3								
G8	G8-1		C40	80	94.6	90.4	80.7	0.85	0.96	3.0	5.8	1.9	131.3	120.0	103.0	0.78	0.91	3.8	13.0	3.5
	G8-2			100	102.1	97.6	85.2	0.83	0.96	3.0	6.5	2.2								
	G8-3			150	113.1	103.5	91.6	0.81	0.92	3.0	7.8	2.6								
	G8-4			200	124.8	110.4	98.0	0.79	0.89	3.0	8.5	2.8								

Group	Test Ref	Sheeting thickness, t (mm)	Concrete Grade	Transverse spacing (mm)	Double Studs								Single Stud							
					F	C	U						F	C	U					
					P_F	P_C	P_U	P_U/P_F	P_C/P_F	δ_F	δ_U	δ_U/δ_F	P_F	P_C	P_U	P_U/P_F	P_C/P_F	δ_F	δ_U	δ_U/δ_F
G9	G9-1	1.5	C12	80	54.3	56.2	62.3	1.15	1.04	1.5	4.3	2.8	82.1	80.0	77.0	0.94	0.97	3.0	11.0	3.7
	G9-2			100	56.3	58.1	63.2	1.12	1.03	1.5	4.3	2.8								
	G9-3			150	62.9	64.3	65.8	1.05	1.02	1.5	5.3	3.5								
	G9-4			200	69.5	69.4	67.0	0.96	1.00	1.8	7.5	4.3								
G10	G10-1		C20	80	67.8	68.9	72.3	1.07	1.02	2.0	5.0	2.5	100.2	98.6	89.2	0.89	0.98	3.0	11.5	3.8
	G10-2			100	71.8	73.0	74.8	1.04	1.02	2.3	6.0	2.7								
	G10-3			150	80.1	80.2	79.5	0.99	1.00	2.3	6.8	3.0								
	G10-4			200	88.4	86.9	83.0	0.94	0.98	2.3	10.3	4.6								
G11	G11-1		C30	80	84.6	84.8	81.5	0.96	1.00	2.3	6.0	2.7	121.1	118.5	102.8	0.85	0.98	3.3	12.0	3.7
	G11-2			100	89.5	89.6	84.8	0.95	1.00	2.3	6.3	2.8								
	G11-3			150	98.9	97.2	91.2	0.92	0.98	2.3	6.8	3.0								
	G11-4			200	109.5	105.5	97.6	0.89	0.96	2.3	10.3	4.6								
G12	G12-1		C40	80	96.8	96.8	88.8	0.92	1.00	3.0	6.5	2.2	135.8	130.0	112.5	0.83	0.96	3.5	13.0	3.7
	G12-2			100	104.5	104.1	93.5	0.89	1.00	3.0	8.5	2.8								
	G12-3			150	115.8	111.0	101.0	0.87	0.96	3.0	8.5	2.8								
	G12-4			200	127.8	117.0	107.5	0.84	0.92	3.0	10.8	3.6								

Group	Test Ref	Sheeting thickness, t (mm)	Concrete Grade	Transverse spacing (mm)	Double Studs								Single Stud							
					F	C	U						F	C	U					
					P_F	P_C	P_U	P_U/P_F	P_C/P_F	δ_F	δ_U	δ_U/δ_F	P_F	P_C	P_U	P_U/P_F	P_C/P_F	δ_F	δ_U	δ_U/δ_F
G13	G13-1	2	C12	80	56.2	56.7	66.5	1.18	1.01	1.8	4.0	2.3	85.7	85.7	88.6	1.03	1.00	3.0	9.0	3.0
	G13-2			100	58.3	58.5	67.4	1.16	1.00	1.8	4.0	2.3								
	G13-3			150	65.2	64.2	70.5	1.08	0.98	2.0	4.0	2.0								
	G13-4			200	71.9	70.4	74.6	1.04	0.98	2.0	4.5	2.3								
G14	G14-1		C20	80	70.2	72.0	83.0	1.18	1.03	2.0	5.5	2.8	108.0	107.8	103.1	0.95	1.00	3.0	10.3	3.4
	G14-2			100	74.3	76.2	85.7	1.15	1.03	2.0	5.8	2.9								
	G14-3			150	82.9	83.8	90.4	1.09	1.01	2.0	6.0	3.0								
	G14-4			200	91.6	90.9	94.0	1.03	0.99	2.0	6.8	3.4								
G15	G15-1		C30	80	87.6	89.0	94.0	1.07	1.02	2.8	7.5	2.7	130.9	130.8	117.8	0.90	1.00	3.3	12.0	3.7
	G15-2			100	92.7	94.0	97.6	1.05	1.01	2.8	8.0	2.9								
	G15-3			150	102.5	102.3	104.2	1.02	1.00	2.8	8.0	2.9								
	G15-4			200	113.4	110.2	111.6	0.98	0.97	2.8	10.5	3.8								
G16	G16-1		C40	80	100.3	102.0	103.0	1.03	1.02	3.0	9.5	3.2	146.0	145.9	126.7	0.87	1.00	3.5	13.0	3.7
	G16-2			100	108.2	110.0	108.5	1.00	1.02	3.0	10.3	3.4								
	G16-3			150	119.9	119.0	116.5	0.97	0.99	3.0	10.3	3.4								
	G16-4			200	132.3	128.0	125.0	0.94	0.97	3.3	11.0	3.4								

Note: F, C, and U indicate favourable, central and unfavourable stud positions respectively. P_F, P_C, P_U are FE loads per stud in kN and δ_F, δ_U are slips in mm.

7.4.3. Effect of profiled sheeting thickness

The effect of the profiled sheeting thickness on the strength and ductility of the single and double studs placed in the favourable, central and unfavourable location is studied. Transverse spacings and concrete strengths are also varied to assess their effect. In order to study the effect of the profiled sheeting thickness, load per stud versus sheeting thickness curves have been plotted for the single and double studs having different transverse spacings and concrete strengths. Mainly, the effect of the sheeting thickness on the behaviour of studs placed in the unfavourable location is of a particular interest.

The load versus profiled sheeting thickness curves for double shear studs placed in the unfavourable position with a transverse spacing of 100 mm are presented in Figure 7.25. It can be observed that the strength of the shear connector increases by 25% when the sheeting thickness is changed from 0.9 mm to 2 mm for C12 concrete. In case of C20, C30 and C40 concrete grades, the change of the sheeting thickness from 0.9 to 2 mm results in 30 % enhancement in the strength of the shear stud. The load versus sheeting thickness plot is linear for all concrete grades except for C12 concrete grade. This is due to the fact that the push test with a sheeting thickness of 2 mm and a concrete grade of C12 failed by a combination of rib punching and concrete cone failure, which is uncommon for a push test with unfavourable studs. All other push tests with unfavourable positioned studs failed by rib punching, which suggested that the shear stud tore away from the steel deck, and splitting in the adjacent steel web in front of the stud occurred.

The comparison of the contour plot of the tensile damage variable, representing cracking in the concrete, for the push test with unfavourable studs having a transverse spacing of 100 mm, a concrete grade of C12, and sheeting thicknesses of 0.9 and 2 mm is shown in Figure 7.26. Due to low concrete strength and high sheeting thickness, the concrete failure cones develop around the shear connector along with some steel deck buckling in case of the push test with 2 mm sheeting. However, the push test with a sheeting thickness of 0.9 mm completely fails due to rib punching. The steel deck buckling is more prominent in push tests where failure occurs only due to rib punching instead of concrete failure as shown by comparison of the push tests with C12 and C40 concrete grades having a sheeting thickness of 2 mm in Figure 7.27.

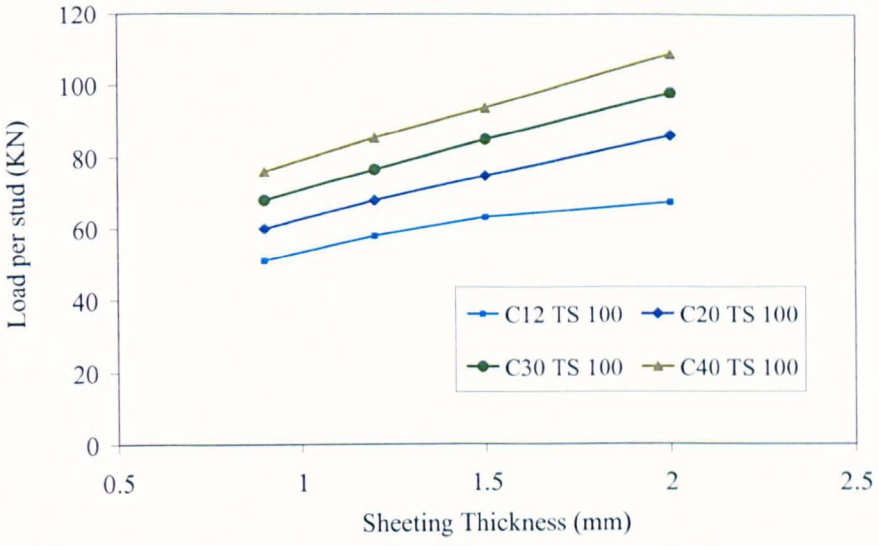

Figure 7.25 Load versus sheeting thickness curve for unfavourable double studs with a transverse spacing of 100 mm

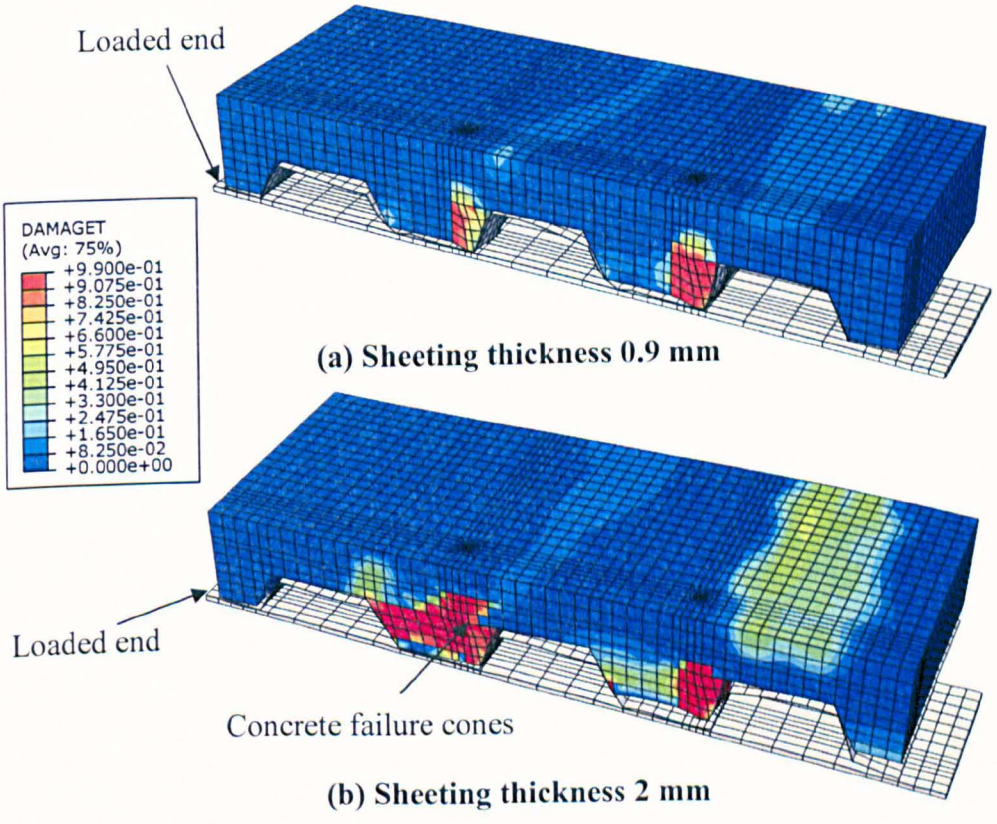

Figure 7.26 Comparison of tensile damage for push test with unfavourable studs having a transverse spacing of 100 mm and a concrete grade of C12

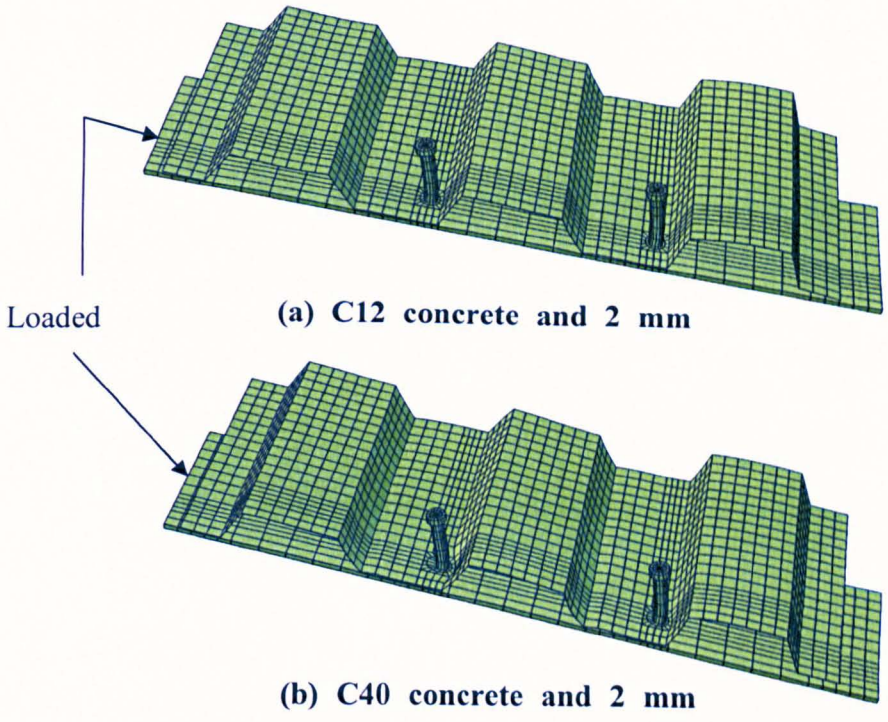

Figure 7.27 Comparison of steel deck deformations for push tests with unfavourable studs having transverse spacing of 100 mm

The load versus profiled sheeting thickness curves for a push test with unfavourable studs having a transverse spacing of 200 mm for different concrete strengths are plotted in Figure 7.28. The shear connector resistance increased by 22% when the sheeting thickness was varied from 0.9 mm to 2 mm for C12 concrete. For C20, C30 and C40 concrete grades, the shear connector resistance increased by about 28% with change in sheeting thickness from 0.9 to 2 mm. The load versus sheeting thickness curves are approximately linear. All push tests failed by rib punching apart from the push test with C12 concrete grade having a sheeting thickness of 2 mm, which failed by a combination of steel deck buckling and concrete cone failure. A push test with double studs placed in the unfavourable location having C40 concrete grade, 0.9 mm thick steel deck and the yield stress of the steel deck as 550 MPa was also analysed. The change in the yield stress of the steel deck from 350 MPa to 550 MPa resulted in an increase in the load per stud from 89 kN to 96 kN for the unfavourable positioned stud. However, the same change did not have any effect on the results of favourable studs. This shows that the strength of the shear connector in the unfavourable position not only depends on the thickness but the strength of the profiled sheeting as well.

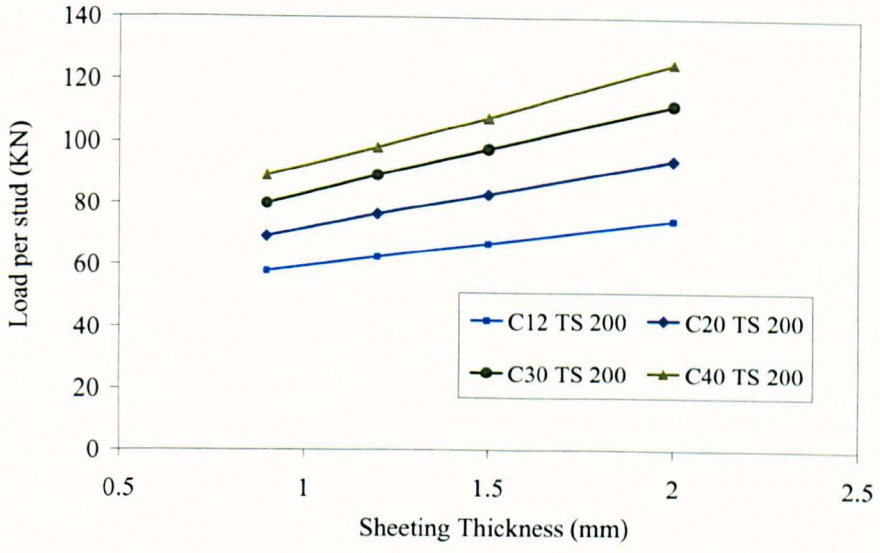

Figure 7.28 Load versus sheeting thickness curve for unfavourable double studs with a transverse spacing of 200 mm

The load versus sheeting thickness curves for a single stud per rib placed in the unfavourable position are plotted in Figure 7.29. These curves show a linear pattern and the shear connector strength enhancement of about 30% when the sheeting thickness is increased from 0.9 mm to 2 mm. Push tests having unfavourable double studs with transverse spacings of 80 and 150 mm follow a similar trend in load versus sheeting thickness curves as that of push tests with unfavourable double studs having transverse spacings of 100 mm and 200 mm. In general, for push tests with unfavourable studs, the shear connector resistance increased by as much as 30% when the profiled sheeting thickness was varied from 0.9 mm to 2 mm.

The load versus sheeting thickness curve for central double studs having a transverse spacing of 100 mm is plotted in Figure 7.30. The strength of the shear connector increased by about 10% with increase in sheeting thickness from 0.9 to 2 mm. The load versus sheeting thickness curves approximately exhibited a linear behaviour. Compared to unfavourable double studs with a transverse spacing of 100 mm, where the shear connector strength increased by 25% when the sheeting thickness was changed from 0.9 mm to 2 mm, the change in the sheeting thickness did not increase the shear connector strength in the same proportion in case of central double studs spaced at 100 mm. In case of central double studs with a transverse spacing of 200mm, the strength

enhancement of 10%, 15%, 17% and 20% was observed for concrete grades of C12, C20, C30 and C40 respectively when the sheeting thickness was changed from 0.9 mm to 2 mm. An increase of 20-25% and 15% in the strength was observed in case of central and favourable single shear studs respectively and only 8% increase was noticed for double favourable studs with change in sheeting thickness from 0.9 mm to 2 mm.

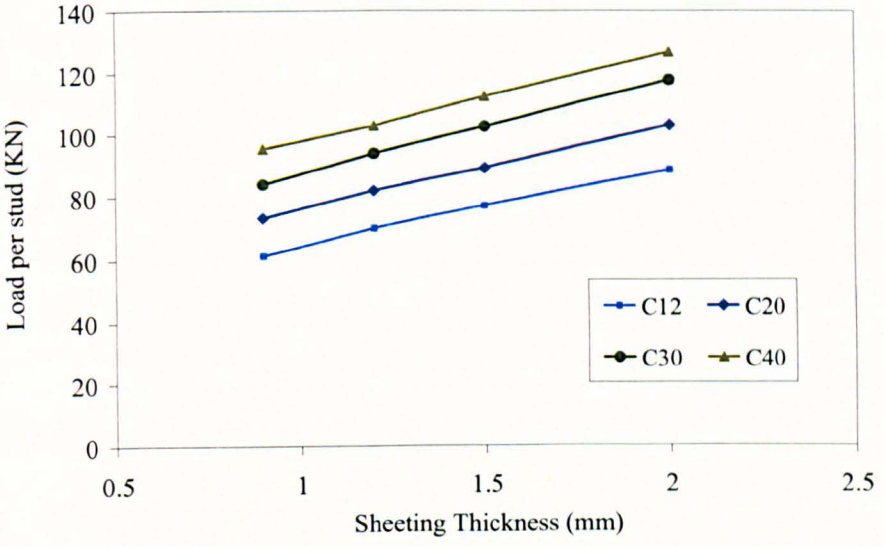

Figure 7.29 Load versus sheeting thickness curve for unfavourable single stud

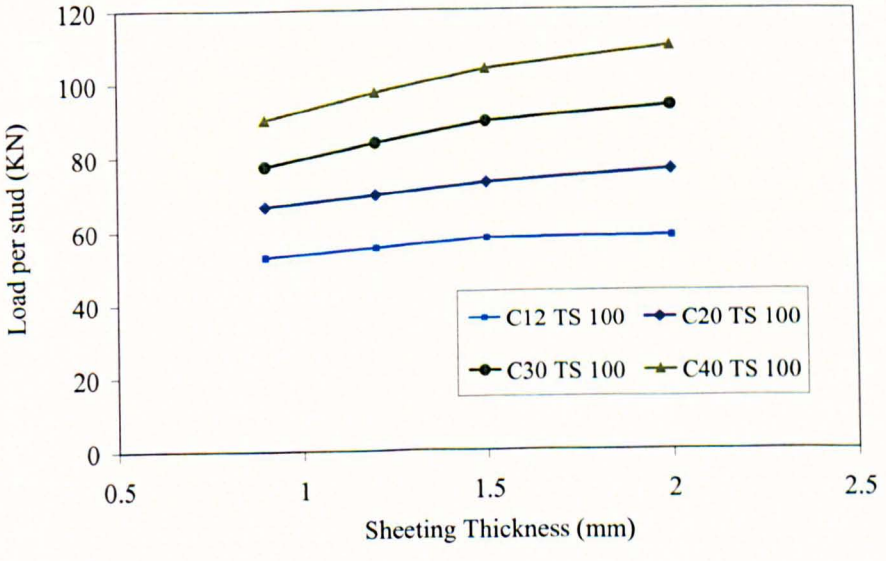

Figure 7.30 Load versus sheeting thickness curve for central double studs with a transverse spacing of 100 mm

The reason for 20% increase in the strength when the sheeting thickness is changed from 0.9 to 2 mm for central shear stud having a transverse spacing of 200 mm and a concrete grade of C40 is that the strong concrete (C40) and the thin steel deck (0.9mm) lead to formation of concrete failure cones only in front of the stud and concrete behind the shear stud remains undamaged as shown in Figure 7.31(a); on the other hand, when the concrete is strong (C40) and the steel deck is thick (2 mm), concrete failure cones develop in the entire rib as shown in Figure 7.31(b) and resultantly larger failure cones lead to an increase in the shear stud strength. Some cracking at the shallow part of the concrete slab also occurred near the free end as indicated by the tensile damage variable in Figure 7.31(b). But still the shear connector resistance of the central stud (C40 TS 200 t = 2 mm) is 3% less than the strength of the corresponding favourable stud, as shown in Table 7.3, on account of less area of concrete failure cones.

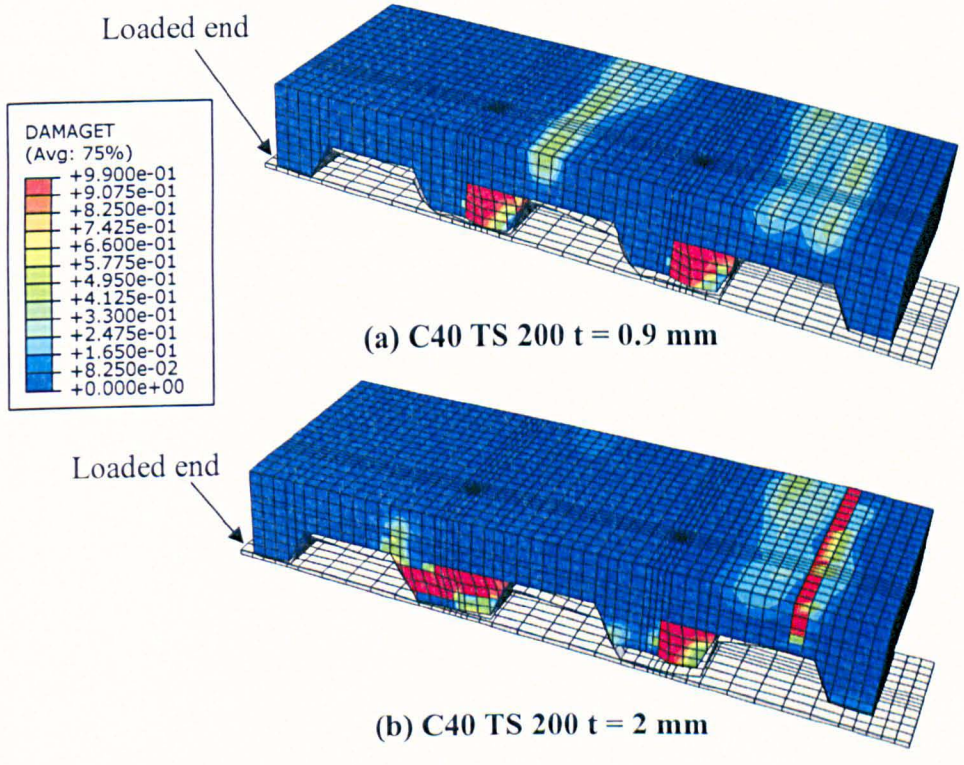

Figure 7.31 Comparison of tensile damage for push test with central studs having transverse spacing of 200 mm and a concrete grade of C40

The stress contours of the profiled sheeting for the push test with central double studs having a transverse spacing of 200 mm and a concrete grade of C40 are plotted in Figure 7.32. It can be observed in Figure 7.32(a) that the web and bottom flange of the profiled sheeting show a clear bulge behind the shear stud in the direction opposite to

the applied shear loading for the push test with central double studs having 0.9 mm thick steel deck and C40 concrete grade. It indicates that the steel deck plays a role in addition to the concrete strength in contributing to overall shear connector resistance when concrete is strong and steel deck is thin for central double studs. Conversely, for the same push test with a sheeting thickness of 2 mm, the steel deck does not deform as much as it does in case of 0.9 mm thick steel deck as shown in Figure 7.32(b). However, some lifting of the steel deck is observed in the loaded direction of the shear stud near the free end. This shows that when the steel deck is thick then it provides an extra confinement to the concrete slab and as a result concrete failure cones are developed.

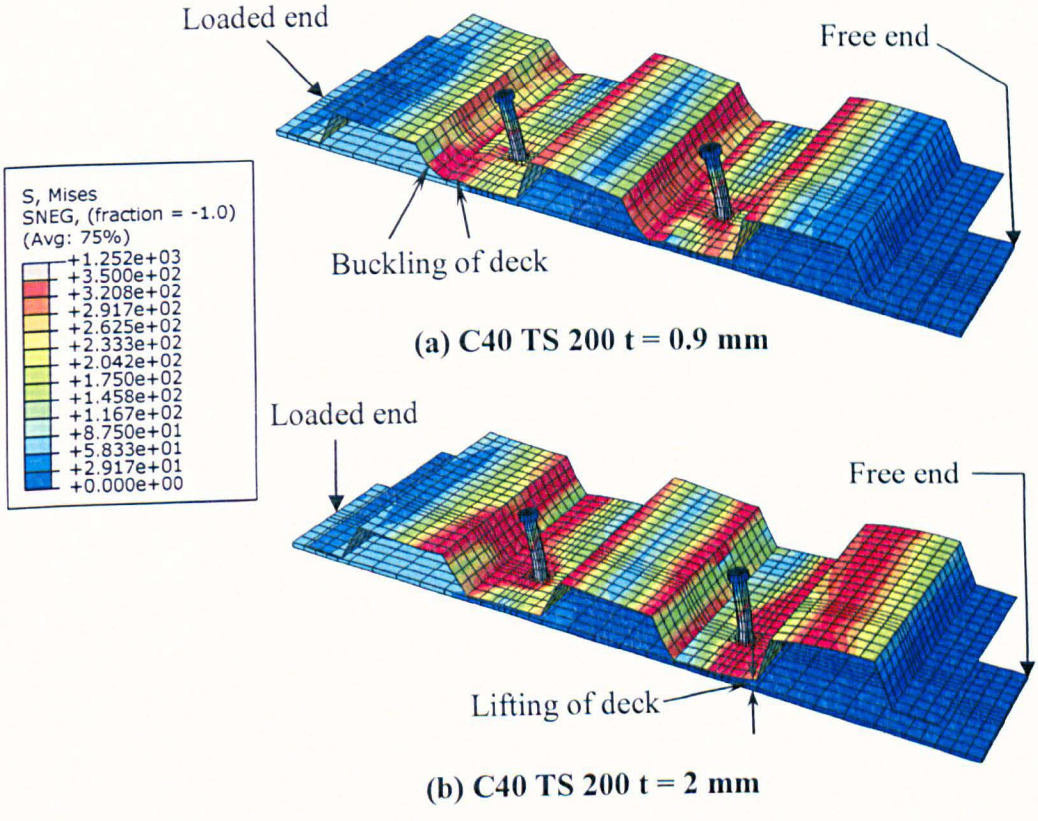

Figure 7.32 Comparison of steel deck stress contours for push test with central studs having a transverse spacing of 200 mm and a concrete grade of C40

7.4.4. Strength prediction equations for unfavourable and central studs

At the moment, there are no guidelines available in Eurocode 4 for shear studs placed in unfavourable and central locations. Therefore, a linear regression analysis of the push test results in unfavourable locations having both single and double studs with transverse spacings of 80, 100, 150 and 200 mm is carried out and Equations 7.1 to 7.3

are proposed. In Equation 7.1 $P_{U\text{-}EQ}$ represents the predicted strength of the shear connector placed in the unfavourable position either as double or single stud in a sheeting pan, $P_{F(0.9t)}$ denotes the shear connector resistance of the favourable stud with a profiled sheeting thickness of 0.9 mm and t is the thickness of the steel deck in mm. For the shear connector resistance of single and double studs placed in the central position Equations 7.2 and 7.3 are proposed. In Equations 7.2 and 7.3 $P_{CS\text{-}EQ}$ *and* $P_{CD\text{-}EQ}$ denote shear connector resistance of single and double studs placed centrally in a deck rib, and all other parameters are same as those of Equation 7.1. The factors α and β can be obtained from Table 7.4, which are based on the average ratio of the unfavourable over favourable and the central over favourable load per stud from Table 7.3 for different concrete grades having a sheeting thickness of 0.9 mm.

$$P_{U-EQ} = \alpha \times P_{F(0.9t)} \times (0.38t + 0.66) \tag{7.1}$$

$$P_{CS-EQ} = \beta \times P_{F(0.9t)} \times (0.25t + 0.78) \tag{7.2}$$

$$P_{CD-EQ} = \beta \times P_{F(0.9t)} \times (0.16t + 0.87) \tag{7.3}$$

Table 7.4 Determination of factors α and β

Concrete Grade	Factor, α		Factor, β	
	Single Stud	Double Studs	Single Stud	Double Studs
C12	0.85	0.94	0.99	0.98
C20	0.81	0.87	0.94	0.96
C30	0.76	0.79	0.9	0.90
C40	0.73	0.77	0.86	0.88

The suitability of the equations proposed in this study for calculating the shear connector resistance of the unfavourable and central studs is assessed by plotting the experimental versus predicted shear stud strengths, drawing the best-fit line and determining its coefficient of correlation, R. This coefficient measures the degree to which the measured and predicted values agree to each other and it is used as a measure of the accuracy of future predictions. The experimental shear stud strengths obtained

from push tests with a single stud per rib placed in the unfavourable position are compared with stud strengths predicted by Equation (7.1) developed in this study for unfavourable position studs in Table 7.5. The load per stud obtained from different experiments, $P_{u\text{-}test}$ in Table 7.5 is plotted against the load per stud obtained from Equation (7.1), $P_{U\text{-}EQ}$ for push tests with an unfavourable single stud per rib as shown in Figure 7.33.

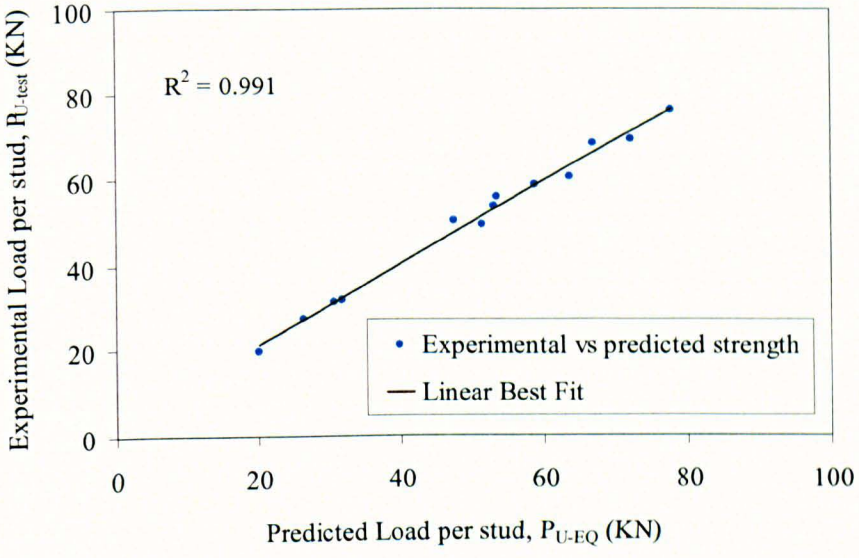

Figure 7.33 Experimental versus predicted load per stud for unfavourable single stud

The coefficient of correlation, R of the best-fit line of the comparison between the experimental and predicted results is 0.991 as shown in Figure 7.33, which indicates that the results obtained from proposed Equation (7.1) agree quite well with the experimental results for a single stud placed in the unfavourable location. In addition, the mean and coefficient of variation of the predicted results are 1.00 and 3.5% respectively. This also shows that the predicted values do not vary much from the mean of the values.

Table 7.5 Comparison of shear connector strength from experiments and developed equations for push tests with unfavourable single stud

Series	Concrete Compressive Strength, f_{cm} (MPa)	Stud Details	Deck details			Average Experimental Load for Favourable position stud, $P_{F\text{-}test}$ (kN)	Average Experimental Load for Unfavourable position stud, $P_{U\text{-}test}$ (kN)	Load per stud from developed equation $P_{U\text{-}EQ}$ (kN)	$P_{U\text{-}test}$ / $P_{U\text{-}EQ}$	Tested by
		Size $d \times h_{sc}$ (mm × mm)	Height, h_p (mm)	Average rib width, b_o (mm)	Thickness, t (mm)					
D1 & D3	30.6	13 × 100	50	150	0.9525	39.0	32.0	31.8	1.01	Rambo-Roddenberry (2002)
D4 & D5	20.1	16 × 100	50	150	0.9525	61.7	55.7	53.6	1.04	
D7 & D9	40.6	13 × 100	50	150	0.9525	40.0	31.6	30.7	1.03	
D10 & D12	48.8	19 × 100	50	150	0.9525	89.7	68.3	67.0	1.02	
D13 & D15	32.5	16 × 100	50	150	0.9525	64.6	49.4	51.4	0.96	
D16 & D18	27.1	10 × 100	50	150	0.9525	24.4	19.9	20.1	0.99	
D17 & D19	27.1	22 × 100	50	150	0.9525	71.2	58.3	58.9	0.99	
D20 & D22	36.1	10 × 127	76	150	0.9525	35.0	27.5	26.3	1.05	
D21 & D23	36.1	22 × 127	76	150	0.9525	60.5	50.2	47.6	1.05	
D26 & D28	34.5	19 × 100	50	150	0.9525	66.7	53.4	53.2	1.00	
D27 & D29	34.5	19 × 100	50	150	0.9525	99.1	76.2	77.8	0.98	
G1F & G5U	35.0	19 × 125	80	140	1.2	91.9*	69.2	72.3	0.96	Johnson & Yuan (1998)
—	31.5	19 × 127	76	150	0.9	83.7	60.3	63.8	0.95	Easterling *et al* (1993)
Mean									**1.00**	
COV									**3.5%**	

Note: **PF(0.9t)* for this test was determined from finite element analysis as 80 kN.

Table 7.6 Comparison of shear stud strength from FE analysis and developed equations for push tests with central studs and unfavourable stud pairs

Ref.	Concrete Strength, f_{cm} (MPa)	Stud Details	Deck details			$P_{F\text{-}test}$ (kN)	$P_{UD\text{-}FE}$ (kN)	$P_{CD\text{-}FE}$ (kN)	$P_{CS\text{-}FE}$ (kN)	$P_{U\text{-}EQ}$ (kN)	$P_{CD\text{-}EQ}$ (kN)	$P_{CS\text{-}EQ}$ (kN)	$P_{UD\text{-}FE}$ / $P_{U\text{-}EQ}$	$P_{CD\text{-}FE}$ / $P_{CD\text{-}EQ}$	$P_{CS\text{-}FE}$ / $P_{CS\text{-}EQ}$	Tested by
		Size $d \times h_{sc}$ (mm × mm)	Height, h_p (mm)	Average rib width, b_o (mm)	Thickness, t (mm)											
D2	30.6	13 × 100	50	150	0.9525	36.9	30.8	35.1	--	32.0	35.5	--	0.96	0.99	--	Rambo-Roddenberry (2002)
D6	20.1	16 × 100	50	150	0.9525	52.8	49.8	52.6	--	50.6	52.7	--	0.98	1.00	--	
D8	40.6	13 × 100	50	150	0.9525	43.8	33.2	37.7	--	34.8	40.0	--	0.95	0.94	--	
D11	48.8	19 × 100	50	150	0.9525	68.4	54.4	62.3	--	53.7	61.4		1.01	1.01	--	
D14	32.5	16 × 100	50	150	0.9525	65.4	53.5	63.2	--	55.6	62.7	--	0.96	1.01	--	
D1	30.6	13 × 100	50	150	0.9525	39.0	--	--	38.1	--	--	37.0	--	--	1.03	
D4	20.1	16 × 100	50	150	0.9525	61.7	--	--	62.4	--	--	61.7	--	--	1.01	
D7	40.6	13 × 100	50	150	0.9525	40.0	--	--	38.9	--	--	36.3	--	--	1.07	
D10	48.8	19 × 100	50	150	0.9525	89.7	--	--	79.8	--	--	78.7	--	--	1.01	
D13	32.5	16 × 100	50	150	0.9525	64.6	--	--	63.8	--	--	60.6	--	--	1.05	
Mean													**0.98**	**0.99**	**1.04**	
COV													**2.5%**	**2.9%**	**2.5%**	

Note: $P_{F\text{-}test}$ = Average experimental load for favourable position stud, $P_{UD\text{-}FE}$ = FE load for unfavourable position stud placed in pairs, $P_{CD\text{-}FE}$ = FE load for central position stud placed in pairs, $P_{C\text{-}FE}$ = FE load for central position stud placed as single stud per rib

Due to limited research in case of unfavourable pairs of shear connectors and central studs, a combination of experimental and numerical shear stud strengths are used to assess the accuracy of the equations developed in this study for unfavourable pairs of studs and central studs. The predicted shear stud strengths and the results obtained from the finite element analysis for unfavourable double shear studs and shear studs placed in the central position both as single and in pairs are presented in Table 7.6. The mean of the numerical over predicted results is very close to 1 with coefficient of variation ranging from 2.5% to 2.9%, which suggests the equations developed in this study give reasonable estimate of the shear connector strength for shear stud placed in the central location, and in the unfavourable position as double studs per rib.

7.4.5. Effect of shear stud position in a deck rib

The position of the shear stud in a sheeting rib is described as favourable or unfavourable depending on which side of the central stiffener it is welded, or as central if it is welded centrally to the profiled sheeting rib. The position of the shear stud is defined in terms of the distance, $e_{mid\text{-}ht}$ from mid height of the profiled sheeting rib. The term $e_{mid\text{-}ht}$ is the distance from the edge of the shear stud shank to the mid-height of the steel deck rib in the direction of the applied shear loading as shown in Figure 7.34. For the profiled sheeting used in this study, the values of $e_{mid\text{-}ht}$ equal to 106 mm, 65.5 mm and 25 mm represent favourable, central and unfavourable studs respectively.

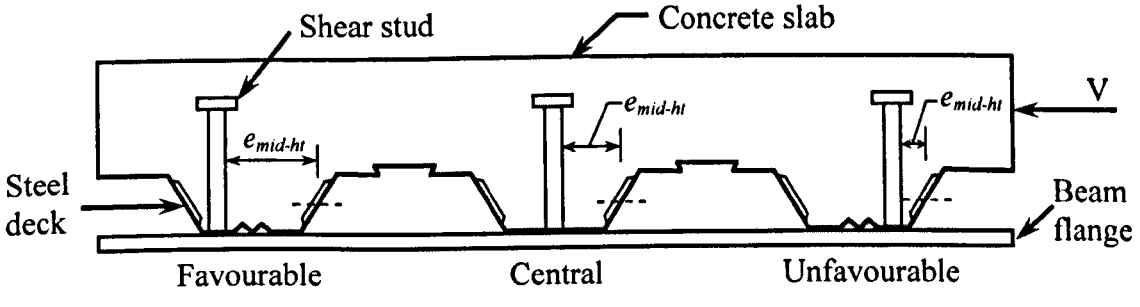

Figure 7.34 Shear stud in favourable, central and unfavourable position

To study the effect of the stud position, a parametric study was conducted for both double and single studs placed in unfavourable, central and favourable positions. The load versus stud positions (expressed in terms of distance $e_{mid\text{-}ht}$) for a transverse spacing of 100 mm and a sheeting thickness of 0.9 mm is plotted in Figure 7.35. It indicates that

as the distance of the shear stud increases from the mid-height of deck rib in the load bearing direction of the stud, the strength of the shear connector increases. The strength of the unfavourable stud is reduced by 4, 12, 20 and 22% as compared with the favourable stud for concrete grades of C12, C20, C30 and C40 respectively. It means that the strength of the shear stud in the unfavourable position does not increase in the same proportion as it does for the favourable stud when the concrete strength is increased. Alternatively, the results suggest that the strength of the unfavourable stud is primarily a function of the strength and thickness of the profiled sheeting rather than the concrete strength.

The strength of central studs is reduced by 1, 2, 9 and 9% as compared to favourable studs for concrete grades of C12, C20, C30 and C40 respectively as shown in Figure 7.35. The failure patterns suggest that for the push test with concrete grades of C12 and C20, the concrete failure cones form in both of the profiled sheeting ribs, which is the reason for similar strength of the central stud to that of the favourable stud. However, in case of C30 and C40 concrete grades with central studs, the complete concrete failure cones develop only in one of the deck rib, while a partial concrete failure cone is observed in the other rib, which is why the strength of central studs is 9% less than that of favourable studs.

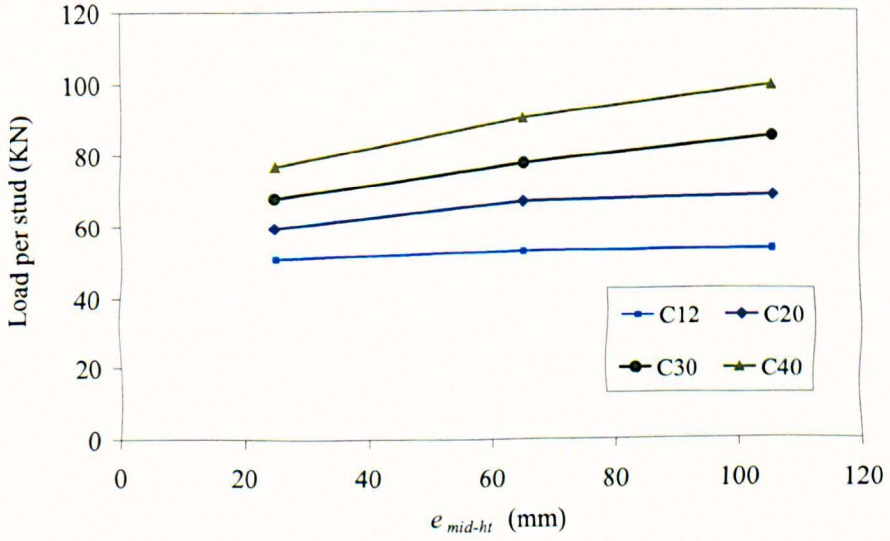

Figure 7.35 Load versus stud position curve for double stud with a transverse spacing of 100 mm and sheeting thickness 0.9 mm

The load versus stud position curve is plotted for double studs with a transverse spacing of 200 mm and a sheeting thickness of 0.9 mm in Figure 7.36. In case of unfavourable studs, the shear connector resistance is reduced by 12, 18, 23 and 27% as compared to the favourable stud for C12, C20, C30 and C40 concrete grades respectively. For central studs, the strength is decreased by 3.6, 8, 12 and 16.6% in comparison with the favourable stud. In case of a single stud in unfavourable and central positions, almost similar reduction in strength is observed as that of double studs with a transverse spacing of 200 mm and a sheeting thickness of 0.9 mm. For favourable studs, the increase in transverse spacing results in formation of larger concrete failure cones, and thus increase in shear connector resistance. While in case of unfavourable studs, the increase in transverse spacing results in longer strip of concrete available to be crushed under the application of the applied shear loading and resultantly the shear connector resistance also increases. For unfavourable stud with C12 concrete grade, this narrow strip crushes more easily as compared to the high strength concrete resulting in 12% lesser shear connector resistance than the favourable stud, which is almost three times more than the difference of 4% observed in the stud with a transverse spacing of 100 mm. For C40 concrete grade this difference is 27%, which is only 5% more than the difference of 22% in case of the transverse spacing of 100 mm. This suggests that the steel deck fails in case of C40 concrete grade and crushing of the narrow strip of concrete in front of the stud is less than that of C12 concrete grade.

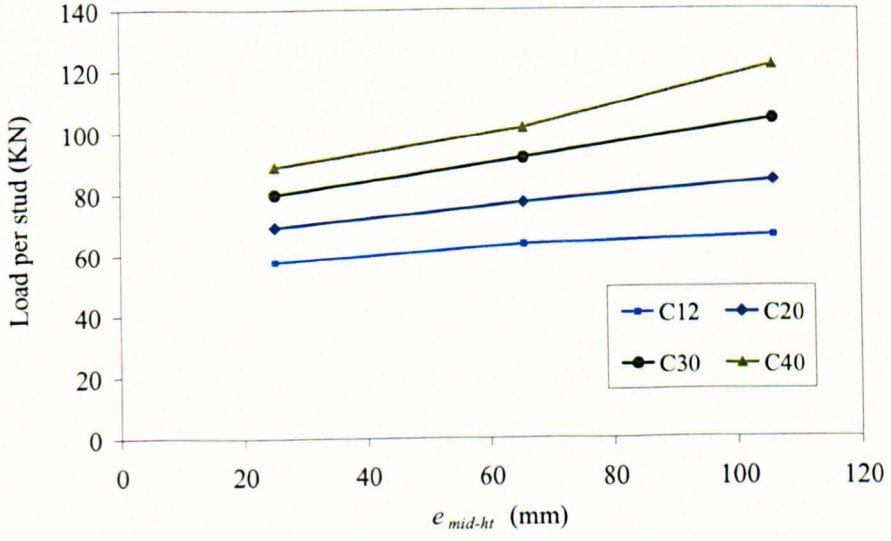

Figure 7.36 Load versus stud position curve for double stud with a transverse spacing of 200 mm and a sheeting thickness 0.9 mm

The load versus stud position curve is plotted for double studs with a transverse spacing of 100 mm and a sheeting thickness of 1.5 mm in Figure 7.37. The strength of the unfavourable double studs is increased by 12% and 4 % for C12 and C20 concrete grades and is decreased by 5% and 11% for C30 and C40 concrete grades as compared to favourable double studs. The strength of central double studs is almost similar to favourable double studs as shown in Figure 7.37. Generally, push tests with unfavourable studs fails by steel deck failure rather than concrete failure, and as a result the strength of the unfavourable stud is less than the favourable stud. However, in case of C12 concrete grade with 1.5 mm thick steel deck, the failure patterns are characterised by not only rib punching but formation of concrete cones as well. For this reason, the shear connector resistance of the unfavourable stud with C12 concrete grade and 1.5 mm thick steel deck is 12% higher than the favourable stud.

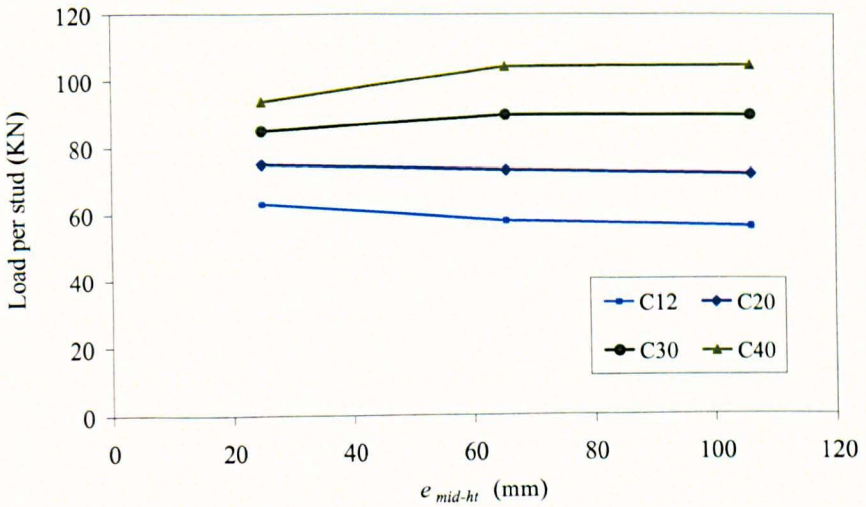

Figure 7.37 Load versus stud position curve for double stud with a transverse spacing of 100 mm and a sheeting thickness 1.5 mm

The load versus distance from the edge of the stud to the mid-height of the steel deck is plotted for double studs with a transverse spacing of 200 mm and a sheeting thickness of 1.5 mm in Figure 7.38. The unfavourable double studs exhibited a reduction of 4, 6, 11 and 14% as compared to the favourable double studs for C12, C20, C30 and C40 concrete grades respectively. This difference is less than the one observed in the same push test arrangement with a sheeting thickness of 0.9 mm as shown in Figure 7.36. On account of 1.5 mm thickness of the profiled sheeting, the reduction in the strength of the

unfavourable double studs in relation to the favourable double studs is less than that for the unfavourable double studs in 0.9 mm thick steel deck.

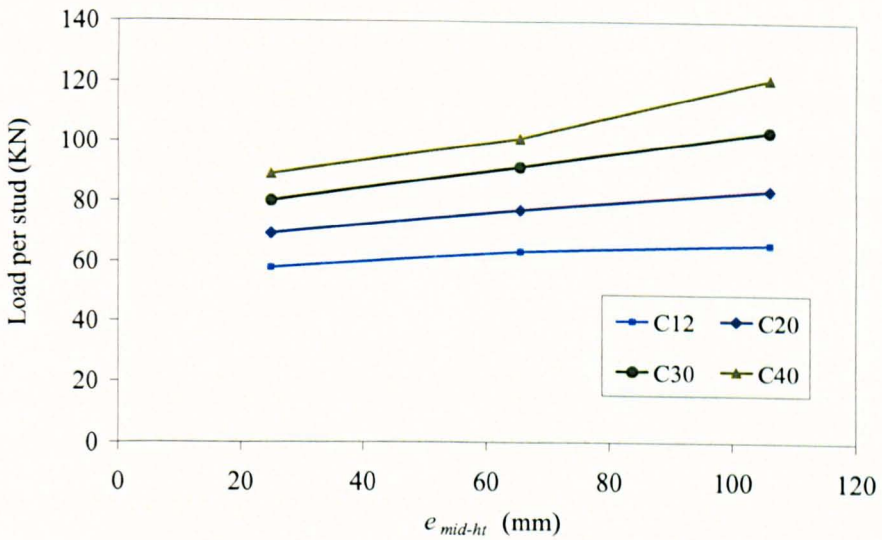

Figure 7.38 Load versus stud position curve for double stud with a transverse spacing of 200 mm and a sheeting thickness 1.5 mm

7.4.6. Ductility of the shear connector

The double shear connectors placed in the favourable position showed average slips of 1.5, 2, 2.5 and 3 mm for C12, C20, C30 and C40 concrete grades, which remained unchanged with variation of the sheeting thickness. For a single stud in the favourable position, a slip of 3-3.5 mm was observed for all concrete grades and sheeting thicknesses. It was observed that the sheeting thickness did not affect the ductility of the shear connector placed in the favourable location. The double shear connectors placed in the unfavourable position had average slips of 4, 5, 6 and 6 mm for C12, C20, C30 and C40 concrete grades respectively with a sheeting thickness of 0.9 mm. In case of unfavourable double studs with 1.5 mm thick steel deck, the average slip increased to 5.5, 7, 7.4 and 8.6 mm for C12, C20, C30 and C40 concrete grades respectively. The slip observed in double studs in the unfavourable position was almost 2-4 times more than the slip obtained from the push test with double favourable studs.

The single shear stud in the unfavourable position exhibited slips of 8.5, 10, 11 and 13 mm for C12, C20, C30 and C40 concrete grades respectively with 0.9 mm thick steel deck, which is almost 3 to 3.5 times the slip observed in a single favourable stud. For

the unfavourable single stud in 1.5 mm thick profiled sheeting, average slips were 11, 11.5, 12 and 13 mm for C12, C20, C30 and C40 concrete grades respectively, which were 3.7 times the average slip observed in the favourable single stud. In case of double studs in the unfavourable position, the transverse spacing of shear studs was also found to have an effect on the ductility of the shear connector. For unfavourable studs in 1.5 mm thick profiled sheeting, the slip increased from 6 mm to 10.3 mm when the transverse spacing was changed from 80 mm to 200 mm. This proves that increase in the transverse spacing improves the ductility of the unfavourable shear connector.

7.4.7. Failure modes of push tests with different stud positions

Mostly, the push test with favourable shear studs failed by formation of concrete failure cones as shown in Figure 7.39. The concrete slab started to crack, characterised by the concrete tensile damage variable, near the underside of the head of the stud and progressing down the diameter of the stud, and thus forming a failure cone or wedge of concrete. As indicated by the concrete tensile damage variable in Figure 7.39, the concrete failure cones are clearly formed around the stud shaft. Some cracking in the shallow part of the concrete slab is also observed near the region where it was bedded to the ground. In the favourable position, some buckling and lifting of the steel deck were also noticed as shown in Figure 7.39 with concrete slab removed for clarity.

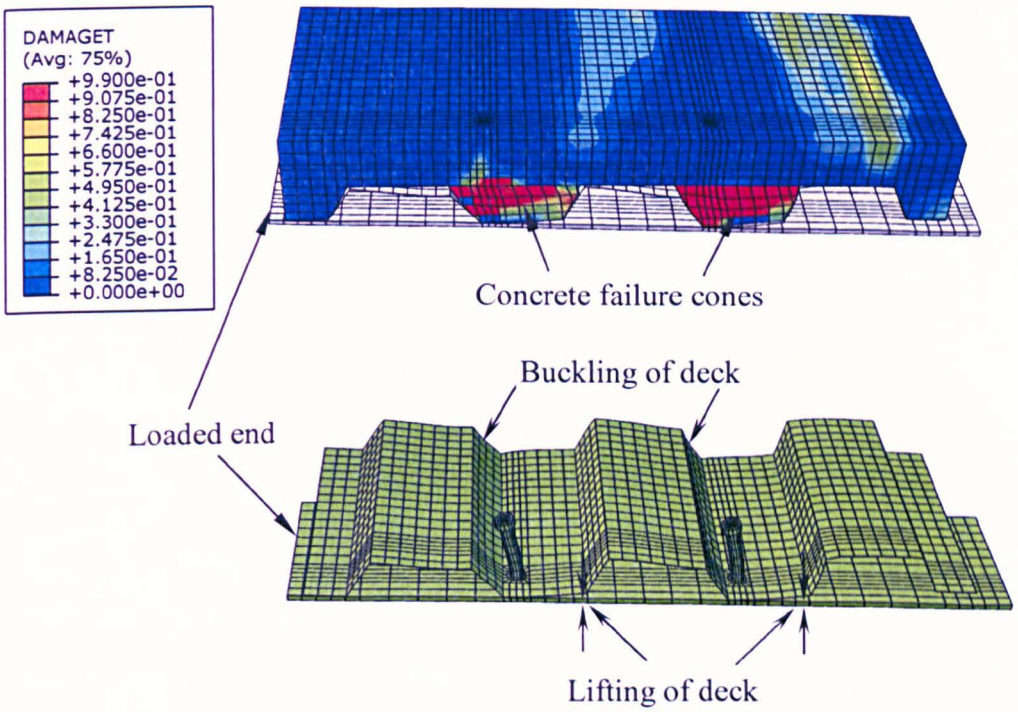

Figure 7.39 Typical failure modes for push tests with favourable position studs

The push test with central studs also failed by formation of concrete failure cones. A complete failure cone formed in a rib near the loaded end of the beam and a partial concrete cone developed around the stud in a rib near the free end as shown in Figure 7.40. For central studs, the steel deck experienced buckling at the back of the shear connector in the direction opposite to the applied shear loading. The bottom flange of the profiled sheeting also exhibited some bulging in case of central studs as shown in Figure 7.40, where the concrete slab has been removed for clarity.

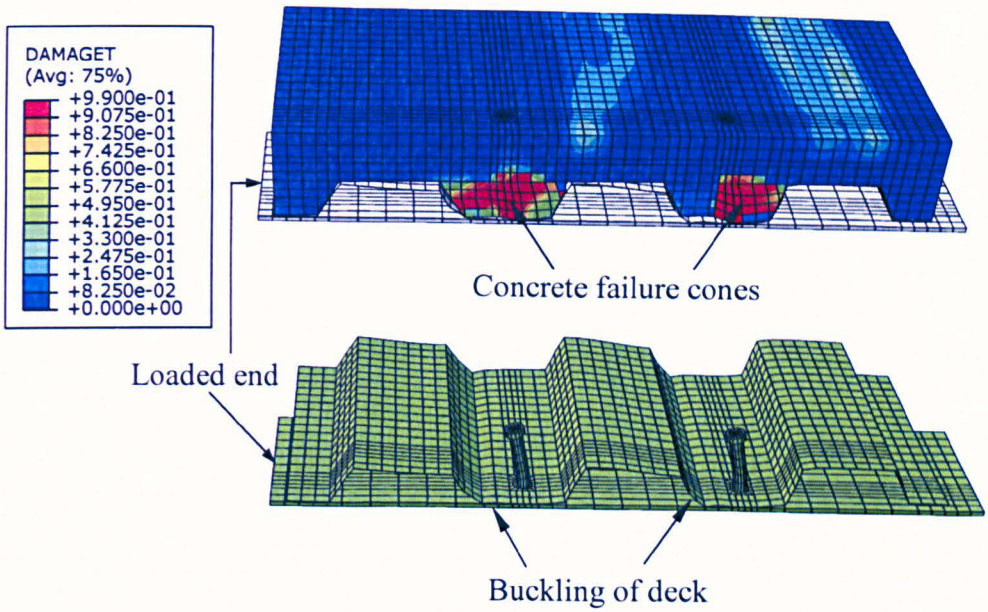

Figure 7.40 Typical failure modes for push tests with centrally placed studs

The failure mode of unfavourable studs was more ductile than that of central and favourable studs. The push test with unfavourable studs failed by crushing of the narrow strip of the concrete in front of the shear stud in its loaded direction and punching of the shear connector through the adjacent web of the steel deck, more commonly known as "rib punching", and eventual tearing of the web of the profiled sheeting as shown in Figure 7.41. It was found that the strength of the shear connector in the unfavourable position was more dependent on the strength and thickness of the steel deck rather than the concrete strength. This suggests that the strength of the shear stud in the unfavourable position is primarily a function of the strength and thickness of the steel deck. However, the strength of concrete cannot be ignored altogether, as crushing of the narrow portion of concrete slab in front of the shear stud in the unfavourable position contributes to the strength of the stud to some extent.

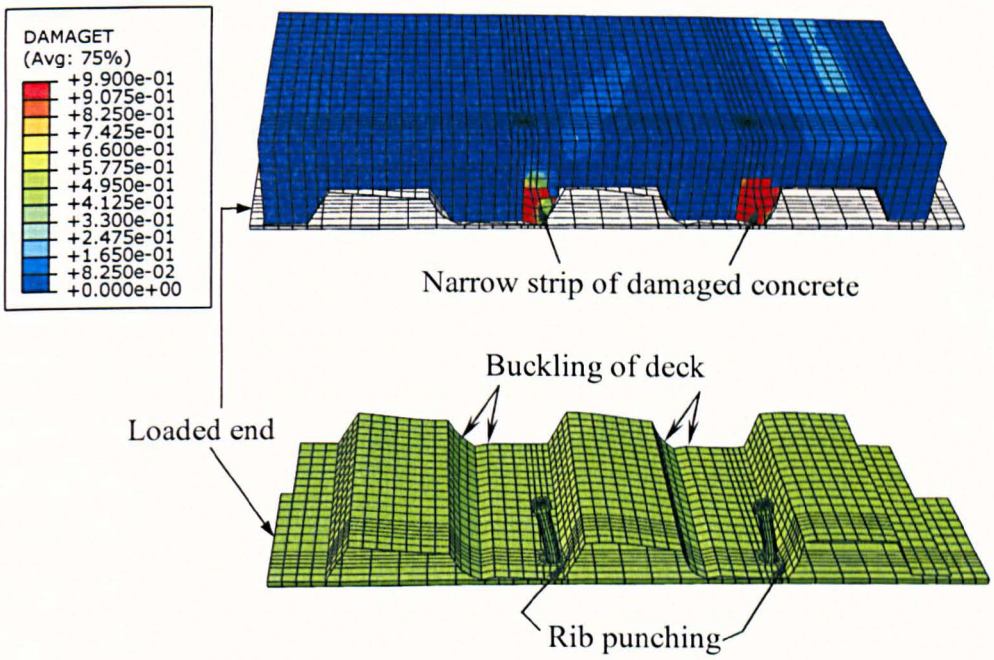

Figure 7.41 Typical failure modes for push tests with unfavourable position studs

7.4.8. Summary and conclusions

The validated three-dimensional finite element model is used in the parametric study to investigate the influence of shear stud position and thickness of the steel deck on the strength, ductility and failure patterns of the headed shear stud welded as single and double studs in the modern profiled sheeting. A total of 240 push tests were analysed using ABAQUS/Explicit with different sheeting thicknesses, positions of the shear stud in a trough, concrete strengths and transverse spacings.

It was found that an increase in the sheeting thickness enhanced the shear connector resistance of the unfavourable stud more than the favourable and centrally placed studs. The shear connector resistance increased by approximately 30%, 15% and 8% for double studs in unfavourable, central and favourable positions respectively when the sheeting thickness was increased from 0.9 mm to 2 mm. An increase of 30%, 20% and 15% in the shear capacity of the single stud was observed for unfavourable, central and favourable positions respectively with a change in the steel deck thickness from 0.9 mm to 2 mm. The equations for predicting the shear connector resistance of the unfavourable and central studs were also proposed. The statistical analysis of the proposed equations showed that the push test results obtained from experiments compared well with the stud strength predicted through these equations

The results of push tests with the unfavourable, central and favourable studs show that the strength of the shear connector increases as the distance of the shear stud increases from the mid-height of the deck rib in the load bearing direction of the stud. The load-slip behaviour of unfavourable studs was more ductile than that of favourable and central studs. The slip of the unfavourable stud was found to be 2-4 times the slip of the favourable stud. The sheeting thickness did not have any influence on the ductility of the favourable stud. However, the sheeting thickness and transverse spacing were found to have improved the ductility of the unfavourable stud. An increase in the concrete strength resulted in more ductile behaviour of the shear stud. The failure modes suggested that predominantly, the push tests with favourable and central studs failed by formation of concrete failure cones. Push tests having unfavourable studs failed by crushing of the narrow strip of concrete in front of the shear stud in its load bearing direction and punching of the stud through the adjacent web of the profiled sheeting.

Chapter 8
Conclusions and future work

Chapter 8
Conclusions and future work

8.1. Conclusions

The behaviour of headed stud shear connectors in composite beams with trapezoidal profiled sheeting laid transverse to the axis of the beam has been studied through experimental and numerical investigations. Following conclusions can be drawn from this study:

1. The most important contribution of this research study is the development of a three-dimensional finite element model to study the behaviour of headed stud shear connectors in steel-concrete composite beams with profiled sheeting. The model developed in this study is different in a number of ways from the models used previously by many researchers. It can accurately predict the shear connector resistance and slip at failure together with failure modes of push tests including stud shearing, concrete cone failure and rib punching as against previous finite element models where it was only possible to predict the shear connector resistance and concrete related failure modes. The separation of the steel deck from the concrete slab, which helped in accurate determination of failure modes, was also modelled in this study which was ignored in previous studies. Although, the finite element model developed in this study predicted well the maximum failure load, slip at failure and failure mechanisms of push tests, it overestimated the ductility of the shear connector beyond peak load.

2. The choice of an appropriate analysis procedure, and material model for concrete was made by trying different material models and analysis procedures available in ABAQUS. As failure of the push test is predominantly concrete related, the use of a proper concrete material model is crucial for accurate modelling of the push test. The combined use of the Concrete Damaged Plasticity model and the dynamic explicit analysis procedure enabled post-failure behaviour of the push test to be modelled, and as a result, the numerical results matched with the experimental results in terms of the maximum failure load, slip at failure and failure modes. It should be noted that the post-failure

behaviour of the push test with profiled sheeting has not been modelled in the past.

3. The developed finite element model was validated extensively against experimental push test results and used in a parametric study to investigate the influence of shear connector spacing and layout, profiled sheeting thickness, and position of shear stud in a rib. The experimental data related to these parameters is either scarce or of limited scope. Moreover, no numerical study has so far been conducted to study the effect of these important variables.

4. The shear connector resistance of double shear studs per rib increased with the increase in transverse spacing between them. The shear connector resistance of pairs of shear connectors per rib placed in the favourable position was found to be nearly equivalent to the shear connector strength of a single stud per rib when the transverse spacing between studs was 200 mm or more. It suggested that individual failure cones formed around shear studs when they were sufficiently apart. However, the transverse spacing limit of 200 mm is only valid for 60 mm deep steel decks and 19×100 mm long shear studs. It is, therefore, concluded that pairs of shear connectors should be placed as farthest apart as practically possible.

5. The results of the numerical analysis suggested that shear connectors placed in the unfavourable position were more ductile than favourable positioned studs; on the contrary, the shear connector resistance of studs in the unfavourable position was less than favourable positioned studs. Therefore, if two shear connectors per rib are to be used, a more beneficial arrangement, in terms of ductility, would be to use staggered layout of shear connectors by placing one stud each in the favourable and unfavourable location rather than placing studs side by side in the favourable position. In this way, the brittle behaviour of favourable studs is compensated by the ductile response of unfavourable studs.

6. The results of the parametric study suggested that the increase in the sheeting thickness enhanced the shear connector resistance of the unfavourable stud more than the favourable and centrally placed studs. It was also shown that the strength of the shear stud placed in the unfavourable position depended more on the thickness of the profiled sheeting than the concrete strength.

7. At the moment, the Eurocode 4 equations for predicting the shear connecter resistance do not take into account the position of the shear stud within a rib. Keeping in view the fact that shear studs placed in unfavourable and central positions are weaker than the studs in the favourable position, the strength prediction equations for unfavourable and central studs have been proposed in this study. The proposed design equations are based on an extensive parametric study and are verified against experimental studies. However, more experimental push tests having different steel decks with studs in unfavourable and central positions should be conducted before these equations could be implemented in design codes.

8. Locating the mesh directly on top of the steel deck or raised above the steel deck with a concrete cover of 30 mm from top surface of the concrete slab did not have any influence on the shear connector resistance. As push tests with a single stud per rib were used to study the effect of mesh position, this conclusion should be considered valid for the shear connector resistance of composite beams with a single stud per rib. Therefore, the common UK construction practice of positioning the mesh at a distance of 25-30 mm below the top surface of the concrete slab for fire design, crack control and longitudinal shear appears to hold true for composite beams with a single stud per rib. However, more testing is required to assess the validity of this conclusion for double studs per rib.

9. The application of normal load of 10% of the horizontal shear load on top surface of the concrete slab in a single-sided horizontal push testing arrangement, in addition to the horizontal shear load, increased the strength of single and double shear studs by 40% and 23% respectively with no significant effect on the ductility of the shear connector. Similarly, using double layers of mesh resulted in 18% increase in the shear connector resistance as compared with a single layer of mesh, while no improvement in the ductility was observed with the use of double layers of mesh.

10. Any lack of improvement in the ductility of the shear stud embedded in a profiled sheeting slab, despite trying different measures such as double layers of mesh, normal load, various push testing arrangements and reinforcement bar at

bottom trough, can be attributed to deficiency in the standard push test arrangement rather than the shear connection. It is recommended that the standard push test arrangement, which represents the real behaviour of composite beams with trapezoidal profiled sheeting, should be developed.

8.2. Proposed future work

Based on the results obtained from this study, following recommendations are proposed for future work:

1. The scope of the research conducted in this study is limited to push tests with 60 mm deep steel deck. The recent availability of steel decks as high as 146 mm in the market makes it necessary to conduct some experimental studies involving very deep trapezoidal profiled sheeting and check the shear connector resistance of deep decks against available design code provisions. This study could be very useful as most of the design code provisions were developed using medium sized steel decks.

2. The experimental data was most scarce for double studs in the unfavourable position, the effect of the position of the stud within a rib, thickness of the steel deck, lightweight concrete, higher number of shear studs in a rib and larger shear stud spacings. It is suggested that some push tests should be conducted to take into account the effect of these parameters on the performance of the headed shear stud.

3. The composite beam tests and companion push tests using different decking profiles 50 mm, 80 mm and 146 mm should be conducted to understand the behaviour of the headed shear stud in a beam and a push test, to identify the factors that lead to discrepancy in the results of composite beams and push tests.

4. The finite element model developed in this study can be extended to take into account the lightweight concrete, different sizes of shear studs, different available steel deck profiles, effect of waveform reinforcement embedded in the concrete slab and fibre reinforced concrete, and parallel sheeting.

5. The finite element model can also be extended to model the full size composite beam with profiled sheeting laid transverse and parallel to the axis of the beam, and to compare its results with the numerical models of push tests. The beam model can also be useful in identifying the causes of different load-slip behaviour of the headed shear stud in a beam and a push test, and understanding different load transfer mechanisms in both composite beams and push tests.

References

References

ABAQUS documentation Version 6.8. 2008 Hibbitt, Karlsson and Sorensen, USA

AISC. 1999. Load and resistance factor design specification for structural steel building. American Institute of Steel Construction. Chicago, USA.

AISC 360-05. 2005. Specification for Structural Steel Buildings. American Institute of Steel Construction. Chicago, Illinois, USA.

Bradford, M.A., Filonov, A. and Hogan, T.J. 2006. Push testing procedure for composite beams with deep trapezoidal slabs. *In: The Eleventh International Conference on Metal Structures,* Rzeszów, Poland.

BS EN 1992-1-1. 2004. Eurocode 2: Design of concrete structures: Part 1-1: General rules and rules for buildings. London: British Standards Institution.

BS EN 1993-1-3: Eurocode 3. 2006. Design of steel structures: Part 1-3: General rules-Supplementary rules for cold-formed members and sheeting, British Standards Institution, London.

BS EN 1994-1-1, Eurocode 4: 2004. Design of composite steel and concrete structures: Part 1.1: General rules and rules for buildings, British Standards Institution, London.

BS5400, Part 5: 1979. Steel, concrete, and composite bridges, British Standards Institution, London.

BS5950, Part 3.1: 1990. Structural use of steelwork in building, British Standards Institution, London.

Burnet, M.J. and Oehlers, D.J. 2001. Rib shear connectors in composite profiled slabs. *Journal of Constructional Steel Research,* **57** (12), pp. 1267–1287.

Collings, D. 2005. *Steel-Concrete Composite bridges*. London: Thomas Telford.

Cornelissen, H.A.W., Hordijk, D.A. and Reinhardt, H.W. 1986. Experimental determination of crack softening characteristics of normal weight and lightweight concrete. *Heron*, **31**(2), pp.45-56.

CP117, Part 1: 1965. Composite construction in structural steel and concrete, British Standards Institution, London.

Easterling, W.S., Gibbings, D.R. and Murray, T. M. 1993. Strength of Shear Studs in Steel Deck on Composite Beams and Joists. *Engineering Journal, AISC*, **30**(2), pp.44-55.

Ellobody, E. 2002. *Finite Element Modeling of shear connection for steel-concrete composite girders.* PhD Thesis. Leeds: School of Civil Engineering, University of Leeds.

Ellobody, E. and Young, B. 2006. Performance of shear connection in composite beams with profiled steel sheeting. *Journal of Constructional Steel Research*, **62**(7), pp.682-694.

Ellobody, E. and Lam, D. 2002. Modeling of headed stud in steel-precast composite beams. *Steel and Composite Structures,* **2**(5), pp.355-78.

Ellobody, E., Young, B. and Lam, D. 2006. Behaviour of normal and high strength concrete-filled compact steel tube circular stub columns. *Journal of Constructional Steel Research*, **62**(7), pp.707-715.

Ernst, S., Bridge, R.Q. and Wheeler, A. 2009. Push-out tests and a new approach for the design of secondary composite beam shear connections. *Journal of Constructional Steel Research,* **65**(1), pp.44-53.

Ernst, S., Bridge, R.Q. and Wheeler, A. 2010. Correlation of Beam Tests with Pushout Tests in Steel-Concrete Composite Beams. *Journal of Structural Engineering, ASCE,* **136**(2), pp. 183-192.

Fisher, J.W. 1970. Design of Composite Beams with Formed Metal Deck. *Engineering Journal, AISC,* 7(3), pp.88-96.

Grant, J.A., Fisher, J.W. and Slutter, R.G. 1977. Composite Beams with Formed Steel Deck. *Engineering Journal, AISC,* **14**(1), pp.24-43.

Hawkins, N.M. and Mitchell, D. 1984. Seismic Response of Composite Shear Connections. *Journal of Structural Engineering, ASCE,* **110**(9), pp.2120-2136.

Hicks, S. 2007. Strength and ductility of headed stud connectors welded in modern profiled steel sheeting. *The Structural Engineer,* **85**(10), pp.32-38.

Hicks, S.J., Couchman, G. 2004. The shear resistance and ductility requirements of headed studs used with profiled steel sheeting. In: Leon RT, Lange J, editors. *Proceedings of composite construction in steel and concrete V.* Kruger Park, South Africa: ASCE.

Hillerborg, A. 1985. The theoretical basis of a method to determine the fracture energy G_f of concrete. *Materials and Structures,* **18**(4) pp.291-96.

Hillerborg, A., Modeer, M., and Petersson, P.E. 1976. Analysis of crack formation and crack growth in concrete by means of fracture mechanics and finite elements. *Cement and Concrete Research,* **6**(6), pp.773-81.

Hu, H.T., Huang, C.S. and Wu, Y.M. 2003. Nonlinear analysis of axially loaded concrete-filled tube columns with confinement effect. *Journal of Structural Engineering, ASCE,* **129**(10), pp.1322-1329.

Jayas, B.S. and Hosain, M.U. 1988. Behavior of Headed Studs in Composite Beams: Push-Out Tests. *Canadian Journal of Civil Engineering,* **15**(2), pp.240-253.

Jayas, B.S. and Hosain, M.U. 1989. Behavior of Headed Studs in Composite Beams: Full-Size Tests. *Canadian Journal of Civil Engineering,* **16**(5), pp.712-724.

Johnson, R.P. 2004. *Composite Structures of Steel & Concrete Beams, Slabs, Column & Frames for Building. 3rd edition.* Oxford: Blackwell Scientific Publications.

Johnson, R.P. 2005. Shear connection in beams that support composite slabs–BS 5950 and EN 1994-1-1. *The Structural Engineer,* **83**(22), pp.21-24.

Johnson, R.P. and Oehlers, D.J. 1981. Analysis and Design for Longitudinal Shear in Composite T-Beams. *Proceedings of the Institution of Civil Engineers, Part 2,* **71**(4), pp.989-1021.

Johnson, R.P. and Yuan, H. 1998. Existing rules and new tests for stud shear connectors in troughs of profiled sheeting. *Proceedings of the Institution of Civil Engineers, Structures and Buildings,* **128**(3), pp. 244-251.

Johnson, R.P. and Yuan, H. 1998. Models and design rules for stud shear connectors in troughs of profiled sheeting. *Proceedings of the Institution of Civil Engineers, Structures and Buildings,* **128**(3) pp. 252-263.

Kim, B., Wright, H.D. and Carins, R. 2001. The behaviour of through-deck welded shear connectors: an experimental and numerical study. *Journal of Constructional Steel Research,* **57**(12), pp.1359-1380.

Lam, D. 2007. Capacities of headed stud shear connectors in composite steel beams with precast hollowcore slabs. *Journal of Constructional Steel Research,* **63**(9), pp.1160-74.

Lam, D. and Ellobody, E. 2005. Behaviour of headed stud shear connectors in composite beam. *Journal of Structural Engineering, ASCE,* **131**(1), pp.96-107.

Lawson, R.M. 1992. Shear Connection in Composite Beams. *In:* Darwin, D. and C. D. Buckner. *Composite Construction in Steel and Concrete II. 14-19 June 1992. Potosi, Missouri, USA,* New York: American Society of Civil Engineers. pp.81-97.

Lloyd, R.M. and Wright, H.D. 1990. Shear connection between composite slabs and steel beams. *Journal of Constructional Steel Research,* **15**(4), pp.255-285.

MC 90. 1993. CEB-FIP Model Code 1990, Thomas Telford, London;

Menzies, J.B. 1971. CP117 and shear connectors in steel-concrete composite beams made with normal-density or lightweight concrete. *Journal of Structural Engineering, ASCE,* **49**(3), pp.137-53.

Mirza, O. and Uy, B. 2009. Behaviour of headed stud shear connectors for composite steel-concrete beams at elevated temperatures. *Journal of Constructional Steel Research,* **65**(3) pp.662-74.

Mirza, O. and Uy, B. 2010. Effects of the combination of axial and shear loading on the behaviour of headed stud steel anchors. *Engineering Structures,* **32**(1): 93-105.

Mottram, J.T. and Johnson, R.P. 1990. Push Tests on Studs Welded Through Profiled Steel Sheeting. *The Structural Engineer,* **68**(10), pp.187-193.

Oehlers, D.J. 1989. Splitting Induced by Shear Connectors in Composite Beams. *Journal of Structural Engineering, ASCE,* **115**(2), pp.341-362.

Oehlers, D.J. and COUGHLAN, C.G. 1986. The Shear Stiffness of Stud Shear Connections in Composite Beams. *Journal of Constructional Steel Research,* **6**(4), pp.273-284.

Oehlers, D.J. and Johnson, R.P. 1987. The Strength of Stud Shear Connections in Composite Beams. *The Structural Engineer,* **65**(14), pp.44-48.

Ollgaard, J.G., Slutter, R.G. and Fisher, J.W. 1971. Shear Strength of Stud Connectors in Lightweight and Normal-Weight Concrete. *Engineering Journal, AISC,* **8**(2), pp.55-64.

Patrick, M. 2000. Experimental investigation and design of longitudinal shear reinforcement in composite edge beams. *Progress in Structural Engineering and Materials*; **2**(2): pp.196-217.

Rambo-Roddenberry, M.D. 2002. *Behavior and Strength of Welded Stud Shear Connectors.* PhD Thesis. Virginia: Virginia Polytechnic and State University, Blancksburg, Virginia, USA.

Robinson, H. 1988. Multiple stud shear connections in deep ribbed metal deck. *Canadian Journal of Civil Engineering*, **15**(4), pp.553-569.

Stark, J. W. B. and Van Hove, B. W. E. M. 1991. Statistical analysis of push-out tests on stud connectors in composite steel and concrete structures. TNO Building and Construction Research, Delft, Report BI-91-163.

Wright, H.D. and Francis, R.W. 1990. Tests on Composite Beams with Low Levels of Shear Connection. *The Structural Engineer,* **68** (15), pp.293-298.

Wright, H.D., Evans, H.R. and Harding, P.W. 1987. The use of profiled steel sheeting in floor construction. *Journal of Constructional Steel Research*, **7**(4), pp.279-295.

Appendix A: The publications from the PhD research

1. Journal papers

Qureshi J, Lam D and Ye J. Effect of shear connector spacing and layout on the shear connector capacity in composite beams. Journal of Constructional Steel Research 2011; 67(4): 706-719.

Qureshi J, Lam D and Ye J. The influence of profiled sheeting thickness and shear connector's position on strength and ductility of headed shear connector. Engineering Structures 2011; 33(5): 1643–1656.

Qureshi J and Lam D. Behaviour of headed shear stud in composite beams with profiled metal decking. Advances in Structural Engineering. 2011 [in press]

2. Conference Papers

Qureshi J, Lam D and Ye J. Finite element modelling of shear connection behaviour in a push test using profiled sheeting. In: The fourth international conference on structural engineering, mechanics and computation (SEMC 2010). Cape Town, South Africa; 2010. ISBN: 978-0-415-58472-2

Lam D and Qureshi J and Ye J. Composite behaviour of headed stud shear connectors in pairs with profiled metal deck flooring. In: Steel & Composite Structures-Proceedings of the 4th International Conference. Sydney, Australia; 2010. ISBN: 978-981-08-6218-3

Lam, D. and Qureshi, J. Modelling Headed Shear Stud in Composite Beams with Profiled Metal Decking. In: Proceedings of the International Workshop on Steel and Composite Structures. Sydney, Australia; 2010. ISBN: 978-1-74108-216-6

Qureshi J, Lam D and Ye J. Behaviour of Headed Shear Stud in a Push Test using Profiled Steel Sheeting. In: 9th International Conference on Steel Concrete Composite and Hybrid Structures. Leeds, United Kingdom; 2009. ISBN: 978-981-08-3194-3

Lam D and Qureshi J. Prediction of longitudinal shear resistance of composite slabs with profile sheeting to Eurocode 4. In: Proceedings of The Regency Steel Asia International Symposium on innovations in structural steel, RSA-ISISS 2008, Singapore; 2008. ISBN: 978-981-08-1727-5

3. Research Reports

Qureshi J and Lam D. Behaviour of headed stud shear connectors using new horizontal push test. Report to The Metal Cladding and Roofing Manufacturers Association (MCRMA) Floor/Deck Group; 2010.

Appendix B: Awards during the PhD research

Second runner up prize for poster presentation at The Institution of Structural Engineers Young Researcher's conference (YRC2010). London, United Kingdom; 2010.

MUET PhD scholarship for UK, 2007-2010: Received Mehran University of Engineering and Technology Jamshoro, Pakistan Scholarship to pursue PhD study in United Kingdom.

HEC PhD scholarship for Austria, 2007-2010: Received "PhD scholarship for study of Sciences, Engineering and Technology, Austria" awarded by Higher Education Commission Pakistan (not taken up).

The author receiving prize from Professor Roger Plank, Senior Vice President of the Institution of Structural Engineers, London